Dissertation
for the doctoral degree in natural sciences
at the Faculty of Applied Computer Science of the University of Augsburg

---

Warm and cold water events in the tropical southeast Atlantic Ocean

---

Karin Romberg

née Lutz

Chair of Physical Geography and Quantitative Methods

University of Augsburg

Augsburg, 2014

Advisor:	Prof. Dr. Jucundus Jacobeit
Reviewers:	Prof. Dr. Jucundus Jacobeit
	Prof. Dr. Karl Wetzel

Thesis Defense: 3.12.2014

To my family

Danksagung

Meinen persönlichen Dank an alle, die maßgeblich am Gelingen dieser Arbeit beteiligt waren, möchte ich informell und damit ohne Nennung sämtlicher akademischer Titel formulieren.

Mein größter Dank gilt meinem langjährigen Chef, Mentor und zuletzt Doktorvater Jucundus Jacobeit. Lieber Herr Jacobeit, ich möchte mich bei Ihnen insbesondere für die unendliche Geduld und die stete Unterstützung bei allen Vorhaben bedanken. Zahlreiche Diskussionen haben mich stets auf dem richtigen Kurs gehalten. Sie waren der beste Chef und Doktorvater, den ich mir hätte wünschen können.

Karl Wetzel möchte ich für die Übernahme des Zweitgutachtens, aber auch für die unermüdliche Motivation und Unterstützung in allen Bereichen des universitären Alltags bedanken.

Ein ausdrücklicher Dank geht auch an die Deutsche Forschungsgemeinschaft (DFG) für die Finanzierung des Projekts JA-831/9-1, in dessen Rahmen die Durchführung dieser Doktorarbeit möglich war. Darüber hinaus möchte ich Herrn Jacobeit und Joachim Rathmann für die Aufnahme im Forschungsprojekt danken.

Ein herzlicher Dank geht an meine fleißigen Korrekturleser und -leserinnen Stefan Romberg, Joachim Rathmann, Irena Ott, Andreas Philipp, Stefanie Seubert und Elke Hertig. Joachim Rathmann möchte ich darüber hinaus für konstruktive Diskussionen im Rahmen des Forschungsprojekts bedanken. Danke, Ena, für ein super Büroklima, die gute Zusammenarbeit und viele hilfreiche Diskussionen!

Lieben Dank auch an Angelika Witt, deren Tür stets für mich offen stand und die sowohl in universitären als auch außeruniversitären Belangen immer ein offenes Ohr für mich hatte.

Meiner Familie möchte ich besonders für die immerwährende Unterstützung und Motivation danken, die mir Studium und Promotion erst ermöglich haben. Danke, dass Ihr immer für mich da wart.

Und nicht zuletzt gilt mein herzlichster Dank meinem lieben Mann Stefan. Lieber Stefan, Du warst immer da, wenn ich nicht mehr weiter wusste. Du hast mir den Weg im Dunklen geleuchtet und mich während aller Höhen und Tiefen dieser Arbeit mit unerschöpflicher Geduld und Zusprache begleitet. Vielen lieben Dank dafür!

Contents

List of Figures

List of Tables

List of Abbreviations

ABA	Angola Benguela Area
ABFZ	Angola Benguela Frontal Zone
AGCM	Atmospheric General Circulation Model
AMJ	April-June
ASO	August-October
ATLN	Atlantic Niño
CA	Cluster Analysis
CCA	Canonical Correlation Analysis
CCP	Canonical Correlation Pattern
DJF	December-February
ENSO	El Niño Southern Oscillation
FMA	February-April
GCM	General Circulation Model
IOD	Indian Ocean Dipole
ISM	Indian Summer Monsoon
ITCZ	Intertropical Convergence Zone
JAS	July-September
JJA	June-August
MAM	March-May
MJJ	May-July
NDJ	November-January
NTA	North Tropical Atlantic
OND	October-December
PC	Principal Component
PCA	Principal Component Analysis
SAA	South Atlantic Anticyclone
SLP	Sea Level Pressure
SON	September-November
SST	Sea Surface Temperature
STA	South Tropical Atlantic
TIO	Tropical Indian Ocean Index
WATL	Western Atlantic Zonal Wind

Abstract

The tropical oceans exhibit high interannual sea surface temperature (SST) variability that strongly impacts the regional climate of the adjacent continents. However, the influence of tropical SST variability is not limited to the regional scale but can be perceived in remote regions all over the globe. Earlier work has mainly focused on the Pacific El Niño Southern Oscillation (ENSO) and its regional and global impacts. Yet, recent studies show that a similar phenomenon exists in the tropical Atlantic Ocean. Warm and cold events in the tropical southeast Atlantic have been described to impact regional rainfall variability and are further assumed to play a role in the development of Pacific ENSO events.

In contrast to the Pacific Ocean two Niño-like phenomena have been described for the eastern tropical Atlantic: one of them centered in the equatorial region, also known as Atlantic Niño, and another one close to the coast of northern Namibia and Angola, referred to as Benguela Niño. Although similar forcing mechanisms are proposed for their evolution, the two Niño types have mainly been analyzed in separate studies and regarded as independent phenomena. Yet, recent studies suggest a possible interdependence.

This thesis thoroughly explores tropical Atlantic SST variability based on long-term observational data aiming at the extraction of robust indices, which are suitable for a further analysis of the link between Atlantic and Benguela Niños. The newly defined indices, which represent both the equatorial and coastal SST variability, are strongly correlated and thus indicate a close connection between anomalous warming and cooling in both regions. Therefore, instead of considering equatorial Atlantic and Benguela Niños as separate phenomena, they are both combined into a classification of one comprehensive Atlantic Niño. With regard to the different regional character of the events, this classification contains the three sub-types major event, minor event and episode.

The newly defined indices and classification of Atlantic Niños are further used to study the influence of tropical southeast Atlantic SST variability on African west coast precipitation. The analyses show that during Atlantic Niños and Niñas anomalous rainfall is observed in different seasons nearly along the entire sub-Saharan west coast. Yet, results indicate a seasonally asymmetric response in some west coast regions. Moreover, a significant impact on precipitation is not limited to major warm or cold water events but is also observed for minor events.

Furthermore, this work studies teleconnections of the tropical Atlantic to the tropical Pacific and Indian Oceans. Analyses are carried out with respect to the dominant influence of the Pacific El Niño Southern Oscillation (ENSO)

system. Therefore, in addition to the investigation of the relationship between the Pacific and Atlantic Oceans, the aim of these analyses is to find links between the Atlantic and Indian Oceans that are not ENSO-dependent. For that, additional analyses are performed that exclude the ENSO signal. Results show a significant anticorrelation between the Atlantic and Pacific Oceans in recent decades and suggest a possible enhancement and delay of the peak of a Pacific La Niña when preceded by a boreal summer Atlantic Niño. By contrast, Indian Ocean SST variability is mainly dependent on the Pacific Ocean. The Atlantic Ocean does not seem to exert a significant influence on the Indian Ocean that is independent of ENSO.

Zusammenfassung

Interannuelle Schwankungen der tropischen Meeresoberflächentemperaturen (SSTs) spielen eine wichtige Rolle für die Klimatologie der angrenzenden Kontinente. Ihr Einfluss ist jedoch nicht regional begrenzt, sondern reicht über Wechselwirkungen mit der Atmosphäre auch bis in weit entfernte Regionen. Besonders ausgeprägte SST Anomalien lassen sich sowohl im tropischen Pazifik als auch im Atlantik und Indik finden. Der Fokus älterer Arbeiten lag dabei vor allem auf dem Pazifischen Warmwasserereignis El Niño und seinen regionalen und globalen Auswirkungen. Neuere Studien zeigen für den Atlantik ähnliche Zusammenhänge auf. Warmwasserereignisse im südöstlichen Atlantik beeinflussen demnach nicht nur die regionale Niederschlagsvariabilität, sondern spielen auch für die Ausprägung von El Niños im Pazifik eine Rolle.

Anders als für den Pazifik wurden für den südöstlichen Atlantik bisher zwei Warmwasserphänomene beschrieben, der Atlantic Niño im äquatorialen Atlantik und der Benguela Niño vor der Küste Südangolas bzw. Namibias. Obwohl ähnliche Entstehungsmechanismen vermutet werden, wurden beide Phänomene bisher hauptsächlich getrennt untersucht. Jüngere Studien zeigen jedoch bereits einen möglichen Zusammenhang dieser beiden.

In dieser Arbeit wird zunächst mittels weiter zurückreichenden Beobachtungsdaten der Meeresoberflächentemperatur die tropisch atlantische SST Variabilität untersucht. Ziel ist die Bildung geeigneter Indizes für die Untersuchung des Zusammenhangs zwischen Atlantic und Benguela Niños. Mittels der neu definierten Indizes, welche sowohl die äquatoriale als auch die küstennahe Variabilität erfassen, kann ein eindeutiger Zusammenhang zwischen den beiden Niño Phänomenen hergestellt werden. Statt einer getrennten Betrachtung werden Warm- und Kaltwasserereignisse in unterschiedliche Klassen eines einzigen Atlantic Niños mit unterschiedlicher Intensität und regionaler Ausprägung eingeteilt: major event, minor event, episode.

Auf der Basis der neu erstellten Indizes und der einheitlichen Klassifikation von Atlantic Niños und Atlantic Niñas werden Zusammenhänge mit Niederschlagsanomalien entlang der subsaharischen Westküste Afrikas untersucht. Hierbei lässt sich feststellen, dass während Atlantic Niños und Niñas nahezu die gesamte Küste zu unterschiedlichen Jahreszeiten deutliche Zu- oder Abnahmen des Niederschlags aufweist. Zudem legen die Ergebnisse der Analysen die Vermutung nahe, dass sich Warm- und Kaltwasserereignisse mögli-

cherweise unterschiedlich stark auswirken. Es kann weiterhin gezeigt werden, dass sich der Einfluss auf den Niederschlag nicht auf größere Ereignisse beschränkt, sondern auch kleinere Ereignisse von Bedeutung sind.

Darüber hinaus werden Wechselwirkungen zwischen dem tropischen Atlantik und dem tropischen Pazifik und Indik untersucht. Dabei wird ein besonderes Augenmerk auf den dominanten Einfluss des El Niño Southern Oscillation (ENSO) Systems gerichtet und für den Indik zusätzliche Analysen unter Ausschluss des ENSO Einflusses durchgeführt. Ziel der Analysen ist es, neben einer Untersuchung des Zusammenhangs von Atlantik und Pazifik auch mögliche Wechselwirkungen zwischen Atlantik und Indik zu finden, welche weitgehend unabhängig vom Pazifik auftreten. Die Ergebnisse zeigen für die letzten drei Dekaden einen deutlichen Zusammenhang zwischen Atlantik und Pazifik. Darüber hinaus geben sie Hinweise auf eine mögliche Verstärkung und Verlängerung einer Pacific La Niña durch einen Atlantic Niño. Dagegen wird die SST Variabilität des Indischen Ozeans maßgeblich durch den Pazifik beeinflusst. Ein signifikanter Einfluss des Atlantiks lässt sich in diesem Zeitraum nicht nachweisen.

1 Introduction

1.1 Motivation

The tropical oceans play a key role in the global climate system. They are the most important regions for large-scale ocean-atmosphere interactions exhibiting variations on various time scales (e.g. Chang et al. 2006b). The Pacific Ocean hosts the most prominent coupled ocean-atmosphere system, namely the *El Niño Southern Oscillation* (ENSO). Numerous studies have analyzed regional and global impacts and have demonstrated its strong influence on both the adjacent continents and regions far from the Pacific Ocean. During an El Niño (warm) event, anomalously high sea surface temperatures (SSTs) are observed in the eastern and central Pacific Ocean. Associated with these SST anomalies severe floods occur in Peru whereas the Indonesian region as well as southern Africa are affected by droughts - just to name a few examples. Its importance goes far beyond climatic changes but also lies in ecological as well as socioeconomic impacts.

For the Atlantic Ocean a similar phenomenon has been described. Interannual SST variations in the tropical southeast Atlantic are linked to rainfall anomalies over northeastern Brazil, southern and western Africa as well as the Sahel region (e.g. Rouault et al. 2003, Xie and Carton 2004, Reason and Rouault 2006). In addition to such climatic impacts, southeast Atlantic SST anomalies further influence the local ecosystem. For instance, they affect marine productivity in the Benguela system (Heymans et al. 2004) with economic consequences for the fisheries.

Despite its unquestioned relevance for both regional and global climate anomalies, comparably few studies have analyzed warm and cold water events in the tropical Atlantic Ocean. And yet, no consensus on the description of these events exists. That is, instead of one phenomenon two Niño-like phenomena are described for the tropical Atlantic Ocean: (1) the Atlantic Niño, centered in the equatorial region (Zebiak 1993) and (2) the Benguela Niño off the coast of Angola and Namibia (Florenchie et al. 2003). Al-

though similar possible forcings of both Niño types and similar impacts on the regional and global climate have been reported, they have mainly been studied in separate studies and regarded as independent phenomena. Only few works assume a possible connection between those two. Thus, from these previous studies the question arises whether the Atlantic Ocean does host two such phenomena or Atlantic and Benguela Niños are in fact part of one Niño phenomenon. This important question not only affects considerations of the SST anomalies themselves, but also has implications for all subsequent analyses considering regional impacts and global interactions.

Therefore, one of the main objectives in this thesis will be the assessment of the question whether there is a connection between the Atlantic Niño and Benguela Niño. Furthermore, this work provides a comprehensive analysis of their regional impacts and global interactions, with respect to both the equatorial and coastal SST variability. A summary of the main contributions of this thesis is given in the subsequent Section 1.2. Section 1.3 then briefly outlines the structure of this thesis.

1.2 Contributions

The main contribution of this thesis can be summarized as follows:

- **Atlantic Niño classification:** Two Niño phenomena have been described for the tropical south Atlantic, one in the equatorial Atlantic termed Atlantic Niño and one off the Angolan coast named Benguela Niño. These have long been analyzed in separate studies. Only recently, it was suggested that they may be related or should even be perceived as one phenomenon. In this thesis, new robust and suitable indices are developed to describe sea surface temperature anomalies in the tropical southeast Atlantic and to analyze the connection between equatorial variability and that further southeast. Furthermore, a new classification of warm and cold water events is derived, which integrates both Niño phenomena with respect to their different regional character.

- **Regional impact on precipitation:** So far, several studies have investigated the relationship between southeast Atlantic SSTs and rainfall over continental Africa but these differ in the selection of regions and seasons, only cover a short period or use different definitions of warm and cold events. Therefore, results from these works are incomplete or not comparable. For this work, comprehensive analyses are carried out, which include the entire west coast facing the south Atlantic, all seasons and one common definition of warm and cold water events in the tropical southeast Atlantic. Furthermore, the present analyses are not limited to warm events and their impact, but also consider cold events.

- **Analysis of tropical teleconnections:** Regarding global interactions between the tropical Atlantic, Pacific and Indian Oceans, most studies have focused on the linear lead-lag relationship and possible mechanisms connecting the Atlantic and Pacific basins. Furthermore, for the Atlantic and Indian Oceans, detailed analyses only

exist for the connection between southeast Atlantic SSTs and the Indian Summer Monsoon. In this work, previous analyses are extended and the proposed mechanisms are evaluated for both the Atlantic Niño and the Niña case. Moreover, a thorough investigation of a possible interaction between the Atlantic and Indian Oceans, both dependent and independent of ENSO, is performed.

Parts of this thesis have been published in peer-reviewed journals: the classification of Atlantic warm and cold water events (see Chapter 5) is described in Lutz et al. (2013). The impact of these events on African west coast precipitation (see Chapter 6) is analyzed in Lutz et al. (2014).

1.3 Thesis Overview

This thesis is organized as follows:

Chapter 2 gives a brief overview of the dominant modes of tropical interannual sea surface temperature variability that are of interest for teleconnection analyses. Chapter 3 briefly describes the datasets used in this work. This chapter further explains necessary computations of variables and data preprocessing. In Chapter 4 the statistical techniques used in this thesis are described.

Chapter 5 then focuses on the tropical southeast Atlantic warm and cold events. After an analysis of patterns of tropical southeast Atlantic SST variability, a new definition and classification of Atlantic Niños and Niñas is introduced. This chapter also includes an analysis of the newly defined indices and events. Chapter 6 explores the regional impact of Atlantic Niños and Niñas in terms of African west coast precipitation. Chapter 7 further discusses Atlantic warm and cold events in the context of global interactions. That is, the chapter investigates the teleconnections of the tropical Atlantic to the tropical Pacific and Indian Oceans. Finally, this thesis closes with conclusions and a brief outlook in Chapter 8.

2

Interannual variability of tropical sea surface temperatures

The tropical ocean and sea surface temperature (SST) variability plays a key role in tropical large-scale atmospheric circulation. Unlike in the extratropics, tropical circulation patterns primarily result from an interaction with the ocean. That is, variability of the atmosphere is strongly coupled to that of the SSTs. Of course, the influence of tropical oceans is not limited to the tropics but can be perceived all over the globe (Chang et al. 2006b, Deser et al. 2010).

In general, the tropical oceans exhibit variability on various time scales. An overview of seasonal, interannual and decadal variability is given in Xie and Carton (2004) for the Atlantic sector and for the Indian Ocean in Schott et al. (2009). A recent review of Pacific interannual and decadal variability associated with the El Niño Southern Oscillation is provided by Wang and Picaut (2004). Additionally, a detailed description of patterns and mechanisms of non-seasonal, i.e. interannual as well as decadal tropical (and extratropical) SST variability is given in Deser et al. (2010).

In this work the focus lies on the interannual time scale. Therefore, the dominant patterns of interannual SST variability in the three tropical ocean basins are discussed in this chapter. Following Deser et al. (2010), for each basin an unrotated covariance-based principal component analysis (PCA) is performed to extract these patterns. This variant of PCA was mainly chosen to produce comparable patterns to those of Deser et al. (2010). As described in Section 4.3, unrotated covariance-based s-mode PCA focuses on the maximum of variability within the field rather than on centers of variation with maximum common variability. Furthermore, instead of using pre-defined indices such as the Niño3.4 index (for an index definition see Section 3.4), here, the principal component (PC) score is used for further analyses of the corresponding time series of each pattern. In addition to the description of each SST pattern and score, associated atmospheric dynamics are discussed.

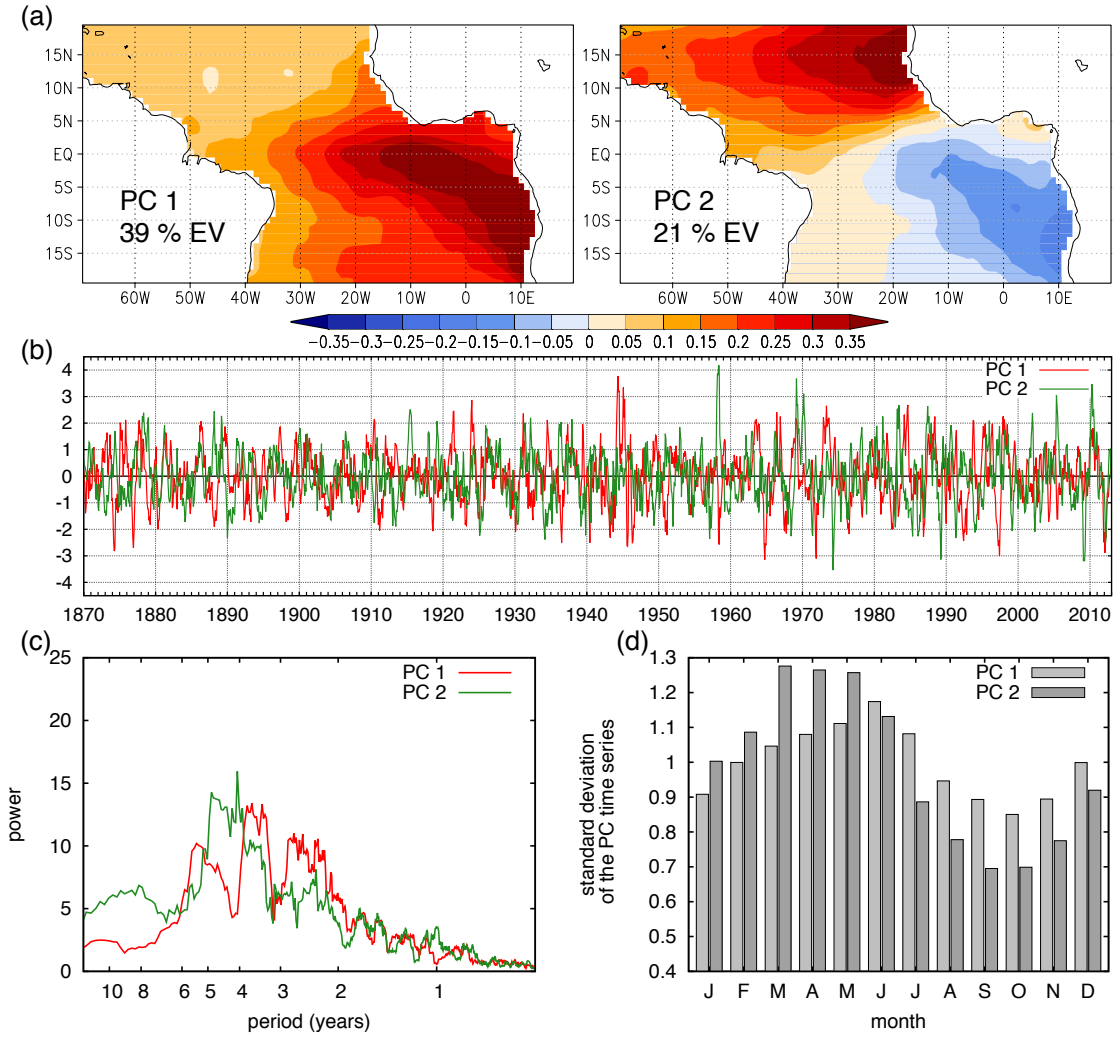

Figure 2.1: First and second principal component of standardized gauss-filtered all-season SSTs in the tropical Atlantic during 1870–2012: (a) loading patterns, (b) monthly PC time series (scores), (c) power spectrum and (d) monthly standard deviation of PC time series. PC1 depicts the Atlantic zonal mode and PC2 the meridional mode. The two modes account for 39 % and 21 % of explained variance (EV), respectively.

2.1 Atlantic zonal and meridional modes

Two major modes of SST variability are described for the tropical Atlantic (Ruiz-Barradas et al. 2000): an equatorial zonal mode (e.g. Merle 1980, Philander 1986, Zebiak 1993) and a meridional mode with cross-equatorial SST gradients (Nobre and Shukla 1996, Chang et al. 1997). A recent review of both modes is given in Xie and Carton (2004) and Chang et al. (2006b).

Atlantic zonal mode

Figure 2.1 shows the two leading principal components of tropical Atlantic SST anomalies between 20°N and 20°S. The leading mode (39 % of explained variance) depicts the equatorial zonal mode, also termed *Atlantic Niño*. The loading pattern (Figure 2.1 (a)) shows an east-west gradient, with its center of variability located in the equatorial Atlantic cold

tongue in the eastern part of the basin off the African coast. A power spectrum (Figure 2.1 (c), for a description of spectral analysis see Section 4.6) of the PC time series (score) shows a dominant range of periods between 2–6 years. The maximum power is centered at a period of about 3.5 years. Smaller peaks are also found for 2.5 and 5.5 years. As indicated by the seasonal cycle of the standard deviation (Figure 2.1 (d)), this mode is also seasonally dependent. High SST variability is observed in boreal summer months and early winter while there is less variation in boreal autumn and late winter. As the Atlantic Niño is the main focus of interest in this thesis, this mode and associated atmospheric dynamics will be discussed in more detail in Chapter 5, which also contains further analyses.

Atlantic meridional mode

The second PC (Figure 2.1 (b)) depicts the pattern referred to as *Atlantic meridional mode*. It appears as an interhemispheric, cross-equatorial SST-gradient and is associated with weaker (stronger) trade winds in the warmer (colder) hemisphere (Nobre and Shukla 1996). The meridional mode is most pronounced in boreal spring (Figure 2.1 (d)) when the intertropical convergence zone (ITCZ) reaches its southernmost position and has been described to be active on decadal time scales (Ruiz-Barradas et al. 2000, Wang 2002). Although the power spectrum of the second PC in our analyses appears shifted to longer time scales compared to the first PC and has a secondary maximum for a period of 8-10 years, the overall maximum is apparent for 4-5 years. This may appear somewhat contradictory at first, but PCA was applied to high-pass filtered data due to our focus on interannual variability. High-pass filtering suppresses decadal variability while it emphasizes interannual variability, which is reflected in the peaks of the spectrum.

Concerning the physical processes involved, Chang et al. (1997) attribute the decadal variation of the meridional mode to an ocean-atmosphere feedback mechanism involving mainly positive thermodynamic feedbacks between wind-induced heat fluxes and SST. This positive wind-evaporation-SST (WES) feedback (originally proposed by Xie and Philander (1994) to explain the northward displacement of the ITCZ over the eastern Pacific and Atlantic) can be summarized as follows: An initial positive anomalous SST gradient (i.e. cold to the south and warm to the north of the equator) is associated with an anomalous northward SLP gradient and thus induces southerly wind anomalies across the equator. When the southern hemispheric southeasterlies cross the equator northwards, they gain a westerly component due to the Coriolis force. Therefore, they decelerate the prevailing northeasterlies north of the equator. The weakened northeasterly trades reduce surface evaporation to the north while the southeasterlies to the south of the equator increase evaporation and thus cooling. Both contribute to a strengthening of the initial SST gradient (Xie and Carton 2004).

The meridional mode is often also referred to as Atlantic dipole mode although the physical existence of such a dipole is questioned and discussed controversially. Instead of a dipole, Houghton and Tourre (1992) find two separate modes of variability north and south of the equator based on a Varimax rotated PCA. Dommenget and Latif (2000) con-

firm that the tropical north and south Atlantic vary independently and are uncorrelated. They describe the dipole as an artifact of the EOF technique used. This is discussed in more detail in Dommenget and Latif (2002). In fact, our results (not shown) confirm that the dipole disappears when using rotated PCA. In contrast, Ruiz-Barradas et al. (2000) reinforce the existence of a dipole when combining SSTs and atmospheric variables in a rotated PCA. Thus, both the choice of the EOF technique and variables included in the analyses severely affect the resultant patterns.

Despite these controversial discussions about empirical modes of tropical Atlantic SST variability in different studies, Xie and Carton (2004) point out three aspects in which these agree: (1) The meridional position of the ITCZ is sensitive to an anomalous cross-equatorial SST gradient. (2) Although rare, an SST dipole maximizes the gradient. (3) Off-equatorial SST anomalies are associated with altered trade winds on both sides of the equator.

It has further been shown that the Atlantic meridional mode is linked to the zonal mode (Servain et al. 1999). Although these two modes may also occur independently, Hu et al. (2013) suggest that they are both statistically and physically connected.

2.2 Pacific El Niño Southern Oscillation

The most prominent mode of global atmosphere-ocean variability is the *El Niño Southern Oscillation* (ENSO) phenomenon. ENSO is a coupled atmosphere-ocean system with El Niño representing the oceanic and the Southern Oscillation the atmospheric component of the system, respectively. The term El Niño refers to sea surface temperature anomalies observed in the central and eastern Pacific while the Southern Oscillation describes a see-saw pattern in sea level pressure between the Indonesian region and the eastern Pacific.

As shown in Deser et al. (2010), the leading empirical orthogonal function (EOF) of global monthly SST anomalies depicts the pattern corresponding to ENSO. Here, the first principal component of a PCA limited to the Pacific domain is shown, which accounts for 45 % of interannual variability. In its positive mode (see loading pattern in Figure 2.2 (a)), which corresponds to an ENSO warm phase, it appears as a horseshoe-like pattern with positive SST anomalies covering the eastern two-thirds of the equatorial Pacific Ocean, flanked by negative anomalies over the western parts. Its corresponding PC score and power spectrum of the score (Figure 2.2 (b) and (c)) indicate that ENSO events last about 1–1.5 years and reoccur every 2.5–8 years. ENSO is seasonally phase-locked with a peak in boreal winter months (see Figure 2.2 (d)). These observations are consistent with earlier work (e.g. Wang and Picaut 2004, Chang et al. 2006b, Deser et al. 2010).

According to Chang et al. (2006b), ENSO can be described as a climate perturbation around the mean state of the coupled atmosphere-ocean system in the tropical Pacific. The oceanic mean state is characterized by an west-to-east SST gradient with a warm pool in the western and a cold tongue in the eastern Pacific. Overlaying easterly trade winds and the ascending (descending) branches of the Walker circulation to the west (east) form the corresponding atmospheric component. Together, ocean and atmosphere

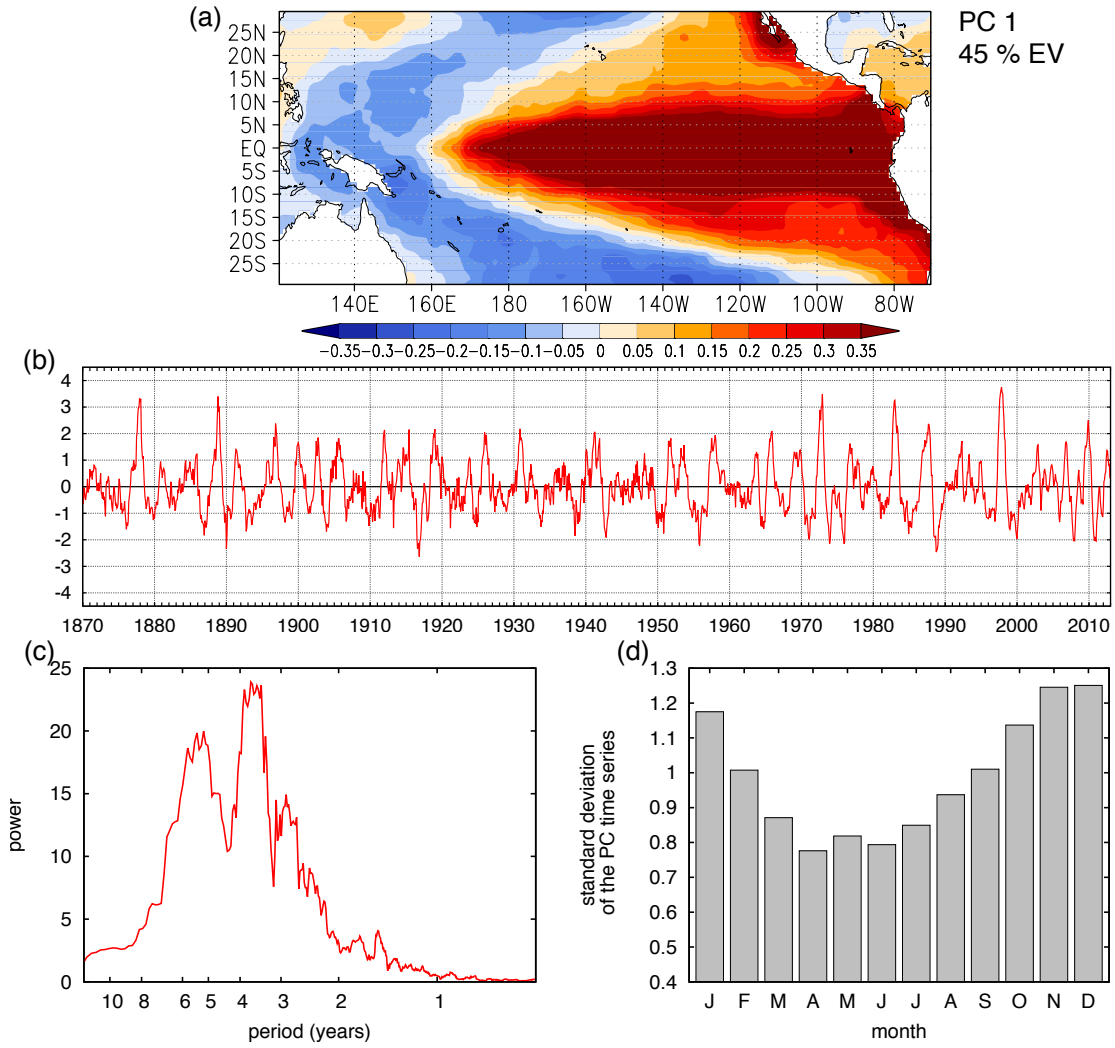

Figure 2.2: Leading principal component of standardized gauss-filtered SSTs in the tropical Pacific during 1870–2012: (a) loading pattern, (b) monthly PC time series, (c) power spectrum and (d) monthly standard deviation of PC time series. The leading PC accounts for 45 % of explained variance (EV) and depicts the SST pattern corresponding to ENSO.

support a positive dynamical feedback: The SST gradient favors large-scale ascent and atmospheric heating over the western equatorial Pacific as well as descent and cooling over the eastern parts. These processes reinforce the strength of the trade winds. Easterly trades in turn act to rise the thermocline and favor associated upwelling in the east, thereby maintaining the climatological distribution of the tropical Pacific SSTs.

Due to the strong atmosphere-ocean coupling, a small change in either the SSTs or the trade winds can trigger a chain reaction in the coupled system. For instance, an initial anomalous SST warming (cooling) in the equatorial eastern Pacific reduces (strengthens) the west-east SST gradient and thus weakens (strengthens) the Walker circulation. The latter is associated with weaker (stronger) trades winds along the equator, which in turn drive ocean circulation changes that further reinforce SST anomalies. This positive atmosphere-ocean feedback proposed by Bjerknes (1969) therefore plays a key role in the development of Pacific Ocean warm (El Niño) or cold (La Niña) events.

The positive Bjerknes-feedback alone would lead to a never-ending warm state of the equatorial Pacific. Therefore, a negative feedback mechanism is required for the termination of a warm or cold phase. In search for such a mechanism, four conceptual oscillator models have been proposed involving the negative feedbacks of (1) reflected Kelvin waves at the western boundary of the ocean (*delayed oscillator*), (2) a discharge process due to Sverdrup transport (*discharge oscillator*), (3) a western Pacific wind-forced Kelvin wave (*western Pacific oscillator*) and (4) anomalous zonal advection due to Rossby and Kelvin wave activity (*advective-reflective oscillator*). For a detailed description of these models see Wang and Picaut (2004), Seubert (2010) and Wang et al. (2012). In addition, assuming that several of these mechanisms may operate in ENSO-like oscillations, Wang (2001) proposes a *unified oscillator* that includes the physics of all other models.

As shown e.g. in Deser et al. (2010) using composite analysis, the evolution of a typical ENSO warm event starts with an incipient positive SST anomaly along the equator and the coast of South America during boreal spring (MAM season, also referred to as *peak phase* by Rasmusson and Carpenter (1982) due to the strong anomalies off the coast). This anomaly subsequently grows over the next several seasons with the center of warming successively moving from the South American Coast to the equatorial central Pacific (*transition phase* in ASO). Negative SST anomalies simultaneously develop to the northwest and southwest of the positive anomaly. The warm event reaches its peak in boreal winter (DJF, *mature phase*), decays in the subsequent year and transitions into a weak cold event in the following boreal summer. The corresponding SLP composites presented by Deser et al. (2010) show the picture of a typical negative Southern Oscillation phase: positive SLP anomalies in the western Pacific and Indonesian region and negative values to the east, also reaching their peak in boreal winter.

Although the origin of the ENSO phenomenon originates in the tropical Pacific, associated changes in the atmospheric large-scale pattern influence the atmospheric circulation and oceanic conditions around the globe (e.g. Alexander et al. 2002). As tropical teleconnections will be the focus of Chapter 7, an interaction between ENSO and Atlantic and Indian Ocean variability will be discussed in more detail in that chapter.

El Niño Modoki

Recent studies report a somewhat different character of El Niño events for the last two decades. The typical horseshoe pattern of the conventional El Niño has its center of maximum warming in the cold tongue region of the eastern equatorial Pacific. In contrast, in recent events the location of the maximum SSTs is shifted to the central Pacific and is flanked by anomalous cooling on both the eastern and western side (Ashok et al. 2007). Consistent with the SSTs, the corresponding atmospheric pattern shows anomalous twin Walker cells with the center of anomalous convection located in the central Pacific and westerly (easterly) trade wind anomalies to its west (east). So far, there is no consensus on a name or typing. While some rather view these anomaly patterns as a different flavor of the conventional El Niño and not as a separate type, other studies propose a new type and name it *dateline El Niño* (Larkin and Harrison 2005), *El Niño* Modoki (or *pseudo El*

Niño, Ashok et al. 2007), *central Pacific El Niño* (Kao and Yu 2009) or *Warm Pool El Niño* (Kug et al. 2009) to emphasize the differences from conventional El Niño (which is also referred to as *eastern Pacific El Niño*). In this work, the name El Niño Modoki - a Japanese expression for "similar but different" (Ashok et al. 2007) - is adopted. Wang and Wang (2013) further classify El Niño Modoki into two types, namely *El Niño Modoki I* and *II*. These two sub-types show different origins and SST anomaly patterns, and thus have different influences on southern China rainfall and typhoon tracks in the western north Pacific.

Despite different names for this phenomenon, these studies agree in the description of SST and atmospheric patterns and thus the existence of a different flavor of El Niño. Furthermore, not only the conditions in the Pacific sector differ in the two types. It is also reported that the new type of El Niño exhibits a different influence on temperature and rainfall in many regions of the world (e.g. Ashok et al. 2007).

An increasing number of events of the new Niño type has been observed since the late twentieth century, and it is assumed that its frequency will further intensify under conditions of global warming (Ashok and Yamagata 2009). That is, more of these events will occur at the expense of the conventional El Niño. Yeh et al. (2009) attribute this development to changes due to anthropogenic warming. However, Yeh et al. (2011) conclude from further coupled general circulation model experiments, that one may not exclude the possibility that the increasing frequency of El Niño Modoki during recent decades may be part of natural variability.

2.3 Indian Ocean Dipole, basin-wide mode and Ningaloo Niño

In the tropical Indian Ocean, the two leading modes of SST variability (Deser et al. 2010) are the *basin-wide mode* and a zonal mode called the *Indian Ocean Dipole* (IOD) (Saji et al. 1999). A recent review of these two modes is given in Schott et al. (2009).

Basin-wide mode

The pattern of the leading PC (37 % of explained variance) depicts the basin-wide mode (Figure 2.3 (a)), which represents negative (positive) SST anomalies covering the entire tropical Indian Ocean. The power spectrum (Figure 2.3 (c)) of the corresponding PC score shows peaks for periods of 3, 3.5 and 5 years. That means that the spectrum of the basin-wide mode is quite similar to that of ENSO (Figure 2.2 (c), p. 9). The seasonal cycle of the standard deviation (Figure 2.3 (d)) shows a peak in late boreal winter and early spring months with maximum values in January, February and March. This is consistent with the results reported by Deser et al. (2010).

As summarized in Schott et al. (2009), the basin-wide mode is closely linked to ENSO and involves a very robust response to ENSO events: During a Pacific warm phase, the Indian Ocean gradually warms. SSTs reach their highest values during boreal spring months March–May, about one season after Niño3 SSTs have peaked in boreal winter. This robust response can be explained by the close connection between the Indian and

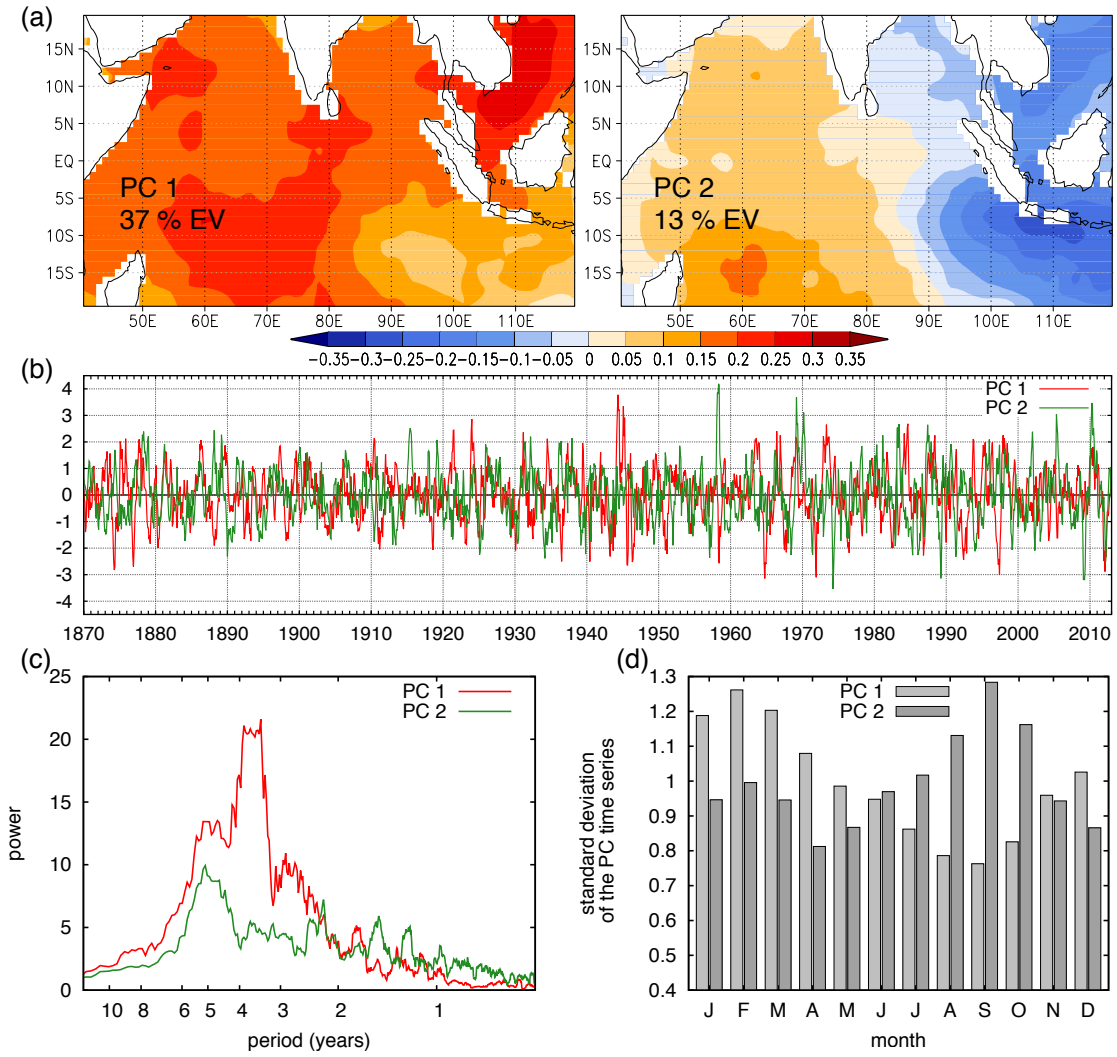

Figure 2.3: (a) First and second principal component of standardized gauss-filtered SSTs in the tropical Indian Ocean during 1870–2012: (a) loading patterns, (b) monthly PC time series, (c) power spectrum and (d) monthly standard deviation of PC time series. PC1 depicts the basin-wide mode and PC2 the dipole mode. The two modes account for 37 % and 13 % of explained variance (EV), respectively.

Pacific Oceans via the *atmospheric bridge* (Alexander et al. 2002): During El Niño, atmospheric convection shifts eastwards. While convection intensifies over the central-to-eastern equatorial Pacific, it is suppressed over the western Pacific and the maritime continent. This leads to changes in surface heat fluxes, especially wind-induced latent heat and cloud-induced solar radiation fluxes. Suppressed convection and increased solar radiation further contribute to a basin-wide warming (Klein et al. 1999). Convective anomalies in turn are modulated by Indian Ocean SSTs in boreal spring that may also play a role in the onset delay of the *Indian Summer Monsoon* (ISM), thereby acting as a climate condenser in response to ENSO (Annamalai et al. 2005a).

Embedded in the basin-wide warming, there is a small region in the *southwest tropical Indian Ocean* (SWIO) between $5-10°$S, which also exhibits a warming in response to ENSO. However, the SWIO warming cannot be explained by surface flux changes, but

may rather be caused by an anomalous deepening of the thermocline ridge normally found in this region (Xie et al. 2002). During the mature phase of El Niño, a region of anomalous anticyclonic wind stress develops in the southeast Indian Ocean due to changes in the Walker circulation. This wind stress anomaly forces westward traveling downwelling Rossby waves, which deepen the thermocline ridge in the SWIO and thus contribute to a SST warming in this region. The SWIO warming reaches its maximum during April-July, about two seasons after the peak of El Niño. For further details see Schott et al. (2009).

Another feature in the tropical Indian Ocean, also linked to ENSO, is an asymmetrical pattern, often occurring during the decay phase of El Niño in boreal spring. While the north Indian Ocean warming weakens during spring, northeasterly and southwesterly wind anomalies appear north and south of the equator, causing an asymmetrical rainfall response (Wu et al. 2008). This asymmetrical pattern may be explained by a wind-evaporation-SST feedback operating on the prevailing easterlies during boreal winter and spring. The pattern persists through early summer and thus is anchored by the SWIO warming (Schott et al. 2009).

Indian Ocean Dipole

The second PC (Figure 2.3 (b)) depicts a dipole pattern with an west-east SST gradient. This zonal mode is also referred to as Indian Ocean dipole. It explains 13 % of total variance, which is consistent with the findings of Saji et al. (1999). The spectrum of this mode (Figure 2.3 (c)) is rather noisy and has two peaks for periods of about 2 and 5 years. This is consistent with results from wavelet analyses presented in Saji and Yamagata (2003b). These authors also show significant decadal variations of the two spectral peaks, which may explain the peaks' moderate magnitude. Furthermore, as shown in Figure 2.3 (d), the dipole mode is seasonally phase-locked with a peak in July-October.

According to Saji et al. (1999), IOD warm events are associated with positive SST anomalies over large parts of the western Indian Ocean basin and negative anomalies in the eastern parts off Sumatra. They also show that IOD events are seasonally phase-locked to boreal autumn. Significant anomalies appear around June, intensify until they peak in October and decay in December. Furthermore, IOD events are associated with increased rainfall over tropical eastern Africa and the western Indian Ocean while decreased rainfall, even drought, is observed over the Indonesian archipelago. As Saji et al. (1999) find a strong connection between equatorial zonal wind anomalies and IOD index variability, they suggest the IOD to be an inherent coupled ocean-atmosphere mode, involving equatorial upwelling and thermocline shoaling. Shinoda et al. (2004) further confirm associated thermocline variability. These observations point to the contribution of the Bjerknes feedback to the evolution of the IOD events in a similar way as it is described for ENSO events. That is, cooling in the eastern Indian Ocean induces easterly wind anomalies, which strengthen equatorial upwelling and shoal the thermocline, thereby reinforcing the initial SST cooling (Deser et al. 2010).

While e.g. Saji et al. (1999) and Webster et al. (1999) believe the IOD to be independent from ENSO due to an insignificant correlation ($r < 0.35$) at lag 0, Allan et al. (2001) questions the existence of such a dipole. The latter authors assume that it is coupled to ENSO or even is an integral part of ENSO. As has already been mentioned in the context of the Atlantic meridional mode, the interpretation of EOFs (as used by Saji et al. (1999)) may be misleading, as they are orthogonal and therefore uncorrelated at lag 0 (Dommenget and Latif 2002). Furthermore, Allan et al. (2001) show, that lead-lag correlations do show a significant connection between the IOD and ENSO. More recent studies suggest that a dipole-like variability does exist in the Indian Ocean but is primarily forced by ENSO (Baquero-Bernal et al. 2002) or at least strongly conditioned by it (Bracco et al. 2005). Furthermore, Roxy et al. (2011) report that the interdependence of ENSO and IOD primarily depends on the season.

Ningaloo Niño

Although small-scale and yet little-known, another interesting Niño mode appears off the coast of western Australia. An unusual SST warming in 2011 with a peak in austral summer of more than 5°C warmer than normal was first described by Feng et al. (2013). This anomaly, which the authors term *Ningaloo Niño*, caused widespread coral bleaching and fish kill. Tozuka et al. (2014) further report an impact on northwestern Australian precipitation with wet (dry) anomalies during a Ningaloo Niño (Niña). The Ningaloo Niño in 2011 was associated with an unusual intensification of the poleward-flowing Leeuwin Current in austral summer, transporting anomalously warm water southward along the coast. The 2011 Ningaloo warm event appeared to be remotely forced by an extraordinary Pacific La Niña in 2010–2011. This phenomenon is further studied in Kataoka et al. (2013), who classify Ningaloo Niños and Niñas into two types. One type is called the *locally amplified mode*, developing trough intrinsic atmosphere-ocean interaction. And a second remotely forced type called *non-locally amplified mode* is mostly associated with ENSO. Due to its close link to the ENSO system, the Ningaloo Niño also shows encouraging predictability with two seasons ahead (Doi et al. 2013). As this phenomenon was only recently identified, a lot of work is still to be done for a better understanding of the mechanisms behind it (Tozuka et al. 2014).

As can be concluded from the descriptions given above, the Indian Ocean shows notable complexity and exhibits several features of different time and spatial scales that may be of interest for subsequent analyses.

3 Data

This chapter briefly describes the datasets used in this work. These include monthly resolved gridded observational datasets of sea surface temperatures (SSTs, Section 3.1), sea level pressure (SLP, Section 3.2) and reanalysis datasets of different atmospheric variables as well as precipitation (Section 3.3). In addition to the gridded fields, preprocessed teleconnection indices as well as indices from own computations are used (Section 3.4). All data are processed according to the procedure described in Section 3.5.

Due to data availability, the 62-year time period from 1951–2012 was chosen as main analysis period. However, some of the analyses, including the Atlantic Niño classification (see section 5), extend back to 1870, as SSTs are available for this period.

3.1 Sea Surface Temperatures

For SSTs, several datasets with different temporal coverage and spatial resolution are available. Deser et al. (2010) give a brief overview of the most commonly used gridded datasets. While in the earlier record period datasets rely on ship observations, buoys and buckets, more recent data, since 1981, also include satellite observations. Data coverage is poor in the earlier record period and mainly concentrated on commercial shipping routes but improves over time (see Figure 3 in Deser et al. 2010). Until today, data coverage in the northern hemisphere is better than in the southern oceans.

For this work, two monthly datasets, namely HadISST and ERSST, are chosen as they both provide a long record period and comparably high spatial resolution. In addition, a third dataset with a shorter temporal coverage, NOAA OISST, is used for validation purposes. The three datasets are briefly described in the following.

ICOADS: Many datasets (including HadISST and ERSST) are based on the International Comprehensive Ocean-Atmosphere Data Set (ICOADS). This dataset provides an

extensive digital collection of quality-controlled surface marine meteorological observations, including SST. The data include non-instrumental ship observations as well as measurements from ships, moored and drifting buoys and also hydrographic profiles. The monthly averaged summary products of version 2.5 are available since 1800 in a $2^\circ \times 2^\circ$ ($1^\circ \times 1^\circ$ since 1960) spatial resolution and are updated monthly in near real-time (Slutz et al. 1985, Woodruff et al. 2011).

HadISST: The monthly sea ice and sea surface temperature dataset HadISST1.1 was developed at the Hadley Center of the UK Meteorological Office and replaces the Global Sea Ice and Sea Surface Temperature (GISST) dataset. The SST fields are reconstructed using an empirical orthogonal (EOF)-based technique, reduced space optimal interpolation (RSOI), in a two-stage process. First, the global pattern of long-term change and second, the residual interannual variability is reconstructed. The superposition of quality-controlled gridded observations is then used to recapture local variance that was lost in the RSOI. With this technique observations are interpolated to a $1^\circ \times 1^\circ$ grid (Rayner et al. 2003). Data are available since 1870 and updated monthly.

ERSST: The Extended Reconstructed Sea Surface Temperature (ERSST) dataset was developed at the National Oceanic and Atmospheric Administration (NOAA). Reconstruction of the SST fields is performed separately for low- and high-frequency components using different filtering techniques and an empirical orthogonal teleconnection (EOT)-approach. The two components are added together to form a total SST anomaly afterwards. ERSST version 3b is available in a $2^\circ \times 2^\circ$ resolution for the period back to 1880 (Smith and Reynolds 2003, Smith et al. 2008).

NOAA OISST: The NOAA Optimum Interpolation (OI) Sea Surface Temperature (NOAA OISST) dataset includes in situ and also satellite observations, namely the Advanced Very High Resolution Radiometer (AVHRR) satellite retrievals (Reynolds et al. 2002). The bias corrected data are available on $1^\circ \times 1^\circ$ grid in a weekly resolution from 1981 to the present. Here, the monthly average is used for comparative analyses.

Due to biases and a different representation of high- or low-frequency variability long-term datasets all have their limitations and in the end it is a decision for the one or the other bias. The main differences between the two long-term datasets HadISST and ERSST lie in the different bias correction techniques and the computation of low-frequency variability (Smith et al. 2008). Pre-analyses for the tropical Atlantic show that differences between the datasets are greater in the earlier period, before 1950, due to the limited data availability, but become smaller after 1950. ERSST has a tendency to be cooler in the earlier record period. In terms of variability, HadISST appears to be more conservative in the tropical Atlantic, showing less fluctuation in the standard deviation. As it also comes with a higher resolution the HadISST dataset is used as main dataset in this work. ERSST and NOAA OISST (for the shorter period) are further used for validation purposes.

3.2 Atmospheric Circulation

Several climate variables in different atmospheric levels are used to analyze the atmospheric circulation. Both observational and reanalysis data are used for long-term and short-term analyses, respectively. A short description of the datasets as well as some mathematical and interpretational details are given in this section.

HadSLP: The Met Office Hadley Centre's mean sea level pressure (HadSLP) dataset was produced using marine observations from ICOADS and terrestrial land and island observations from 2228 stations. Marine and terrestrial data were blended, quality-controlled and finally interpolated to a global 5° grid using reduced-space optimal interpolation (Allan and Ansell 2006). The data are available for the period 1850–2004. The near-real time version HadSLP2r now also provides updates until the present.

NCEP-NCAR reanalysis: The NCEP-NCAR Reanalysis is a joint project between the National Centers for Environmental Prediction (NCEP) and the National Center for Atmospheric Research (NCAR). Their global dataset is based on a frozen (unchanged over the period) data assimilation system and produced using a T62 model with 28 vertical levels. The NCEP-NCAR Reanalysis 1 is available in a 4-times daily, daily but also monthly resolution for the period 1948–2012. In this work, only the monthly data are used. Data are available on a $2.5° \times 2.5°$ grid. For further details refer to Kalnay et al. (1996) and Kistler et al. (2001).

20thCR: The Twentieth Century Reanalysis (20CR) dataset (Compo et al. 2011) is a comprehensive global atmospheric circulation dataset, extending back to 1871. In contrast to other reanalyses, only surface pressure reports were assimilated. Observed monthly SST and sea-ice distributions are used as boundary conditions. It is available in a 6-hourly temporal and a 2° spatial resolution. This dataset was only used in pre-analyses comparing reanalysis and observational data. However, results from the latter led to the decision to exclude the data from further analyses in this work.

The following variables used in this work have been directly obtained from their provider: SLP, geopotential heights (HGT), stream function (PSI), velocity potential (CHI), horizontal wind velocities, vertical velocity (OMEGA) and specific humidity. Moisture flux convergence (MF) was not available for download and had to be computed following the procedure described below.

Convergence (or negative divergence) of moisture flux (MF) integrated from bottom (p_{src}) to the 300 hPa level (p_{top}) is computed from U- and V- components (horizontal velocities $\vec{v_h} = (u, v)$) of wind stress and specific humidity q using the following formula (Palmén and Holopainen 1962):

$$-\nabla \cdot \vec{Q} = -\frac{1}{g} \nabla \cdot \int_{p=p_{sfc}}^{p=p_{top}} \vec{v_h} q dp \tag{3.1}$$

where ∇ denotes the horizontal divergence operator and g is the gravity constant. In addition to the integrated MF, moisture flux convergence for six levels between 1000 and 300 hPa is computed for a detailed analysis of single levels.

For an interpretation of the stream function Ψ and the velocity potential $\mathcal{X}$, which may appear less intuitive, some mathematical background is useful. As explained by Wang (2002), horizontal wind velocity v can be divided into a non-divergent (or rotational) part v_Ψ and a divergent (or irrotational) part $v_\mathcal{X}$:

$$v = v_\Psi + v_\mathcal{X} = k \times \nabla\Psi + \nabla\mathcal{X}. \tag{3.2}$$

The rotational part is usually larger but the divergent part is more important for the consideration of atmospheric cells associated with divergent fields and vertical motion (Wang 2002). Walker and Hadley cells are thermally driven. Atmospheric heating is associated with convection, which induces atmospheric convergence-divergence driving atmospheric vertical motion and circulation. Therefore, the velocity potential $\mathcal{X}$ in combination with the vertical velocity OMEGA can be used to identify atmospheric circulation cells (Wang 2002). In addition, the stream function Ψ indicates regions with cyclonic or anticyclonic flow. As there is no mass transport perpendicular to the streamlines but parallel to them, the latter variable gives additional information about the direction of the flow. For better readability, thereafter Ψ and $\mathcal{X}$ are written in latin letters PSI and CHI, respectively.

3.3 Precipitation

Most precipitation datasets either have a coarse resolution or a relatively short temporal coverage. Parker et al. (2011) give an overview of monthly datasets, which are globally available or at least cover Africa. For the analysis of sub-Saharan precipitation, in this work, three land-surface datasets with relatively high (0.5°) spatial resolution and a temporal coverage of at least 50 years are selected.

CRU: The Climate Research Unit (CRU) dataset version 3.10 is available for the period 1901 to 2009. It includes station data from the Global Historical Climatology Network (GHCN) version 2, the Hulme precipitation database as well as monthly climate bulletins (CLIMAT, internationally exchanged between countries within the World Meteorological Organization (WMO)) and Monthly Climate Data for the World (MCDW), which is provided by National Climate Data Center (NCDC) in the USA. While for the earlier version 2.1 angular-distance weighted (ADW) interpolation was applied (Mitchell and Jones 2005), now triangulated linear interpolation is used to produce a half-degree resolution (Harris et al. 2014). Note that, in the latest version, for several grid points anomaly time series were replaced by climatological values. Time series of these grid points therefore show zero variance and need to be removed for some of the analyses.

GPCC: The Global Precipitation Climatology Centre (GPCC) dataset version 6 is available for the period 1901 to 2010. Data sources include meteorological synoptic data (SYNOP), CLIMAT, national data contributions by WMO members, data collections from several international regional projects, data from CRU and FAO as well as GHCN. SPHEREMAP, a spherical adaptation of Shepard's empirical weighting scheme (Willmott et al. 1985), is used to interpolate the data to a 0.5° grid (Rudolf and Schneider 2005).

UDEL: The University of Delaware terrestrial precipitation dataset (UDel) version 3.02 is available for the period from 1900 to 2010. Station data were compiled from several data sources, which include, amongst others, GHCN version 2, Global Surface Summary of the Day (GSOD), the Legates and Willmott archive and Nicholson's (2001) extensive African gauge data collection (Matsuura and Willmott 2012). According to Parker et al. (2011), this dataset strongly benefits from the latter data and is therefore recommended for usage for the African domain. The dataset is interpolated using a spherical version of the Shepard's distance-weighting method (Willmott et al. 1985) - as it was used for GPCC - as well as Climatologically Aided Interpolation (CAI, Willmott and Robeson 1995).

All three datasets were compared in pre-analyses and showed no major differences except for the zero variances in CRU described above. This work therefore follows the recommendation by Parker et al. (2011) and uses the UDel dataset as main source.

3.4 Teleconnection Indices

Several tropical teleconnection indices were used in this work. These include the well-known El Niño Southern Oscillation (ENSO) SST and SLP indices, two El Niño Modoki indices as well as the Indian Ocean Dipole (IOD) and the Tropical Indian Ocean Index (TIO). All indices are displayed in Figure 3.1.

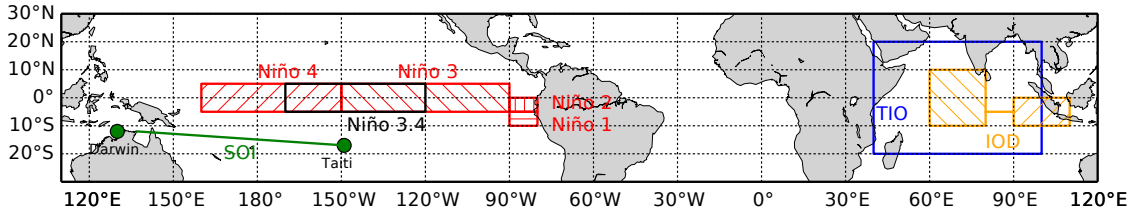

Figure 3.1: Tropical teleconnection indices: ENSO SST index regions Niño 1, 2, 3, 4, 3.4 and SLP index Southern Oscillation Index (SOI) in the Pacific sector; SST index regions for the Indian Ocean Dipole (IOD) and Tropical Indian Ocean Index (TIO) in the Indian Ocean.

El Niño SST indices: To analyze the oceanic component of ENSO variability and its relationship to the Atlantic, the four SST indices Niño1, Niño2, Niño3 and Niño4 (corresponding SST index regions are indicated as red boxes in Figure 3.1) as well as a fifth index Niño3.4 (black box in Figure 3.1) are used. According to Trenberth (1997), ENSO variability is best represented by Niño3.4, but the Niño3 index is also commonly used

in teleconnection studies (e.g. Keenlyside and Latif 2007, Rodríguez-Fonseca et al. 2009). Therefore, initially all five indices are considered. In addition to the indices, ENSO event dates are taken from NOAA CPC (2014). Their definition of warm (El Niño) and cold (La Niña) events is based on the Oceanic Niño Index (ONI), which is computed from the Niño3.4 ERSST SST anomalies (for further details please refer to NOAA CPC 2014). As HadISST was chosen as main dataset, in this work, all ENSO indices were computed using HadISST SSTs.

El Niño Modoki indices: Two additional indices are used to represent central Pacific SST variability associated with El Niño Modoki (for a description of this phenomenon see Section 2.2), namely the Trans-Niño index (TNI, Trenberth and Stepaniak 2001) and the El Niño Modoki index (EMI, Ashok et al. 2007). The TNI is computed using the standardized ENSO indices Niño1+2 and Niño4 and thus represents the SST gradient between the dateline and the American coast:

$$TNI = SST_{Niño1+2} - SST_{Niño4}. \tag{3.3}$$

With respect to the tripolar nature of the SST pattern of the El Niño Modoki, the EMI is defined as

$$EMI = SST_A - 0.5 * SST_B - 0.5 * SST_C \tag{3.4}$$

where SST_A, SST_B, SST_C refer to the SST anomalies in the regions A (165°E–140°W and 10°S–10°N), B (110°E–70°W and 15°S–5°N) and C (125°E–145°W and 10°S–20°N). As all ENSO indices and the TNI index, the EMI index is computed using HadISST data. Due to the lack of space, the latter three regions are not included in Figure 3.1.

Southern Oscillation Index (SOI): The SOI (indicated in green in Figure 3.1) is defined as the difference between normalized monthly mean sea level pressure at Tahiti and Darwin (Trenberth 1984). It is representative for the atmospheric component of ENSO. Data was obtained from NCAR (2014).

Indian Ocean Dipole (IOD): Intensity of the IOD is represented by an anomalous SST gradient between the western equatorial Indian Ocean (50°E–70°E and 10°S–10°N) and the southeastern equatorial Indian Ocean (90°E–110°E and 10°S–0°N) (Saji et al. 1999). The western box was later updated to 60°E–80°E and 10°S–10°N (Saji and Yamagata 2003a). Here, the updated definition is used (yellow boxes in Figure 3.1).

Tropical Indian Ocean Index (TIO): The TIO index covers the whole tropical Indian Ocean between 40°E–100°E and 20°S–20°N (blue box in Figure 3.1) and is used in this work as an indicator for the Indian Ocean basin-wide mode (Schott et al. 2009).

3.5 Data processing

Time series of all datasets described in the previous sections are processed in the same way, following four steps:

1. Temporal aggregation to seasonal sections
2. Spatial aggregation (where necessary)
3. High-pass-filtering
4. Standardization

Small-scale and large-scale processes are active on different time scales. African precipitation shows fast variations on a monthly scale and the response to changes in the regional SSTs or circulation appears within a short term. In contrast, global interactions rather appear on longer time scales. Therefore, both monthly and seasonal analyses are necessary. Data are aggregated to overlapping seasonal sections of 2-monthly up to 12-monthly means. Monthly and seasonal means add up to 144 seasonal sections. These are abbreviated using first letters of each month contained, e.g. J for the month January, JF for the 2-monthly mean January-February, JFM for 3-monthly mean January-March et cetera. These abbreviations will be used in both text and figures.

For region indices such as the teleconnection indices (see Section 3.4), spatial aggregation is carried out for particularly selected grid points.

Furthermore, Rathmann (2009) found significant long-term trends in the South Atlantic SSTs and SLPs and in African precipitation, which also show some non-linear character. However, the primary focus of this work lies on interannual variability and not on long-term trends or on decadal or multi-decadal variability. To remove such low frequency variability or trends, all data are filtered using a 11-year Gaussian high-pass filter. For a detailed description of Gaussian filtering refer to Schönwiese (2013).

Finally, the filtered time series are standardized. If not indicated otherwise, all analyses are based on aggregated, filtered and standardized data.

4 Methods

This Chapter briefly summarizes the statistical techniques used in this work. In addition to a short description of the basics of each technique, further details in terms of application and interpretation are discussed. The order of their description in this Chapter corresponds to their relevance and frequency of usage in this work.

4.1 Bivariate and multivariate correlation analysis

4.1.1 Pearson correlation, partial and multiple correlation coefficients

The two-dimensional Pearson product-moment coefficient of linear correlation, also referred to as Pearson correlation coefficient, is a measure of the linear association between two random variables a and b. The correlation coefficient r_{ab} or r can be expressed as the ratio of the covariance s_{ab} to the two standard deviations s_a and s_b

$$r_{ab} = \frac{s_{ab}}{s_a s_b} = \frac{\sum_{i=1}^{n} (a_i - \bar{a})(b_i - \bar{b})}{\sqrt{\sum_{i=1}^{n} (a_i - \bar{a})^2 \sum_{i=1}^{n} (b_i - \bar{b})^2}} \tag{4.1}$$

where a_i and b_i denote the i-th elements and $\bar{a}$ and $\bar{b}$ the mean values of two variables a and b with sample size n (Wilks 2005, Schönwiese 2013).

The Pearson correlation coefficient has two important properties: First, its values range between -1 and 1. Values of -1 and 1 describe a perfect negative or positive relationship, respectively. Second, for an interpretation of the results in terms of explained variability, the squared correlation coefficient r^2, also called the coefficient of determination, plays an important role. It specifies the proportion of variability of a variable that is described by the other. r^2 is also often described as the ratio of explained variance to the total variance. This interpretation may sometimes be misleading as the relationship described by

r provides no physical explanation for a causative link (Wilks 2005). Additional analyses for a dynamical interpretation are therefore necessary.

A helpful method to assess the possibility of a causal relationship and to detect spurious correlations is provided by partial correlation. The partial correlation coefficient provides a measure of the association between two random variables a and b, excluding the possible controlling effect of a third disturbing random variable c. The three-dimensional linear partial correlation coefficient $r(part)_{ab*c}$ is defined as:

$$r(part)_{ab*c} = r_{ab*c} = \frac{r_{ab} - r_{ac}r_{bc}}{\sqrt{(1 - r_{ac}^2)(1 - r_{bc}^2)}} \tag{4.2}$$

where r_{ab} and r_{ac} denote the two-dimensional correlation coefficients of two variables a and b, and a and c, respectively. Note that expressions such as the exclusion or removal of the controlling effect or influence of a third variable actually mean that this variable is explicitly added to the analyses and not excluded. However, by computing its contribution to the relationship between a and b, one may also estimate the proportion of variability of a described by b that is independent of c. That is, the variance that c has in common with a and with b is removed.

For the interpretation of the results, the two-dimensional correlation coefficient r_{ab} and the partial correlation coefficient $|r(part)_{ab*c}|$ are compared. The result is one of four possible cases:

- $|r(part)_{ab*c}| < |r_{ab}|$: overestimation of r_{ab} due to the influence of c. In the extreme case $|r(part)_{ab*c}|$ drops to 0, i.e. a spurious correlation is detected.
- $|r(part)_{ab*c}| > |r_{ab}|$: underestimation of r_{ab} due to the influence of c. The partial correlation is more suited to explain the relationship between a and b.
- $|r(part)_{ab*c}| \approx |r_{ab}|$: no disturbance. r_{ab} is perfectly suitable to describe the link.
- $|r(part)_{ab*c}|$ and $|r(part)_{ac*b}|$ are both significantly different from zero. Therefore multiple correlation may be considered.

If, for the fourth case, the decision falls for a three-dimensional model that includes all three variables, a is to be understood as predictand (dependent variable) and b and c as predictors (independent variables) b and c. The multiple correlation coefficient $r(mult)_{a*bc}$ is then computed as follows:

$$r(mult)_{a*bc} = r_{a*cb} = \sqrt{\frac{r_{ab}^2 + r_{ac}^2 - 2|r_{ab}r_{ac}r_{bc}|}{(1 - r_{bc}^2)}} \tag{4.3}$$

where r_{ab}, r_{ac} and r_{bc} denote all possible two-dimensional correlation coefficients (Schönwiese 2013).

4.1.2 Test for significance

The Pearson correlation coefficient assumes a minimum sample size (≥ 30), normal distribution and stochastic independence of the data. Normal distribution is tested using a Shapiro Wilks test (as described in Sachs and Hedderich 2009). In addition, the autocorrelation function is plotted for the first few time lags. Results for both normal distribution test and autocorrelation vary across different variables, regions and seasons, and is also different for filtered and unfiltered data. In general, normal distribution cannot be assumed for all datasets, especially not for precipitation. Concerning independence, in some cases autocorrelation is eliminated by high-pass filtering, as is the case e.g. in the tropical Indian Ocean SSTs. However, for precipitation (and also for some regions in the SSTs and other variables) high negative correlation coefficients for lag 1 appear after filtering.

Therefore, a modified significance testing procedure that has already been applied in Philipp (2003) and Seubert (2010), was adapted for all correlation analyses. To account for non-normal distribution, a Fisher-transformation is applied before estimating the confidence intervals (as described in Sachs and Hedderich 2009). Furthermore, the standard *t*-test is computed using reduced degrees of freedom (as suggested by Schönwiese 2013 in case of autocorrelation).

4.1.3 Graphical presentation of correlation results

In addition to common line or point plots, a more complex plot type is chosen for the graphical presentation of results from cross-correlation analysis.

Cross-correlation analyses applied to several seasonal sections leads so quite an abundance of results, i.e. for example 3600 correlation coefficients for 144 seasonal sections and 25 time lags. Therefore, in this thesis a plot type used in Seubert (2010) is adopted and modified for the present analyses. The plot incorporates four dimensions, namely central month (x-axis), length of a seasonal section (y-axis), strength of the correlation coefficient (color scale) and the time lag of maximum correlations coefficients (labels in boxes). An example for cross-correlation analysis applied to the Atlantic Niño 3 (ATLN3) and Tropical Indian Ocean (TIO) indices is shown in Figure 4.1.

Significant correlation coefficients (at the 95% level) are displayed centered on the corresponding central month of a seasonal section, e.g. the FMA season is plotted at the position of central month M, DJF at J, JASO at A, et cetera. Furthermore, for each 1- to 12-month seasonal section only the absolute (positive or negative) maximum for time lags -12–12 months (TIO lagging in this case) is shown. The label denotes the corresponding time lag of the maximum. The overall maximum and minimum of all 3600 correlation coefficients computed in this analysis is highlighted by a white frame. Additionally, the title contains the value of both overall maximum and minimum.

Depending on the purpose, in some figures used in this work only positive **or** negative maxima are displayed. The figure then contains only positive **or** negative correlation coefficients and not both. That is, there are three versions of the plots that display (1) absolute maxima, (2) positive maxima or (3) negative maxima, respectively.

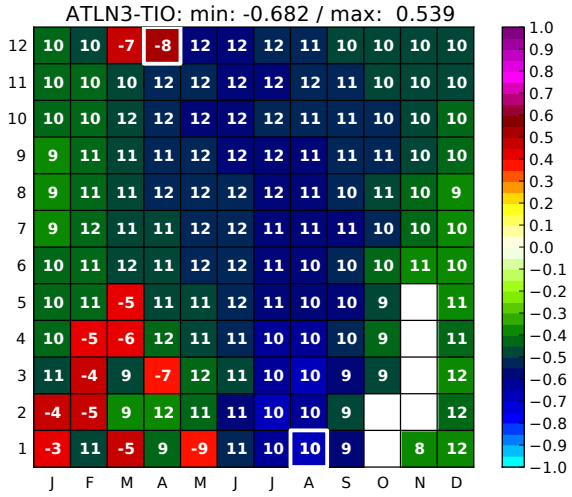

Figure 4.1: Cross-correlation analysis between Atlantic Niño index 3 (ATLN3) and Tropical Indian Ocean Index (TIO) for the period 1981–2012. For each 1- to 12-month seasonal Section (y-axis) only the absolute (positive or negative) maximum correlation for time lags -12–12 months (TIO lagging) is shown. The label denotes the corresponding time lag of the maximum. The overall maximum is highlighted by a white frame. Only significant results (95% level) are shown and displayed based on the central month (x-axis), e.g. the FMA season is plotted at the position of central month M. For a detailed description of this example plot please see text.

4.2 Composite analysis

A composite is the mean of a selected data sample. The selection is based on a certain criterion, e.g. an event (e.g. Indian dipole events in Saji et al. 1999), wet/dry conditions (rainfall) or warm/cold conditions (temperature). Depending on the question analyzed, composite differences are also used, such as wet minus dry (e.g. to analyze the relationship between rainfall and atmosphere in the tropical Atlantic sector, Hastenrath 1984) or warm minus cold.

In this work, compositing is mainly used for the analysis of selected events, i.e. Atlantic Niños and Niñas (see classification in Section 5.5) to learn more about the events themselves and associated atmospheric conditions. To account for a possible asymmetric response, Atlantic Niños and Niñas are explicitly examined separately.

Similar to the correlation analyses in this work, composites are computed for selected time lags, seasonal sections and also for both fields and station time series.

A two-sided Wilcoxon-Mann-Whitney rank sum test or *U*-test (for computational details see Bahrenberg et al. 1990, Sachs and Hedderich 2009) was applied to estimate significant differences of composites. In this case, the warm (Niño) or cold (Niña) sample is tested against the remaining data.

An advantage of the *U*-test over the likewise commonly used *t*-test is that it is a non-parametric test. It does not assume normal distribution of the data, but only an equal shape of the distribution. Another advantage is that it can also be applied to small sample sizes.

4.3 Principal component analysis (PCA)

Principal component analysis (PCA) is a widely used multivariate statistical technique in the atmospheric sciences that reduces a larger set of variables to a smaller number of new variables, termed principal components (PCs). The PCs are linear combinations of the original variables, which represent the maximum possible fraction of the variability in the original data. PCA not only compresses the original data, but also removes linear dependencies as the extracted PCs span a new coordinate system and are orthogonal and thus uncorrelated. PCA can therefore be used to identify the dominant modes of variability in an atmospheric field and to compress the data for subsequent analyses (such as canonical correlation analysis, see Section 4.5). A detailed description including the mathematical definition can be found e.g. in Bahrenberg et al. (1992), Preisendorfer (1988), von Storch and Zwiers (1999), Wilks (2005) and Jolliffe (2002). Note that, instead of PCA, empirical orthogonal functions (EOFs) are also widely used. The computation of PCA and EOF is fairly similar, although a different scaling is applied to their corresponding eigenvectors.

In atmospheric sciences, the most commonly used PCA variants are t-mode or s-mode PCA. In t-mode, PCA input variables are spatial patterns (grid points) of a homogeneous data field (e.g. SSTs) at successive time steps within a given period, whereas for an s-mode PCA input variables are the time series of a data field at successive grid points, in its simplest application. The latter is the main mode used in this work.

Based on the correlation or covariance matrix, the first principal component represents the linear combination of the input variables that has the largest variance. All subsequent PCs are computed such that the linear combinations have the largest possible variances and are uncorrelated with the remaining PCs. The extraction of PCs can be continued until 100 % of total variance of the original data is explained. This is the case when the number of PCs reaches the number of input variables. As a large portion of variance is already explained by the first few PCs, the remaining ones represent rather unimportant modes. Therefore the number of PCs is often limited based on a certain criterion. In this work, the so-called dominance criterion (Jacobeit 1993) was used.

As output of a PCA, PC loadings and scores are retained. In the s-mode case, the PC loadings represent the spatial patterns or spatial centers of variation reflecting the importance of a PC in the space dimension. The PC scores are corresponding time coefficients. In t-mode PCA, the PC loadings are time scores that indicate the importance of the spatial patterns (represented by the PC scores) in the time dimension.

4.3.1 PCA based on covariance matrix versus correlation matrix

Mathematically speaking, the correlation matrix is the covariance matrix of a vector of standardized variables. The difference between correlation-based and covariance-based PCA is therefore that it analyzes the joint variance structure of standardized or non-standardized variables, respectively. As PCA seeks to find variables successively maximizing the proportion of the total explained variance, PCs computed based on the co-

variance matrix emphasize the variables that have the largest variances. Thus, the first few eigenvectors tend to align near the direction of the variables with biggest variances. Conversely, correlation-based PCA weights all variables equally (as they are standardized and therefore have unit variance). Thus, the main difference between correlation-based and covariance-based PCA is one of emphasis.

Choosing one or the other variant of PCA is a question of the aim of an analysis. If one wants to identify the strongest variations in a data set, it is better to use covariance-based PCA. For example, Overland & Preisendorfer (1982, cited in Wilks (2005)) analyzed gridded numbers of extratropical cyclones. They found that covariance-based PCA performs better identifying the regions with the highest variability in cyclone numbers, but correlation-based PCA more effectively locates the primary storm tracks.

4.3.2 Unrotated versus rotated PCA

Standard unrotated PCA may pose problems when attempting a physical interpretation. While the first PC is solely determined by the direction of the maximum variation in the data and subsequent PCs are by definition orthogonal and thus uncorrelated (as discussed above), its interpretation as independent mode is limited, as underlying physical processes may not be independent. Therefore, although the first PC may represent an important mode of variability or physical process, it may also include aspects of other processes and thus mix several distinct processes together (Wilks 2005).

Regardless of the procedure selected for the rotation of the PCs, it aims to seek a result called simple structure. That means, the loadings vector of a correlation-based PCA only contains values near zero or near 1, i.e. a PC optimally represents a set of original variables but leaves the representation of other variables to other PCs. In other words, variables are grouped such that they are highly correlated with a particular PC, but uncorrelated with other PCs.

A widely used rotation procedure is the Varimax rotation. The extracted PCs are orthogonally rotated such that the sum of variances ${s_i}^2$ of the squared loadings of 1..k rotated PCs

$$\sum_{i=1}^{k} {s_i}^2 \tag{4.4}$$

is maximized (Bahrenberg et al. 1992).

In this work, two PCA variants are used. On the one hand, unrotated covariance-based PCA is applied to identify the main modes of SST variability (Chapter 2) and therefore regions of maximum variance. That way, results comparable to those in literature are produced. On the other hand, for a better physical interpretation, rotated correlation-based PCA is used to locate regions of joint variability in the southern Atlantic Ocean (Section 5.2) without a specific focus on the maximum of a field but on groups containing highly correlated variables.

4.4 SANDRA cluster analysis

Cluster analysis or clustering is used to group a sample of objects (e.g. monthly SST patterns) to homogeneous clusters comprising those objects with highest similarity while the resulting groups are heterogeneous, i.e. dissimilar to each other. Each group or class can be represented by its mean, referred to as cluster centroid.

Cluster analysis is not a specific algorithm but the task described above. A range of different procedures involving various algorithms exists that are summarized under the term cluster analysis. These procedures can be mainly distinguished with respect to two aspects: the selection of (1) the proximity measure (measure for similarity or dissimilarity) and (2) the clustering algorithm. That is, clustering always starts with the choice of an appropriate proximity measure and clustering algorithm. Furthermore the number of clusters has to be chosen. An overview of different algorithms and proximity measures is given in Backhaus et al. (2011).

A common distance measure (e.g. Philipp et al. 2007) is the within-cluster sum of squares of deviations (WSS) with

$$WSS = \sum_{j=1}^{k} \sum_{i \in C_j} D(X_i, \bar{X}_j)^2 \tag{4.5}$$

where k denotes the number of clusters C, i the object number and $\bar{X}$ the cluster centroid. The Euclidean Distance D between the objects assigned to a cluster and its corresponding cluster centroid is defined as

$$D(X_i, \bar{X}_j) = \sqrt{\sum_{l=1}^{m} (X_{il} - \bar{X}_{jl})^2} \tag{4.6}$$

where m denotes the number of elements of each object (e.g. grid points of the SST patterns in this work).

For the comparison of different clustering solutions and thus an evaluation of their quality, the explained cluster variance (EV) is useful, which is defined as

$$EV = 1 - \frac{WSS}{TSS} \tag{4.7}$$

where the TSS (total sum of squares) is computed as the sum of all squared Euclidean Distances between all objects and the overall centroid. In this work, the EV and several other evaluation metrics are used, including the Pseudo-F statistic, within-type standard deviation, confidence interval of the mean, pattern correlation ratio and the Silhouette index. For a detailed description of those please see Beck and Philipp (2010).

For the clustering algorithm, a non-hierarchical clustering approach called *simulated annealing and diversified randomization (SANDRA)* is applied in this thesis. In order to reduce the probability to step into a local optimum during the iterative optimization process in cluster analysis, two optimization approaches are combined in *SANDRA*: Instead of using unchanged seed partitions, cluster analysis is run multiple times using different

randomly created seed partitions (*multistart technique*) and selecting the best solution in terms of EV. Furthermore, *diversified randomization* also randomizes the ordering of objects and cluster numbers throughout the iterative process in which clusters are evaluated and objects are reassigned. In addition, the *simulated annealing* technique, which simulates the process of a slowed down tempering by reheating of particles in a melt pot, is transferred to the objects in cluster analysis. Unlike in other clustering techniques, objects are not irreversibly assigned to a cluster, but may leave it at any stage even when increasing at first the cost function (distance measure WSS). This way *SANDRA* seeks to approximate a global optimum.

The number of clusters is determined based on an evaluation of several solutions with different numbers using the evaluation metrics described above. An additional tool for the determination of an appropriate cluster number is the application of a t-mode PCA (if spatial patterns are to be clustered) to the data set (Philipp et al. 2007). The number of PCs selected according to the dominance criterion can be used as an indicator for an optimal cluster number.

4.5 Canonical correlation analysis (CCA)

Canonical correlation analysis (CCA) is a multivariate statistical technique that is used to describe the relationship between two multivariate data sets. For example, it can be used to link large-scale atmospheric or oceanic patterns such as SST and regional precipitation fields, as is the case in this thesis.

CCA identifies a sequence of pairs of patterns in the two data sets and constructs corresponding transformed variables, termed canonical variates. The canonical variates are computed by projecting the original data onto the patterns. CCA is somewhat similar to PCA, but unlike the latter, CCA searches for patterns in two multivariate datasets instead of one. Furthermore, the aim of CCA is not to find patterns that represent maximum amount of variation in the data sets as is the case in PCA. Instead, the pairs of patterns are chosen such that the canonical variates exhibit maximum correlation between them but are uncorrelated with any of the other identified variates. In other words, CCA aims to maximize the interrelationship between two data sets.

The Pearson correlation coefficient between a pair of canonical variates is termed the canonical correlation coefficient r_C. It is a measure for the quality of the relationship between the two canonical variates of a pair. The number of significant canonical correlations is determined using Rao's F-test (Rao 1973, cited in Hertig 2004).

The canonical loading patterns (thereafter referred to as CCP) include, mathematically speaking, the correlation coefficients between the original data and the canonical variates. That is, they represent the relationship between original and transformed data. Therefore, high positive or negative loadings in a pair of CCP maps can also be interpreted as positive or negative coupling of the two corresponding variables.

The canonical variates, the corresponding time scores, can be interpreted in terms of the polarity and strength or importance of the patterns. That is, for positive score values,

the corresponding pattern is in its positive mode and positive loadings are representative for positive (e.g. SST or precipitation) field anomalies. For more details including a mathematical description see e.g. von Storch and Zwiers (1999) and Wilks (2005).

In this work, CCA is not applied to the fully resolved SST and precipitation fields, but to PCs extracted from these fields. As highly intercorrelated data fields may have unwanted effects on the computation of CCA and interpretation of results, Barnett and Preisendorfer (1987) suggest to combine CCA with PCA. A prefiltering and orthogonalizing using PCA reduces noise in the data and helps to find more stable results.

Application of CCA assumes stochastic independence and normal distribution. This is tested following the procedure already described in Section 4.1.2. Not all of the data meet these conditions. This is accepted as CCA is mainly used as additional tool and results are compared with analyses based on other techniques.

4.6 Time series analyses

Any time series has certain, often combined, characteristics such as a trend, cyclical features (e.g. determined by the annual cycle) or a stochastic component (noise). The detection and description of such behavior and the separation of superimposed signals are important for the understanding of atmospheric processes and for forecasting future events or long-term developments. A general overview of time series analysis and the techniques available is given in von Storch and Zwiers (1999), Wilks (2005).

To learn more about the characteristics of the index time series used in this work, such as the Atlantic Niño indices (see Chapter 5) and the teleconnection indices (see Chapter 7), three techniques in time series analyses for the time and frequency domain including autocorrelation, spectral analysis and wavelet analysis are applied. Note that no trend analyses were performed except in pre-analyses, as trends were explicitly removed by high-pass filtering (see Section 3.5).

Autocorrelation: Autocorrelation is the cross-correlation of a time series with itself. The autocorrelation coefficient r_A for subsequent time lags τ can be represented by the autocorrelation function $r_A(\tau)$. Beyond the use for the test for data independence (e.g. prior to correlation analyses, see Section 4.1), the autocorrelation function can further be used for the detection of persistent signals or also repeating patterns. If, in the first case, $r_A(\tau)$ declines rather slowly, the time series contains a signal with a certain persistency, i.e. it serves as a *memory*. For the second case, $r_A(\tau)$ shows some oscillatory behavior, i.e. alternately turning negative and positive, this may indicate a cyclical feature of a time series. Such a cyclical signal can then further be explored in spectral analysis (e.g. Schönwiese 2013).

Spectral Analysis: Spectral analysis is a tool to analyze recurring signals by detecting frequencies and corresponding periodicities in a time series. For that purpose the time series can be transformed to a function of frequency f, $S(f)$ which is called the power

spectrum or spectral density. Using Fourier analysis, each time series can be represented by an infinite series of sine and cosine functions. The transformation to the spectral representation is termed Fourier transform, accordingly. In the ideal case of a purely periodic process, a time series' spectrum would only contain a single line while a very irregular process produces a rather smooth and continuous spectrum.

For a more detailed description of spectral analysis see Ghil (2002), Wilks (2005) and Schönwiese (2013). In this work, the so-called Multitaper Method (e.g. Ghil 2002) was selected for the spectral estimation.

In the graphical representation the x-axis displays the period in months and the y-axis the energy (percentage of variance).

Wavelet Analysis: Wavelet analysis allows the analysis of a time series in both time and frequency domain. While spectral analysis only detects frequencies in a time series, wavelet analysis can also analyze how such frequencies, i.e. dominant modes of variability, vary in time. Unlike sine and cosine functions in Fourier transform, local base functions, termed wavelets, are used in Wavelet transform. These wavelets have flexible windows that can be stretched and translated in both frequency and time. For a more detailed description of the mathematical background see e.g. Lau and Weng (1995), Torrence and Compo (1998) and Mélice and Servain (2003)

Results for wavelet analysis are displayed in contour plots, where time is depicted on the x-axis and the period on the y-axis.

5

Classification of warm and cold water events in the tropical southeast Atlantic

For an analysis of warm and cold water events in the tropical southeast Atlantic and their impact on regional and global scales, a solid definition of such events is necessary first. This chapter explains how these events are defined, categorized and characterized. After an introduction into related work in Section 5.1, tropical southeast Atlantic variability is discussed in more detail in Section 5.2. In Section 5.3 three new Atlantic Niño regions are defined and further analyzed in Section 5.4. The definition and classification of warm and cold events is explained in Section 5.5. The newly defined Atlantic Niño and Niña events are then further characterized in Section 5.6, and Section 5.7 discusses influences contributing to their evolution.

Parts of the work described in this chapter have been published in Lutz et al. (2013). Results presented in that paper have been updated to the period 1870-2012.

5.1 Introduction

The tropical southeast Atlantic exhibits high interannual sea surface temperature anomalies, which show some similarity to those observed in the Pacific Ocean during El Niño, although weaker and less frequent (e.g. Zebiak 1993, Carton and Huang 1994). Warming in the southeast Atlantic has been discussed as the positive expression of a coupled ocean-atmosphere mode which is associated with weakened trade winds, less intense upwelling in the Benguela system, a deepened thermocline and an increase in sea level height. Similar to the Pacific, the positive Bjerknes feedback contributes to the evolution of Atlantic SST anomalies, although it is weaker and mainly active in boreal spring and summer months (Keenlyside and Latif 2007). Nevertheless, all three elements of the feedback mechanism also exist in the equatorial Atlantic: the coupling between (1) eastern

Atlantic SSTs and western Atlantic zonal winds, (2) western Atlantic winds and upper-ocean heat content in the east as well as (3) heat content and SSTs in the east.

However, in contrast to the Pacific, two Niño-like phenomena instead of one have been described for the Atlantic Ocean. One of the two, termed *Atlantic Niño*, is centered in the equatorial region and described as part of the Atlantic zonal mode (Merle 1980, Philander 1986, Zebiak 1993). It peaks in boreal summer when the ITCZ reaches its northernmost position. The other one is referred to as *Benguela Niño* (Shannon et al. 1986, Shannon and Nelson 1996) and peaks in spring. It appears off the coast of northern Namibia and Angola, near where the *Angola-Benguela frontal zone* (ABFZ, Meeuwis and Lutjeharms 1990) divides the cooler waters in the Benguela upwelling system from the warmer waters of the Angola Current. In addition to these two separately described phenomena, Okumura and Xie (2006) discuss SST anomalies in November and December in the equatorial Atlantic in terms of an *Atlantic Niño II*. Furthermore, Nnamchi et al. (2011) describe the Atlantic Niño as part of a *South Atlantic Ocean Dipole* (SAOD) with opposite SST anomalies in the Atlantic Niño sector and the southwest Atlantic off the southern South American coast.

Although Atlantic SST anomalies are less frequent, shorter and less intense compared to their Pacific counterparts, they have striking effects on regional rainfall (e.g. Rouault et al. 2003, Reason and Rouault 2006) and the local ecosystem. Heymans et al. (2004) report reduced plankton production and a decreased seal population due to high pelagic fish mortality during Benguela Niños. Fish mortality also involves sardines and anchovies and therefore further affects the fisheries.

Multiple causes and influences contribute to the development of warm and cold events. A recent discussion and summary of involved processes are provided by Lübbecke (2013) and Richter et al. (2013).

In *canonical events*, as they are termed by Richter et al. (2013), ENSO-like dynamics including the Bjerknes feedback are involved. A weakening of the southeasterly trade winds in the western equatorial Atlantic excite Kelvin waves, which deepen the thermocline and outcrop in the *Angola Benguela Area* (ABA). This leads to reduced upwelling in the eastern equatorial Atlantic and thus causes a warming of the cold tongue region (e.g. Zebiak 1993, Keenlyside and Latif 2007, Lübbecke et al. 2010). This canonical evolution is phase-locked to the seasonal cycle: equatorial wind variability and SST variability in the ABA region peak in boreal spring months March–May, whereas SST variability in the equatorial region peaks in boreal summer months June–August.

Furthermore, Okumura and Xie (2006) describe a cooling in November and December, resulting from a secondary peak in equatorial wind and SST variability. They name a warm event appearing in this season an Atlantic Niño II to distinguish it from the Atlantic Niño that peaks in boreal summer. Although the Atlantic Niño II follows the same canonical evolution involving easterly wind anomalies, a shoaling of the thermocline and the Bjerknes feedback, the authors also report important differences between those two types. Neither the seasonal cooling in November-December nor an anomalous warming or cooling extends all the way to the west African coast. Furthermore, the authors em-

phasize that the Atlantic Niño II is not a simple extension of the summertime Niño, as in some years they appear to be a recurrence of the latter, but in others they are not.

In addition to the canonical events, Richter et al. (2013) describe *non-canonical events*, which cannot be explained by ENSO-like dynamics. For the latter events they propose a mechanism involving meridional and zonal temperature advection from the *north tropical Atlantic* (NTA). As non-canonical warm events are preceded by easterly wind anomalies, one would expect a cooling in the tropical southeast Atlantic. But this cooling is opposed by horizontal advection of warm water from the anomalously warm NTA. The NTA warming is due to reduced surface latent heat flux and near-surface winds, which are characteristic of the meridional mode described in Section 2.1. Thus, the latter seems to play an important role for the development of non-canonical events, although a NTA warming is not always followed by such an event. Other factors such as the preconditions in the equatorial Atlantic and possibly remote influences from the equatorial Pacific may play a role. Despite the suggested link between the meridional mode and the non-canonical events, Richter et al. (2013) emphasize that these two are separate phenomena.

Lübbecke and McPhaden (2012) and Lübbecke (2013) suggest an alternative pathway for the influence of the NTA. According to those authors, an altered wind pattern during a NTA warming associated with the meridional mode or caused by a Pacific El Niño generates off-equatorial westward propagating warming Rossby waves and eastward propagating cooling Kelvin waves. The Rossby waves are then reflected into eastward propagating warming Kelvin waves. As a result, first cooling and then warming is observed in the tropical southeast Atlantic. The two competing cooling and warming Kelvin wave types are also discussed in terms of a delayed negative feedback to El Niño, which may be more or less dominant, and thus either an Atlantic Niño or an Atlantic Niña is caused.

Similarly, the wind forcing is still controversially discussed in terms of a *remote* and *local* forcing. Most authors attribute a warming in the southeast Atlantic to the remote influence from western equatorial wind anomalies (e.g. Servain et al. 1982, Delecluse et al. 1994, Florenchie et al. 2003, Rouault et al. 2007), although altered local wind regimes may also modulate the events (Florenchie et al. 2004). As described above, western equatorial zonal wind anomalies trigger Kelvin waves that propagate to the east thereby deepening the thermocline, and outcrop in the ABA causing reduced upwelling. This mechanism is referred to as *remote forcing*. By contrast, Polo et al. (2008) report that Kelvin waves might not reach as far as the ABA and suggest instead, that anomalous local alongshore wind stress over the Angola Benguela upwelling region cause the SST anomalies. Due to the locally observed wind stress anomalies, this forcing is also discussed in terms of a *local forcing*. Richter et al. (2010) further endorse the importance of alongshore wind anomalies and associated reduced upwelling, which they partly attribute to a weakening of the South Atlantic high. Furthermore, they suggest that a basin-scale weakening of the anticyclone causes wind stress anomalies in both the equatorial and coastal southeast Atlantic. Thus, both remote and local forcings are simultaneously active and contribute to the evolution of SST anomalies in the corresponding region. That means that the two Niño types develop due to different forcings (remote and local), but nearly at the

same time, which explains the high correlation between Atlantic and Benguela Niños. Lübbecke et al. (2010) also emphasize the role of the South Atlantic anticyclone and associated variability of the southeasterly trade winds although some of these authors emphasize the influence of the anticyclone on the equatorial region and thus support the remote forcing for both regions in the latter and in more recent papers (as already described above, Lübbecke and McPhaden 2012, Lübbecke 2013).

A list of warm and cold events in the equatorial and/or coastal southeast Atlantic can be collected from the literature. Strong and therefore well-studied Benguela Niños have been described for the years 1934, 1949, 1963, 1984 (Shannon et al. 1986), 1995 (Gammelsrød et al. 1998) and 2001 (Rouault et al. 2007). Strong cold events developed in 1978, 1982, 1983, 1991/92, 1997 and 2004 (Florenchie et al. 2004, Reason et al. 2006). A moderate but persistent warm episode is described during 1972–1975 and a cold period in 1969–1971 (Walker 1987). Less intense warm events occurred in 1986, 1988, 1991, 1996, 1997/98 and cold events in 1969, 1982/83 (Carton and Huang 1994, Boyd et al. 1987, Reason et al. 2006). According to Florenchie et al. (2004), many events peak in boreal spring following the seasonality in the interannual SST variability, although some of them reach a maximum of intensity in boreal summer months. For the equatorial Atlantic, Wang (2002) describes 11 Atlantic Niños during the 50-year period 1950 – 1999, including 1963, 1968, 1973, 1981, 1984, 1987, 1988, 1995, 1996, 1998, 1999. Eight of the latter events peak in boreal summer but three peak in boreal winter. Furthermore, boreal winter warm events (Atlantic Niño II) are described for 1987, 1993, 1997 and 2003 while cold events occurred in 1986, 1991, 1996 and 2001 (Okumura and Xie 2006).

Duration of the events varies from a few months to half a year or more, recurring every 3–5 years. Florenchie et al. (2004) also mention that on average, cold events seem to last longer than warm ones.

Despite the description of similar mechanisms behind the events, such as the equatorial west Atlantic wind forcing and Kelvin wave propagation, Atlantic and Benguela Niños have long been analyzed in separate studies and regarded as independent events. But a few recent studies describe a strong relation between SST variability off the Angolan coast and the equatorial Atlantic (e.g. Reason et al. 2006, Huang 2004). Lübbecke et al. (2010) further suggest that both Niños should be perceived as one phenomenon as they are highly correlated. However, recent studies maintain a separate Benguela Niño (e.g. Rouault 2012).

Thus, several questions arise from the previous studies described above:

- When discovering anomalous warming or cooling in the tropical southeast Atlantic, do these SST anomalies belong to a Benguela or an Atlantic Niño or Niña?
- Is there a connection between the two phenomena or might they even be part of one Niño type?
- And which type or phenomenon should any subsequent analyses be based on, such as the study of an impact on regional precipitation and teleconnections to remote regions?

To assess the question whether the two Niño phenomena Atlantic and Benguela Niño are connected, a new robust definition of warm and cold water events in the tropical southeast Atlantic is needed. Therefore, it is necessary to find suitable patterns or regions and corresponding indices that represent the SST variability of the whole region and not just the coastal or equatorial part. The newly defined indices can then be further used in the definition of warm and cold events.

In this work, two main approaches are considered for the construction of the required SST indices: (1) the extraction of representative PCA patterns and the use of their corresponding time scores as indices (Section 5.2), and (2) the definition of distinct regions based on the SST standard deviation and their application to spatially averaged region indices (Section 5.3).

5.2 Patterns of south tropical Atlantic SST variability

For the first approach, s-mode principal component analyses are carried out for annual as well as monthly and seasonally averaged high-pass filtered time series. In contrast to Chapter 2, rotated PCA is applied. Here, our focus lies on regions with a maximum of shared variability and not on an overall maximum within the field.

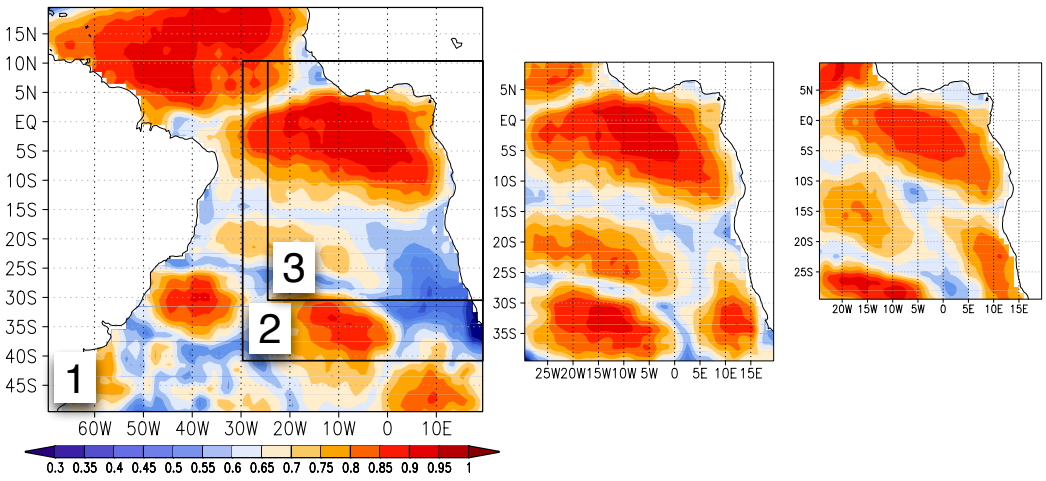

Figure 5.1: Centers of variation of the SST PCs for the month of March 1870–2012. Rotated PCAs are carried out for different domain sizes, from left to right: domain 1 (70°W - 20°E, 20°N - 50°S), 2 (30°W - 20°E, 10°N - 40°S) und 3 (25°W - 20°E, 10°N - 30°S).

Different domain sizes are examined in order to separate equatorial variability from that off the Angolan coast. Figure 5.1 depicts the SST PC patterns for the example of March. Despite a stepwise reduction in domain size, there is only one pattern extracted in the tropical southeast Atlantic, which covers both regions. This pattern resembles the first PC extracted from unrotated PCA described in Section 2.1, although the center of maximum loadings is located closer to the equator. This difference is due to the rotation of the PCs. Other PC patterns extracted are located too far south to be relevant for consideration, i.e. in the central south Atlantic or in the Benguela Current south of the ABFZ.

Similar results as for March are obtained for all other months. Thus, PCA is unable to separate equatorial and coastal variability but extracts a single pattern representing tropical southeast Atlantic SST variability. Although the position and extension of the center of variation of the pattern varies across different seasons, the principal pattern remains similar. To illustrate this, Figure 5.2 depicts examples of the centers of variation for the months of January, April, July and October. In boreal autumn and winter the PC 1 pattern, referred to as tropical southeast Atlantic pattern thereafter, is centered furthest north in the equatorial Atlantic. The pattern has its largest extent in spring and reaches furthest south along the west African coast in July with its maximum loadings also located further southeast.

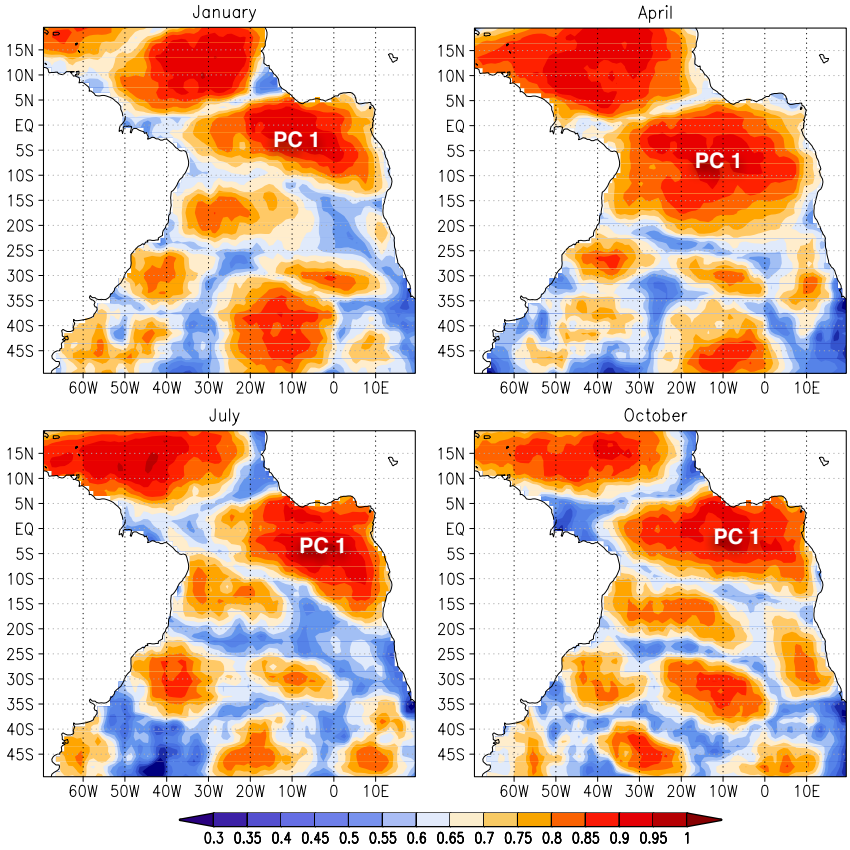

Figure 5.2: Centers of variations extracted from rotated PCA of monthly mean SST data for the south Atlantic domain: examples for January, April, July and October 1870–2012. The first PC (PC 1) always depicts the tropical southeast Atlantic pattern.

Furthermore, only part of the equatorial Atlantic and Benguela Niños and Niñas listed in Section 5.1 are found in the monthly PC scores (not shown) of the tropical southeast Atlantic pattern. This is not surprising as the PC only represents part of the variability and thus smaller events that are limited to the equatorial or the coastal region may not be captured. Therefore, an index based on a PC score is not suitable for the detailed study of warm and cold events in the southeast Atlantic, which potentially differ in their regional character.

Although the PCA approach does not provide an adequate solution for a pattern or region definition that separates equatorial and coastal SST variability, it is still worth having a closer look at this very prominent pattern in the southeast Atlantic. Therefore, an approach applied by Hertig and Jacobeit (2010) to determine large-scale SST regimes is modified for the description of the SST patterns in the south Atlantic between 20°N and 50°S. The modified procedure consists of the following steps:

1. Rotated s-mode PCA is applied to all 144 overlapping 1-month to 12-months seasonal sections. The number of PCs is selected according to the dominance criterion.

2. All patterns (PC loadings) of all seasonal sections are then joined together and clustered using SANDRA cluster analysis (see Section 4.4). Note that here, clustering is preferred to the PCA approach applied in Hertig and Jacobeit (2010) as it simplifies the procedure and by definition provides a classification of patterns. In this step, each PC loading pattern is assigned to a distinct cluster, which is represented by its cluster centroid.

3. To select an optimal number of clusters from several clustering solutions, different evaluation metrics (see Beck and Philipp 2010) are applied (see Figure 5.3). An additional criterion is the selection of the number of PCs of a t-mode PCA according to the dominance criterion (see Section 4.3), 9 PCs in this case. Most criteria point to an optimal solution of 10 clusters. Centroids are finally calculated for each cluster and displayed in Figure 5.4.

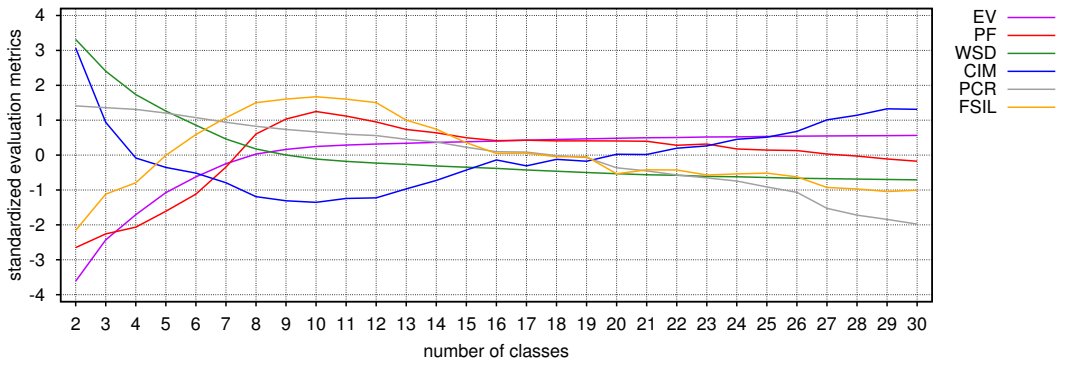

Figure 5.3: Comparison of different SST PCA pattern clustering solutions with a number of 2 to 30 clusters. Evaluation metrics include explained variance (EV), Pseudo-F statistic (PF), within-type standard deviation (WSD), confidence interval of the mean (CIM), pattern correlation ratio (PCR) and the Silhouette index (FSIL). All evaluation metrics are standardized. For a description of the different evaluation metrics see Beck and Philipp (2010).

4. To analyze the temporal persistence of each (centroid) pattern, the scores of those PCs of consecutive sub-periods that are members of the same cluster, are correlated with each other (Figure 5.4).

Following the steps described above, 10 centroid patterns are obtained for the south Atlantic domain. Figure 5.4 displays the 10 centroid patterns and corresponding results

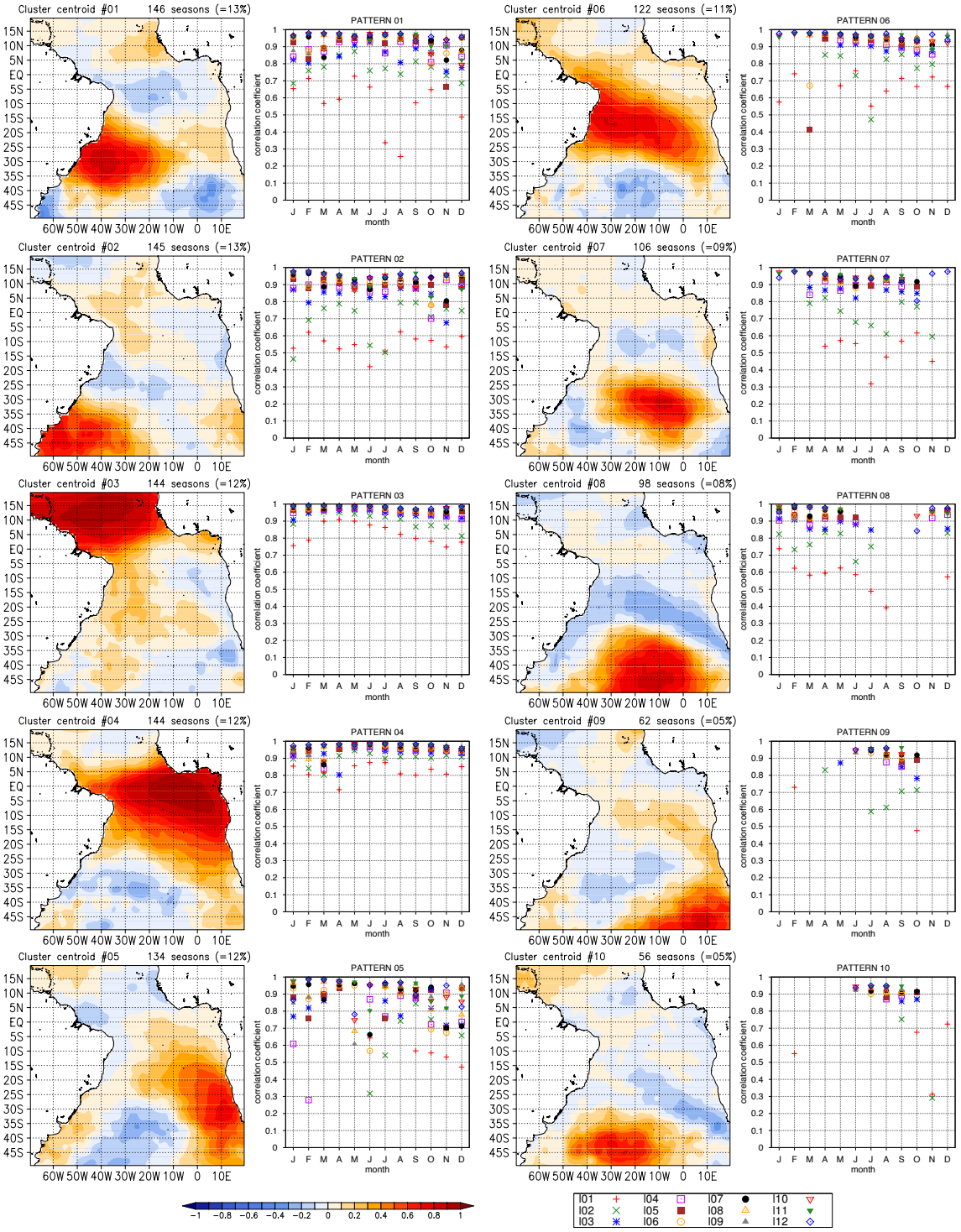

Figure 5.4: Centroid patterns derived from the clustering of SST PC loadings (contour plots, left). Correlation coefficients (right) between the corresponding PC time coefficients from consecutive 1- to 12-month seasonal sections (l01-l12 in legend). Clusters are ordered by highest to lowest number of seasonal sections in each cluster.

from correlation analysis of consecutive PC score sub-periods. In addition, Figure 5.5 shows the seasonal occurrences of the 10 patterns.

One can easily recognize pattern 4 as the tropical southeast Atlantic pattern that has already been described above. This pattern can appear in all seasons (and thus in all 144

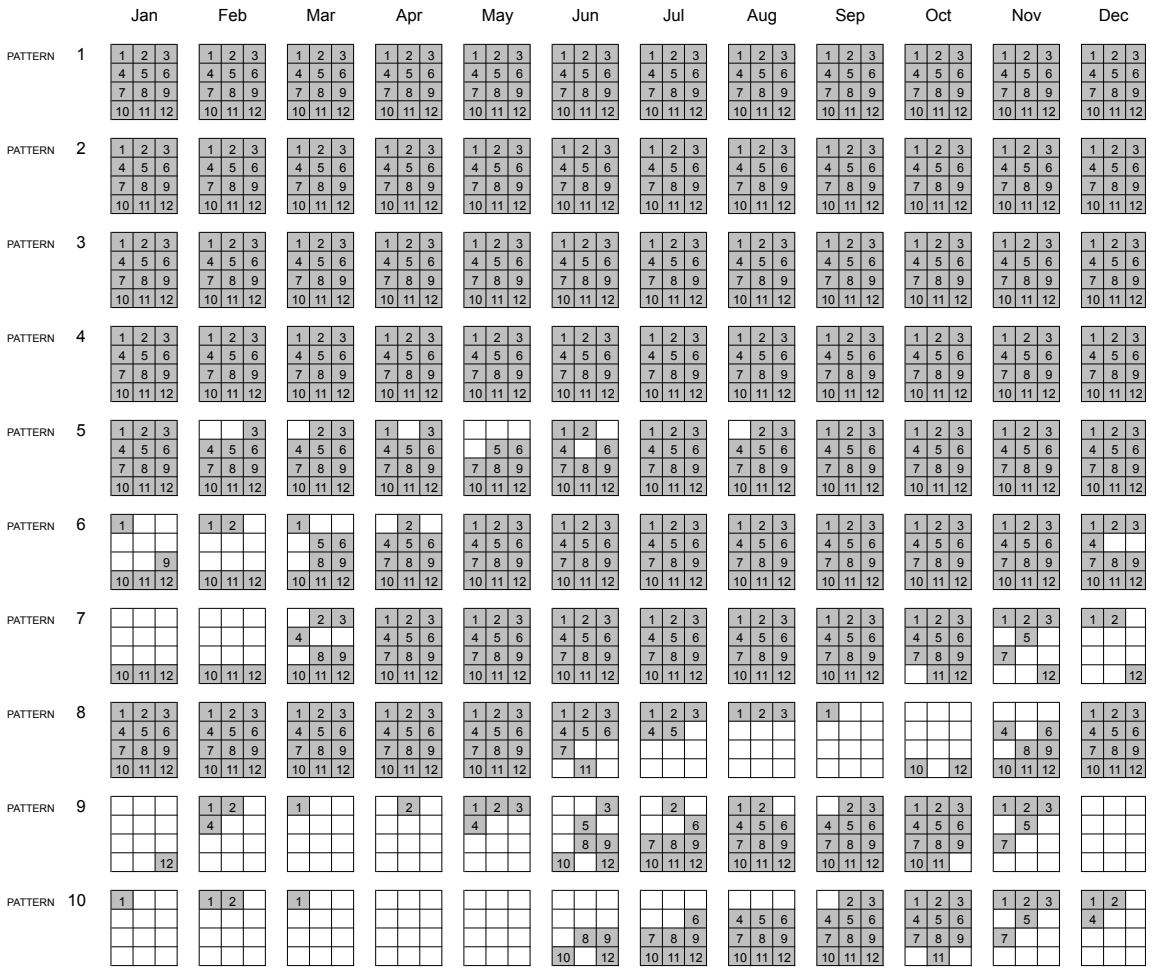

Figure 5.5: Occurrence of pattern 1 to 10 (rows) for the 1- to 12-month seasonal sections (numbers in cells). The column title indicates the central month of a seasonal section. For example, the first row of pattern 1 Jan contains J, JF, DJF. See corresponding centroid patterns in Figure 5.4.

seasonal sections, as seen in Figure 5.5) and shows a remarkable temporal persistence throughout the year. A small drop of the correlation coefficient is observed in spring. The spring season is the season with maximum SST variability in the tropical southeast Atlantic and also the season where some of the events peak while summer events just start.

A second remarkably persistent pattern is present in the tropical north Atlantic. Like the southeast Atlantic pattern, it can occur in all 144 seasonal sections (Figure 5.5). As described in Section 2.1, several studies (e.g. Ruiz-Barradas et al. 2000) have described tropical north Atlantic variability as part of a meridional dipole mode, while others (e.g. Houghton and Tourre 1992, Dommenget and Latif 2000) find an independent mode, which is uncorrelated with south tropical Atlantic variability. Here, using rotated PCA (in contrast to unrotated in Section 2.1), an independent mode is found instead of a dipole pattern, as described in the latter papers.

To investigate a possible connection between the tropical Atlantic north and south of the equator, simple indices are constructed for the tropical north (NATL index, $5° - 20°$N and $60° - 30°$W) and south Atlantic (SATL index, $0° - 20°$S and $30°$W$-10°$E) and used in cross-correlation analyses. Significant correlations (at the 95% level) are found for time

lags between -2 (NATL leading) and 0 in boreal winter months NDJ (months for SATL), but these do not reach magnitudes greater than 0.36 and thus only represent a weak link.

Two main conclusion can be drawn from the analyses described above: First, a separation of the tropical southeast Atlantic into regions representative for the equatorial Atlantic and the Benguela Niño cannot be achieved by the application of PCA. This also indicates that the equatorial and the coastal region share a great portion of variability and the two Niño types may not be independent or at least co-occur at certain times. Second, the SST pattern in the tropical southeast Atlantic Ocean derived by PCA and subsequent SANDRA cluster analysis appears to be a relatively dominant pattern that can occur in any of the seasons and also shows temporal persistence over several months. This may point to the fact that warm and cold water events can appear at any time of the year and also possibly last several months or even a whole year.

5.3 Definition of Atlantic Niño regions und corresponding indices

As the PCA approach is unable to separate equatorial and coastal Atlantic variability, the second approach explored in this work is the manual definition of SST regions. So far several different regions have been used in literature. Regions defined in the equatorial Atlantic are for example ATL3 (3°N−3°S and 20° − 0°W, Zebiak 1993) and CTA (3°N−3°S and 15°−W0°E, Reason et al. 2006). The latter was also used under different names, e.g. as central equatorial Atlantic index (Okumura and Xie 2006) and as ACT1 (Richter et al. 2013). A region extending further south is the Atlantic cold tongue region (ACT, 2°N−6°S and 20° − 0°W, Ding et al. 2012). Off the coast of Angola the Angola Benguela Area (ABA, Florenchie et al. 2003) is defined for 3°N−3°S and 15°W-0°E. Thus, the previously defined regions vary in latitudinal and longitudinal position and their extension. As a result the corresponding indices (Figure 5.6) show a similar temporal evolution but also expected differences. Therefore, a simple adoption of previously defined regions and corresponding indices is not possible.

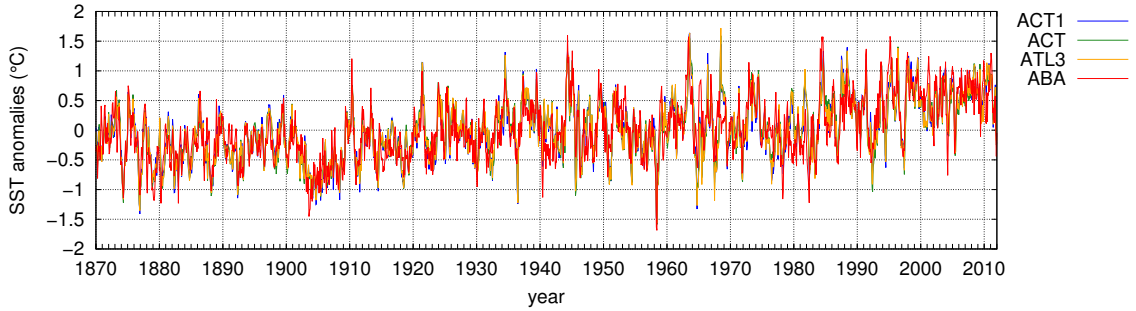

Figure 5.6: Examples of tropical southeast Atlantic SST anomaly indices for index regions used in the literature: ATL3 (3°N−3°S and 20° − 0°W, Zebiak 1993), ACT1 (3°N−3°S and 15°W-0°E, Richter et al. 2013), Atlantic cold tongue region (ACT, 2°N−6°S and 20° − 0°W, Ding et al. 2012) and Angola Benguela Area (ABA, 3°N−3°S and 15°W-0°E, Florenchie et al. 2003)

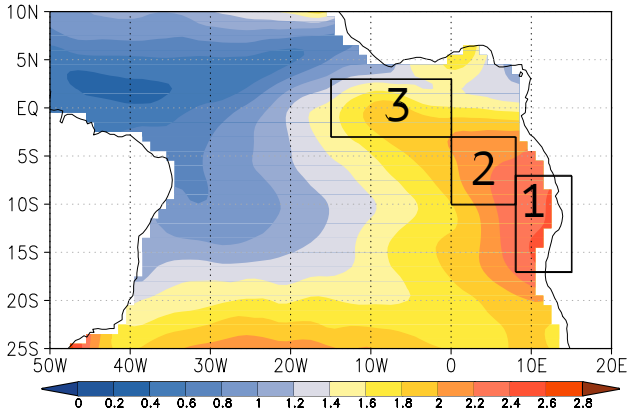

Figure 5.7:
Standard deviation of SST anomalies for the period 1870–2011 (°C) and Atlantic Niño regions ATLN1, ATLN2 and ATLN3.

There are several principal ways to define new regions. In any case, they should fulfill the following criteria:

- The regions should cover the whole area affected by known warm and cold water events, i.e. the equatorial region, the Angolan coast and also the area in between.
- The regions should be located within the area of highest southeast Atlantic SST variability.

To estimate the area generally affected by warm and cold events, composite analyses are carried out (1) for known warm events and (2) based on an index threshold. For the latter composites, those months are selected as event months, for which a normalized high-pass filtered ABA index exceeds one standard deviation. These pre-analyses again confirm the findings above, that the temperature anomaly may affect a greater area including both equatorial and coastal regions.

The two kinds of composites above were first considered as basis for a region definition, but the idea had to be dismissed as the selection of events for a composite would be already biased. That is, composites based on known events may omit yet undiscovered and undescribed events. Furthermore, an index-based selection again only includes one index of one region.

Therefore, a different approach is chosen. As in Florenchie et al. (2004), the standard deviation is used to identify regions of similar SST variability in the tropical Atlantic between 10°N and 25°S. As can be seen in Figure 5.7, a large area of high variability reaches from the southwest African coast far into the equatorial Atlantic. The area with highest variability, located off the coast of Angola and northern Namibia, is selected as Atlantic Niño (ATLN) region ATLN1 (corresponding to a northward moved ABA region). ATLN3 (resized ATL3) region represents equatorial Atlantic variability, and a third transition region ATLN2 is fit in between to finally cover the whole cold tongue area. The resulting three Atlantic Niño (ATLN) regions (rectangles in Figure 5.7) are defined as follows:

- ATLN 1: 17°S−7°S and 8°E−15°E
- ATLN 2: 10°S−3°S and 0°W−8°E
- ATLN 3: 3°S−3°N and 15°W−0°W

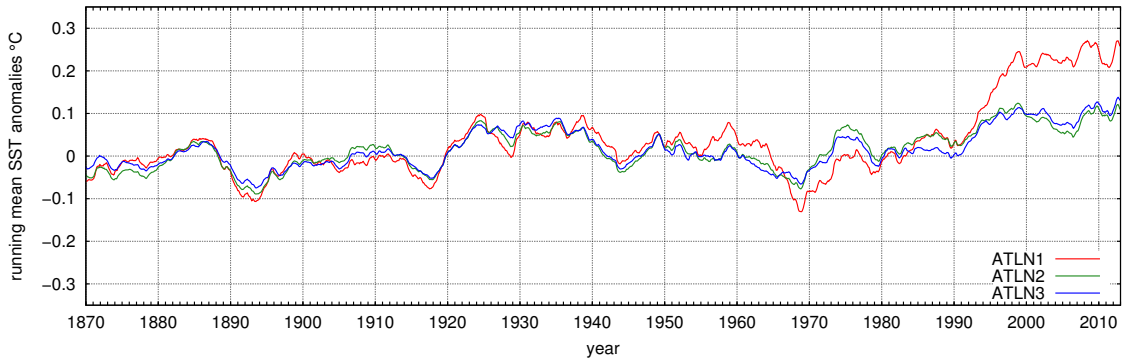

Figure 5.8: ATLN1–3 30-year running mean SST anomalies for the period 1870–2012.

Based on these newly defined regions, new suitable indices can now be computed. But before proceeding, for this step, further considerations in terms of low-frequency variability are necessary.

It has already been shown that there are substantial trends in the tropical southeast Atlantic SSTs (Rathmann 2009). Figure 5.8 depicts ATLN1–3 index anomalies, low-pass filtered using a 30-year running mean. Low-pass filtering reveals both decadal variations as well as a trend, which is most pronounced in ATLN1 in the last four decades. Consequently, in an index containing a positive trend, one would find mainly cold events at the beginning and mainly warm events at the end of the index time series. As trends in the three indices are not linear, a linear trend removal cannot be applied. On the other hand filtering techniques such as Gaussian high-pass filtering may eliminate frequencies that are still of interest in subsequent analyses.

Therefore, to remove trends and to compute robust indices, an approach is chosen that was used by NOAA CPC (2014) for the construction of the Oceanic Niño Index. Instead of one single reference period, multiple moving 30-year reference periods (termed base periods by NOAA CPC 2014) are used to calculate anomalies for successive 5-year periods. The latter are centered in their corresponding reference period. For example, to compute index anomaly values during 1976–1980, the 1961–1990 reference period is used. The most recent 30-year reference period (1981–2010) is used for the years from 1996 until now and may be updated when the next reference period 1986-2015 can be calculated. Average SST anomalies for all 23 30-year reference periods for the ATLN1 index are shown in Figure 5.9. An additional advantage of this procedure over common trend removal and filtering techniques is that most of the index period does not need to be recalculated when the time series is updated as all reference periods are kept.

Furthermore, SST variability varies spatially across the three indices. The decreasing standard deviation with larger distance to the Angolan coast seen in Figure 5.7 is, of course, also contained in the three indices. Therefore, to achieve comparable indices for all regions despite their different location and seasonal cycle, standardization is applied as a last step. As 1996–2000 is the last period which does not need to be recalculated, the reference period 1971–2000 is used to calculate the standard deviation.

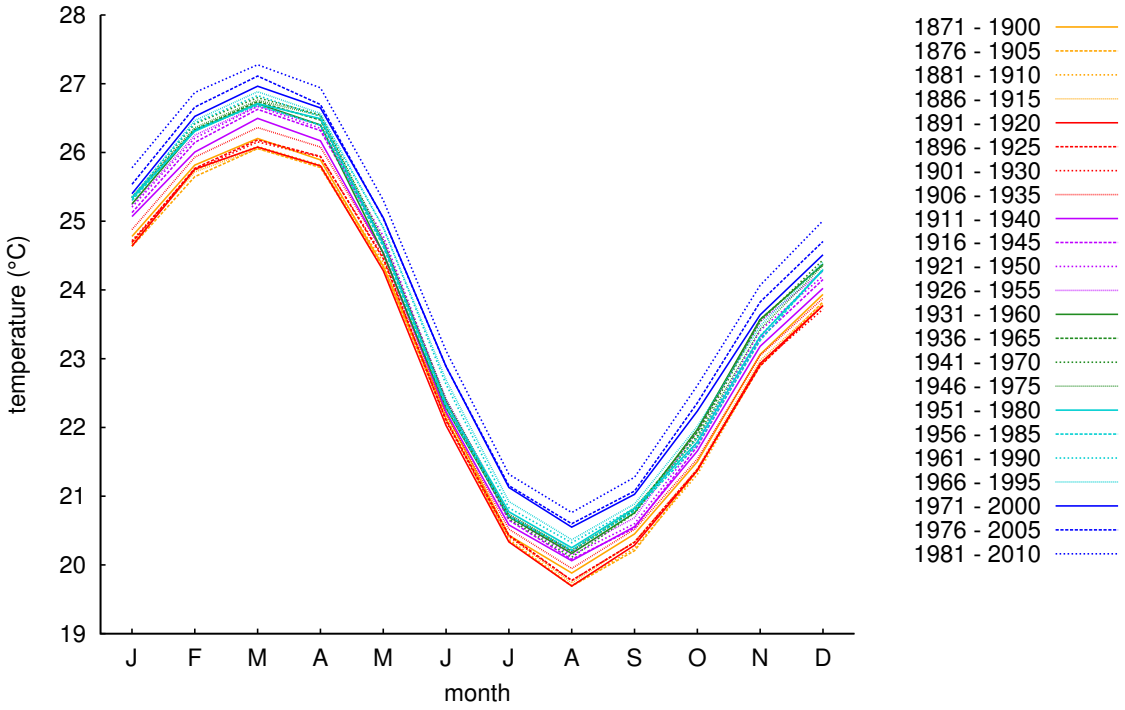

Figure 5.9: Average SSTs in the ATLN1 region for the 23 30-year reference periods between 1870 and 2012.

The steps described above to compute the three ATLN indices can be summarized as follows:

1. Average 1° x 1° SST anomalies for ATLN regions 1–3.
2. Calculate monthly SST anomalies with respect to 30-year reference periods updated every 5 years.
3. Standardize these anomalies using the standard deviation from the 1971–2000 period.

The resulting three indices are now comparable and can be used to define warm and cold events with respect to their contemporary climatology.

Figure 5.10 depicts the three Atlantic Niño indices ATLN 1–3. All three indices show a great resemblance in their time series for the whole study period 1870–2012. Well-studied warm events such as 1934, 1949, 1963, 1984 and 1995 (e.g. Shannon et al. 1986, Gammelsrød et al. 1998) and cold events such as 1982/83, 1997 and 2004 (e.g. Florenchie et al. 2004, Reason et al. 2006) can be identified in all three indices. For a list of more events see Section 5.1.

Cross-correlation as well as 30-year running correlation analysis for lag zero is performed for the ATLN indices (Figure 5.11). The striking similarity of the three indices is confirmed by their correlation coefficients: for lag zero, ATLN1 and 3 indices are significantly (99% level) correlated at 0.74, ATLN1 and 2 at 0.84, and ATLN2 and 3 at 0.91. Cross-correlation coefficients reach their peak at lag zero, although the ATLN3 region has a tendency to lag ATLN1.

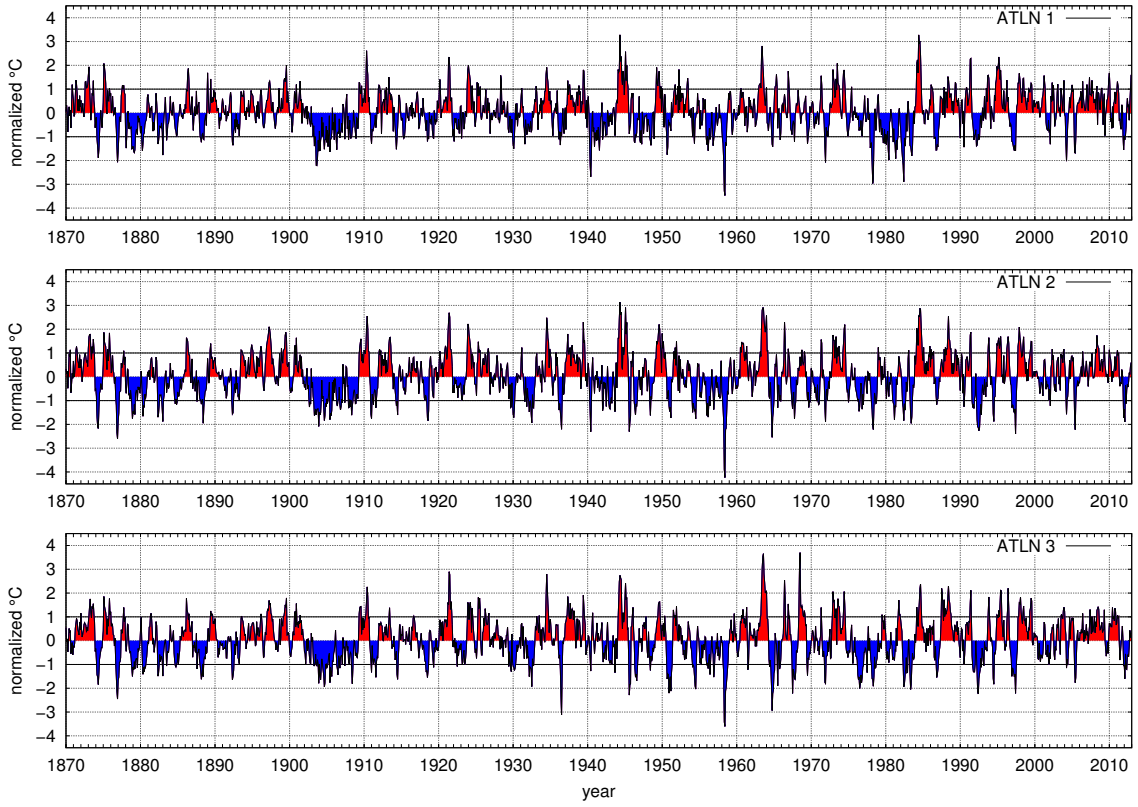

Figure 5.10: Atlantic Niño indices 1, 2 and 3 (top to bottom) calculated for the period 1870–2012.

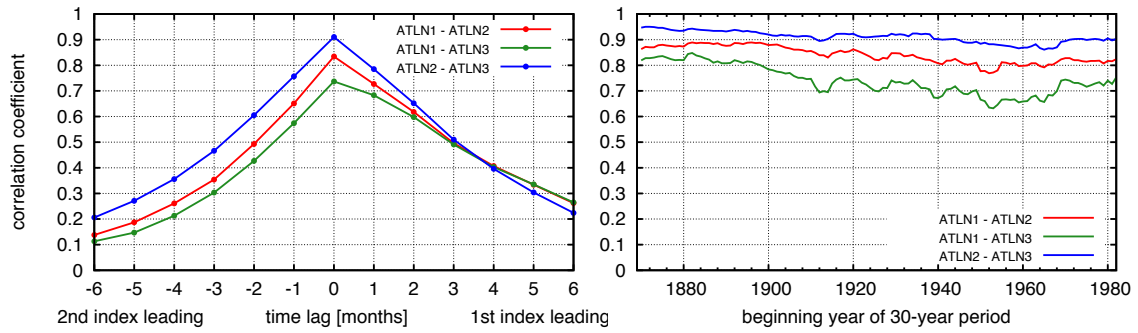

Figure 5.11: Cross-correlation (left) and 30-year running correlation (right) coefficients for ATLN 1 and 2 (red), ATLN 1 and 3 (green), ATLN 2 and 3 (blue), for the period 1870–2012. All values are significant at the 99% level.

Annual index correlation analyses are repeated with the more recent OISST data for the period 1981–2012. Results are consistent with the findings from HadISST data. All three indices are significantly correlated at comparable magnitudes: for lag zero, ATLN1 and 3 indices are correlated at 0.69, ATLN1 and 2 at 0.75, and ATLN2 and 3 at 0.83.

Furthermore, monthly correlation analysis (not shown) shows a slight seasonal cycle with minima in boreal spring and autumn, although all values are still above 0.6. Maxima are reached in boreal winter (absolute maximum, $r > 0.7$ for all indices) and winter. Results further indicate that ATLN3 has a tendency to lag those in ATLN1 in boreal spring months March and April.

5.4 Spectral characteristics of the Atlantic Niño indices

Although there is a consensus regarding a recurring anomalous warming and cooling in the tropical southeast Atlantic in the literature, different frequencies are suggested. Some studies report that moderate anomalies off the Angolan coast occur quite frequently while pronounced warming and cooling only occurs roughly every decade (Shannon et al. 1986, Reason et al. 2006). Latif and Grötzner (2000) also describe a quasi-biennial oscillation for the equatorial Atlantic, whereas Keenlyside and Latif (2007) interpret the spectral characteristics as hardly discernable from red noise. To address the question whether a recurring signal exists with comparable frequencies in both the equatorial and the coastal region, a closer look at the newly defined Atlantic Niño indices is necessary.

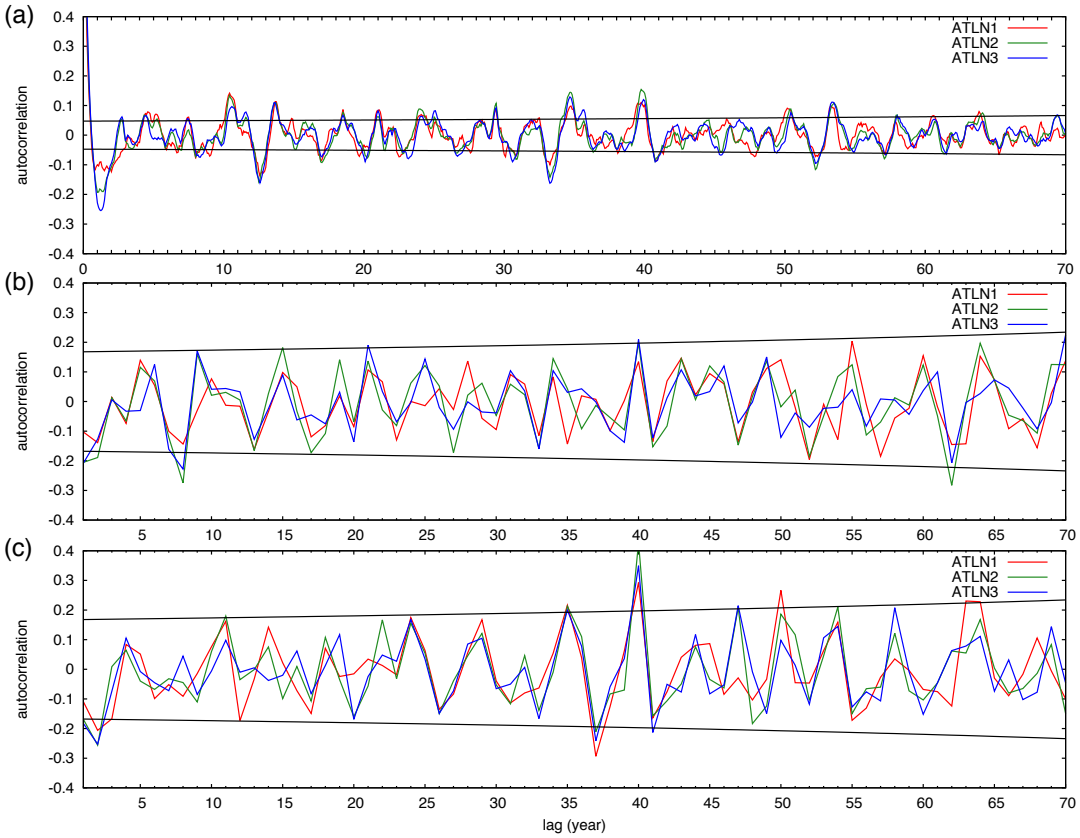

Figure 5.12: Autocorrelation functions for the ATLN1–3 indices for the period 1870–2012. ACFs for the (a) annual anomaly time series and the monthly time series of (b) January and (c) July. Black lines indicate 95 % significance: for the upper line, positive correlation coefficients above this line are significant, for the lower line negative correlation coefficients below this line are significant.

To gain a first insight into cyclic variations that may be contained in the index time series, autocorrelation functions (ACFs) are plotted in Figure 5.12 for the annual anomaly time series as well as for the 1-month seasonal sections January and July. Although weak and mainly insignificant (at the 95 % level), the autocorrelation functions of all three indices reveal a cyclic signal with a period of about 3–5 years.

To further analyze this cyclic feature, spectral analysis is applied for the whole study period 1870–2012 and also for a shorter period 1951–2012. Figure 5.13 displays the power

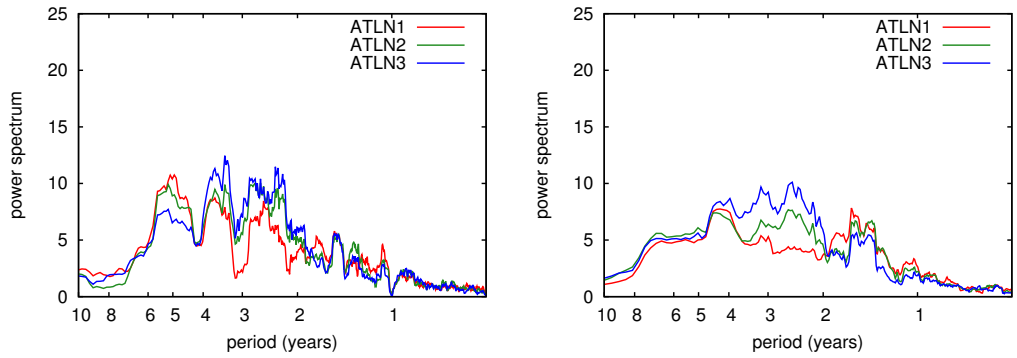

Figure 5.13: Power spectra of the ATLN1–3 indices for the period 1870–2012 (**left**) and for 1951–2012 (**right**). The x-axis denotes the period (1/frequency), the y-axis displays the power as a proportion of spectral variance.

spectra for all three indices for the two selected time periods. All spectra show enhanced variability at interannual time scales, with peaks centered at about 2.5 and 3.5 years. This is consistent with results in Latif and Grötzner (2000) who describe a quasi-biennial oscillation for the ATL3 index. For ATLN1 and ATLN2, there is also a peak for a period of 5 years. Behavior of the three indices is similar, although the power in the ATLN1 index is less pronounced in peak times. The two selected time periods 1870–2012 and 1951–2012 show similar peaks at higher frequencies, although peaks are lower, especially in the ATLN1 index. For lower frequencies, i.e. a period of more than 4 years, spectra differ between the two selected time periods. Therefore, wavelet analysis is applied to the three ATLN indices to learn more about the evolution of index frequencies over time.

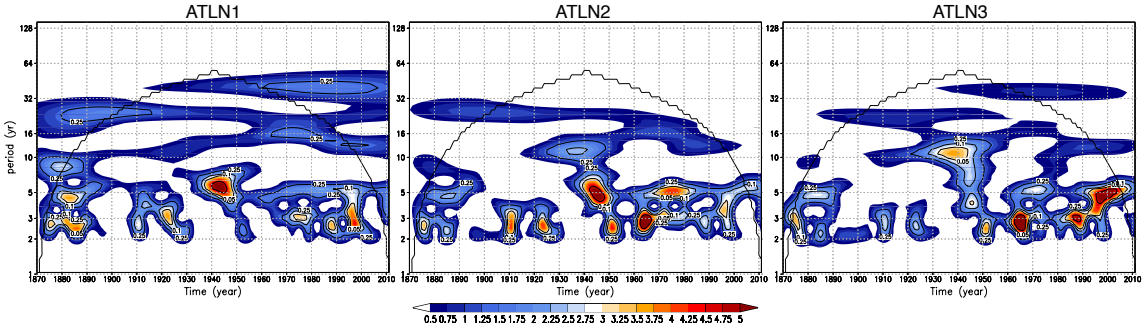

Figure 5.14: Wavelet power spectrum of the ATLN1–3 indices for the period 1870–2012. Time is shown in the x-direction, the period in the y-direction. Shading represents the power and contour lines indicate the significance levels α of 0.25, 0.10, 0.05 and 0.01.

Figure 5.14 depicts the wavelet power spectra of the three ATLN indices. The time evolution of the wavelet power reveals strong interdecadal changes in their oscillation peaks. The 2–3 year oscillation was strongest during the period 1950–1980, as was already reported by Latif and Grötzner (2000). All indices also show increased power in the 5 year band throughout 1950–2012, most pronounced in ATLN3 index during the last three decades. The strong variation in wavelet power also explains the weakness of the overall signal.

Despite the detection of rather weak signals compared to those seen in the power spectrum of the Pacific ENSO (see Figure 2.2 in Section 2.2), all three analyses point to a similar interannual oscillation with a period of 2–5 years which corresponds to the frequency of occurrence reported for warm and cold events in the tropical southeast Atlantic. These events are discussed in more detail in the following section.

5.5 Classification of Atlantic Niños and Niñas

As was already shown in the previous sections, the three ATLN indices show a quite similar behavior in their temporal evolution, and significant correlation coefficients further point to a strong interdependence. Furthermore, the three indices' spectral characteristics are comparable and reveal an interannual oscillation with a period of 2-5 years, which has already been associated with warm and cold events in the tropical southeast Atlantic.

For a first analysis of strong warm and cold anomalies, composites are computed separately for the ATLN1–3 indices exceeding a threshold of one standard deviation. The following characteristics can be observed in the composites as well as single events and corresponding time series:

- The composite patterns show a warm or cold anomaly that affects a greater region and is not limited to the equatorial or the coastal region.
- For the case of strong events, including the well-known historical events, all three indices exceed the threshold.
- If only one index or two indices exceed(s) the threshold, the remaining one or two indices at least show(s) less pronounced anomalies of the same sign in most cases.

These observations provide additional evidence that there is a connection between the three regions and therefore also between the equatorial and the coastal region, for which separate Niño phenomena have been described.

It can be concluded that events found in the different indices do not seem to be independent and in most cases the whole cold tongue region is affected by a warming or a cooling. Therefore, all three indices are included in the new definition of warm and cold events presented in this section.

As for the indices, so far, there is no universal threshold or minimum duration for warm and cold events. For example, Florenchie et al. (2004) define warm and cold episodes based on ABA SST anomalies exceeding a threshold of 1°C. Lübbecke et al. (2010) use a different threshold and define their Niño (Niña) events as periods with ABA (or ATL3) SST anomalies exceeding a value of +0.7 (-0.7) standard deviations for at least three consecutive months. According to Wang (2002) warm and cold events are periods of at least 1 month of ATL3 index anomalies exceeding 0.7°C. Therefore, different threshold values and durations are evaluated in the present experiments in order to find definite ones which include all well-known historical events in the Atlantic and Benguela Niño regions. Finally, a threshold of one standard deviation σ and three consecutive months

are chosen, as this choice best reflects the already known events. Expressed in degree Celsius, one standard deviation is 0.74°C (ATLN1), 0.50°C (ATLN2), 0.48°C (ATLN3).

Based on this threshold, finally all three indices are included in one classification of warm and cold events with the following three Atlantic Niño and Niña sub-types:

Major event: all ATLN indices exceed the threshold of one positive (negative) standard deviation for at least three consecutive months (warm (cold) event criterion).

Minor event: at least one index meets the warm (cold) event criterion, the other indices exceed an average of half a standard deviation for at least one three-month period.

Warm (cold) episode: period consisting of multiple connected events, including at least one major event. SST anomalies between two events do not change the sign and the event-break does not last for more than 6 months.

To prevent a split-up into multiple events that are actually part of one single event, index time series are allowed to drop below the threshold by $0.2 * \sigma$ in one index for one month if at least three consecutive months exceeding the threshold were already found. Accordingly, in warm (cold) episodes, splitting of an event is prevented by tolerating a small ($0.2 * \sigma$) sign change for only one month of one index.

This new classification is now based on all three ATLN index regions and does not treat them separately anymore. Thus, Atlantic and Benguela Niños are now combined into one comprehensive Atlantic Niño with different regional characters. While the sub-type major event represents strong events with a spatially extensive anomaly, the sub-type minor event also considers anomalies with a greater magnitude in only one region, e.g. the equatorial or the coastal region. In addition, the sub-type episode characterizes events with prolonged duration. Based on this classification, 13 major warm events, 20 minor warm events, 6 warm episodes as well as 12 major cold events, 23 minor cold events and 2 cold episodes are identified in the study period 1870–2012. Only 3 individual cold events and 2 individual warm events cannot be classified as one of the sub-types. For these cases, Niña/Niño conditions are found in only one ATLN region but no significant warming or cooling in the other two regions. These 5 regional events are all short and SST anomalies in the corresponding region are less pronounced.

To confirm the present results and test the stability of this new classification, it was also run on the OISST dataset (for a description of the dataset see Section 3.1). All major warm and cold events and the majority of the minor events found in the HadISST classification are also found in the OISSTs. Minor differences in event onset, decay, duration and peak lie within the expected range of random deviations between different datasets.

Table 5.1 summarizes all classified events and specifies sub-type, event period, duration and peak month. Figures 5.15 and 5.16 show distinct examples of the different Atlantic Niño and Niña sub-types: Figure 5.15 displays two examples of major events, the major warm event 1963–1964 and the major cold event 1958. The lower two examples include the minor warm event 2001 and the minor cold event 2004 with their main warming (cooling) centre in the ATLN1 region. Figure 5.16 shows two examples of minor

Table 5.1: Atlantic Niño and Niña events between 1870 and 2012 with corresponding beginning and ending year/month, duration (dur.) in months, Niño type and peak month. Niño types are Major (M), minor (m) and Episode (E). For type minor, the indices exceeding the threshold are added in parentheses. For ATLN1 and 3 regions, both are indicated if affected.

Atlantic Niños				Atlantic Niñas			
begin – end	dur.	sub-type	peak	begin – end	dur.	sub-type	peak
1871/05 – 1871/07	3	m (2)	5	1874/03 – 1874/06	4	M	5
1872/08 – 1873/10	15	M	2	1876/10 – 1877/02	5	M	12
1875/02 – 1876/01	12	E	11	1878/11 – 1879/04	6	M	12
1886/03 – 1886/07	5	M	6	1880/03 – 1880/09	7	M	5
1889/06 – 1889/09	4	m (3)	6	1882/05 – 1882/07	3	m (3)	5
1893/07 – 1893/09	3	m (2)	7	1888/01 – 1888/06	6	m (3)	6
1894/11 – 1895/02	4	m (2)	12	1892/04 – 1892/07	4	m (3)	5
1896/02 – 1896/04	3	m (2)	3	1903/04 – 1905/09	30	E	6
1896/12 – 1897/08	9	M	4	1906/05 – 1906/07	3	m (3)	5
1899/03 – 1899/08	6	M	8	1906/10 – 1907/02	5	m (2)	11
1909/05 – 1910/09	17	E	5	1908/05 – 1908/07	3	m (3)	6
1913/05 – 1913/08	4	m (0)	7	1914/04 – 1914/07	4	m (1)	7
1920/11 – 1921/10	12	E	6	1918/05 – 1918/09	5	M	8
1923/11 – 1924/05	7	M	12	1930/01 – 1930/05	5	M	2
1925/05 – 1925/08	4	m (3)	5	1932/02 – 1932/07	6	m (3)	7
1934/06 – 1934/10	5	M	7	1936/02 – 1936/08	7	m (3)	7
1937/04 – 1938/03	12	m (3)	5	1940/04 – 1940/07	4	m (1)	6
1939/06 – 1939/08	3	m (1)	6	1945/08 – 1945/10	3	m (3)	8
1944/02 – 1945/06	17	E	5	1946/04 – 1946/09	6	m (3)	8
1949/04 – 1950/03	12	E	8	1948/05 – 1948/08	4	m (1)	6
1953/05 – 1953/07	3	m (1)	6	1950/09 – 1951/04	8	m (3)	12
1960/07 – 1960/12	6	m (2)	9	1954/02 – 1954/07	6	m (3)	7
1963/01 – 1964/03	15	M	8	1956/01 – 1956/06	6	m (2)	3
1966/05 – 1966/07	3	m (3)	6	1958/02 – 1958/10	9	M	6
1968/05 – 1969/03	11	m (3)	7	1964/08 – 1965/02	7	m (3)	10
1972/11 – 1973/11	13	E	7	1967/07 – 1967/12	6	m (3)	7
1974/04 – 1974/08	5	M	7	1976/04 – 1977/01	10	m (3)	7
1984/03 – 1984/11	9	M	6	1977/12 – 1978/06	7	M	4
1986/02 – 1986/04	3	m (1)	2	1981/01 – 1981/08	8	m (1)	5
1987/07 – 1988/10	16	M	6	1982/02 – 1982/09	8	M	6
1993/09 – 1993/12	4	m (1,3)	11	1983/04 – 1983/08	5	M	5
1994/10 – 1995/07	10	M	3	1986/07 – 1987/01	7	m (1,3)	10
1996/04 – 1996/07	4	m (3)	6	1991/08 – 1992/11	16	E	7
1997/10 – 1998/03	6	M	12	1996/12 – 1997/07	8	M	6
1999/05 – 1999/08	4	M	7	2004/03 – 2004/05	3	m (1)	4
2001/03 – 2001/05	3	m (1)	4	2005/05 – 2005/07	3	M	6
2003/11 – 2004/01	3	m (3)	12	2011/12 – 2012/02	3	m (3)	2
2008/05 – 2008/08	4	m (3)	5				
2009/12 – 2010/02	3	m (1)	1				

events centered on the ATLN3 region, the minor warm event 2003–2004 and the minor cold event 1984–1985. The remaining two examples include the warm episode 1944–1945, which consists of two major events, and the cold episode 1991–1992, which consists of a minor and a major event. All eight examples clearly show that, notwithstanding the sub-type, warming or cooling affects the whole eastern tropical Atlantic reaching from the Angolan coast to the equatorial Atlantic.

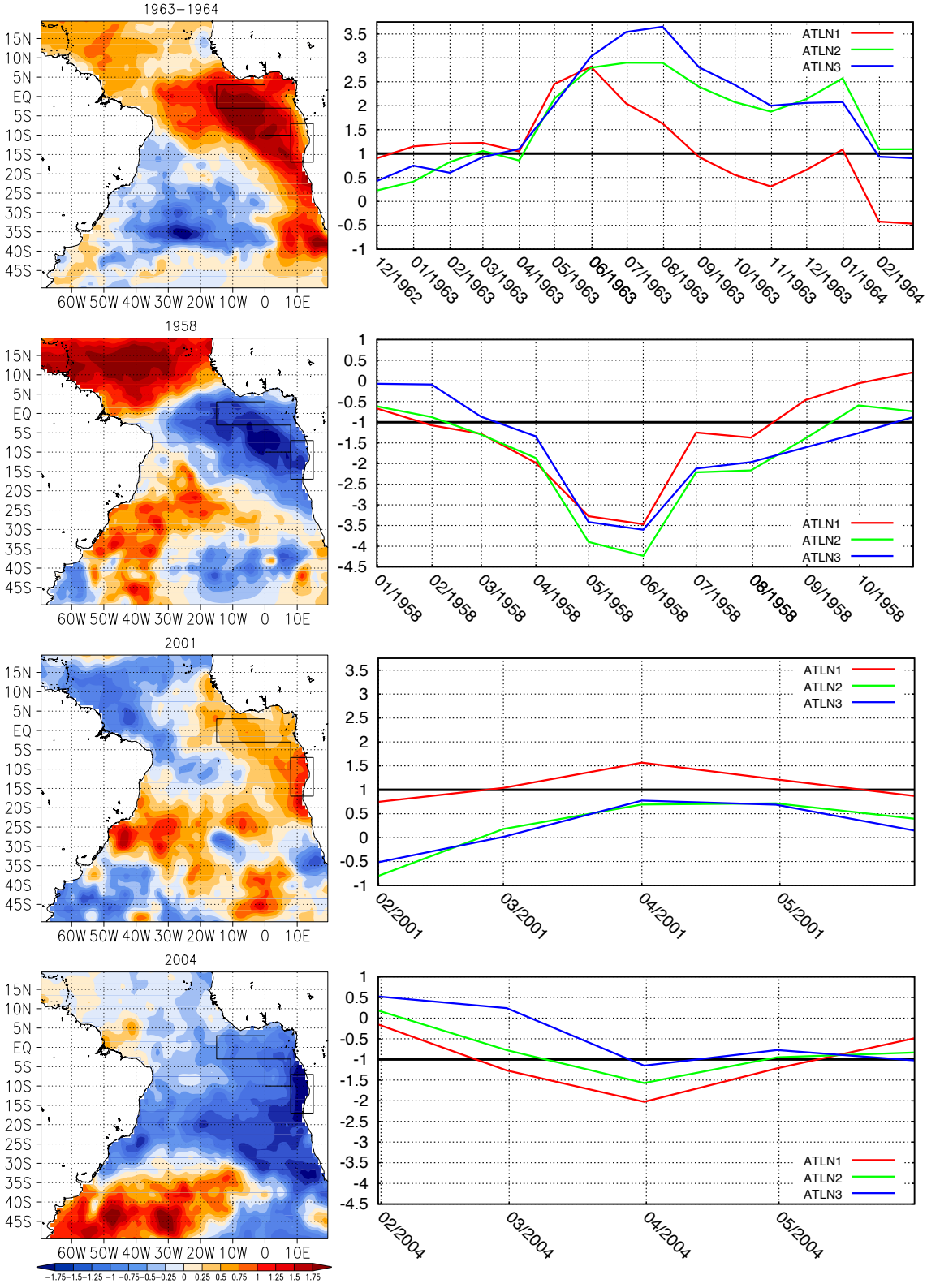

Figure 5.15: Examples of the Atlantic Niño and Niña sub-types (from top to bottom): major warm event 1963–1964, major cold event 1958, minor warm event 2001 and minor cold event 2004. For each example, composites of high-pass filtered SST anomalies and index time series are shown. Index regions are indicated as black rectangles.

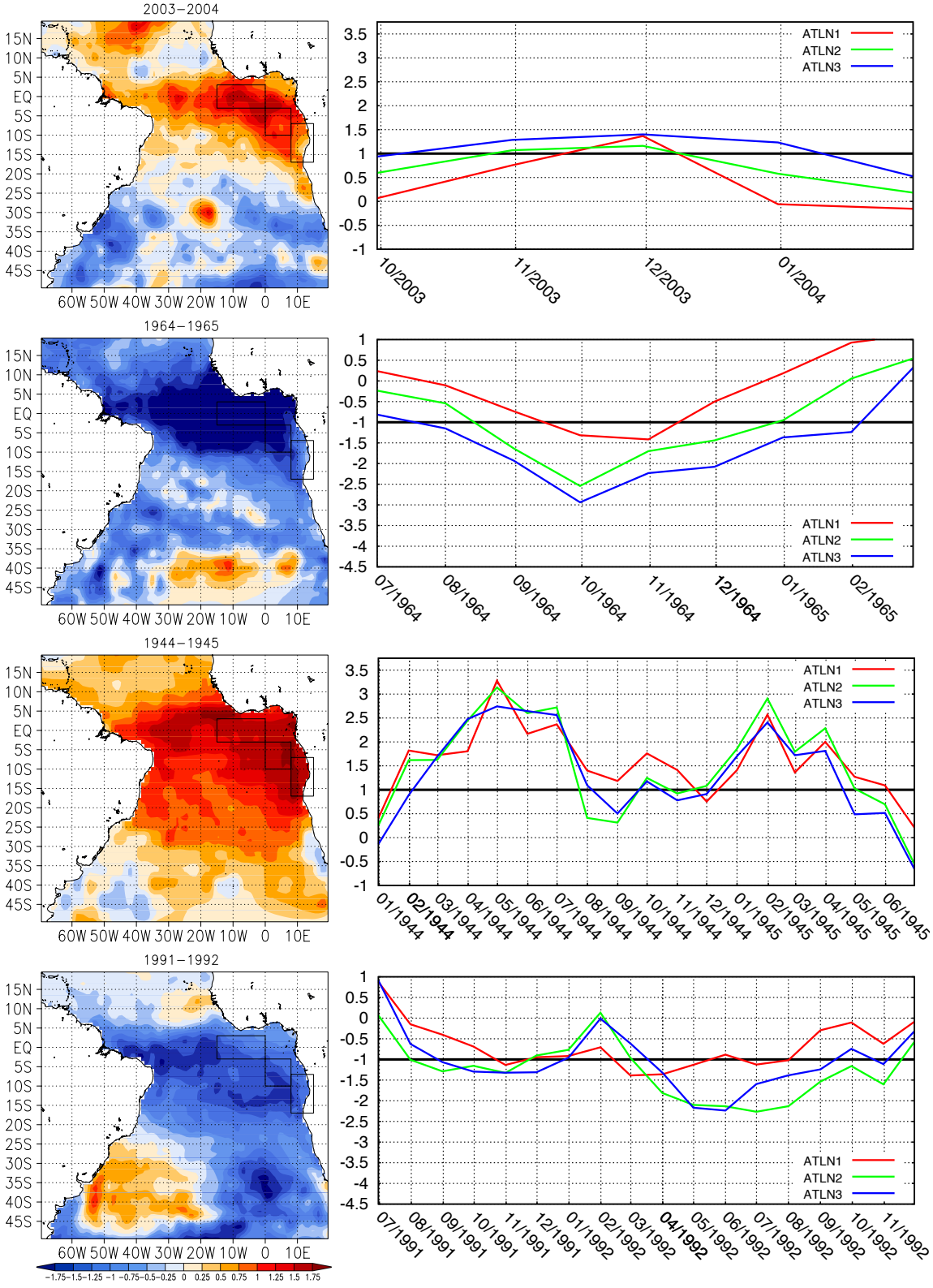

Figure 5.16: Examples of the Atlantic Niño and Niña sub-types (from top to bottom): minor warm event 2003–2004, minor cold event 1964–1965, warm episode 1944–1945, cold episode 1991–1992. For each example, composites of high-pass filtered SST anomalies and index time series are shown. Index regions are indicated as black rectangles.

5.6 Analysis of Atlantic Niño and Niña events

To characterize Atlantic Niño and Niña events in general, and also the different sub-types in terms of onset, duration and peak, event durations are computed. Additionally, the frequencies of months classified as Atlantic Niño and Niña months are plotted in Figure 5.17 (a) and (c). Onset months are shown in Figure 5.17 (b) and (d), and Figure 5.18 depicts peak months.

The different event sub-types are characterized by different event durations: minor warm (cold) events last for 5 (4) months on average, major events for 9 (6) months and episodes for 14 (23) months. The difference in duration between cold major and minor events is smaller than that for warm events.

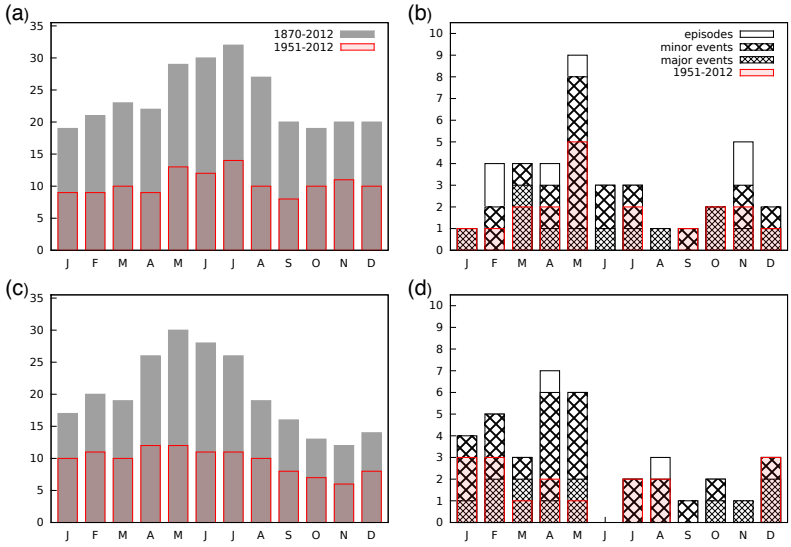

Figure 5.17: Left column: monthly frequencies of Atlantic Niño (a) and Niña (c) events (all types) between 1870 and 2012. **Right column:** Monthly occurrence of onsets of Atlantic Niño (b) and Niña (d) events (subtypes minor, major events and episodes) for the same time period. The x-axis displays the peak year of each event, not the onset year. Monthly frequencies and onsets of events for the period 1951-2012 are highlighted in red.

As can be seen from Figure 5.17 (a) and (c), any month of the year can be an Atlantic Niño and Niña month and these are quite well distributed across the year, although boreal summer months are favored. One can also notice a slight asymmetry with cold events favoring earlier months than warm events. This feature is less pronounced in the more recent period 1951–2012 (indicated in red). Another feature visible in both periods is a boreal autumn minimum in the occurrence of cold event months.

Considering the events' onset (Figure 5.17 (b) and (d)) - notwithstanding the type - most of them start in boreal spring months with a peak in May for warm events and in April for cold events. But some of the events also start in late boreal autumn or winter months. This is consistent with earlier studies, which report that conditions are favorable for warm or cold water events twice a year (Okumura and Xie 2006, Rouault 2012). For the more recent period, the spring onset peak in cold events disappears and in general the double-peak of onset months is less noticeable in cold events.

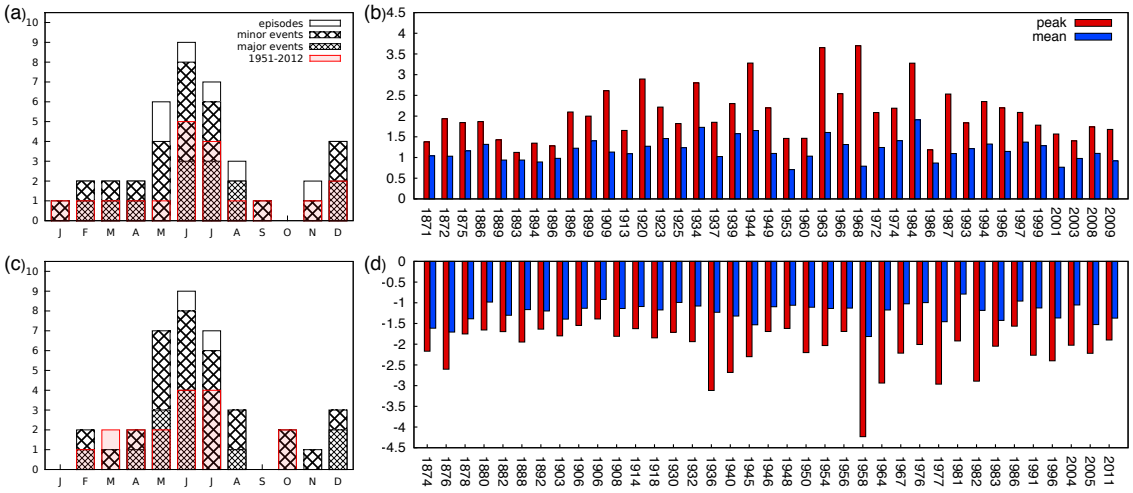

Figure 5.18: Left column: monthly occurrence of peaks of Atlantic Niño (a) and Niña (c) events (subtypes minor, major events and episodes) between 1870 and 2012. The total of event peaks for the period 1951-2012 is highlighted in red. **Right column:** peak and mean values of all Atlantic Niño (b) and Niña (d) events for the same time period, computed across all three ATLN indices. The x-axis displays the peak year of each event, not the onset year.

Figure 5.18 displays the monthly occurrence of peaks of Atlantic Niño (a) and Niña (c) events. About 50 % of warm (a) and cold (c) water events peak in late boreal spring and early summer months May to July, but peaks are also found in boreal winter month December and throughout the remaining months of the year. This is similar for both the shorter and the longer record periods. Another important finding is that the different sub-types do not favor a specific peak month. The same can be concluded for sub-types with different peak region from Table 5.1. Although one might expect a minor sub-type centered in the ATLN1 region to rather peak in spring and one centered in the ATLN3 region to peak in summer, there is no clear indication for such favoring. Figure 5.17 (b) and 5.17 (d) depict the peak and mean values of each classified events, computed across all three ATLN indices. These include well-studied major warm events such as 1934, 1963 and 1984 (e.g. Shannon et al. 1986, Florenchie et al. 2004), which all show remarkably high peaks. Strong cold events are found e.g. in 1936, 1958, 1977 and 1982.

Summarizing the findings above, Atlantic Niños and Niñas can appear all year round with many of them starting in boreal spring or autumn and peaking in boreal summer. Results indicate a potential asymmetry in duration, onset and monthly occurrence, which is also visible in a classification run on the ERSST data set. Still, these findings need to be interpreted with care due to the limited number of overall events. However, such an asymmetry is not unusual and has already been reported for the Pacific ENSO system (Okumura and Deser 2010) and may therefore also be present in the Atlantic Ocean.

5.7 Remote versus local wind forcing

In general, the southeasterly trade winds in the south Atlantic can either be altered by variations in the intertropical convergence zone (ITCZ) or by variations in the strength of the South Atlantic Anticyclone (SAA). While equatorial winds are weakest in boreal spring when the ITCZ reaches its southernmost and thus closest position to the equator (Xie and Carton 2004), variations in the SAA in early spring may also affect trade wind and SST variability in the following months (e.g. Lübbecke et al. 2010, Richter et al. 2010).

However, as already described in the Introduction (Section 5.1), it is still controversially discussed whether Atlantic warm and cold events are *remotely* forced by western equatorial zonal wind anomalies exciting Kelvin waves or *locally* forced by variations in the SAA and associated alongshore wind anomalies along the Angolan coast altering coastal upwelling. That is, it is unclear, whether a weakening of the trades is more important in the equatorial or in the coastal region. Here, both the remote and local influences are examined for the three ATLN regions:

1. For an analysis of the *remote influence*, cross-correlation analyses are performed between the three ATLN indices and a western Atlantic zonal wind index (WATL, 2.5°S−2.5°N and 40° − 20°W, similar to that of Richter et al. 2010).

2. Furthermore, the *local influence* is investigated by correlating the ALTN indices with a high-pass filtered SLP index representing South Atlantic Anticyclone variability (SAA, 20°S−40°S and 30° − 10°W, as also used by Lübbecke et al. 2010).

Correlation analyses are carried out for monthly and 2-/3-month seasonal sections for different time lags (-6 to 0 months, negative lag indicates WATL or SAA leading). Results are summarized in Figure 5.19 showing the maximum correlation coefficients of all time lags for each SST seasonal section. In addition, Figure 5.20 depicts selected results of an analysis of specific time lags, i.e. the lags for which the overall maximum correlation was found. Therefore, lag 0 is selected for the correlations between the ATLN and WATL indices and lag -2 (SAA leading) for those between the ATLN and SAA indices.

Results from cross-correlation analyses reveal strong seasonality in the strength of the relationship between SSTs and wind or SLP index. Regarding the *remote influence*, high significant positive correlations, i.e. westerly (easterly) wind anomalies associated with warm (cold) SST anomalies, are found between all three indices and the WATL index in late spring and boreal summer. This may be explained by the abovementioned migration of the ITCZ and associated trade wind variability. Peak values of more than or close to 0.8 are reached for the equatorial region ATLN3, but ATLN1 and 2 still show remarkable correlation coefficients with a tendency to lag the zonal wind index by one or two months. For ATLN2 and 3, a secondary peak is apparent in boreal winter, which is consistent with findings in Okumura and Xie (2006), who attribute late autumn easterly anomalies to a change in South American convection. However, in contrast to the latter authors, Keenlyside and Latif (2007) suggest that the Bjerknes feedback is mainly active during spring and summer months. This may explain why this secondary peak in winter

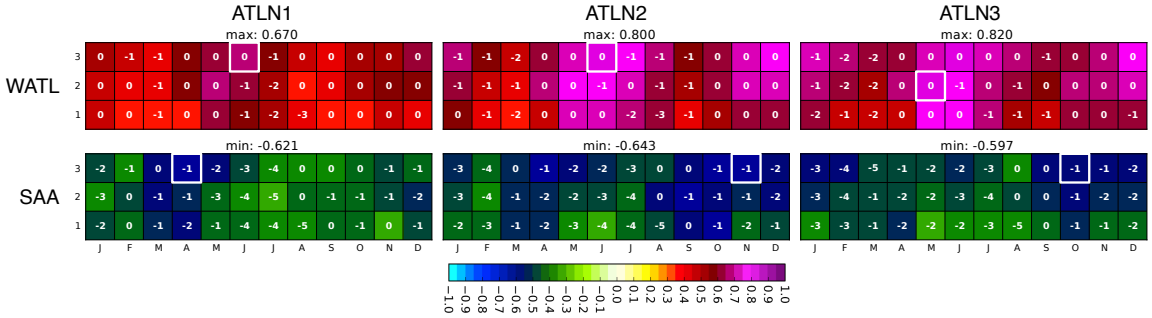

Figure 5.19: Monthly and seasonal correlation coefficients between ATLN 1–3 indices (columns) and the WATL index (first row) as well as the SAA index (second row) for the period 1951–2012. For each 1 to 3-month seasonal section (y-axis), only the absolute (positive or negative) maximum for time lags -6 to 0 months (negative lags indicate WATL/SAA index leading) is shown. The labels denote the corresponding time lag of the maximum. The overall maximum is highlighted by a white frame. Only significant results (95 % level) are shown based on the central month (x-axis) of the ATLN index, e.g. the FMA season is plotted at the position of central month M.

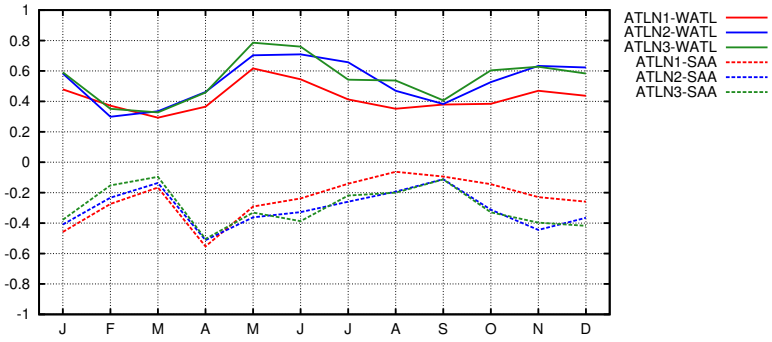

Figure 5.20: Monthly correlation coefficients between ATLN 1–3 indices and the WATL index (solid curves) as well as the SAA index (dashed curves) for the period 1951–2012. Time lags were selected according to the overall maxima indicated in Figure 5.19. For the ATLN–WATL only correlations for lag 0 and for ATLN–SAA only those for lag -2 (SAA leading) are displayed. Months for the ATLN index are indicated on the x-axis.

is not visible in the ATLN1 region. An equatorial SST anomaly forced by westerly wind anomalies in boreal autumn does not always seem to reach the coast. However, when looking up winter peak events in Table 5.1 (p. 51), major and equatorial minor events with winter peaks do exist although no coastal minor events have winter peaks. Thus, the ATLN1 region does not seem to play an important role in the evolution of boreal winter events whereas a major event can still reach the coast.

Concerning the *local influence*, correlation coefficients between the ATLN and SAA indices indicate a strong link in boreal spring with warmer (colder) than normal SSTs lagging a weakening (strengthening) of the south Atlantic high. This is consistent with the findings of Lübbecke et al. (2010). As all three indices are well correlated, the influence of the south Atlantic anticyclone and associated trade wind anomalies on SST anomalies appears not to be limited to the coastal region but also reaches as far as the equator, as has also been reported by Richter et al. (2010). A second peak is found in boreal autumn, although less pronounced in the ATLN1 index. Comparable results are achieved with the HadSLP2r data set when selecting the same period 1951–2012 (not shown).

Unlike in spring, the WATL and SAA indices in boreal winter are also significantly correlated (not shown). According to Robertson et al. (2003), in boreal winter the South Amazonian convergence zone is related to the strength and position of the SAA. Although Okumura and Xie (2006) describe South American convection to cause easterly equatorial wind anomalies, they do not report a connection to the subtropical high. Therefore, partial correlation is used in the present analysis to exclude spurious correlation and to investigate the individual contributions of equatorial wind anomalies and the subtropical high, respectively. The influence of the equatorial winds appears to be robust, whereas the partial correlation with the SSA index indicates an overestimation of this influence but remains significant. For the ATLN1 and ATLN2 regions, correlations become insignificant when excluding the influence of equatorial wind anomalies. Therefore multiple correlation analysis is only performed for the ATLN3 region. Comparison of the bivariate and multiple correlation coefficients shows that a small increase in explained variance can be achieved when both influences are included. Although altered equatorial zonal wind seem to be the main influence, at least a small contribution of the subtropical high is likely. From these results it may be speculated that simultaneous changes over the south Atlantic and South America could explain why in some rare cases stronger warm or cold water events, i.e. major events, either develop or peak in late boreal autumn and winter months.

In summary, it can be concluded that remote and local forcings are both relevant, but their influence is seasonally dependent. While the SAA mainly contributes to the evolution of warm or cold events in boreal early spring, equatorial Atlantic zonal wind anomalies play a more important role in boreal summer and again to a lesser extent in boreal autumn. From the present correlation analyses it is also visible that in these months all three SST regions are affected, although the strength of the link varies. This further confirms the close connection between the three ATLN regions and also indicates that they share at least some of the forcings and mechanisms contributing to anomalous warming or cooling.

5.8 Summary

In this chapter tropical southeast Atlantic SST variability has been described using PCA and cluster analyses in a first part. In the remaining part of the chapter, robust regions and indices are defined, which were further used in a classification and characterization of warm and cold events.

First, when analyzing patterns of tropical Atlantic SST variability, a dominant and persistent pattern is found in the tropical southeast Atlantic, which can appear at any time of the year. PCA could not be used to split up the southeast Atlantic into regions, which are representative of the equatorial Atlantic and the Benguela Niño. But instead, analyses clearly demonstrate that both the equatorial and the coastal regions share a great portion of variability. This indicates that the two Niño types may not be independent or at least co-occur at certain times.

Second, by defining three Atlantic Niño regions covering most of the Benguela cold tongue area and calculating new robust SST anomaly indices for each of them, a strong connection between SST variability in all three regions was found. This confirms the link between equatorial Atlantic and coastal SST variability and also the great portion of variability shared within the whole tropical southeast Atlantic area already indicated by the PCA analyses. Therefore, in this thesis a new classification of warm and cold events is proposed that is based on all three SST indices. Thus, Atlantic and Benguela Niños, previously considered as separate phenomena, are now integrated into a single classification. They are classified into three sub-types of one comprehensive Atlantic Niño with different regional characters. This classification now serves as a solid base for further research on the dynamics of warm and cold events in the eastern tropical Atlantic and their regional impact and global interactions.

6

Impact on African west coast precipitation

After a detailed analysis of Atlantic Niños and Niñas in the previous chapter, this chapter now discusses the impact of such events on regional precipitation, namely African west coast precipitation. After an introduction and overview of previous studies in Section 6.1, Section 6.2 explains the determination of precipitation regions, which are then used in Section 6.3.1 to analyze co-variability of Atlantic SSTs and precipitation. Co-variability is further assessed using CCA analyses in Section 6.3.2. Non-stationarities in the SST–rainfall relationship of selected regions are briefly discussed in Section 6.3.3. Section 6.4 then focuses on Atlantic warm and cold events classified according to the ATLN classification explained in the previous chapter and investigates their impact on African west coast precipitation. This is further discussed in the context of the overlaying atmospheric circulation in Section 6.5. Due to the limited availability of higher level quality circulation and precipitation data (see data description in Chapter 3), analyses in this chapter are limited to the period from 1951 to 2010.

Parts of the work described in this chapter have been published in Lutz et al. (2014).

6.1 Introduction

One important driver of African rainfall variability is tropical southeast Atlantic sea surface temperature. In general, an increase in SSTs enhances evaporation and therefore increases water vapor content of the atmospheric boundary layer. Dependent on the direction of low-level winds, moisture is then transported towards the landmass. If atmospheric conditions are favorable for advective or convective processes, the arriving moist air contributes to the generation of rainfall. One can therefore expect a change in tropical southeast Atlantic SSTs to have an impact on African rainfall at least in some regions or seasons.

A general overview of SST influence, including south Atlantic SSTs, on sub-Saharan rainfall and associated atmospheric dynamics is given by Camberlin et al. (2001). Their analysis considers both low and high frequency variability and also includes remote influences from the Pacific ENSO system. The authors find the clearest response to interannual south Atlantic SSTs anomalies along the Atlantic shore with the strongest signal in West Africa. Positive correlations are reported for Angola in boreal spring months March–May, which then move to Gabon and reach the Guinean West Africa in boreal summer months July–September. For the latter regions, negative correlations are found during the dry season. These changes can be mainly explained by variations in the latitudinal position of the ITCZ. A boreal summertime south Atlantic SST warming reduces the temperature gradient between the ocean and the overheated continent. This results in a reduced northward excursion of the ITCZ, thus leading to positive rainfall anomalies along the Gulf of Guinea. In boreal winter, positive SST anomalies are associated with an abnormal southerly shifted ITCZ staying closer to the equator over the ocean rather than over the continent. As a consequence, precipitation along the Guinean coast is significantly reduced. However, this study does not consider time lags nor distinguishes between the influence of SST anomalies in the equatorial region and in the Benguela system off the Angolan coast.

Apart from this comprehensive study by Camberlin et al. (2001), most studies investigate only selected smaller regions or the rainy season. Many of these regional studies examining SST-rainfall links focus on the northern hemisphere. Here, Kouadio (2003) shows a statistical connection between tropical Atlantic SSTs and Ivory Coast rainfall during the summer monsoon season. Changes in the Ivorian rainfall distribution are linked to an abnormal position of the ITCZ. Reason and Rouault (2006) provide evidence of a connection between boreal spring SST anomalies in the tropical southeast Atlantic and rainfall in subsequent boreal summer months (JJAS) over coastal West Africa. Based on the analyses of moisture flux and heat content, they identify SSTs off the coast of Angola and northern Namibia as a moisture source for West African rainfall. For May rainfall they also describe a weak inverse relationship with SSTs in the previous months. The authors suppose that stronger convection over Angola associated with positive SST anomalies may occur at the expense of the developing convection over West Africa, thus reducing precipitation in the latter region. Furthermore, Polo et al. (2008) use extended maximum covariance analysis to extract time-evolving patterns of Atlantic SSTs in relation to anomalous boreal summer rainfall in West Africa. Their leading mode confirms the positive relation between SST anomalies in the southeast Atlantic and precipitation anomalies in the Guinea Coast region. Hermes and Reason (2009) analyze the relationship between southeast Atlantic winds and SSTs and coastal West African as well as Angolan and Namibian precipitation on an intra-seasonal scale. Concerning coastal West Africa, they find anomalous rainfall to be related to changes in the low-level meridional wind transporting moisture from the tropical southeast Atlantic towards the continent, which confirms earlier studies described above.

The equatorial region of the African west coast has received the least attention so far. Balas et al. (2007) show that, among other influences on rainfall variability in western equatorial Africa, the SST anomalies in the tropical southeast Atlantic play an important role in boreal summer months (JJA). Consistent with a southward displacement of the ITCZ during an Atlantic Niño event, their results show positive precipitation anomalies for the southern sub-regions of their study area and negative anomalies for the northern ones. However, the region is quite complex and Atlantic SSTs may also contribute to rainfall variations in other seasons. Two recent studies use a study region similar to that of Balas et al. (2007) but larger and with different sub-regions to further investigate western equatorial African rainfall variability and the relation of the latter to tropical ocean and atmospheric circulation: Nicholson (2013) focuses on boreal spring, and Dezfuli and Nicholson (2013) investigate boreal autumn. Both studies clearly confirm the complexity of the study region, where rainfall is either largely locally controlled or modulated by orographic effects. Nevertheless, especially the coastal sector does show a strong link to Atlantic SSTs. However, the authors suggest that the link between rainfall and local SSTs mainly reflects remotely forced changes in the large-scale atmosphere-ocean system.

In the southern hemispheric regions of the African west coast, Hirst and Hastenrath (1983) first found a positive correlation between southeast Atlantic SSTs and rainfall along the coast of Angola in boreal spring months March-April. They suggest a causality chain of atmosphere-ocean anomalies, which involve a relaxation of the easterly wind stress over the western equatorial Atlantic that in turn forces a warming of the eastern tropical Atlantic SSTs. As a result of associated changes in atmospheric moisture and stability, rainfall along the Angolan coast is increased. Shannon et al. (1986) and Nicholson and Entekhabi (1987) show that during warm water events in the tropical southeast Atlantic, abnormal high rainfall also occurs along the Namibian coast as well as further inland. They attribute these anomalies to changes in local SSTs but also in the large-scale atmospheric circulation. Rouault et al. (2003) further suggest that the extent inland of the precipitation anomalies may depend on the regional moisture convergence and atmospheric circulation anomalies. Angolan and Namibian rainfall anomalies are greatest for those events with a circulation being favorable for a strengthened westward moisture flux from the Indian Ocean and a weakened southeasterly flux away from the southeast Atlantic coast. While the latter authors suggest the Indian Ocean to be the dominant moisture source, Hermes and Reason (2009) also emphasize the role of the Atlantic. A stronger Angolan low and strengthened low-level winds feeding into the low are associated with enhanced moisture advection from the Atlantic towards the land and thus increased precipitation. Furthermore, Muller et al. (2008) describe the case of an unusual wet austral summer in 2005-2006 in Namibia associated with the co-occurrence of anomalously warm southeast Atlantic SSTs and a Pacific La Niña. At the southern tip of the continent, Vigaud et al. (2009) connect South African precipitation anomalies to a dipole-like pattern with SST anomalies centered further south. During a positive mode of their South Atlantic mid-latitude mode, moisture availability and thus precipitation is reduced over subtropical southern Africa. Reason and Rouault (2006) also mention a potential negative link between southeast tropical Atlantic SSTs and southwest African rainfall.

Recent studies, most of which are focused on West Africa and the Sahel, have also addressed non-stationarities in the SST-rainfall relationship. Positive SST anomalies in the Atlantic associated with a southward displacement of the ITCZ causes positive rainfall anomalies over the Gulf of Guinea and negative anomalies over the Sahel, thus forming a dipole pattern (Janicot et al. 1998, Mohino et al. 2011b, Losada et al. 2010a). Furthermore, Sahel precipitation was also found to co-vary with Pacific SSTs (Janicot et al. 1998, Giannini et al. 2003). But after the 1970s the dipole pattern in response to Atlantic SSTs changed to a monopole pattern with both the Guinean coast and the Sahel region showing positive rainfall anomalies during Atlantic warm periods. While the SST-rainfall relationship appears to be quite stationary for the Guinean coast, it is non-stationary for the Sahel and collapses after the 1970s (Polo et al. 2008, Joly and Voldoire 2010, Rodríguez-Fonseca et al. 2011). In the same recent decades, a significant anti-correlation between the Atlantic and Pacific Oceans appears (Rodríguez-Fonseca et al. 2009). The non-stationarity in the link between Atlantic SSTs and Sahel precipitation may therefore be due to the counteracting effects of the Pacific and Atlantic Oceans on Sahel precipitation (Joly and Voldoire 2010, Mohino et al. 2011a). Losada et al. (2012) report a seasonal dependence, i.e. constructive mechanisms at work for May–June and destructive effects for July–August.

Earlier studies, including the ones that have been described above, have mainly focused on either a specific region and a selected season or cover only a short period. Moreover, different techniques and definitions, including those for SST regions and indices as well as warm and cold events, have been used. Thus, results are incomplete or not comparable across different studies.

Therefore, in this work, comprehensive analyses are carried out considering all regions facing the south Atlantic and all different seasonal sections with 1–3 month length throughout the year. All analyses are based on the newly defined ATLN indices and the Atlantic Niño classification described in Chapter 5. Thus, for the first time, one common definition of warm and cold events is used to study their relationship to rainfall along the entire west coast of sub-Saharan Africa. Furthermore, the impact of both warm and cold water events on coastal rainfall is considered.

6.2 Determination of precipitation regions

To reduce dimensions of the fully resolved precipitation field of sub-Saharan Africa (20°N to the southern tip of the continent) for subsequent analyses and in order to determine regions with similar rainfall variability, rotated s-mode PCA was applied to the annual standardized precipitation anomaly time series first. Common criteria for the selection of an appropriate number of PCs including the dominance criterion suggest a number too small and thus regions too big to e.g. separate coastal variability from that further inland. The number of 39, explaining 60.6% of total variance, was therefore subjectively chosen with respect to climatological aspects (circulation, wet and dry seasons).

A precipitation region is defined by all grid points having their maximum PC loading on the same PC. Instead of using the PC scores as corresponding time series, the

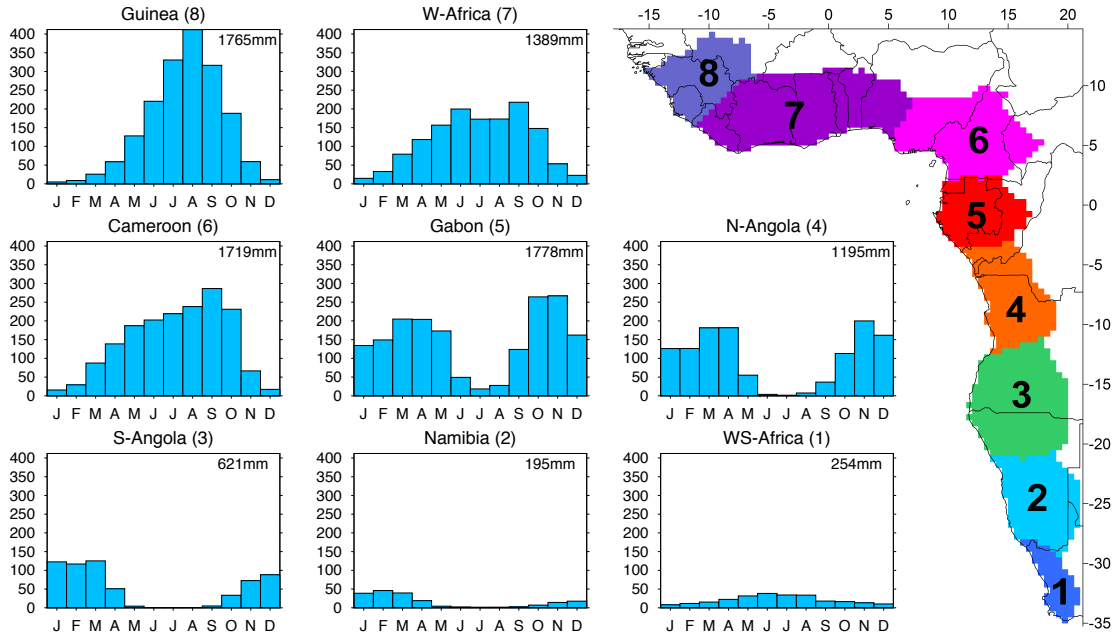

Figure 6.1: Selected regions of similar precipitation variability derived from s-mode PCA (Chapter 4.3) based on standardized 1951–2010 precipitation time series. Bar charts show corresponding seasonal cycles and annual precipitation sums. Numbers in brackets in the bar chart title correspond to the regions' numbers in the map.

weighted regional mean rainfall is used. Time series of grid boxes assigned to the same precipitation region are weighted by their corresponding PC maximum loading, divided by the sum of weights, and then spatially averaged to form an index.

For further analyses, only the regions along the west coast, which are facing the Atlantic Ocean, are selected. Figure 6.1 depicts the selected eight coastal African precipitation regions and their mean annual cycle. The names of the regions are chosen according to the country or sub-region with the highest areal percentage. The regional selection consists of five tropical regions (4, 5, 6, 7, 8), one marginal tropical region (3), and two subtropical regions (1, 2). From north to south, the position and intensity of three circulation systems, namely the ITCZ, the subtropical highs and the mid-latitude westerlies dominate the seasonal cycle of the different regions. Precipitation in tropical regions is mainly dependent on the north-south excursions of the ITCZ. *Guinea (8)*, *W-Africa (7)*, and *Cameroon (6)* receive most of their precipitation in boreal summer caused by the West African monsoon. In *Gabon (5)* rainfall maxima follow the equinoxes. The southwest monsoonal flow into the Angola low causes the precipitation in austral summer months over *N-Angola (4)*. The latter receives most of the annual rainfall between November and April whereas winter months are dry. The seasonal cycle in *S-Angola (3)* is similar but includes a pronounced dry season between April and September when the subtropical anticyclones over the Atlantic and Indian Oceans are located further north. *Namibia (2)*, mainly influenced by the subtropical highs, shows a typical semi-arid climate with small amounts of rainfall in austral summer and autumn. The maximum in austral winter

in *WS-Africa (1)* reflects the influence of extra-tropical cyclones within the mid-latitude westerlies. Note that hereafter the eight precipitation regions are written in italics and their numbers are added in parentheses to distinguish them from the actual countries.

6.3 Links between variability of southeast Atlantic SSTs and African west coast precipitation

The influence of tropical Atlantic Ocean variability on African west coast precipitation is assessed by means of bivariate correlation analyses in Section 6.3.1 as well as multivariate canonical correlation analyses in Section 6.3.2. Section 6.3.3 further analyzes selected regions and seasons in terms of non-stationarities.

6.3.1 Correlation analyses of SST and precipitation indices

Monthly and seasonal correlation analyses between the three ATLN and the eight precipitation indices are carried out for different time lags (0 to 4 months, precipitation lagging SST). Correlation coefficients are then analyzed region by region, from north to south, and described below. Due to the abundance of results, Figure 6.2 shows only the maximum correlation coefficients of all time lags for each SST seasonal section.

The strongest link between SST and rainfall variability is evident for *W-Africa* (region 7, see Figure 6.1) in boreal summer months during the monsoon season. This is consistent with results from previous studies (e.g. Camberlin et al. 2001, Reason and Rouault 2006). The overall maximum correlation of 0.76 is found for the June–August ATLN3 SST and the July–September precipitation indices, i.e. precipitation is lagging SSTs by one month. Maximum values for ATLN1 and 2 indices are found earlier in May–July. This indicates, that the development of anomalies in the more southeastern regions precedes equatorial (ATLN3) anomalies. Correlations for lag 1 and 2 are at similar magnitude and remain significant (95 % confidence level) for lags 3 and 4. As described by Reason and Rouault (2006), it takes up to 4 months to build up moisture evaporated over the tropical Atlantic off the Angolan coast that can significantly contribute to boreal summer rainfall in West Africa. In addition, results from the present analyses suggest that SST influence and evaporation is not limited to the coastal region (ATLN1) but is also apparent for ATLN2 and 3 regions.

In contrast to the strong SST-precipitation link of positive sign found for *W-Africa (7)*, there is only a minor or no significant connection in the boreal summer months July–September for the adjacent *Guinea (8)* region. Instead, correlation coefficients are negative ($r = -0.38$ to -0.44) for the 2- and 3-month seasonal sections April–May and April–June, which is the pre-onset and onset season.

For *Cameroon (6)*, a positive link is found in boreal summer between May–July ATLN1 SSTs and June–August precipitation. This link is weaker for ATLN2 and 3 indicating that those two SST regions influence tropical central Africa in boreal summer to a lesser extent. In the ATLN2 and 3 regions, weak negative correlations appear in boreal autumn months.

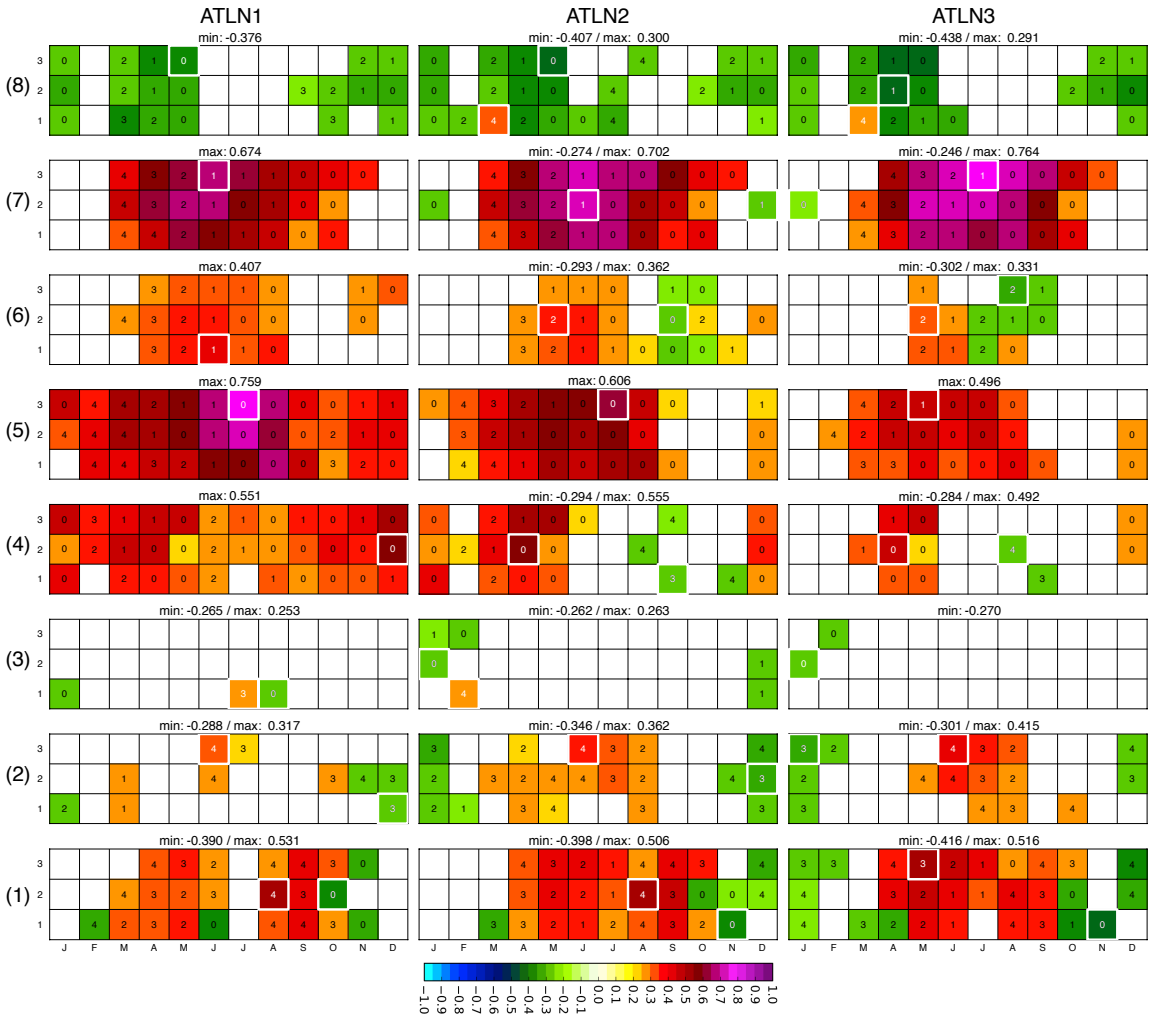

Figure 6.2: Monthly and seasonal correlation coefficients between ATLN 1-3 indices (columns) and precipitation indices 1-8 (rows). Precipitation regions are sorted from north to south (8 to 1). For each 1 to 3-month SST seasonal section (y-axis), only the absolute (positive or negative) maximum for time lags 0-4 months (precipitation lagging) is shown. The labels denote the corresponding time lag of the maximum correlation. The overall maximum is highlighted by a white frame and white label. Only significant results (95 % level) are shown and displayed based on the central month (x-axis), e.g. the FMA season is plotted at the position of central month M.

Further south down the coast, another strong link between boreal summer SSTs and rainfall (dry season) appears for *Gabon (5)*. ATLN1 and precipitation indices are correlated at 0.76. Correlations for the ATLN2 and 3 regions are weaker indicating that coastal SSTs are more important for the Gabon precipitation than equatorial ones. A second weaker link is found in boreal winter months December-February.

For *N-Angola (4)*, correlations reach their maximum ($r = 0.50 - 0.55$) in austral summer months December–January for the ATLN1 region and in autumn months April–May for ATLN2 and 3. No significant link appears to exist between SST and rainfall variability is in *S-Angola (3)* except for a weak signal in austral spring months December–January.

Results for *Namibia (2)* suggest a possible link between austral winter (May–July) SSTs and spring (September–November) precipitation with the maximum correlation of 0.41 for the ATLN3 region. Furthermore, a weak influence of austral summer ATLN2 and 3

SSTs on autumn rainfall is indicated. For *WS-Africa (1)* the correlations are negative in austral summer months October and November. Positive correlations are found for ATLN1 and ATLN2 late austral winter (August–September) SST and austral summer rainfall (December–January, $r = 0.53 - 0.51$) at moderate magnitudes whereas ATLN3 April–June SST is correlated ($r = 0.52$) with late austral winter precipitation.

Summarizing the findings from index correlation analyses discussed above, it is evident that the influence of Atlantic variability is not limited to certain months or regions (as might be thought from previous studies). It plays an important role throughout the year although with regional differences. Another important insight is that coupled variability is present on different time scales. Some links are only discovered on a monthly scale while others are stronger on the seasonal scale.

6.3.2 Canonical correlation analyses

To further explore the links discussed in the previous section, monthly and seasonal canonical correlation analyses (CCAs, for a description of the method see Section 4.5) for time lags 0 – 4 months are computed and compared with the bivariate results. The canonical correlation patterns (CCPs) provide a more detailed insight as they include the entire spatial resolution. Due to the abundance of patterns (for all seasons and time lags), only selected examples can be described below.

The first pair of CCPs (Figure 6.3 (a), $r = 0.83$) for the 3-months seasonal section June–August consists in its positive mode of a SST pattern with positive anomalies in the tropical southeast Atlantic and a corresponding precipitation pattern showing positive anomalies over Gabon, Congo and southern Cameroon as well as West Africa. The patterns clearly confirm the links described in the previous section between boreal summer SSTs and precipitation in the regions *Gabon (5)* and *Cameroon (6)* as well as the well-known link to *W-Africa (7)*. Furthermore, it is evident that the influence of SST anomalies on boreal summer precipitation is not limited to West Africa, but affects the whole coastal region between Liberia and Gabon. Another interesting feature is the positive link to southeast African rainfall. Although not further discussed, the latter region is also included in one of the seasonal rainfall response types classified by Camberlin et al. (2001). Moreover, when analyzing the same month for SST pattern and precipitation lags 1-2 months (i.e. July–September and August–October seasons), a positive link to west South African precipitation appears (not shown), which also confirms the results of bivariate correlation analyses. Note that these patterns do not show the above-described connection to *Gabon (5)* and *Cameroon (6)*. The latter patterns therefore resemble the patterns derived by maximum covariance analysis for the shorter period 1979–2002 described in Polo et al. (2008).

The second example (Figure 6.3 (b)), i.e. the first pair of December–January patterns, represents the positive connection of tropical southeast Atlantic SSTs and *N-Angola (4)* precipitation. The precipitation pattern also shows anomalies reaching into the African continent as far as the east coast and confirms previous findings (e.g. Nicholson and Entekhabi 1987). Furthermore, this pattern also indicates a weak positive link to *Gabon (5)*

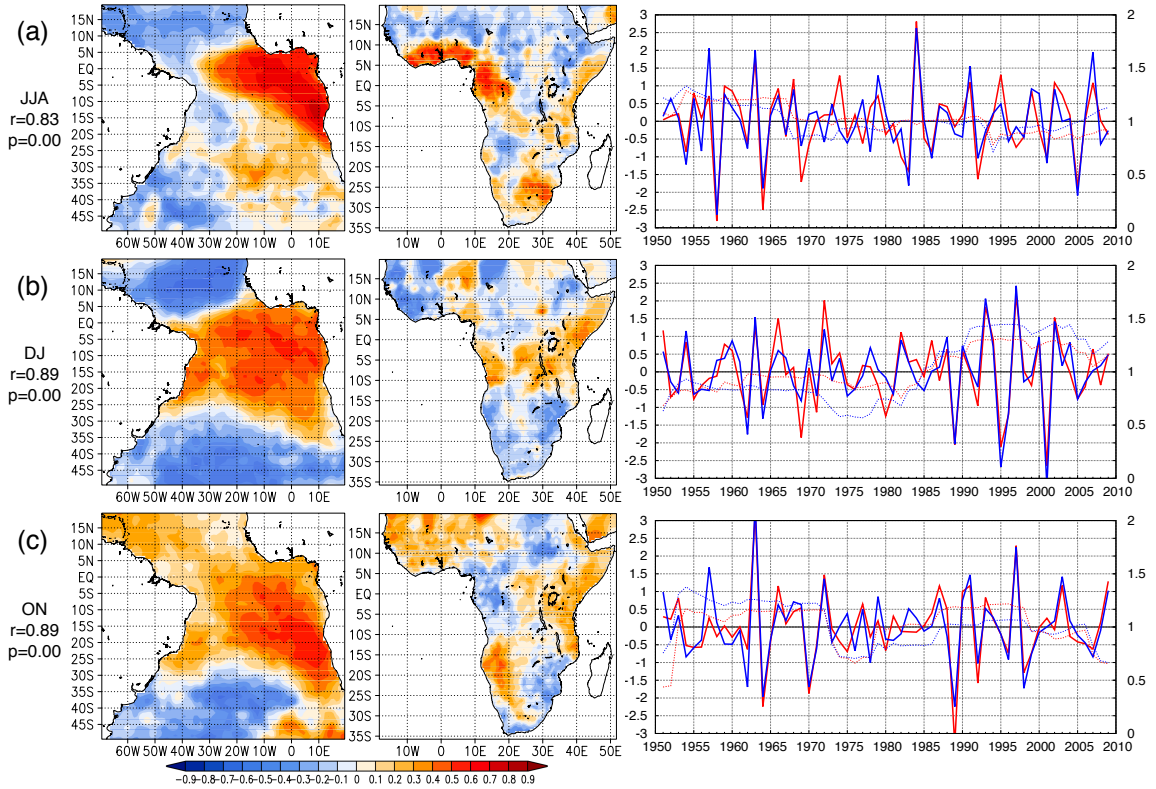

Figure 6.3: The first CCA patterns (CCPs) for south Atlantic SSTs (left column) and sub-Saharan African precipitation (middle column) for the period 1951–2010, corresponding SST (red) and precipitation (blue) canonical scores (time coefficients, right column, solid curves, left axis), and 20-year running standard deviations (dotted curves, right axis). Rows depict examples of JJA (a), DJ (b) and ON (c) seasons. For each example canonical correlation coefficients r and levels of significance p are given.

and *Cameroon (6)* and a weak negative link to *Guinea (8)*.

The third example (Figure 6.3 (c)) depicts the first pair of October–November CCPs, which capture the negative link between tropical southeast Atlantic SSTs and precipitation in *WS-Africa (1)* already described in the bivariate correlation analyses. Although no time lag was applied in this example, this pair of patterns also represents the positive link to Namibian precipitation described earlier.

The corresponding canonical scores of the three pairs of patterns (right column in Figure 6.3) additionally include information about specific years including warm and cold water events. In Figure 6.3 (a) for warm water events such as 1963, 1966, 1968, 1984 and 1995, anomalies are positive, whereas negative values occur in cold water events, e.g. 1958, 1964, 1983 and 2005. Canonical scores of the latter two examples also include positive peaks e.g. in 1963 and 1966, but negative anomalies are found for the warm events 1984 and 1995. This is due to the fact that some of the events are short and do not last throughout all seasons. Furthermore, CCA patterns may cover areas with a different precipitation response to the same events.

The time series plots in Figure 6.3 also contain the 20-year running standard deviations (*rsd*) of the CCA scores. As can be seen from both the scores and their corresponding *rsd* time series, pattern strength (amplitude) and also the frequency of a change in polarity

vary over time. Changes are rather moderate in the first example (Figure 6.3 (a)). In contrast, in the second example (Figure 6.3 (b)) a higher *rsd* indicates a stronger amplitude after the 1980s with both strong positive and negative modes. Multi-decadal changes in amplitude and frequency are also visible in the third example. These non-stationarities will be discussed in more detail in the following section.

6.3.3 Non-stationarities in the SST-precipitation link in selected regions

To assess non-stationarities in the link between Atlantic SSTs and coastal rainfall before and after the so-called *climate shift* in the second half of the 1970s (Miller et al. 1994), cross-correlation analyses discussed in Section 6.3.1 are additionally carried out for the two 30-year sub-periods 1951-1980 and 1981-2010 and tested for significant differences using a Fisher z-transformation. Furthermore, running 30-year correlations are calculated for all 3-months seasonal sections. From these results it can be concluded that the general pattern remains similar before and after the climate shift. But results also point to changes in specific seasons for some regions. Running correlations for the two most remarkable examples are shown in Figure 6.4.

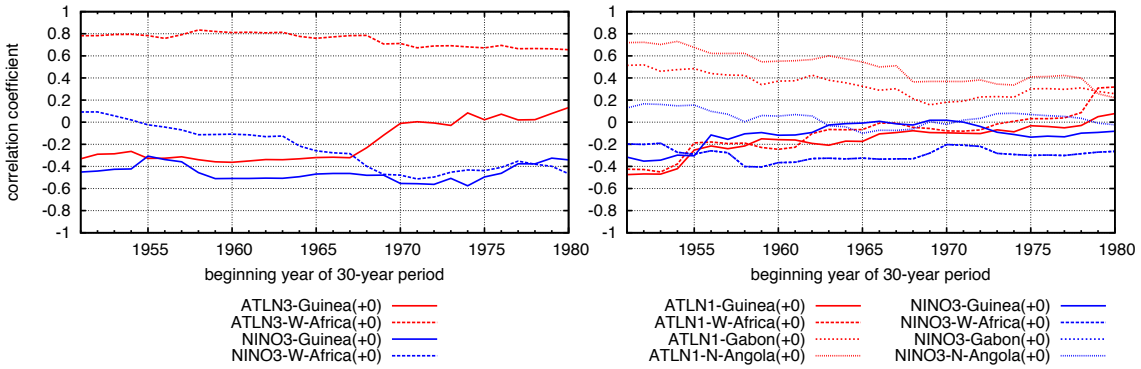

Figure 6.4: Examples of 30-year running correlation coefficients between 1951 and 2010 for selected SST and precipitation indices. **Left:** July–September (lag 0) ATLN3 (red) and Niño3 (blue) indices correlated with *Guinea* (solid curves) and *W-Africa* (dashed curves). **Right:** March–May (lag 0) ATLN1 (red) and Niño3 (blue) indices correlated with *Guinea* (solid curves), *W-Africa*, *Gabon* and *N-Angola* (curves with different dashed types). The beginning year of a 30-year period is displayed on the x-axis. Confidence levels: 90 % for $r > 0.32$, 95 % for $r > 0.38$ and 99 % for $r > 0.50$

The first example (left plot in Figure 6.4) shows results for the July–September season in *Guinea (8)* and *W-Africa (7)*. While the link between ATLN3 SST and *W-Africa (7)* precipitation is stationary for the whole period, correlation coefficients collapse for *Guinea (8)* after 1965. At the same time, significant negative correlation coefficients appear between the Niño3 index and *W-Africa (7)*. These changes coincide with the appearance of a significant anti-correlation between the Atlantic and Pacific Oceans as reported in Rodríguez-Fonseca et al. (2009). These results are similar to the findings for the Sahel region (e.g. Mohino et al. 2011b, Rodríguez-Fonseca et al. 2011, Losada et al. 2012). *Guinea (8)*, located at the western edge of the Sahel, still seems to be affected by the competing effects of the Atlantic and Pacific Oceans described in these studies. Positive SST anomalies in

the Atlantic Ocean are associated with a southward shift of the ITCZ and thus cause negative precipitation anomalies over the Sahel. By contrast, negative Pacific SSTs contribute to the establishment of anomalous convergence over West Africa and thus an increase in rainfall over the Sahel. Due to the anti-correlation between the Atlantic and Pacific Oceans after the 1970s, these two effects are now competing and their combination leads to a cancellation of each other. Although *Guinea (8)* is not a typical Sahel region and results differ from these studies for May and June, similar processes appear to affect this region in July to September.

The second example (right plot in Figure 6.4) depicts running correlation coefficients for the March–May season in *Guinea (8)*, *W-Africa (7)*, *Gabon (5)* and *N-Angola (4)*. Here the ATLN1 index is selected instead of ATLN3 due to its stronger connection to *Gabon (5)* and *N-Angola (4)* (see Figure 6.2). The relationship to the tropical Atlantic SSTs gradually weakens and becomes insignificant in both the regions north and south of the equator. In contrast, no significant changes are found for the correlations with the Niño3 index, which are generally weak. Still, it is worth mentioning that a similar anticorrelation between Atlantic and Pacific SSTs - as it is seen in boreal summer months - also appears in spring months in recent decades although developing more continuously. One may speculate that the position and strength of the ITCZ are influenced by counteracting processes in a similar way as in boreal summer, but further analyses are necessary to investigate this in more details. However, this lies beyond the scope of this work.

6.4 Impact of Atlantic Niño and Niña events on African west coast precipitation

As discussed in Section 6.3, co-variability in a certain month or season does not necessarily indicate a symmetric response and thus an impact of both warm and cold water events on precipitation. Therefore, to analyze the specific impact of both of them on African west coast precipitation, Atlantic Niño and Niña composites of rainfall anomalies for time lags of 0-4 months (precipitation lagging SSTs) are computed for the eight precipitation regions. These composites (and all others in this chapter) are computed separately for each month or season and include all months classified as Atlantic Niño or Niña month in the period 1951–2010. That means, they include all event sub-types as classified and described in Section 5.5 and summarized in Table 5.1 (p. 51). Monthly frequencies of warm and cold events , which correspond to the composite sample sizes, vary between 6 and 14; the exact numbers can be taken from Figure 5.17. Note that numbers for 1951–2010 and 1951–2012 are identical except for a difference of 1 month in December, January and February for Atlantic Niñas. The cold event in 2011 occurred outside the considered time period.

As most composite results are significant at the 95 % level (for details on compositing and significance testing see Section 4.2) at lags 0 or 1 and differences between results of the latter are small, Figure 6.5 only summarizes results for lag 0. For the remaining lags significant results are discussed in the text.

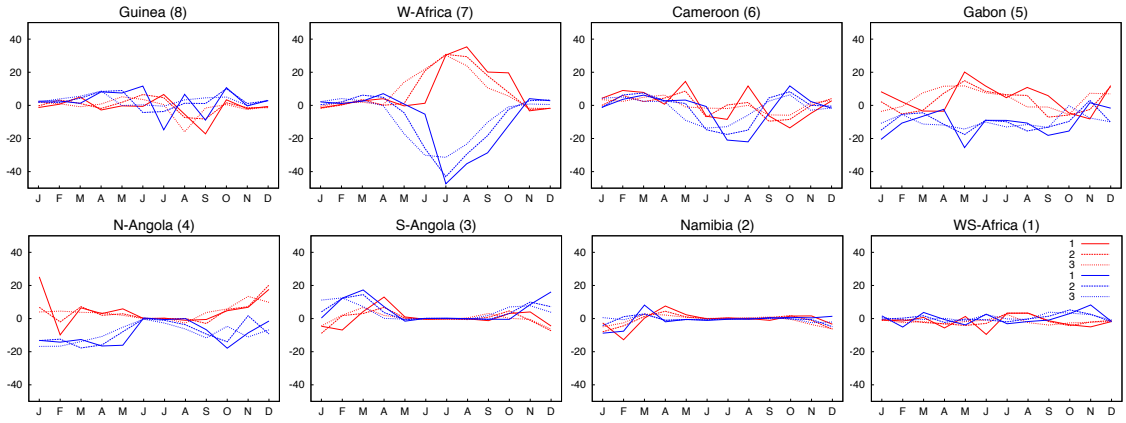

Figure 6.5: Atlantic Niño (red) and Niña (blue) composite mean values of rainfall anomalies for all 1- to 3-month seasonal sections (line type) for the selected eight precipitation regions. All Niño and Niña sub-types are included in the composites. The x-axis denotes the central month, e.g. the FMA season is plotted at the position of central month M. Only lag 0 results are displayed.

For the *Guinea (8)* region, a significant warm water impact is only found in March, which is still in the dry season. Precipitation appears to be increased during Atlantic Niños. Cold water events are associated with an increase in boreal winter and spring months except for March. The maximum increase is found in the April–July season, when the annual rainfall amounts are already higher than in the drier winter months. This is also the season where the ATLN SST indices and the Guinea (8) precipitation index are correlated at their maximum ($r \leq -0.38$) as described in Section 6.3.1.

Consistent with the results of bivariate correlation analyses presented in Section 6.3.1 and that of previous studies (e.g. Reason and Rouault 2006), warm (cold) water events significantly contribute to an increased (decreased) boreal summer and early autumn precipitation in *W-Africa (7)* at time lags of 0 or 1 months. Remarkably, in July the mean decrease (-47.3 mm) during Niña events is more pronounced than the increase (+30.4 mm) during Niño events. Furthermore, Niño composite peak values tend to lag the Niña composite peaks by one month. As discussed in Section 5.6, the distribution of monthly frequencies and also onset months (Figure 5.17) is not quite symmetric. Therefore, the asymmetric rainfall response may either be an artifact of the ATLN event classification or a real asymmetry due to the fact that cold events start earlier and thus atmospheric conditions favorable for decreased precipitation build up earlier resulting in a stronger impact. Unfortunately, sample sizes are too small to proof the latter assumption. Still, this is an interesting observation that should be further explored in future work.

In *Cameroon (6)* a significant increase in precipitation during warm water events is observed in boreal winter months December–January. For cold water events, there is a significant decrease in boreal summer months June–September.

In *Gabon (5)* significant results are found almost throughout all seasons. Warm water events contribute to a significant increase in precipitation in boreal spring and summer months with composite peaks in April-June and July–September seasons. Cold water events contribute to an even stronger decrease from May (-25.5 mm) throughout September and also in boreal winter months December–February.

For *N-Angola (4)* warm and cold water impacts not only differ in magnitude but also in season. While Niño events mainly contribute to an increase in austral summer rainfall in December and January, for Niña events a significant decrease can be observed throughout January to May and also in austral autumn months with a maximum mean decrease of 17.9 mm in October.

During warm water events June–July, rainfall is increased in *S-Angola (3)* and April–June rainfall in *Namibia (2)*. In both regions there is also an increase in November at lag 3-4 (not shown). For cold water events, significant increase is found for *S-Angola (3)* in March as well as a decrease in Namibia in the 2-months seasonal sections December–January and January–February (lag 2-4).

In *WS-Africa (1)* warm water events are associated with an increase in August precipitation (lag 4) and a decrease in November (lag 0-3). During cold water events an increase in October–November precipitation as well as a decrease in February is observed.

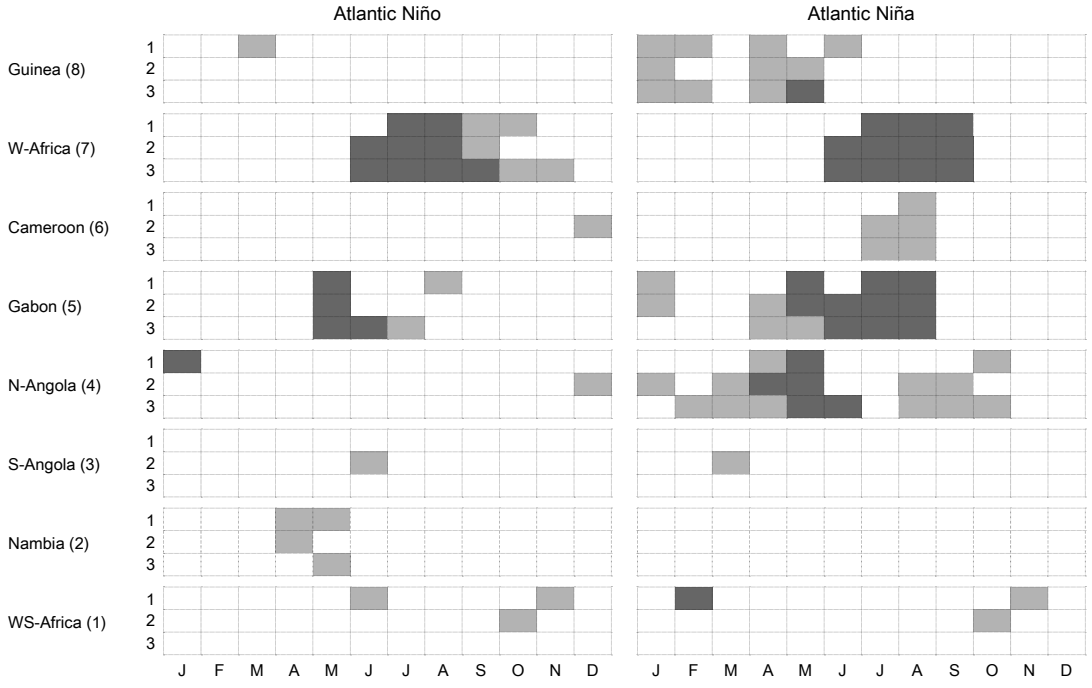

Figure 6.6: Significance of Atlantic Niño and Niña composites for all precipitation regions and 1- to 3-month seasonal sections. 99 % (dark grey) and 95 % (light grey) levels are displayed.

Figure 6.6 shows significance of all lag 0 composite means displayed in Figure 6.5 and described above. It summarizes all results being significant at 95 % (light grey boxes) and 99 % (dark grey boxes) levels. Thus, it can be concluded that both warm and cold water events have a significant impact on African west coast rainfall throughout the year. The main influence forms a cluster in both Atlantic Niño and Niña composites. These two clusters are concentrated on the months of May throughout November and the tropical regions *Gabon (5)* and *W-Africa (7)*. But there are also significant results in the remaining seasonal sections and coastal regions. The figure also reveals that cold water impacts are more extensive, affecting more seasons.

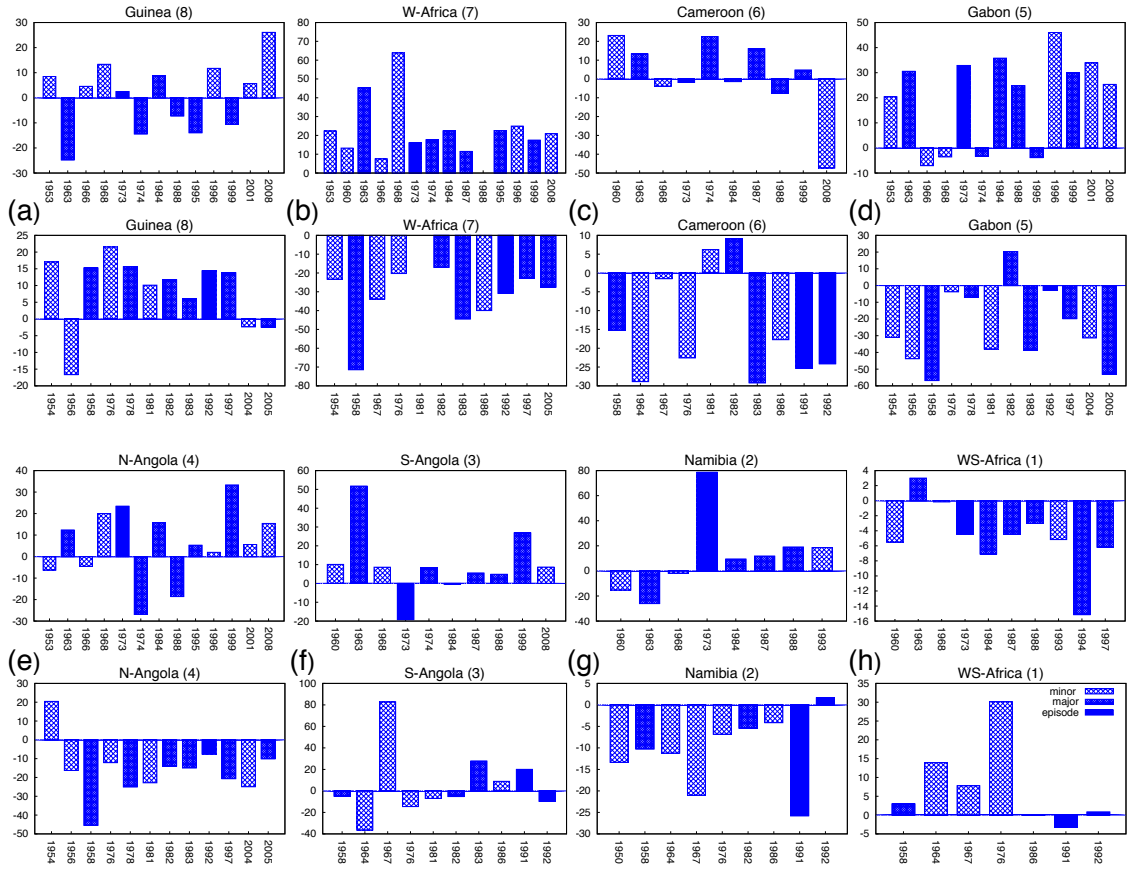

Figure 6.7: Precipitation anomalies in Atlantic Niño or Niña years for selected seasonal sections and time lags. Each example (a–h) consists of both Atlantic Niño (upper plot) and Niña (lower plot) years. Only seasonal sections that were part of an event are shown. The sub-types major event, minor event and episode are indicated with different fill styles. Lag is 0 if not specified. The selection includes the following examples: Guinea (8) AMJ, W-Africa (7) JJA, Cameroon (6) AS, Gabon (5) May, N-Angola (4) May, S-Angola (3) Nov lag 3 (i.e. Jul SST), Namibia (2) JF lag 4 (Sep SST), WS-Africa (1) Nov lag 1 (Oct SST).

For a closer look at specific event years that are included in the composites discussed above, precipitation anomalies for all event years are plotted for all regional indices, seasons and time lags. Figure 6.7 displays an example of each region where a significant increase or decrease is observed in either Niño or Niña years or both. In all cases, both cold and warm composite members are shown.

The first example depicts April–June precipitation anomalies in *Guinea (8)*. While there is apparently no response to warm events, in the cold case this region shows a clear increase in 9 out of 12 events with an average of 8.7 mm. Negative anomalies are found for three years, 1956, 2004 and 2005. An explanation for these exceptions can be seen in the SST indices (not shown). The minor event 1956 was mainly centered on ATLN1 and ATLN2 index regions, whereas values of ATLN3 index do not exceed the threshold in the months April and May. A similar situation is true for minor event 2004. For major event 2005, the time lag between onset in ATLN1 and ATLN3 causes the missing precipitation response. While the events' peak is already visible in ATLN1 around May and June, it appears delayed in ATLN3 in July–August. For April and May, this region is even

still warmer than average. This shows that although the region is still clearly influenced by the tropical eastern Atlantic SSTs, the precipitation response is very sensitive to the actual temperatures. Due to the more distant location to the main warming center, it mainly depends on the influence of ATLN3 SST.

In *W-Africa (7)* SST anomalies contribute to anomalous June–August rainfall in all events in both Niño and Niña years, notwithstanding the event type. Only for 1981 and 1988 no response was found. This again confirms the strong link between SSTs and rainfall in this region discussed in the previous sections. In *Cameroon (6)* there is no clear rainfall response in warm events, whereas a decrease is observed in all Niña years except for 1981 and 1982. This cannot be explained by an analysis of the SSTs alone. As explained earlier, the region is rather complex and orographic effects as well as local convection modify its precipitation response to SST anomalies. Furthermore, atmosphere dynamics associated with specific events may play an important role in this case. Possible processes are further discussed in Section 6.5.

Similar to the *W-Africa (7)* region, *Gabon (5)* shows a systematic response to both warm and cold water events in May with an increase in precipitation in the former and a decrease in the latter. In the same month, anomalous cooling contributes to a decrease in *N-Angola (4)*, but warming has no clear effect. For the remaining examples, November rainfall (lag 3) in *S-Angola (3)*, January–February (lag 4) in *Namibia (2)* and November rainfall in *WS-Africa (1)*, the response is rather asymmetric and thus mainly found in the warm or cold case.

Overall, there is no clear dependency of the magnitude of precipitation response on the Atlantic Niño subtype. That means, although one might expect major events to be associated with a stronger increase or decrease in precipitation than minor events, this is not the case. However, as described above, in most cases it is not important if a minor event is centered on one or the other ATLN region. This is an important finding, as previous studies (e.g. Rouault et al. 2003) mainly focused on events off the Angolan coast. Results presented in this work emphasize that both equatorial and the coastal southeast Atlantic SSTs contribute to rainfall along the Atlantic coast. Therefore, Atlantic and Benguela Niños should not be considered as separate phenomena in impact analyses. This confirms the conclusion drawn from Chapter 5, that the two Niño types may better be perceived as one.

Summarizing the findings discussed above, composite analyses of Atlantic Niño and Niña events lead to two important conclusions. First, if an increase or decrease in rainfall in a specific region and season is found for warm water events, the opposite is not necessarily true for cold water events. This is the case e.g. for boreal summer months in *Gabon (5)* and *Cameroon (6)*. Second, an increase (decrease) in warm (cold) events does not always occur at the same magnitude. In some cases cold water impacts are more pronounced than warm water ones, e.g. in *Gabon (5)* and *W-Africa (7)*, or vice versa. To exclude a possible bias as a consequence of high-pass filtering, results of filtered and unfiltered data were compared. Unfiltered data composites indeed confirm the two effects described above.

6.5 Associated atmospheric dynamics

In the previous section significant impacts of Atlantic warm and cold water events on rainfall in African west coast regions have been discussed. To address the question, which mechanisms possibly contribute to an increase or decrease in specific months or seasons, a closer look at the overlaying atmospheric dynamics is necessary.

As was already briefly discussed in Section 6.2, the complex climatology of sub-Saharan Africa is mainly dominated by the position and intensity of three circulation systems. That is from north to south: (1) the intertropical convergence zone, (2) the southern subtropical highs (Indian and South Atlantic anticyclones) and the associated south-easterly trade winds as well as (3) the mid-latitude westerlies with their extra-tropical cyclones at the southern tip of the continent. Southward movement in austral summer months and northward movement in winter months of these three systems cause the typical seasonal rainfall variations in different regions (for further details see Buckle 1996, Preston-Whyte and Tyson 1989). Rainfall variability is therefore also sensitive to any anomalous displacement or intensity of one of these systems. In addition, positive (negative) SST anomalies act to increase (decrease) atmospheric instability and therefore further contribute to anomalous rainfall (Hirst and Hastenrath 1983).

To analyze changes in the atmospheric conditions during Atlantic Niño and Niña events, composites of monthly mean moisture flux convergence and precipitation were calculated (see Figures 6.8 to 6.11). SST composites provide additional information about the monthly mean extent of warming or cooling in the southeast Atlantic. Starting at the beginning of the year - in austral summer - the most remarkable changes in precipitation during Niño and Niña events are discussed below.

Figures 6.8 and 6.10 show that during Niño events in December and January, moisture flux into the Angolan low is weakened, whereas low latitude westward moisture flux from the Indian Ocean far into the continent is increased, contributing to an increase in precipitation along the Angolan coast. As suggested by Gimeno et al. (2010) and Gimeno et al. (2012), terrestrial regions such as tropical southern Africa (also termed as Winter Africa (WAF) in Gimeno et al. 2010) and the Sahel region also serve as moisture sources in addition to oceanic ones. Water precipitated onto land is again partially available for evaporation and can therefore contribute to rainfall variations in a secondary way. Although WAF serves as a moisture source preferably in austral winter, weakened convergence and small shifts in source and sink regions may also add to a change in regional rainfall patterns. At the same time the low-level southwest monsoonal flow (850 hPa level, not shown) into Gabon and Cameroon is enhanced causing increased rainfall in the latter regions. During Niña events the situation is not completely inverse (Figures 6.9 and 6.11). There is no significant change in the influence of the Indian Ocean, while the southwest monsoon appears to be weakened. Therefore, the southern Angolan region is not significantly affected, whereas Gabon receives less rainfall.

In boreal spring months February to April, Rouault et al. (2003) found that the increase in Angolan and Namibian precipitation is greatest when westward moisture flux from

the Indian Ocean is strengthened and the southeasterly flux away from the southeast Atlantic coast is weakened. Local evaporation as well as enhanced atmospheric instability over the southeast Atlantic further contribute to increase precipitation, but they are not considered to provide the dominant source of moisture. In contrast, Hermes and Reason (2009) emphasize the possibly stronger influence of enhanced moisture advection from the Atlantic Ocean. Therefore the southeast Atlantic serves as an additional moisture source, although in a less dominant way than the Indian Ocean. The present composite results suggest that both processes are important but that the prevailing influence also depends on the month considered. In March the influence of the Indian Ocean is present but does not appear to be significantly strengthened. Therefore the above-average rainfall in the northern regions may be mainly caused by a weakened southeasterly moisture flux away from the coastal regions. In April enhanced southeasterly flow from the Indian Ocean into the southern part of the continent contributes to precipitation anomalies that extend further south.

In May enhanced southwesterly flow from the Atlantic into central Africa increases rainfall along the coast of Gabon and southern Cameroon in Atlantic Niño years, whereas precipitation along the West African coast is reduced. Reason and Rouault (2006) suggest that this may be due to stronger convection over Angola at the expense of the developing convection over West Africa, but they do not further discuss this feature. In the present study, results show enhanced flow into the Angolan low and reduced moisture flux towards the West African coast during Niño events, while the reversed case in Niña years leads to an even more pronounced and significant decrease in precipitation (see also Figures 6.8 and 6.9).

Boreal summer months June–September have already been discussed intensively in the literature. A warmer than normal southeast Atlantic associated with a southward displacement of the ITCZ contributes to enhanced moisture flux into West Africa and stronger convection. This causes increased precipitation along the Guinean coast (e.g. Reason and Rouault 2006). The inverse is true for the cold SST case. Results depicted in Figures 6.10 and 6.11 clearly reflect these changes in the boreal summer monsoon and thus confirm previous studies. Interestingly, the area significantly affected by the decrease in Atlantic Niña years appears to be larger than that showing increased precipitation in Niño years.

For austral spring months, the focus is now moved to South Africa. Here, in October and November in Atlantic Niño years, the South Atlantic Anticyclone as well as the mid-latitude westerlies appear to be displaced to the south and weakened. As a consequence, South Africa receives below-average rainfall. In contrast, during November in Niña years when the anticyclone and the westerlies appear to be shifted northward, enhanced southwesterly flow towards the South African coast increases rainfall. These results agree with earlier studies, which found that wet and dry austral summers over subtropical southern Africa are linked with latitudinal shifts of the mid-latitude westerlies (Vigaud et al. 2009).

It can be concluded that warm and cold water events in the southeast Atlantic Ocean are accompanied by changes in the overlaying atmospheric circulation that contribute

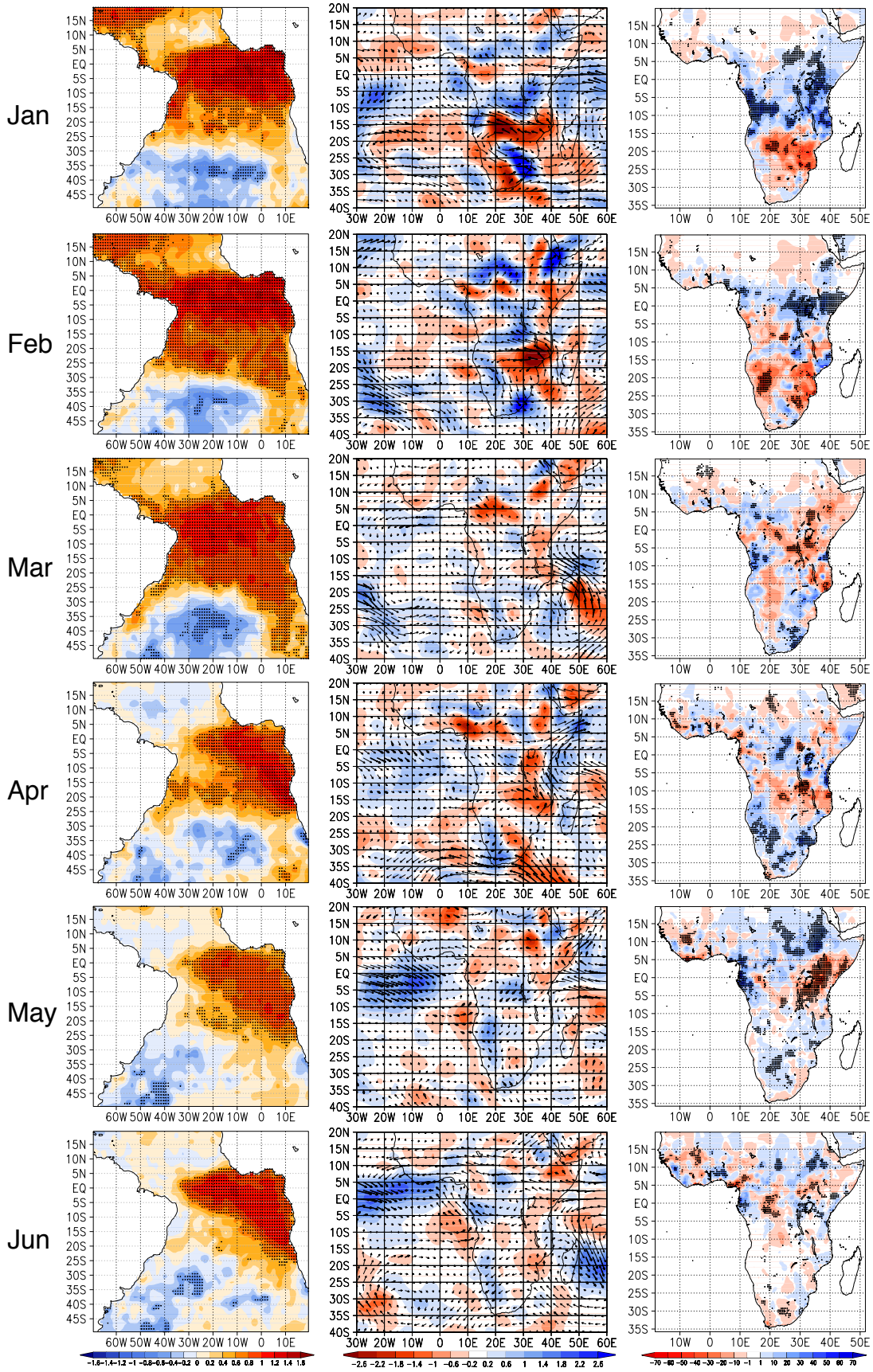

Figure 6.8: Monthly January to June Atlantic Niño (all types) composites for high-pass filtered standardized SST, high-pass filtered moisture flux convergence ($g\ kg^{-1}\ m\ s^{-1}$) and precipitation (mm). Significant values (95 % level) are highlighted with symbols (SST and precipitation) or bold arrows (moisture flux convergence).

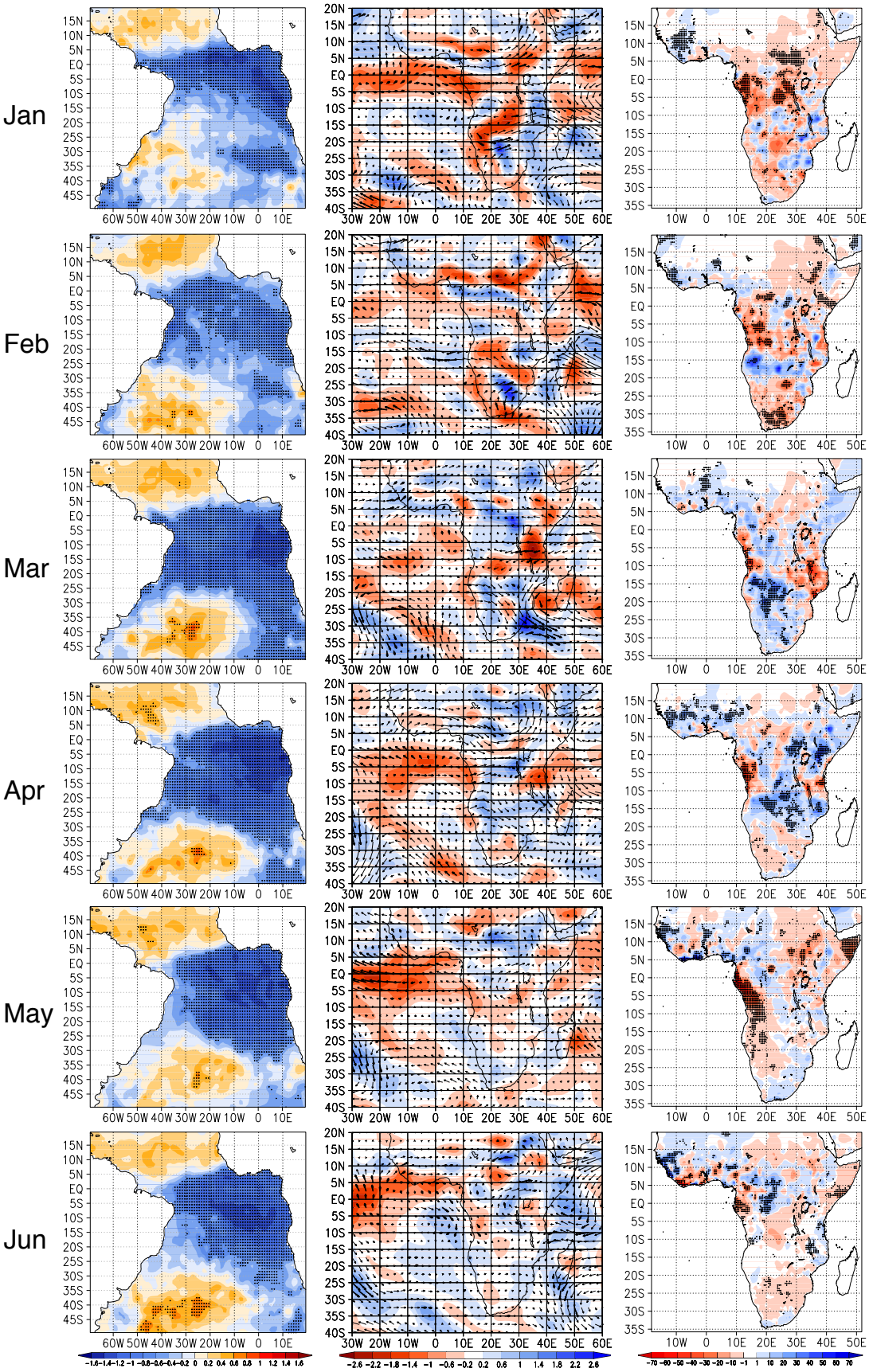

Figure 6.9: Same as Figure 6.8 but for Atlantic Niña composites.

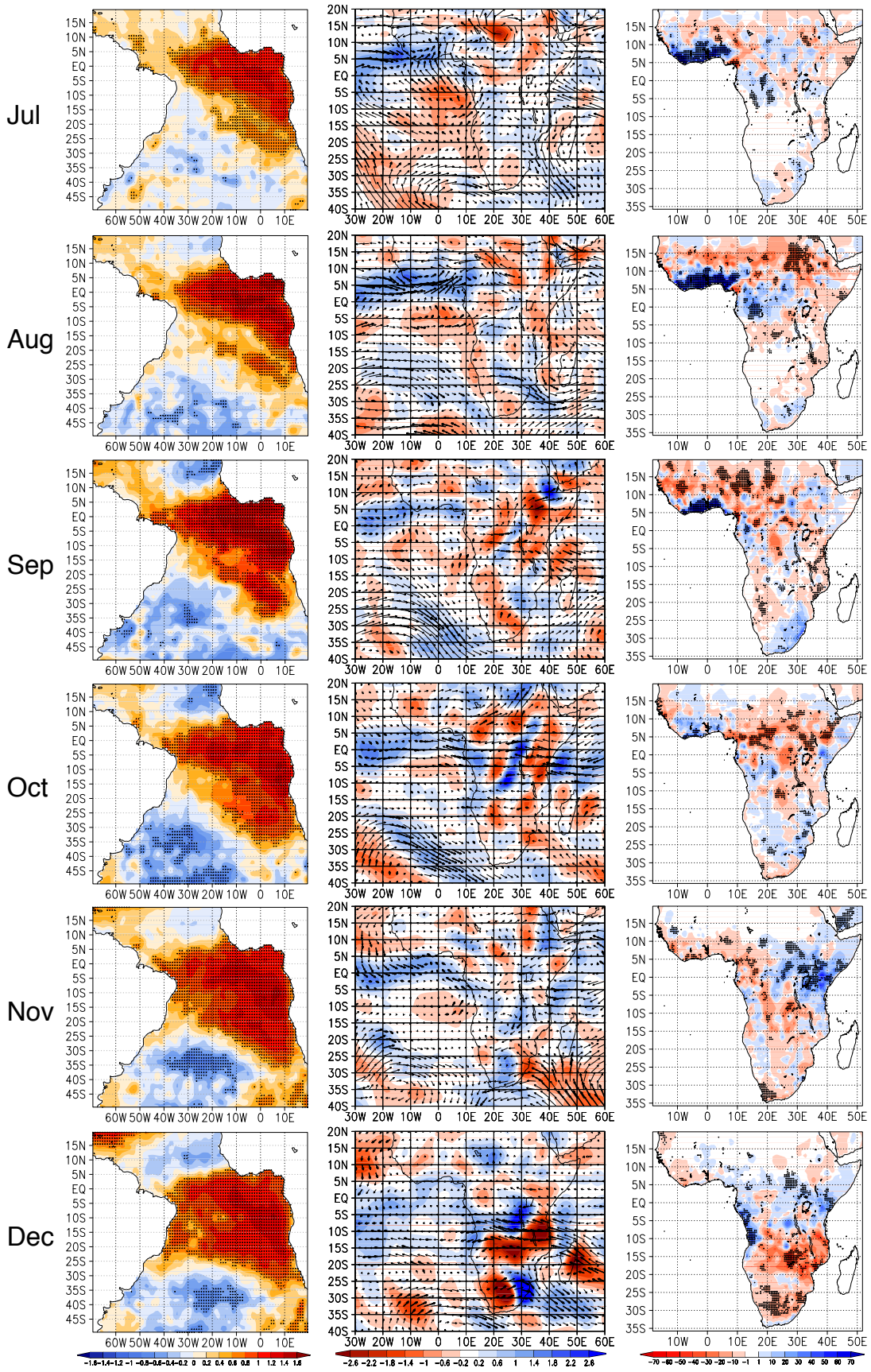

Figure 6.10: Monthly July to December Atlantic Niño (all types) composites for high-pass filtered standardized SST, high-pass filtered moisture flux convergence ($g\ kg^{-1}\ m\ s^{-1}$) and precipitation (mm). Significant values (95 % level) are highlighted with symbols (SST and precipitation) or bold arrows (moisture flux convergence).

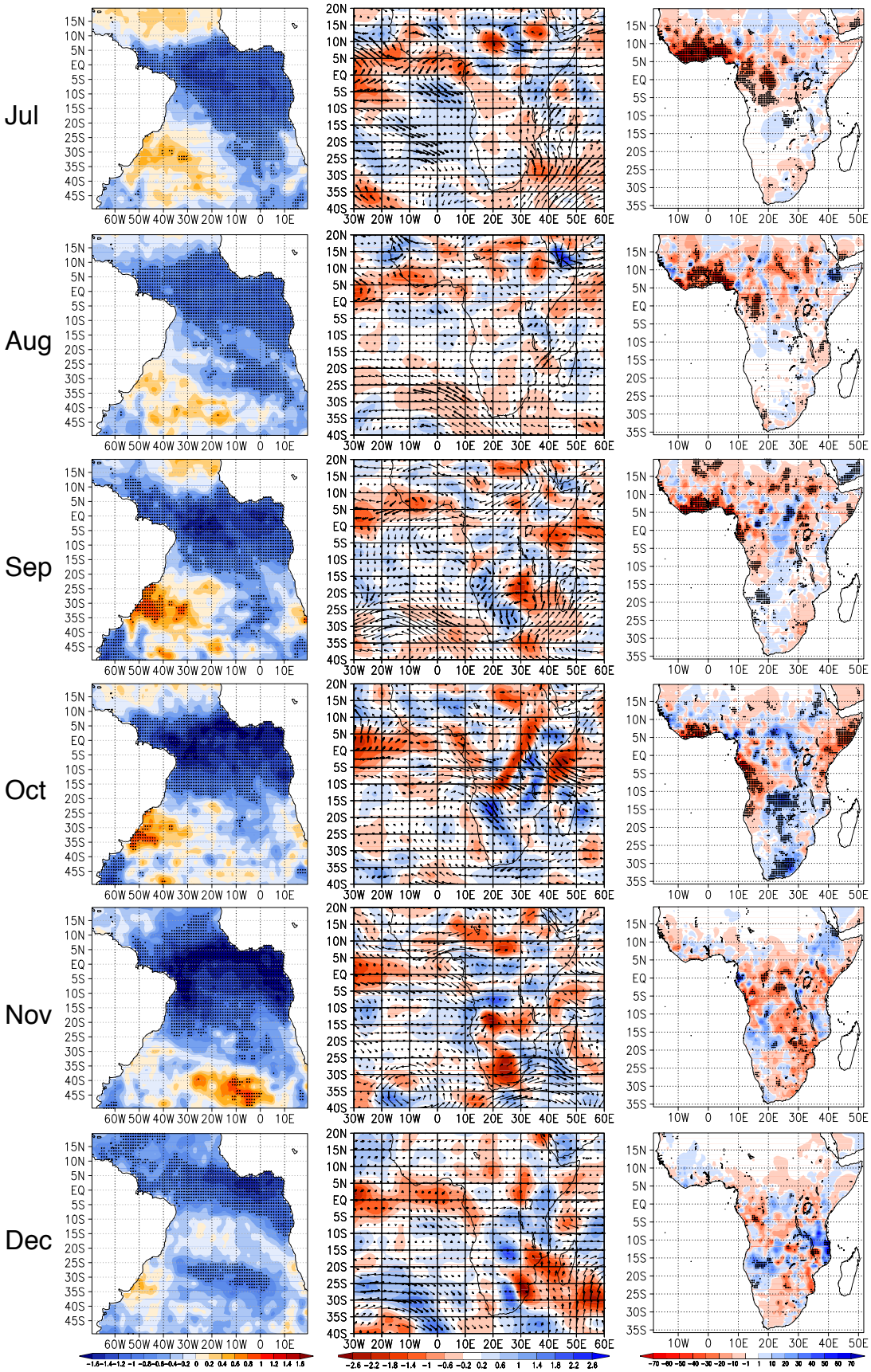

Figure 6.11: Same as Figure 6.10 but for Atlantic Niña composites.

to rainfall anomalies over different regions along the African Atlantic coast in different ways. In the northern regions, anomalous rainfall is caused by changes in the strength of the monsoonal flow, moisture transport from the Atlantic and local convection. All these factors are dependent on the position and intensity of the ITCZ. In the southern part of the continent, a modification of the location and strength of the southern hemispheric anticyclones as well as moisture transport from the Indian Ocean contribute to modified rainfall patterns. In this context, the Atlantic Ocean plays a less dominant role as moisture source. In addition, changes in local evaporation and atmospheric stability also contribute to anomalous rainfall. Therefore the northern regions are directly connected to the events via moisture transport from the Atlantic, whereas the southern regions are indirectly connected to the events through changes in the overlaying large-scale circulation.

6.6 Summary

In this chapter links between southeast Atlantic SST and African west coast precipitation variability have been extensively studied using correlations analyses and CCA. Furthermore, the impact of warm and cold water events (as defined in Chapter 5) on coastal precipitation as well as associated atmospheric dynamics have then been discussed in detail based on composites.

Results show that links between southeast Atlantic SSTs and precipitation are present throughout the year on a monthly or seasonal time scale. Depending on the season considered, several regions along the African west coast are subject to rainfall anomalies during warm and cold water events. A significant impact on precipitation is not limited to major warm or cold water events, but is also observed for minor events.

Furthermore, the rainfall response to Atlantic Niño and Niña events may be asymmetric in season or magnitude in some regions. In several cases, it is stronger in the Niña case than it is in the Niño case.

As can be concluded from the composite analyses, changes in the interacting atmospheric circulation during warm and cold water events lead to particular rainfall anomalies in different regions along the African Atlantic coast. The northern regions are directly connected to the events via enhanced or weakened moisture transport from the Atlantic, which is dependent on the intensity of the monsoonal flow towards the continent. In contrast, the southern regions are indirectly connected to the events through changes in the location and strength of the southern hemispheric anticyclones as well as the moisture transport from the Indian Ocean.

Results also reveal that not all of the links between SSTs and precipitation are stationary over time. A detailed study of these non-stationarities is beyond the scope of this thesis but should be subject of future work.

7

Teleconnections of the tropical Atlantic to the tropical Pacific and Indian Oceans

The previous chapter has given an insight into regional impacts of warm and cold water events in the tropical southeast Atlantic. This chapter now discusses interactions on global scale, i.e. the teleconnections between the tropical Atlantic Ocean and the tropical Pacific and Indian Oceans. An introductory Section 7.1 summarizes previous work on teleconnections between the three tropical oceans. The subsequent Section 7.2 focuses on the interactions between the Atlantic and Pacific Oceans. In the first part of this section (Section 7.2.1), a general overview of the co-variability of the two oceans is given. The second part (Section 7.2.2) describes a case study of selected Atlantic and Pacific warm and cold events. Furthermore, Section 7.3 discusses teleconnections between the Atlantic and Indian Oceans taking into account the close connection between the Pacific and Indian Oceans. After an analysis of co-variability including and excluding the Pacific influence, the remaining sections describe the links of the tropical Atlantic to the two main modes of Indian Ocean SST variability, namely the basin-wide mode (Section 7.3.3) and the Indian Ocean Dipole (Section 7.3.4).

7.1 Introduction

The term *teleconnection* refers to the linkage of climate anomalies over great distances, which are seemingly unrelated. According to Liu and Alexander (2007), the term itself is assumed to be first used by Ångström (1935) in the context of an analysis of the North Atlantic Oscillation (NAO). As discussed in Philipp (2003) and Liu and Alexander (2007), earlier studies refer to teleconnections as simultaneous correlations between temporally fluctuating meteorological variables. However, for climate prediction and other purposes, it is useful to include temporal lags or other relevant components of the climate system, such as the ocean. That way, a more generalized concept of teleconnection is received.

Teleconnections are fed by atmospheric and oceanic energy transports and wave propagation. The atmosphere thereby acts like a *bridge* between different parts of the ocean whereas the ocean acts like a *tunnel* connecting different parts of the atmosphere (Alexander et al. 2002, Liu and Alexander 2007). Almost all involved atmospheric processes are fast, reaching equilibrium within a season and being fully effective for climate variability on interannual or longer timescales. By contrast, oceanic processes vary on longer timescales and therefore only play an important role for very low-frequency climate variability (Liu and Alexander 2007).

In the tropics, changes in SSTs can force changes in convection and thus the Walker and Hadley circulations. Atmospheric Kelvin and Rossby waves and other involved processes transport the signal via the *atmospheric bridge* to remote regions in both the tropics and extratropics (Alexander et al. 2002, Liu and Alexander 2007).

Teleconnections between the tropical Atlantic and Pacific Oceans

Numerous studies have discussed the relationship between the tropical Atlantic and Pacific Oceans and have come to quite different conclusions concerning direction and sign of the response.

Due to the prominence of the ENSO phenomenon, in many studies a primary focus lies on the direction from the Pacific to the Atlantic, i.e. on the leading role of the Pacific Ocean. However, a robust response to Pacific warming is only found for the *northern tropical Atlantic* (NTA). Several studies (e.g. Hastenrath 1984, Saravanan and Chang 2000, Czaja et al. 2002, Huang 2002) show that during boreal spring, after the mature phase of a Pacific El Niño, a weakening of the northeast trade winds and an increase in SSTs can be observed in the NTA region. Furthermore, Ham et al. (2013a;b) recently suggested that NTA warm (cold) SSTs during boreal spring in turn may also serve as a trigger for Pacific La Niña (El Niño) events in the following winter.

In contrast, the response in the southern tropical Atlantic is still controversially discussed. While Latif and Grötzner (2000) and Lohmann and Latif (2007) find positive SST anomalies in the tropical southeast Atlantic Ocean in boreal summer in response to an ENSO warm event in the previous winter, Huang (2004) reports negative SST anomalies. Consistent with the observation that both Atlantic Niño and Niña may follow a Pacific El Niño, the two oceans are uncorrelated when the Pacific Ocean leads (Keenlyside and Latif 2007). According to Chang et al. (2006a), the inconsistent relationship between Pacific El Niño and the Atlantic Niño is a result of the *destructive interference* between atmospheric and oceanic processes in response to a Pacific warming. Namely these competing processes over the Atlantic basin are cooling produced by the Bjerknes feedback and tropospheric-temperature-induced warming (for a detailed description of the tropospheric temperature mechanism see Chiang and Sobel 2002, Chiang and Lintner 2005). A different mechanism is suggested by Lübbecke and McPhaden (2012) and Lübbecke (2013), that was originally introduced by Foltz and McPhaden (2010) to explain the interaction between the Atlantic meridional and zonal modes. As was already explained in detail in Section 5.1, the former authors propose a delayed negative feedback to El Niño,

which may be more or less dominant, and thus may either cause an Atlantic Niño or an Atlantic Niña.

On the other hand, recent studies have suggested that south Atlantic variability may also influence ENSO. Mélice and Servain (2003) are among the first to describe a link between south Atlantic variability and the Southern Oscillation. However, they do not yet provide a dynamical explanation. Wang (2006) further explores the connection between tropical Atlantic and Pacific Oceans using the ATL3 and Niño3 SST indices. Although this study finds no contemporaneous correlation, it demonstrates, that the two oceans are connected via an inter-basin SST gradient that is coupled to the overlaying atmosphere. Subsequent analyses, using both observational data (Keenlyside and Latif 2007, Polo et al. 2008) and model experiments (Jansen et al. 2009), do find significant correlations between the two oceans when the Atlantic leads by 6 months. Rodríguez-Fonseca et al. (2009) and Losada et al. (2010b) further explore the dynamical explanation for this anticorrelation. While the former analysis is based on both observational and model data, the latter uses an AGCM multimodel approach. Their results show that a boreal summer warming in the tropical southeast Atlantic is associated with an anomalous Walker circulation with a strengthened ascending branch over the tropical Atlantic and a descending branch over the central equatorial Pacific. Associated increased surface wind divergence and accelerated easterly trades over the latter ocean contributes to an eastward propagating shoaling of the thermocline. Furthermore, the Bjerknes feedback is active during the whole process and further acts to increase SST anomalies in the eastern Pacific. Altogether, this leads to an enhancement of the development of La Niña conditions. Due to this physical mechanism, an Atlantic warming in the 20th century might even have suppressed a Pacific warming (Kucharski et al. 2011). According to the results of Rodríguez-Fonseca et al. (2009), there is no significant connection between the Pacific and Atlantic Oceans before the late 1960s. The connection only establishes about a decade before the abrupt changes in the atmosphere-ocean system in the middle of the 1970s, also termed as *climate shift* (Miller et al. 1994). By contrast, Ding et al. (2012) report that a significant anticorrelation already exists before the 1970s with Atlantic SSTs leading by 9 months in their model results. In addition, they mention that the lead-lag relationship between Atlantic and Pacific SSTs in both observational and model data is also found in other seasons, but the authors do not find an explanation for these results.

Furthermore, Jansen et al. (2009), Frauen and Dommenget (2012) and Keenlyside et al. (2013) report that equatorial Atlantic variability potentially enhances El Niño prediction. Moreover, recent studies analyzing the representation of the Atlantic-Pacific teleconnection in CMIP5 simulations suggest their general capability of modeling this relationship. However, the models still show notable biases in both the Atlantic and Pacific Oceans. These biases lead to several differences of the modeled link compared to the observed one such as a weaker representation of the teleconnection and an incorrect frequency of co-occurring events (Richter et al. 2014, Kucharski et al. 2014, Ott et al. 2014).

Teleconnections between the tropical Pacific and Indian Oceans

Although this chapter mainly focuses on the teleconnections of the Atlantic Ocean to the Pacific and Indian Oceans, the relationship between the latter oceans themselves needs to be considered when analyzing teleconnections between the Atlantic and the Indian Oceans. As has already been discussed in Section 2.3, the Pacific and Indian Oceans are closely linked to each other via a tropical atmospheric bridge and thus via altered Walker and Hadley cells (e.g. see Figure 4 in Klein et al. 1999). Therefore, the first of the two main modes of Indian Ocean variability, namely the basin-wide mode, shows a robust response to ENSO. That is, the tropical Indian Ocean gradually warms during a Pacific warm event, reaching highest SST values approximately 3-6 months after El Niño peaks (e.g. Klein et al. 1999, Trenberth et al. 2002, Deser et al. 2010). For the second mode, the Indian Ocean Dipole, it is still controversially discussed whether it is ENSO-dependent or not. It is significantly correlated with ENSO in boreal autumn months, but IOD events can also occur independently (Schott et al. 2009, Roxy et al. 2011). For further details on the atmospheric dynamics of these modes and their response to ENSO see Section 2.3.

The eastward shift of the Walker circulation and the associated suppressed convection over the Indonesian Archipelago during a Pacific El Niño does not only result in increasing Indian Ocean SSTs. These changes also lead to a drier than normal Indian Summer Monsoon (ISM) during the summer season preceding an El Niño peak (Rasmusson and Carpenter 1983, Klein et al. 1999, Krishnamurthy and Kirtman 2003). However, the ENSO-ISM relationship has substantially weakened since the late 1970s (Krishna Kumar et al. 1999). This weakening has been attributed to a broad range of causes such as natural low-frequency variability, global warming, changes in the teleconnection patterns or the co-occurrence of ENSO and IOD events. A summary of these and other proposed hypotheses is given in Kucharski et al. (2007). The authors further suggest that tropical Atlantic SSTs may also modulate the ENSO-ISM relationship, which will be discussed in more detail in the next subsection.

Several recent studies have also investigated the reversed influence of the Indian Ocean on the ENSO system (e.g. Behera and Yamagata 2003, Annamalai et al. 2005b, Kug and Kang 2006). Model experiments suggest that interannual SST variability in the Indian Ocean increases ENSO variability modulating both amplitude (Yu et al. 2002) and period (Wu and Kirtman 2004). Furthermore, it is shown that El Niño is stronger with a co-occurring IOD while it is weaker when a basin-wide warming co-occurs (Annamalai et al. 2005b; 2010). Moreover, El Niño decays more rapidly following an IOD (Kug and Kang 2006). Dommenget et al. (2006) point out that the interpretation of such results is rather difficult due to the primary forcing of ENSO on the Indian Ocean SST. However, from their modeling results they also conclude that an improvement of ENSO predictions is likely when both the tropical Indian and Atlantic Oceans are considered.

In summary, it can be concluded that the two main modes of Indian Ocean variability, namely the basin-wide mode and the IOD, both depend on or interact with the ENSO system to some extent. Therefore, subsequent analyses of the relationship between the Atlantic and Indian Oceans have to be carried out with respect to the interaction between Indian and Pacific Ocean SST variability.

Teleconnections between the tropical Atlantic and Indian Oceans

Concerning teleconnections between the Atlantic and Indian Ocean basins, most studies have focused on the Indian Summer Monsoon (ISM) so far. In boreal summer, south tropical Atlantic SSTs are significantly correlated with rainfall over the Indian peninsula (Kucharski et al. 2007; 2008, Yadav 2008, Rajeevan and Sridhar 2008) and are further shown to contribute to the modulation of the ENSO-ISM relationship (Kucharski et al. 2007). The physical mechanism proposed to explain the ISM response to south tropical Atlantic SST anomalies in boreal summer months is a Gill-Matsuno-type quadrupole (Kucharski et al. 2009). Warm (cold) SST anomalies cause upper-level divergence (convergence) in the Atlantic sector. Upper-level westerly (easterly) wind anomalies then transport the signal as Kelvin waves to the east, leading to low-level divergence (convergence) over India. Consequently, reduced (increased) monsoon rainfall is observed over the Indian peninsula. Further AGCM model experiments by Losada et al. (2010b) and Barimalala et al. (2011) confirm the mechanism proposed by Kucharski et al. (2009). Due to the anticorrelation between Atlantic and Pacific since the 1970s, competing effects are at work in recent decades. While an Atlantic warming weakens the ISM, the simultaneous development of a Pacific La Niña is linked to stronger convection over South Asia, thus resulting in a stronger ISM. Therefore, the contributions from the Atlantic and Pacific Oceans tend to cancel each other and thus the net effect of both influences is reduced (Wang et al. 2009).

Less attention has been paid to the SST response in the Indian Ocean basin. Wang et al. (2009) notice that the tropical Atlantic-Indian basin teleconnection discussed above also induces changes in the Indian Ocean SSTs. In their observational study they show a connection of boreal summer SSTs in the *southern tropical Atlantic* (STA) to 850 hPa winds and SSTs in the western Indian Ocean sector. Positive STA SST anomalies are associated with a weakening of the Somali jet, which contributes to positive SST anomalies in the western tropical Indian Ocean due to decreased evaporation and anomalous ocean downwelling. Losada et al. (2010b) and Barimalala et al. (2011) also show a connection between boreal summer SSTs in the tropical southeast Atlantic and the western Indian Ocean. According to their results both SST and precipitation response in the Indian Ocean sector are consistent with the Gill-Matsuno-type mechanism proposed by Kucharski et al. (2009). However, although Ding et al. (2012) confirm the SST response in the western Indian Ocean, they note that this relationship does not necessarily reflect a direct influence of the tropical south Atlantic on this region. Instead, it may rather be interpreted as the indirect influence of the induced Pacific Ocean variability.

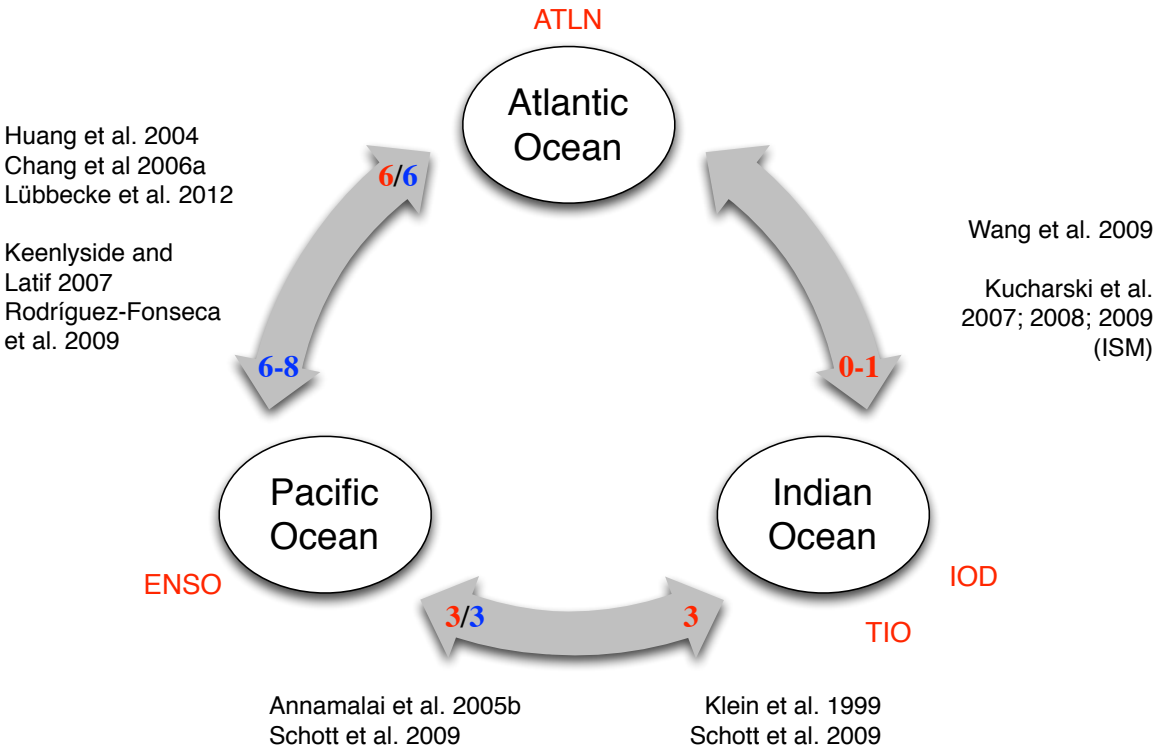

Figure 7.1: Scheme of tropical teleconnections: overview of important time lags in the lead-lag relationships between the modes of tropical SST variability (red letters outside circles) and corresponding key literature. Numbers in the arrow heads indicate the direction towards an ocean. Red and blue correspond to a positive and negative response, respectively. For example, the blue time lags 6-8 in the arrow head pointing towards the Pacific Ocean indicates a cooling (warming) of the Pacific Ocean in response to warm (cold) Atlantic SSTs. The relevant studies are placed close to the corresponding time lags.

Figure 7.1 provides a schematic overview of the teleconnections between the tropical oceans that have been discussed in this introduction. The figure summarizes known teleconnections between the main modes of tropical SST variability with corresponding time lags and key publications.

This summary has given an insight in the complexity of the interactions between the tropical oceans. The remaining part of this chapter now focuses on the teleconnections of the tropical Atlantic to the Pacific and Indian Oceans. Previous studies analyzing those have mainly focused on the linear lead-lag relationship and possible mechanisms connecting the basins. However, several studies have shown a nonlinear asymmetric behavior of Pacific ENSO events regarding the spatial distribution, magnitude and duration of associated Pacific SST anomalies as well as their regional and global response (e.g. Hoerling et al. 1997, An and Jin 2004, Okumura and Deser 2010). A similar asymmetric character may apply to the response to Atlantic events. Indeed, an asymmetry has already been indicated by composite analyses for the regional precipitation response (see Chapter 6). Thus, a similar behavior may also be assumed for the global scale. That means, it is yet unclear whether the proposed mechanism for the teleconnection of the tropical southeast Atlantic to the tropical Pacific and Indian Oceans produces similar patterns - although

inverse - for Atlantic Niño and Niña events. Furthermore, concerning the Indian Ocean, most attention has been given to the Atlantic influence on the Indian Summer Monsoon whereas only few studies have analyzed the interaction between Atlantic and Indian Ocean SSTs. This chapter therefore addresses several yet unanswered questions:

- Rodríguez-Fonseca et al. (2009) and other authors discuss an enhancement of a Pacific Niña by an Atlantic Niño revealed by linear regression analyses. Does their proposed mechanism apply to both the response to an Atlantic Niño and a Niña in a similar way or may this teleconnection have an asymmetric character?
- Is there a difference in the SST and atmospheric patterns for a Pacific Niña or Niño with and without a previous Atlantic Niño or Niña? That is, is there observational evidence for the suggested enhancement in both the warm and cold case, and is the response symmetric?
- Kucharski et al. (2007) show that Atlantic Ocean variability may further influence the Indian summer monsoon. Does the proposed connection also affect Indian Ocean SST variability?
- Is there a connection of Atlantic SSTs to both the basin-wide mode and Indian Ocean Dipole variability?
- For the Atlantic and Indian Oceans, it further needs to be investigated whether a potential link reflects an ENSO-independent connection of these two oceans or whether is it dominated by the strong influence of the Pacific Ocean.

To assess these questions, separate experiments are performed for the Atlantic-Pacific teleconnection in Section 7.2 and the Atlantic-Indic teleconnection in Section 7.3. Analyses for the latter are carried out with respect to the strong link between the Pacific and Indian Oceans.

7.2 Links between the tropical southeast Atlantic and the Pacific ENSO system

This section analyzes the relationship between the tropical Atlantic and Pacific Oceans. As a first step, co-variability is assessed by means of bivariate correlation analyses (Section 7.2.1). The subsequent section provides a detailed analysis of the connection between Atlantic warm and cold events to Pacific ENSO events with a focus on their peak seasons, namely boreal summer and the following winter season (Section 7.2.2).

7.2.1 Co-variability of the tropical Atlantic and Pacific Oceans

For a first overview of co-variability of the tropical Atlantic and Pacific Oceans, cross-correlation analyses are carried out between the three ATLN indices and the Niño1, 2, 3, 4 and 3.4 indices. Analyses are performed for all 1 to 12-month seasonal sections and for time lags -12 to +12 with the Atlantic SST indices leading (lagging) for positive (negative) lags. Furthermore, three different time periods are used to account for different

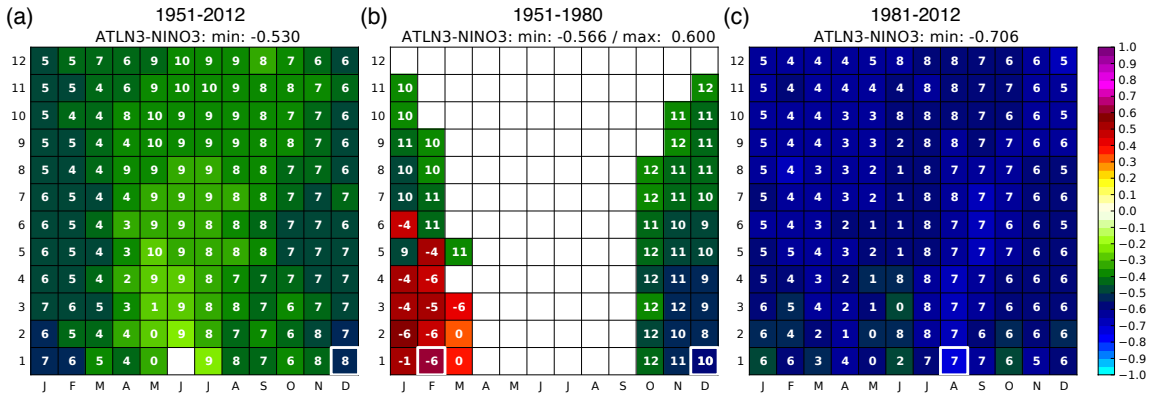

Figure 7.2: Cross-correlation analysis between the ATLN3 and Niño3 indices for the different periods: (a) 1951–2012, (b) 1951–1980, (c) 1981–2012. For each 1- to 12-month seasonal section (y-axis) only the absolute (positive or negative) maximum correlation for time lags -12–12 months (NIÑO3 index lagging) is shown. The label denotes the corresponding time lag of the maximum. The overall maximum is highlighted by a white frame. Only significant results (95% level) are shown and displayed based on the central month (x-axis), e.g. the FMA season is plotted at the position of central month M.

conditions before and after the 1970s as they were reported by e.g. Rodríguez-Fonseca et al. (2009) (also see Section 7.1): (a) the entire study period 1951–2012, (b) the first half 1951–1980 and (c) the second half 1981–2012.

Figure 7.2 displays the results for the example of the ATLN3 and Niño3 indices. This example is chosen as these two indices show the strongest connection of all index combinations. Due to the abundance of results, Figure 7.2 only contains the maximum correlation coefficients of all time lags for each seasonal section. Results for the three time periods clearly differ. For the entire study period (Figure 7.2 (a)), all maximum correlation coefficients are negative with corresponding positive lags, i.e. ATLN3 leads Niño3. In this period, the overall maximum anticorrelation between the two indices is found for boreal winter at lag 7 to 8. That is, the boreal winter ATLN3 index is linked to the following boreal summer Niño3 index. Weaker but significant correlations are observed for the remaining seasons. On the contrary, results for the sub-periods are contradicting. In the earlier period 1951–1980 (Figure 7.2 (b)), maximum correlation coefficients are centered on boreal winter months. The overall negative maximum is found in December where the Atlantic leads the Pacific by 10 months (following October), whereas a positive maximum in February indicates a Pacific lead of 6 months (previous September). There are no significant values throughout boreal spring and summer. By contrast, in the 1981–2012 period the overall maximum is found in boreal summer with the Atlantic leading the Pacific in the following winter by 6 to 8 months, which is consistent with earlier studies (e.g. Keenlyside and Latif 2007, Polo et al. 2008, Rodríguez-Fonseca et al. 2009). Furthermore, all maximum values are negative and all corresponding time lags are positive. That is, the overall picture for this period is that of a significant anticorrelation between the Atlantic and Pacific Oceans with the Atlantic leading the Pacific throughout the year, although at differing magnitudes and time lags.

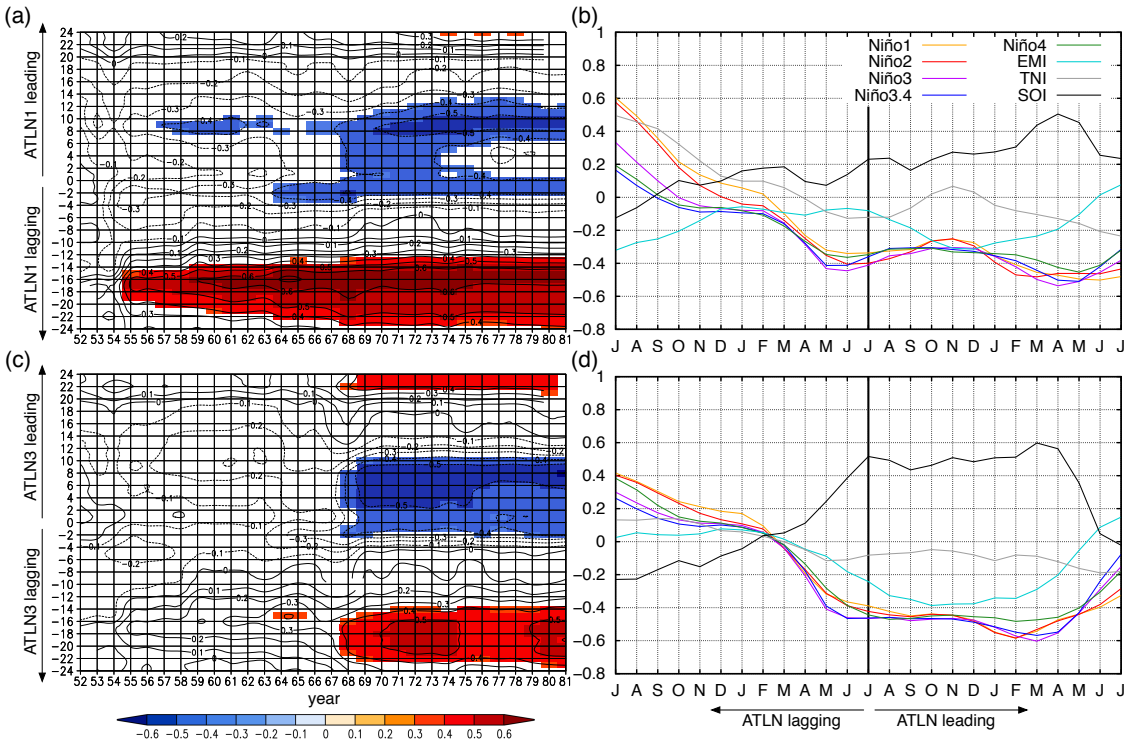

Figure 7.3: Left: 30-year lead-lag correlations, running one year from 1951–1980 to 1981–2012 between the boreal summer (JJA) ATLN1 (a) and ATLN3 (c) indices and the Niño3 index. **Right:** lead-lag correlations for the JJA ATLN1 (b) and ATLN3 (d) indices and the ENSO indices Niño1, 2, 3, 4 and 3.4 indices, the Trans-Niño index (TNI), the El Niño Modoki index (EMI) as well as the SOI (for all index definitions see Section 3.4). X-axis labels indicate the central month of the 3-months season of the indices. The black vertical line indicates the JJA ATLN1 or 3 index season and thus time lag 0.

For a closer look at the non-stationary anticorrelation between the Atlantic and Pacific Oceans discussed in Section 7.1, the peak season of the Atlantic Niño, namely boreal summer months June–August, is selected. Figure 7.3 displays running 30-year lead-lag correlations for the JJA season of the entire study period 1951–2012 between the ATLN1 (Figure 7.3 (a)) and ATLN3 (Figure 7.3 (c)) and Niño3 indices. For both the ATLN1 and ATLN3, indices significant correlation coefficients at lags 6–9 months (ATLN indices leading) exceed a magnitude of 0.5 after the late 1960s. Thus, SST variability of the Atlantic Ocean in boreal summer is linked to that of the following winter and spring seasons in the Pacific Ocean. The significant positive correlations at time lags 12–18 months with Niño3 index leading are due to the autocorrelation of this index and confirm the inherence of the ATLN1 and 3 indices' signal in the Niño3 index. This is consistent with results presented by Rodríguez-Fonseca et al. (2009).

To further illustrate the relationship between the boreal summer (JJA) Atlantic SSTs and the leading or lagging Pacific Ocean during the recent decades, Figure 7.3 (b) and (d) depict seasonal lead-lag correlations for the period 1981–2012 and for the different ENSO SST indices as well as the SOI SLP index (see Section 3.4 for a detailed description of these indices). The black vertical line in the two plots indicates lag 0, i.e. the JJA season for ATLN1 or 3 indices as well as the ENSO indices. Negative lags (ATLN indices

lagging) are plotted to the left and positive lags (ATLN indices leading) to the right of the line. Correlation coefficients for all five Niño indices show a fairly similar evolution from boreal winter and spring (JFM, lag -5) preceding the Atlantic summer season to boreal winter following that summer.

Starting in the preceding boreal winter (Pacific leading), Atlantic and Pacific Niño SST indices are uncorrelated. In the following months an anticorrelation establishes, reaching significant (95 % level) values of about -0.4 around the April–June season. As suggested by Chang et al. (2006a), the presence of significant correlations at negative lags (i.e. Pacific leading) may indicate an influence of the Pacific on the Atlantic. However, as also noted by Rodríguez-Fonseca et al. (2009), the Atlantic Niño is in its mature phase in boreal summer while the Pacific event is only in its onset or development phase. Therefore, the correlation coefficients are either coincidental or indicate a possible influence of the Atlantic on the Pacific Ocean.

Correlation coefficients keep their magnitude until the following boreal winter. Peak correlation coefficients of around -0.6 are then reached in the following boreal spring. That means that the actual peak correlation appears about 2–3 months after the Pacific events typically peak. Other studies including that of Rodríguez-Fonseca et al. (2009) report similar results but do not discuss this observation as their main focus remains on boreal winter. Whether this observation is a coincidental result or a real delay and strengthening of the Pacific SST peak exist, will be analyzed in further pattern correlation and composite analyses later in this chapter.

Correlation results of the SOI index follow a very similar development compared to the ENSO SST indices but with opposite sign. As the latter indices and the SOI index are anticorrelated, these results further confirm the existence of a link of the Atlantic Ocean to the coupled ENSO system.

The remaining two indices in Figure 7.3 (b) and (d), namely the EMI and the TNI, were chosen to represent El Niño Modoki. As can be seen from the results for both the ATLN1 and 3 indices, correlation coefficients do not reach magnitudes as high as those of correlation analyses with the remaining Niño indices. It can be concluded that the link between Atlantic Niños and conventional Pacific ENSO events is stronger than that with the Modoki events. This is consistent with the results of Ham et al. (2013a), who suggest that the conventional Pacific El Niño is connected to the Atlantic Niño while the central Pacific Modoki events are connected to SST anomalies in the tropical north Atlantic.

However, there are also differences in both magnitude and time lag in the results for the ATLN1 and 3 regions. Some of these results may be attributed to their different geographical location and thus to the time lag of about one month in the development of SST anomalies, as discussed earlier (Chapter 5 and 6). Furthermore, in a typical Pacific ENSO event, the center of SST anomalies successively moves from the coast to the central Pacific (see Chapter 2.2 and Rasmusson and Carpenter 1982). In contrast, not all summer peak Atlantic Niños have pronounced anomalies in the coastal region (ATLN1). This may provide an additional explanation why the link between the southern regions in both oceans, i.e. the ATLN1 and the Niño1 and 2 regions, is weaker.

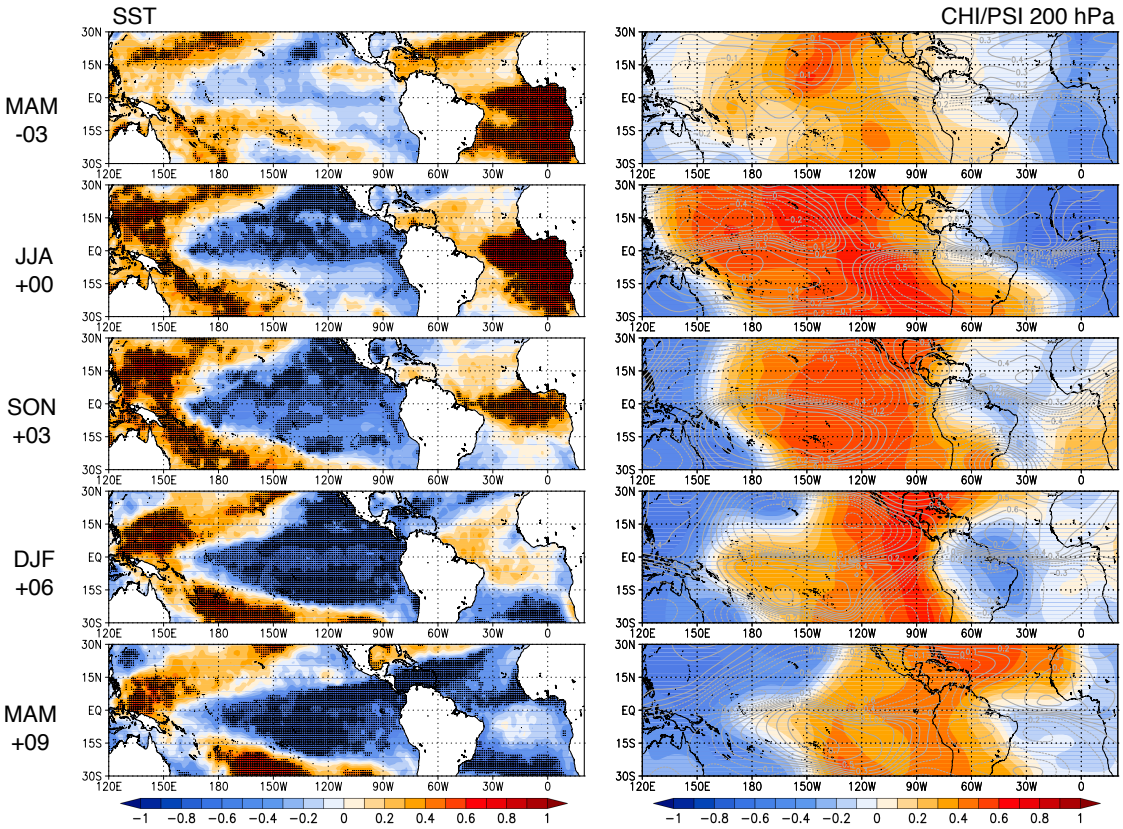

Figure 7.4: Spatial correlation patterns between the JJA ATLN3 index and standardized high-pass filtered SST, 200hPa CHI (shading) and PSI (contour) fields for the period 1981–2012. Selected time lags from the boreal spring leading the ATLN3 index to the following boreal spring lagging the ALTN3 index are shown: -03 (MAM, spring), +00 (JJA, summer), +03 (SON, autumn), +06 (DJF, winter) and +09 (MAM, spring). Significant values (95 % level) for the SSTs are highlighted with dots. For better readability of the patterns, symbols indicating significance are omitted in the CHI/PSI plots.

In addition to the index correlation analyses, spatial patterns of correlation coefficients are computed. Figure 7.4 depicts patterns of SST, 200 hPa velocity potential (CHI) and stream function (PSI) correlated with the boreal summer (JJA) ATLN3 index for the Pacific-Atlantic domain during 1981–2012. Consistent with the index correlation analyses the SST correlation patterns show an Atlantic-Pacific anticorrelation with negative correlation coefficients that develop in boreal spring and strengthen throughout boreal summer and autumn, reaching their peak in the following winter and spring. The correlation pattern represents the typical horseshoe pattern of a La Niña.

The corresponding atmospheric correlation patterns (right panel in Figure 7.4) show the typical Gill-type quadrupole response that has been discussed in several recent studies (e.g. Rodríguez-Fonseca et al. 2009, Losada et al. 2010b, Barimalala et al. 2011): The velocity potential at the 200 hPa level (shading in Figure 7.4) depicts anomalous upper-level divergence over the Atlantic Ocean and anomalous convergence over the eastern Pacific Ocean, corresponding to anomalous upward and downward motion, respectively. The 200 hPa stream function (contour lines) shows two anticyclones straddling the equator to the east and two cyclones west of the center of anomalous convergence. Therefore, both upper-level CHI and PSI indicate an altered Walker circulation with an anomalous

ascending branch over the tropical south Atlantic and a strengthened descending branch over the central equatorial Pacific Ocean. This atmospheric pattern, i.e. a strengthening of the Pacific Walker circulation, is consistent with a Pacific La Niña event.

The upper-level anticyclones as well as the divergence over the Atlantic Ocean already appear in spring (MAM, -03). The quadruple and thus the anomaly in the Walker circulation is then best developed during boreal summer (JJA, lag +00), i.e. in the mature phase of an Atlantic Niño. This provides further evidence for a connection of the two ocean basins. Moreover, it confirms the hypothesis that an Atlantic Niño in its mature phase may enhance a developing La Niña. The above-described altered Walker circulation may provide the physical explanation for the Atlantic influence on the Pacific Ocean. In the following two seasons (SON and DJF) the Atlantic upper-level divergence associated with the anomalous ascending branch weakens while the anomaly in the Pacific sector is retained. In the next spring season the anomaly also starts to dissolve in the eastern Pacific region.

Similar results are achieved when the ATLN1 and 2 indices instead of ATLN3 are correlated with the SST, CHI and PSI fields (not shown). Both SST and atmospheric patterns clearly resemble those described above and depicted in Figure 7.4. However, as for the index correlation analyses (Figure 7.3), magnitudes of the correlation coefficients are smaller when the ATLN1 and 2 indices are used. As the links between the equatorial tropical Atlantic and Pacific Oceans appear to be strongest and most stable, further analyses in this chapter will be based on ATLN3 and Niño3 indices.

The results presented above clearly show that there is a statistical connection between the two ocean basins. Furthermore, a dynamical explanation points to the existence of a causal link. To further investigate whether the mechanism applies to both the Atlantic Niño and the Niña case, a case study of Atlantic and ENSO events is performed and discussed in the following section.

7.2.2 A case study of boreal winter ENSO events with and without preceding summer Atlantic events

Correlation analyses in the previous section have clearly shown a connection between boreal summer SSTs in the tropical southeast Atlantic and those of the following winter and spring in the tropical Pacific Ocean in the 1981–2012 period. To further shed some light on the question whether the summer Atlantic Niños are just coincidentally followed by Pacific La Niñas or actually enhance the latter, an additional case study is carried out in this section. For that, all Pacific ENSO events with and without a preceding Atlantic event within the period from 1981 to 2012 are analyzed. This leads to the following four cases:

Case 1: Pacific La Niña preceded by a summer Atlantic Niño

Case 2: Pacific La Niña without preceding summer Atlantic Niño

Case 3: Pacific El Niño preceded by a summer Atlantic Niña

Case 4: Pacific El Niño without preceding summer Atlantic Niña

Here, the term summer Atlantic Niño or Niña refers to those events that have their peaks in the June–August season or show strong anomalies exceeding the event threshold (as defined in Section 5.5) at least in the equatorial region (ATLN3). Events that just start or end in summer and show anomalies below the event threshold in the ATLN3 region are not included in the selection. Their impact is assumed to be smaller than that of events with pronounced anomalies in boreal summer. Interestingly, all events that meet this criterion, and are followed by a Pacific event, are major events or minor events centered on the equatorial region. This indicates that this region plays a more important role in tropical teleconnections than the southern SST regions. This may be either due to the season of its peak - summer in this case - or due to the fact that equatorial SSTs more effectively impact the Walker circulation. For the Pacific ENSO events, no preselection is necessary as they reliably peak in boreal winter or at least have reached strong SST anomalies at that time. Note that two years, namely 1987 and 1991, are excluded from this case study, as they suit none of the four cases. In these years, both Atlantic Niña and an ENSO event exist, but the Atlantic Niña does not peak in summer. Therefore, these two years are not representative for Case 3. Table 7.1 contains the corresponding years for the four selected cases.

Table 7.1: Years selected for the composite case study: Pacific Niñas (1) with and (2) without preceding summer Atlantic Niño as well as Pacific Niños (3) with and (4) without preceding summer Atlantic Niña. Years refer to the peak year of the Atlantic events and to the onset / development year of the Pacific events.

Pacific Niñas		Pacific Niños	
(1) preceding Atlantic Niño	(2) no preceding Atlantic Niño	(3) preceding Atlantic Niña	(4) no preceding Atlantic Niña
1984	1983	1982	1994
1988	2005	1997	2002
1995	2007		2004
1999	2010		2006
2008	2011		2009

For each of the four cases, composites are computed for the following variables: SST, SLP as well as CHI, PSI, geopotential heights (HGT), wind and vertical velocity (OMEGA) of all available atmospheric levels. As the SST, SLP, CHI and PSI fields best summarize and represent the anomaly picture, the remaining variables are used for the interpretation of the results but are not depicted in the figures.

Note that the sample size of each of the cases is small due to the availability of events within the period of the strongest Atlantic-Pacific link between 1981 and 2012. Therefore, results from the composite analyses carried out in this section need to be interpreted with care. The results cannot provide clear evidence for differences between the selected cases but may only serve as indication for a different evolution of ENSO events with and without preceding Atlantic event. However, an analysis of these limited events is still justified as it provides valuable insights that may not be achieved with methods such as correlation or regression analysis.

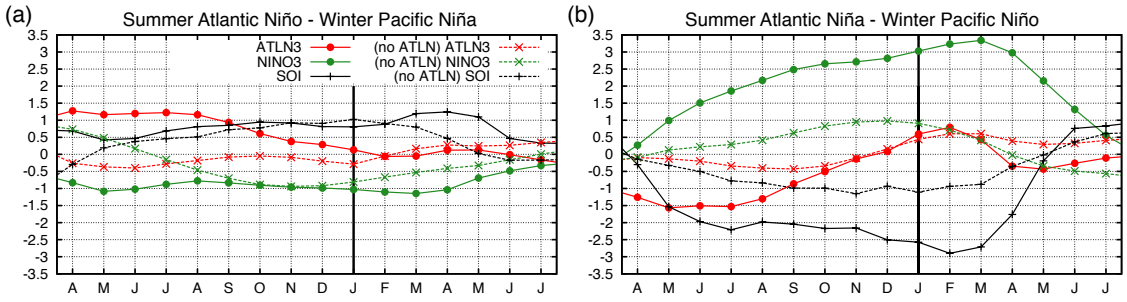

Figure 7.5: Composite time series of seasonal mean ATLN3, Niño3 SST and SOI SLP indices for ENSO events selected according to the following four cases: (a) Pacific Niñas (1) with and (2) without preceding summer peak Atlantic Niño (ATLN) as well as (b) Pacific Niños (3) with and (4) without preceding summer peak Atlantic Niña. X-axis labels indicate the center month of each 3-month seasonal mean, i.e. DJF is plotted at central month J. Time lag 0 (black vertical line) corresponds to the ENSO mature season boreal winter (DJF). Negative (positive) lags of the lagging (leading) indices are plotted to the left (right) of the line.

From the four cases described above, Figure 7.6 depicts the composites patterns for Case 1 and 2, i.e. for a Pacific La Niña with and without preceding Atlantic Niño. Case 3 and 4, i.e. a Pacific El Niño with and without preceding Atlantic Niña are presented in Figure 7.7. In addition, Figure 7.5 contains composite time series of the ATLN3, Niño3 and SOI indices for Case 1 and 2 in Figure 7.5 (a) and Case 3 and 4 in Figure 7.5 (b).

Case 1: Pacific La Niña with preceding summer Atlantic Niño: As can be seen from the top set of composites in Figure 7.6, SSTs in the tropical Atlantic show a typical pattern of an Atlantic Niño with strong positive anomalies in boreal spring and summer, which dissolve during autumn. In the tropical Pacific, negative anomalies already appear in spring, strengthen in the following seasons and are still well developed in the following spring. The SST composite patterns are similar to the correlation patterns in Figure 7.4, although SST anomalies during the preceding spring season (MAM, lag -09) are more pronounced. Furthermore, SLP anomalies are negative in the Atlantic sector in spring and summer. At the same time, positive (negative) anomalies develop over the eastern (western) Pacific Ocean, corresponding to a positive SOI phase. The corresponding 200 hPa velocity potential and stream function fields show the picture of a strengthened Pacific Walker cell.

Case 2: Pacific La Niña without preceding summer Atlantic Niño: Due to the selection of years without Atlantic Niños, the bottom set of SST patterns in Figure 7.7 contains no positive anomalies in the tropical southeast Atlantic during boreal spring and summer (lag -09 and -06). In the Pacific Ocean, a decaying El Niño is still visible in spring, which then transitions into a La Niña in the following months. Maximum negative SST anomalies are reached in the boreal winter season. In the following spring, the negative anomalies dissolve already. As for the SSTs, there are no pronounced SLP anomalies in the Atlantic sector while a typical positive SOI phase is still developing in the Pacific sector. The CHI and PSI fields show anomalous upper-level divergence over the eastern Pacific Ocean in the preceding boreal spring, which corresponds to the anomalous ascending branch of the decaying El Niño. In the following seasons, upper-level

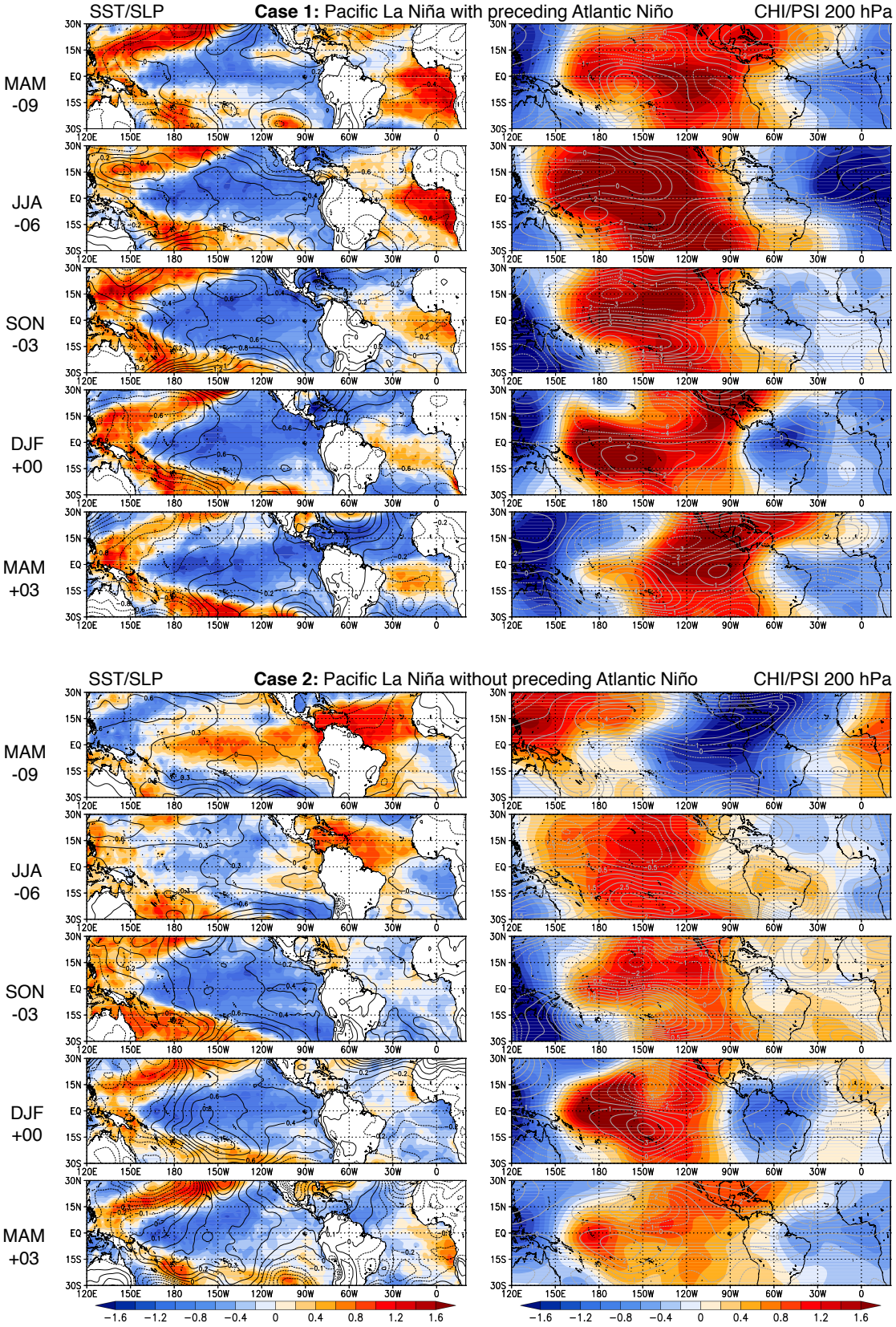

Figure 7.6: Composites of seasonal mean standardized high-pass filtered SST (shaded) and high-pass filtered SLP (hPa, contours), 200 hPa velocity potential (CHI, $10^6 m^2 s^{-2}$, shaded) and stream function (PSI, $10^6 m^2 s^{-2}$, contours) for ENSO events selected during 1981–2012 according to the following two cases: **Case 1** (top): Pacific La Niña with preceding summer Atlantic Niño and **Case 2** (bottom): Pacific La Niña without preceding summer Atlantic Niño. The time lags correspond to the ENSO mature season boreal winter (DJF).

convergence and descending motion replaces the divergence and ascent. Thus, in boreal winter composites clearly show the mature phase of the Pacific La Niña and an associated strengthened Walker circulation.

Comparing the two cases of a Pacific La Niña with and without a preceding Atlantic Niño, the most obvious differences may be observed in the SST patterns (Figure 7.6) and the composite time series of the Niño3 and ATLN3 indices (Figure 7.5): in the case of a preceding warming in the southeast Atlantic, negative anomalies in the Pacific Ocean develop one season earlier, i.e. in boreal spring instead of summer. This does not mean that the Atlantic Niño influences the onset of a La Niña. However, an early onset of a Pacific La Niña with an associated Walker circulation anomaly enables the development of an atmospheric bridge. This further creates the possibility of an influence of the Atlantic Niño on an enhanced development of the Pacific anomalies.

Furthermore, as seen in both the composite patterns and the time series, the La Niña with a preceding Atlantic Niño is still well developed in boreal spring and decays later than without an Atlantic warming. Results shown in Figure 7.5 further indicate that the peak of the Niño3 index in a La Niña with a preceding Atlantic Niño is delayed to the spring season (FMA). Thus, the peak occurs two months after the typical mature phase and even appears stronger in magnitude. As already mentioned above, these results are based on a limited number of events and cannot prove a different development in Case 1 and 2. However, it is still interesting to note that results point to a delayed and enhanced peak in the early boreal spring season. Indeed, these results are consistent with the correlation analyses discussed earlier. The maximum correlation coefficient between the ATLN3 and Niño3 indices is observed for the June–August and January–March seasons, respectively (Figure 7.3 on p. 91). Thus, the Niño3 index lags the ATLN3 index by 8 months with the peak correlation in spring.

Note that Kayano et al. (2011) also mention a reinforcement and longer duration of Pacific La Niña conditions due to a previous summer Atlantic Niño. However, their composite analysis includes events of the entire period between 1900 and 2006. Thus, the events are not selected with respect to a significant correlation between the Pacific and Atlantic Oceans. Their analysis therefore provides only limited representativeness for the recent decades in which a significant Pacific-Atlantic anticorrelation is observed.

Another interesting aspect in the SST patterns of Case 2 in Figure 7.6 is that the strongest anomalies are centered in the central equatorial Pacific while they are less pronounced off the South American coast. That is, the pattern with a preceding Atlantic Niño resembles a conventional Pacific La Niña. By contrast, although the SSTs do not show the typical tripole pattern of a Pacific La Niña Modoki, without an Atlantic warming the pattern is somewhat similar to a Modoki event. This is consistent with the results of Ham et al. (2013a) who suggest that an Atlantic Niño is linked to a conventional La Niña but not to a Modoki event.

Case 3: Pacific El Niño with preceding summer Atlantic Niña: The top set of SST composite patterns in Figure 7.7 shows the negative anomalies of an Atlantic Niña during boreal spring and summer which already disappears in autumn. In the tropical Pacific,

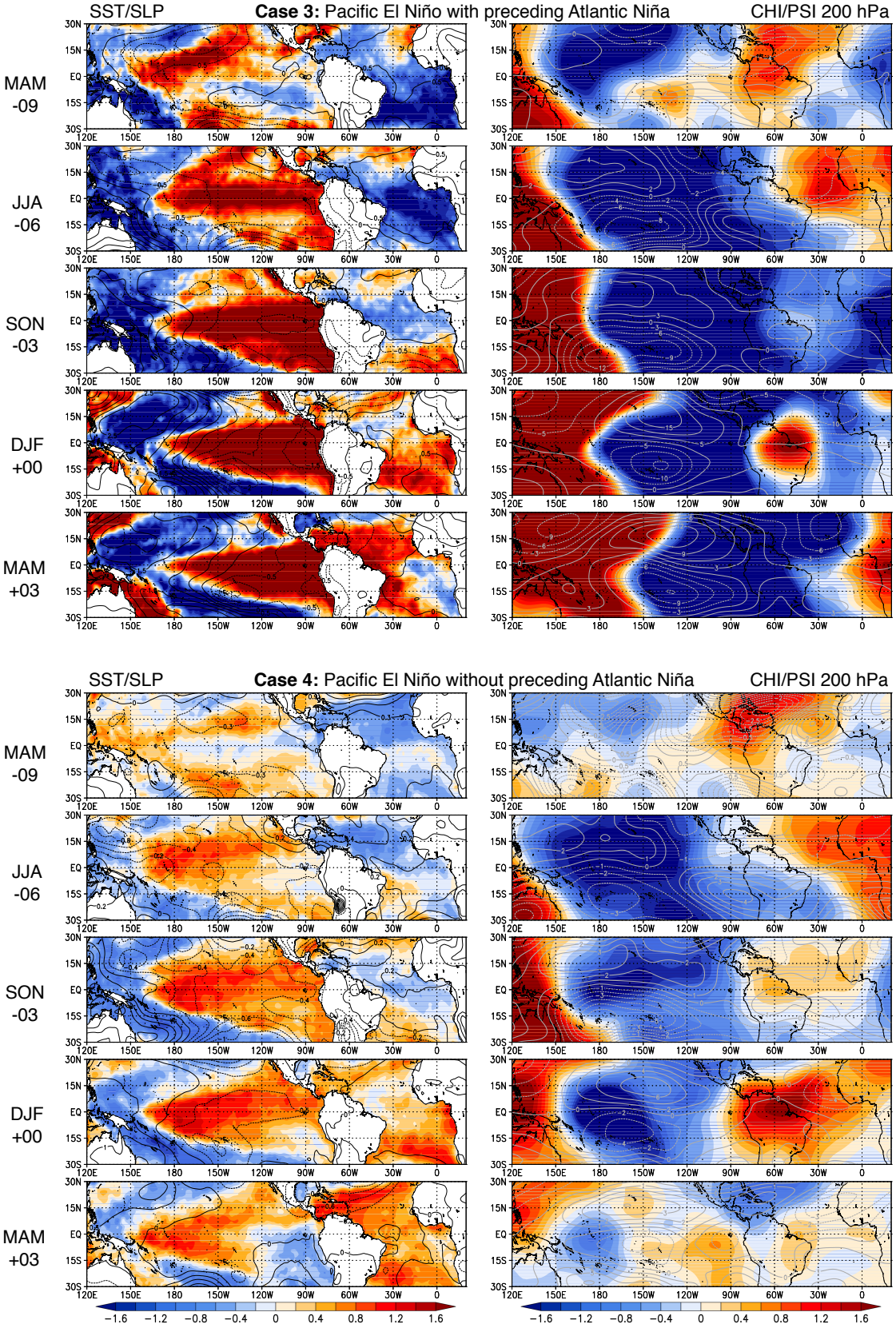

Figure 7.7: Composites of seasonal mean standardized high-pass filtered SST (shaded) and high-pass filtered SLP (hPa, contours), 200 hPa velocity potential (CHI, $10^6 m^2 s^{-2}$, shaded) and stream function (PSI, $10^6 m^2 s^{-2}$, contours) for ENSO events selected during 1981–2012 according to the following two cases: **Case 3** (top): Pacific El Niño with preceding summer Atlantic Niña and **Case 4** (bottom): Pacific El Niño without preceding summer Atlantic Niña. The time lags correspond to the ENSO mature season boreal winter (DJF).

positive anomalies appear in summer and show the typical horseshoe pattern of an El Niño throughout the following spring. As for Case 1, the SST composite patterns are similar to the correlation patterns in Figure 7.4 except for the preceding spring season (MAM, lag -09). This spring pattern indicates a decaying La Niña that transitions into an El Niño in summer. The corresponding SLP composites show a positive anomaly over the south Atlantic in spring and summer. In the Pacific sector, an SLP gradient corresponding to a negative SOI phase is depicted in the plots. Consistent with the SST and SLP composites, the 200 hPa CHI and PSI fields show the picture of a weakened Pacific Walker cell.

Case 4: Pacific El Niño without preceding summer Atlantic Niña: Similar to Case 2, without an Atlantic Niña, the bottom set of SST composite patterns in Figure 7.7 depicts no negative anomalies in the tropical southeast Atlantic during boreal spring and summer, as one would expect. In the Pacific Ocean, an El Niño develops comparably late. Positive SST anomalies in the central Pacific increase during boreal autumn and winter. In the following spring the negative anomalies already replace the positive ones off the South American coast. As for the SSTs, the negative SOI phase seen in the SLP composites is best developed during autumn and winter. The corresponding CHI and PSI fields show a weakened Pacific Walker circulation from boreal summer throughout winter. However, this anomaly has nearly dissolved in the following spring season.

Due to the different sample sizes, one may not draw conclusions from a different magnitude of the composite anomalies from a comparison of the two cases of a Pacific El Niño with and without a preceding Atlantic Niña. That is, the strong differences in the Niño3 and SOI composites (Figure 7.5) simply show that the sample of Case 3 contains two strong Pacific El Niños. However, comparing the evolution of the SST patterns, two interesting aspects may be pointed out: (1) a 2-month delay in the ENSO peak season and (2) a difference in the general pattern of the Pacific warming. Both observations are similar to those from the comparison of Case 1 and 2. That is, the Niño3 index in Figure 7.5 shows a delayed peak in boreal spring after the typical Pacific mature phase, again consistent with the time lag of 8 months observed in the correlation analyses. Furthermore, the SST patterns in Figure 7.7 for the case with a preceding Atlantic Niña resembles a typical conventional Pacific El Niño. Yet it is more similar to an El Niño Modoki in the case without an Atlantic cooling.

In summary, the case study described above does indeed support an enhancement of ENSO events by preceding Atlantic events in both the warm and the cold case and its corresponding inverse response. Furthermore, consistent with the correlation analyses, peaks of ENSO events with a preceding Atlantic warm or cold event are not only stronger but also delayed by two months to the spring season. However, from these experiments another important conclusion may be drawn. While recent studies (e.g. Kayano et al. 2011) claim that an Atlantic Niño (Niña) triggers a Pacific La Niña (El Niño), results presented here clearly point to an enhancement rather than a triggering as was also suggested by Keenlyside et al. (2013). In fact, especially in Case 1, i.e. a Pacific La Niña with preceding Atlantic Niño (see Table 7.1), SST anomalies in the Pacific appear early

in the year. Therefore, it is unlikely that the Pacific SST anomalies are caused by those in the Atlantic. However, as also indicated by the present results, Atlantic events may contribute to a substantial enhancement and delay of the Pacific SST peak. Future work should focus on these two aspects and further analyze these using both observational data and GCM experiments.

7.3 Links between the tropical southeast Atlantic and the Indian Ocean

This section analyzes the relationship between the tropical Atlantic and Indian Oceans. Similar to the previous section, co-variability is first assessed by means of bivariate correlation analyses (Section 7.3.1). However, as discussed in Section 7.1, the Indian Ocean SST variability is strongly coupled to the Pacific ENSO system. Therefore, additional partial correlation analyses excluding the influence of the Pacific Ocean are carried out. Section 7.3.2 first discusses examples of partial correlation patterns with regard to the selected time lag for the disturbing variable. Results of the partial correlation analyses for the two main modes of Indian Ocean SST variability are then presented and discussed in two separate sections, i.e. for the basin-wide mode in Section 7.3.3 and for the Indian Ocean Dipole in Section 7.3.4. Furthermore, these two sections provide a detailed analysis of the connection between Atlantic warm and cold events to the two Indian Ocean SST modes using composite analyses.

7.3.1 Co-variability of the tropical Atlantic and Indian Oceans

To assess co-variability of the tropical Atlantic and Indian Oceans, cross-correlation analyses are carried out between the three ATLN indices and the TIO and IOD indices, representing the basin-wide mode and the Indian Ocean Dipole, respectively. Analyses are performed for all 1 to 12-months seasonal sections and for time lags -12 to +12 with the Atlantic SST indices leading (lagging) for positive (negative) lags. As for the analyses of the Atlantic and Pacific Oceans, three different time periods are used to account for differences in the link between the two oceans before and after the 1970s: the entire study period 1951–2012, the first half 1951–1980 and the second half 1981–2012.

Figure 7.8 displays the results for the ATLN3 and the TIO indices (Figure 7.8 (a-c)) as well as for the ATLN3 and IOD indices (Figure 7.8 (d-f)). Due to the abundance of results, Figure 7.8 only contains the maximum correlation coefficients of all time lags for each seasonal section. For both Indian Ocean indices, results for the three time periods clearly differ. Considering the ATLN3 and TIO indices (Figure 7.8 (a-c)) for the entire study period 1951–2012, maximum negative correlation coefficients appear in the boreal summer season with the Atlantic leading by 12 months. A positive simultaneous correlation exists in boreal winter. The summer link is also apparent in the 1951–1980 period although weaker and only contained in the monthly correlations. There are no significant seasonal correlation coefficients throughout boreal spring and summer. The winter/early spring link is stronger with maximum values of up to $r = 0.74$ when the Atlantic is leading by 1 to 3 months. By contrast, the period 1981–2012 is mostly dominated by negative

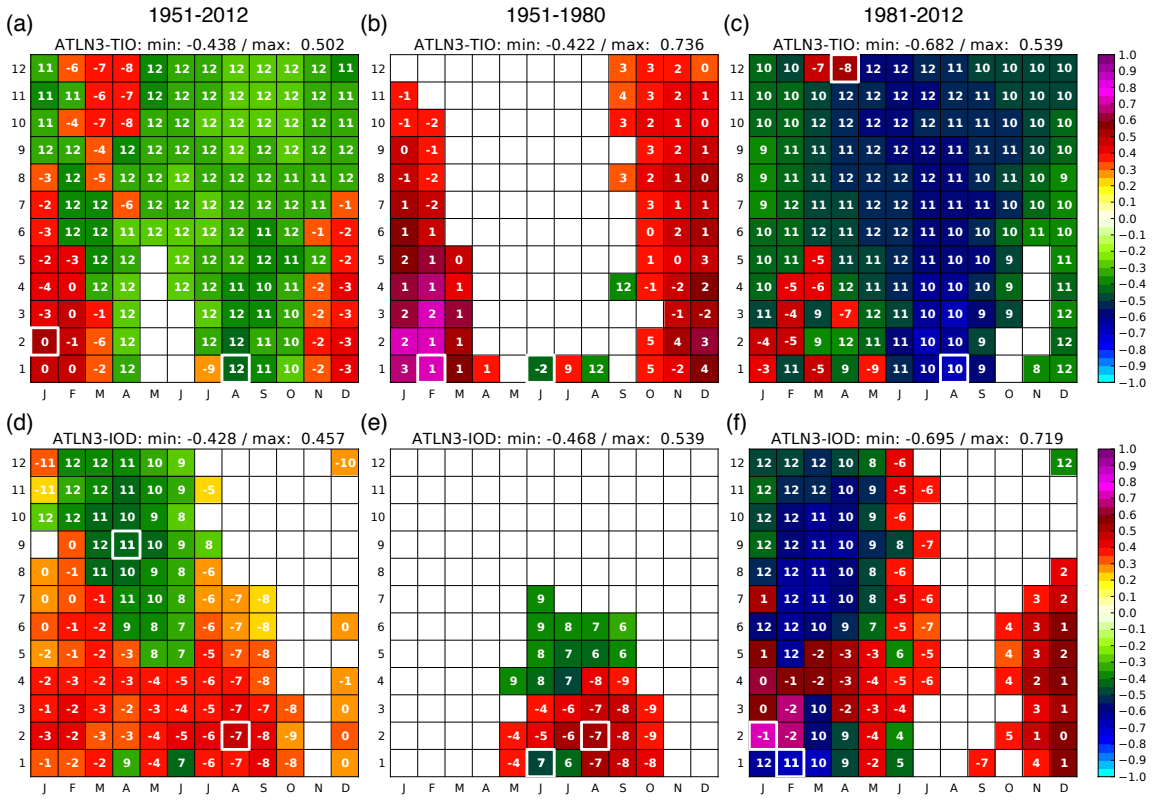

Figure 7.8: Cross-correlation analysis between ATLN3 and TIO (a-c) and IOD (d-f) indices for the different periods: (a)+(d) 1951-2012, (b)+(e) 1951-1980, (c)+(f) 1981–2012. For each 1- to 12-month seasonal section (y-axis) only the absolute (positive or negative) maximum correlation for time lags -12 to 12 months (TIO or IOD index lagging) is shown. The label denotes the corresponding time lag of the maximum. The overall maximum is highlighted by a white frame. Only significant results (95% level) are shown and displayed based on the central month (x-axis), e.g. the FMA season is plotted at the position of central month M.

correlations with a maximum in boreal spring when the Atlantic leads by 10 months. That is, the tropical Atlantic summer SSTs are linked to those of the basin-wide mode in the following spring. A weaker link exists between the boreal winter ATLN3 and the TIO indices in the preceding autumn (lag -3 to -5).

Regarding the correlation coefficients between the ATLN3 and IOD indices (as shown in Figure 7.8 (d-f)), for both periods of 1951 to 2012 and 1951 to 1980, positive values are found for boreal summer Atlantic SSTs and the following winter season of the IOD (lag +7) as well as the previous winter season (lag -7). However, the Indian Ocean Dipole is only active between boreal spring and winter with its peak in autumn. Therefore, significant values for winter are not representative for an actual link to the IOD in this season. Instead, these correlations rather indicate a link to one of the poles of the IOD, i.e. the western or eastern part of the tropical Indian Ocean. For a definition of the IOD index and its two poles, referred to as IODW and IODE thereafter, see Section 3.4. A similar situation applies to the recent record period 1981–2012: in the relevant boreal autumn season no significant link exists to the Atlantic Ocean. That means that either there is no connection between the Atlantic Niño and the Indian Ocean Dipole or an existing connection is concealed by the disturbing influence of ENSO.

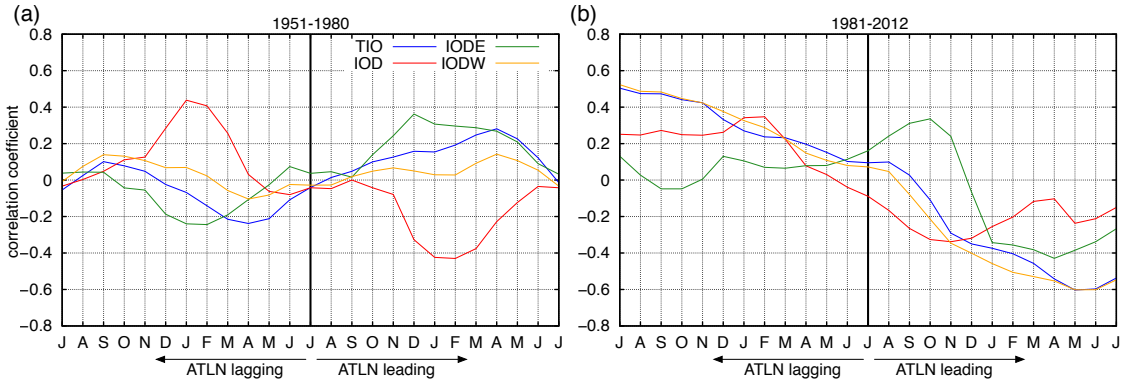

Figure 7.9: Lead-lag correlations for the JJA ATLN3 indices and the TIO, IOD, a western Indian Ocean (IODW) and an eastern Indian Ocean (IODE) index the sub-periods (a) 1951–1980 and (b) 1981–2012. X-axis labels indicate the central month of the 3-month seasons of the different leading and lagging Indian Ocean indices. The black vertical line indicates the JJA ATLN3 index season and thus time lag 0.

To further explore connections of boreal summer tropical Atlantic SST variability to the basin-wide mode and the Indian Ocean Dipole, lead-lag correlations with a focus on the summer season (JJA is time lag 0) are shown in Figure 7.9. This figure also contains correlations for the western (IODW) and eastern part (IODE) of the Indian Ocean basin to explain significant values in seasons where no typical IOD occurs. Regarding the basin-wide mode, in the earlier record period 1951–1980 (Figure 7.9 (a)), the ATLN3 index is insignificantly correlated with the TIO at both negative and positive lags. But insignificant positive values for a leading Atlantic Ocean turn to significant (95 % level) negative values of $r = -0.6$ in the period 1981–2012 (Figure 7.9 (b)) when the ATLN3 index is leading by 10 months. As was explained in Section 7.1, a tropical Indian Ocean basin-wide warming peaks about 3 to 6 months after the mature phase of a Pacific El Niño. Consistent with the anticorrelation between the Atlantic and Pacific Oceans, the negative link to the Indian Ocean found here clearly points to a basin-wide cooling following a Pacific La Niña. However, these results may not answer the question whether this anticorrelation between the ATLN3 and TIO indices represents a significant contribution of the Atlantic Ocean to an anomalous Indian Ocean cooling or simply confirms the strong link of Indian Ocean variability to ENSO. Additional partial correlation analyses are necessary to further investigate the relationship between the Atlantic and Indian Oceans excluding the influence of ENSO variability.

Furthermore, regarding the correlations between the ATLN3 and IOD indices, Figure 7.9 (a) indicates that in the earlier sub-period, the link to both the preceding and the subsequent boreal winter IOD indices might reflect a connection to the eastern Indian Ocean instead. However, for IODE index all values are insignificant. In the period 1981–2012 (Figure 7.9 (b)), a weak link to the IOD appears in boreal autumn, which is confirmed by the opposite signs of the correlations to the IODW and IODE. Values are insignificant though and may again reflect an IOD phase accompanying an ENSO event (see Section 7.1). As for the results of the TIO index, additional partial correlation analyses need to be carried out to validate this potential link.

Before partial correlation analyses are described for both the basin-wide mode and the Indian Ocean Dipole, some important aspects concerning the time lag selection for the disturbing variable are discussed in the following section. Note that the remainder of this chapter focuses on the sub-period 1981–2012, as there are no significant bivariate correlations for the two modes in relevant seasons of the earlier sub-period 1951–2012.

7.3.2 Examples of partial correlation patterns excluding the ENSO signal

For the use of partial correlation analysis in lead-lag relationships such as teleconnection analysis, the selection of the time lag for the exclusion of the effect of a disturbing variable may affect results. Therefore, pre-analyses with different time lags for the exclusion of the ENSO influence are carried out.

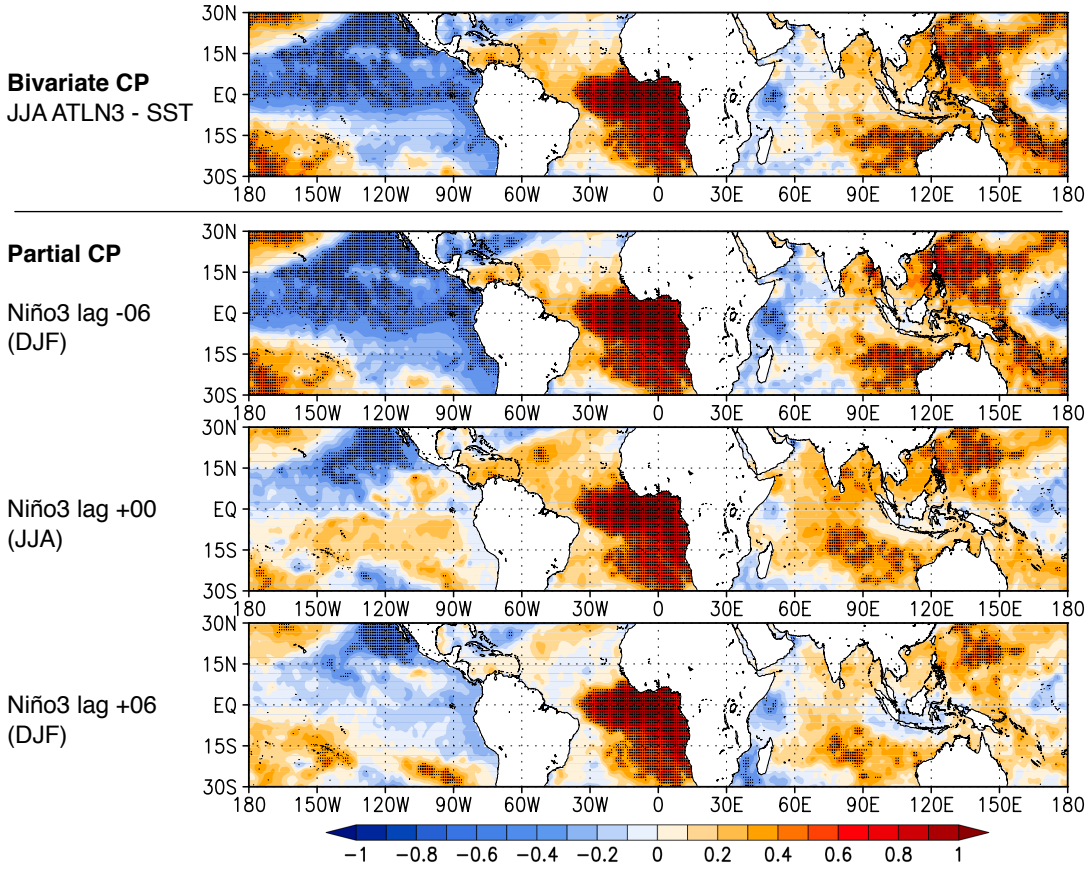

Figure 7.10: Spatial correlation patterns (CP) of bivariate and partial correlation analysis between the boreal summer ATLN3 index and the global tropical SST field for the period 1981–2012. The ENSO signal (Niño3 index is used as disturbing variable) is excluded at different time lags: for the preceding boreal winter (DJF, lag -06), summer (JJA, lag +00) and the subsequent winter (DJF, lag +06). Significant values (95 % level) are highlighted with dots.

Figure 7.10 depicts the results of bivariate (top pattern) and multivariate partial correlation analyses (remaining patterns) between the ATLN3 index and the global tropical SST field applied to the boreal summer season June–August during 1981–2012. For partial correlation, the Niño3 index is used as disturbing variable, which is excluded at different time lags. Note again that expressions such as the exclusion or removal of the effect or influence of a third variable - the Niño3 index in this case - does not mean that the variable

is excluded from the partial correlation analyses. By computing its contribution to the relationship between two variables in question - the ATLN3 index and each time series of the global tropical SST field in this case - one may estimate the remaining proportion of variability of one variable described by the other that is independent of the third one. That is, the variance that the third variable has in common with the other two variables is removed. For more description on partial correlation analysis see Section 4.1.

For the first one of the three partial correlation patterns, the preceding boreal winter Niño3 index (lag -06) is used as disturbing variable. For the second and third patterns, the influence of the simultaneous summer (lag +00) and subsequent winter (lag +06) Niño3 indices is removed, respectively. For an interpretation of the partial correlation patterns, results from bivariate correlation analysis of the ATLN3 and Niño3 indices (see Figure 7.3 (d) in Section 7.2.1) provide important additional information about the linear relationship between these two indices: insignificant correlation coefficients near zero for a negative lag of 6 months (Niño3 index leading) as well as significant negative correlations are observed for lag 0 and positive lags (Niño3 index lagging). In other words, in the first example of partial correlation analyses presented in Figure 7.10, there is no disturbing influence due to the fact that the ATLN3 and Niño3 indices are uncorrelated. Therefore, bivariate and multivariate correlations are expected to be very similar. The second and third of the three examples are representative for the exclusion of the disturbing influence of a developing and a subsequent maturing La Niña.

Comparing the bivariate and multivariate results, the pattern of the partial correlation analysis without the influence of the leading Niño3 index (DJF, lag -06) is fairly similar to the bivariate correlation pattern anywhere in the tropics, as one would expect. In the Pacific, the negative correlations north and south of the equator slightly intensify. One may assume a strengthening of the link of the Atlantic Niño to a developing Pacific La Niña due to a removed preceding El Niño. However, this quite small difference in the correlation patterns is most likely random noise. This result is consistent with the insignificant positive bivariate correlation between the ATLN3 and Niño3 indices when the Niño3 index is leading by 6 months (see Figure 7.3 (d)).

In the second case, the negative correlation coefficients in the equatorial Pacific Ocean are replaced by positive values. Furthermore, positive values appear in the northern tropical Atlantic. That is, removing the influence of a simultaneously developing Pacific La Niña leads to a correlation pattern resembling that of a decaying El Niño. However, partial correlation coefficients are insignificant in the equatorial Pacific and northern tropical Atlantic. Thus, great portions of the ENSO signal are removed in this case.

In the third case, in which the Niño3 index lags by 6 months, correlation coefficients in the equatorial Pacific are all near zero. That is, with the removal of the influence of a subsequent ENSO event in its mature phase, the signal of a developing event in the previous boreal summer months is also removed. From all three cases, the third case, i.e. the use of the subsequent boreal winter Niño3 index (DJF, time lag +06) as disturbing variable in the partial correlation analyses, most effectively removes the ENSO signal. Therefore, this time lag is chosen for the remaining analyses in this chapter if not indicated otherwise.

Another important conclusion can be drawn from the analyses presented above: in all cases the positive correlation coefficients in the tropical southeast Atlantic corresponding to the Atlantic Niño are nearly undisturbed. That means that this mode is inherent to the Atlantic Ocean and not dominated by the Pacific ENSO system. As an important consequence, its influence on remote regions other than the Pacific Ocean is maintained in partial correlation analyses.

7.3.3 Teleconnections to the Indian Ocean basin-wide mode

This section further explores co-variability between the tropical southeast Atlantic Ocean and the first mode of Indian Ocean SST variability, namely the basin-wide mode. In addition to the bivariate index correlation analyses described in Section 7.3.1, partial correlation analyses excluding the influence of the Pacific ENSO are carried out. Figure 7.11 depicts results for the boreal summer (JJA) ATLN3 index correlated with the TIO index of the following four seasons: JJA (lag +00), SON (lag +03), DJF (lag +06), MAM (lag +09). The black vertical line indicates the season of the TIO index. The partial correlation coefficient is displayed as red curve. The corresponding bivariate correlation coefficient between the ATLN3 and TIO indices, which is a scalar, is plotted as green horizontal line to facilitate the comparison of the bivariate and multivariate results. The figure further contains the bivariate results for the relation of the boreal summer ATLN3 and TIO indices to the disturbing variable, i.e. the ATLN3 and Niño3 indices (blue curve) as well as TIO and Niño3 indices (orange curve). X-axis labels correspond to the central month of the 3-month season of the disturbing variable (Niño3 index). To give an example: the peak in the red curve in Figure 7.11 (a) denotes the partial correlation coefficient between the JJA ATLN3 and the JJA TIO indices excluding the influence of the leading AMJ Niño3 index. The corresponding bivariate correlation coefficient between the JJA ATLN3 (TIO) and AMJ Niño3 indices can be taken from the blue (orange) curve.

As can be seen in Figure 7.11 (a) and (b), for the boreal summer and autumn seasons, bivariate correlation coefficients between ATLN3 and TIO indices are close to zero and thus insignificant. If the signal of a developing La Niña is removed, i.e. the AMJ Niño3 index in Figure 7.11 (a) and the JJA Niño3 index in Figure 7.11 (b), partial correlation coefficients are significant (at the 95 % level). This suggests an underestimation of the bivariate correlation between the Atlantic and Indian Oceans due to the disturbing influence of ENSO. The positive link revealed by partial correlation analysis indicates that positive SST anomalies in the Atlantic Ocean contribute to a warming of the Indian Ocean and thus counteracts the influence of the Pacific Ocean. Due to the anticorrelation of the Atlantic and Pacific Oceans, the latter induces a cooling in the western Indian Ocean basin at the same time. However, when removing the effect of the Niño3 index for the boreal autumn season and the ENSO mature phase, partial correlations are equal to the bivariate results (close to zero) for the summer (Figure 7.11 (a)) and insignificant for the autumn (Figure 7.11 (b)) examples, respectively. That means, that the relationship between the Atlantic and Indian Oceans is not stable and the significant partial correlation for negative Niño3 index lags appears to be an artifact of the choice of the time lag.

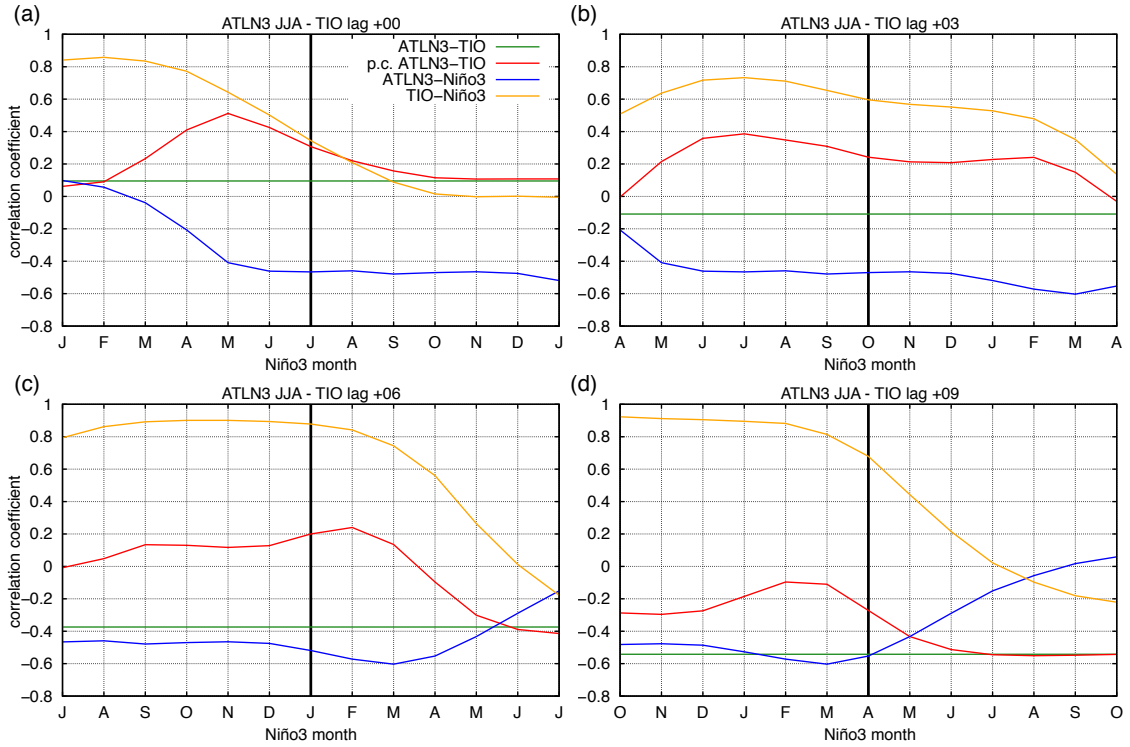

Figure 7.11: Partial correlations (red curve) between the boreal summer (JJA) ATLN3 and the TIO index for the (a) boreal summer (JJA, lag+00), (b) following autumn (SON, lag +03), (c) winter (DJF, lag +06) and (d) boreal spring (MAM, lag +09), excluding the effect of the Niño3 index (disturbing variable). The black vertical line indicates the season of the TIO index. The single value of the corresponding bivariate correlation coefficient between the ATLN3 and TIO indices is displayed as green curve. The blue (orange) curve indicates the bivariate correlations between the ATLN3 (TIO) and the Niño3 index. X-axis labels indicate the central month of the 3-month season Niño3 index.

As summarized in Section 7.1, recent studies report a significant influence of tropical southeast Atlantic SST variability on the Indian Summer Monsoon (Kucharski et al. 2007; 2008, Losada et al. 2010b) as well as Indian Ocean SSTs (Wang et al. 2009) in boreal summer months. However, the above-described results from the present analyses do not confirm a significant impact on Indian Ocean SST variability.

In the remaining two seasons, namely boreal winter (Figure 7.11 (c)) and spring (Figure 7.11 (d)), the leading JJA ATLN3 index is significantly anticorrelated with the TIO index in the bivariate case. However, removing the effect of the DJF Niño3 index reveals an overestimation of the relationship between the ATLN3 and TIO indices. Thus, the link between the two indices may be mainly attributed to the strong relationship of both the ATLN3 and TIO indices to the Niño3 index. Both the Atlantic and Indian Oceans are linked to the Pacific Ocean, but they are not significantly linked to each other.

Index correlation analyses focus on the link to only one specific SST mode in the tropical Indian Ocean, the basin-wide mode in this case. However, tropical southeast Atlantic SST variability may also be linked to a different pattern that is not well represented by an index such as the TIO index. Therefore, additional spatial patterns of partial correlation coefficients between the ATLN3 index and the SST field of the Atlantic-Indic sector are

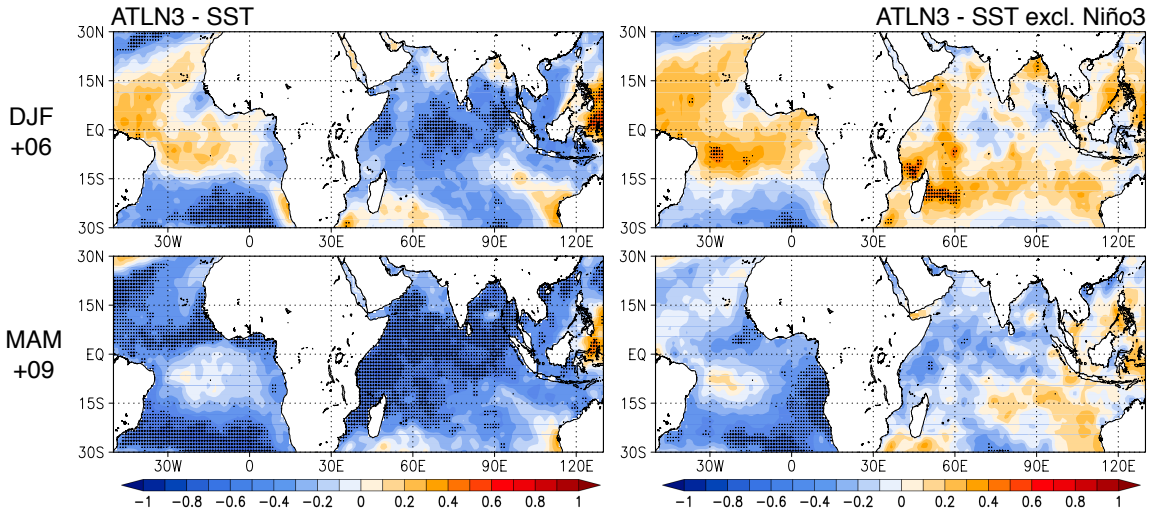

Figure 7.12: Spatial patterns of bivariate (left) and partial correlation analyses (right) between the boreal summer ATLN3 index and the following winter and spring SST fields of the Atlantic-Indic sector for the period 1981–2012. The ENSO signal is removed using the DJF Niño3 index as disturbing variable. Significant values (95 % level) are highlighted with dots.

displayed in Figure 7.12. This section focuses on the winter and spring seasons following an Atlantic Niño - yet neglected in literature - while the summer and autumn seasons are discussed in the context of the dipole mode in the subsequent Section 7.3.4.

As can be seen from the bivariate correlation results in Figure 7.12 (left patterns), the boreal winter and spring SST fields correlated with the preceding summer JJA ATLN3 index shows the typical pattern of a basin-wide warming that usually develops in response to a Pacific El Niño (e.g. Deser et al. 2010). Consistent with the anticorrelation between Atlantic and Pacific, the Indian Ocean is also anticorrelated with the ATLN3 index. That is, a basin-wide cooling is the response to a southeast Atlantic warming. However, when removing the effect of the Niño3 index in partial correlation analysis (right patterns in Figure 7.12), the basin-wide pattern disappears. A weak positive response is observed in the southern parts of the tropical Indian Ocean in boreal winter while a negative response appears in the northwestern parts in the spring season. Though, correlation coefficients are mostly insignificant at the 95 % level. These results clearly show that the basin-wide cooling in response to an Atlantic Niño indicated by significant bivariate results does not reflect an ENSO-independent link between those two modes. This link mainly exists due to the significant anticorrelation between the Atlantic and Pacific Oceans. Therefore, the basin-wide cooling is in fact the response to a Pacific La Niña while there appears to be no significant contribution of the Atlantic Niño.

Results discussed above have shown that there is no linear relationship between the Atlantic and Indian Oceans when the effect of the ENSO signal is removed. However, an ENSO-dependent interaction via a "Pacific bridge" may still exist. As discussed in Section 7.2, results for the Pacific Ocean have indicated a delayed and increased peak of ENSO events following Atlantic events. This observation gives rise to the assumption that this signal is propagated to the Indian Ocean and thus a stronger and probably delayed or prolonged basin-wide warming might follow an itself enhanced ENSO event.

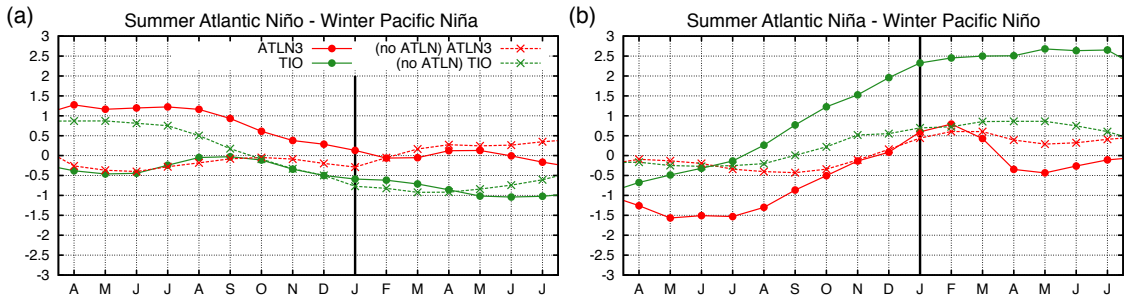

Figure 7.13: Composite time series of seasonal mean ATLN3 and TIO SST for ENSO events selected according to the following four cases: (a) Pacific Niñas (1) with and (2) without preceding summer peak Atlantic Niño (ATLN) as well as (b) Pacific Niños (3) with and (4) without preceding summer peak Atlantic Niña. X-axis labels indicate the center month of each 3-month seasonal mean, i.e. DJF is plotted at central month J. Time lag 0 (black vertical line) correspond to the ENSO mature season boreal winter (DJF). Negative (positive) lags of the lagging (leading) indices are plotted to the left (right) of the line.

To assess the question whether an enhancement of an ENSO event preceded by an Atlantic event also affects the Indian Ocean basin, the case study carried out in Section 7.2.2 is extended to the Atlantic-Indic sector. Composite time series are additionally computed for the TIO index and displayed together with the ATLN3 index composites in Figure 7.13 for the two (a) Pacific La Niña cases and the (b) El Niño cases. As can be seen from both the La Niña and the El Niño composites, in an event with a preceding Atlantic event the TIO index reaches its peak in the AMJ season and exhibits high values in the following months. This indicates that the peak is delayed by one month and also prolonged by about two months. Strong anomalies are maintained until the following boreal summer season. As noted in Section 7.2.2, the strong differences in the TIO index composites for the cases of a Pacific El Niño with and without preceding Atlantic Niña (Figure 7.13 (b)) are probably the result of a small sample size. Therefore, one may not draw conclusions from the large differences in magnitude.

Additional composites of SST, SLP as well as upper-level velocity potential and stream function (200 hPa CHI and PSI) fields of the Atlantic-Indic domain are computed for the four cases of a Pacific La Niña (El Niño) with and without a preceding Atlantic Niño (Niña). Consistent with the composite time series, the most remarkable differences are found in the boreal summer season following an ENSO event. Therefore, this season is selected for presentation in Figure 7.14. The lag +06 denotes the months after the ENSO event. The corresponding time lag for the Atlantic event is +12, e.g. the figure depicts the summer season one year after the Atlantic Niño (Case 1) or the Atlantic Niña (Case 3).

As can be seen from the patterns in the left column of Figure 7.14, negative (positive) SST anomalies corresponding to a basin-wide cooling (warming) still prevail in the summer season after a Pacific La Niña (El Niño) with a preceding Atlantic Niño (Niña). While the basin-wide cooling appears mainly in the central and western part of the Indian Ocean, warming affects the entire basin. By contrast, without a preceding Atlantic event, only weak anomalies are still left at that time whereas strong anomalies appear

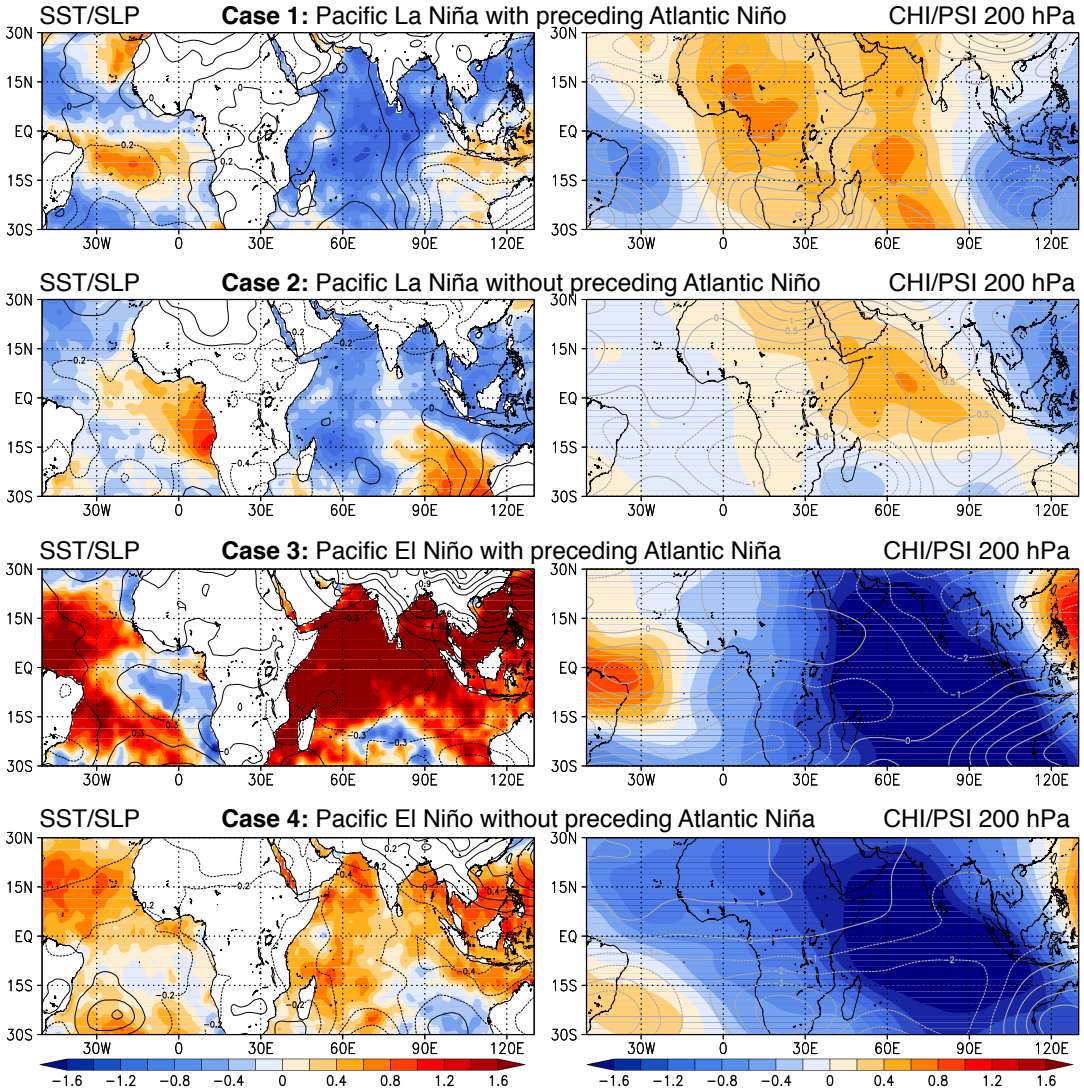

Figure 7.14: Composites of boreal summer (JJA) mean standardized high-pass filtered SST (shaded) and high-pass filtered SLP (hPa, contours), 200 hPa velocity potential (CHI, $10^6 m^2 s^{-2}$, shaded) and stream function (PSI, $10^6 m^2 s^{-2}$, contours) for ENSO events selected during 1981–2012 according to the following four cases from top to bottom: Pacific La Niña with (**Case 1**) and without (**Case 2**) preceding summer Atlantic Niño as well as Pacific El Niño with (**Case 3**) and without (**Case 4**) preceding summer Atlantic Niña. The selected JJA season is the summer season one year after the Atlantic event and 6 months after the corresponding ENSO event.

off the coast of northwestern Australia. These SST anomalies are already observed in the winter and spring season (not shown). They probably represent a Ningaloo Niño (Niña) - for a description of this phenomenon see Section 2.3.

The corresponding atmospheric anomalies differ in location for the La Niña and El Niño cases and are thus explained separately. In the case of a Pacific La Niña with preceding Atlantic Niño, Figure 7.14 (left patterns) shows an SLP gradient with positive anomalies over the western and negative anomalies over the eastern parts of the Indian Ocean basins. The corresponding CHI and PSI fields (patterns in the right column of Figure 7.14) depict large-scale anomalous upper-level convergence over the western Indian basin and anomalous divergence over the Indonesian region. Convergence and

divergence correspond to downward motion in the west and upward motion in the east, respectively. Associated anomalous westerlies maintain latent heat flux and thus surface cooling as it is described to be the typical Indian Ocean response to an ENSO event (e.g. Schott et al. 2009). However, the main region of cooling appears to be limited to the western Indian Ocean. By contrast, without an Atlantic Niño, there is no similar SLP gradient; instead positive anomalies appear in the Australian region. The corresponding CHI and PSI anomalies are generally weak. Altogether, the atmospheric picture only reveals diminishing anomalies from a decaying basin-wide cooling. A similar but reverse situation applies to the Pacific El Niño cases. Though, the SLP gradient and anomalous downward motion over the Indian Ocean basin appear shifted to the east. Warming due to a decrease in wind-induced latent heat flux may play a less dominant role in this case. Instead, an increase in solar radiation due to suppressed convection over the Indian Ocean (also see Schott et al. 2009) probably contributes to maintain the basin-wide warming which therefore covers the entire basin. The main difference between the El Niño cases with and without preceding Atlantic Niña is the magnitude of their anomalies. However, no conclusion can be drawn from this difference due to the small sample size.

Despite the small sample size of any of the cases, results do indicate a potential contribution of the Atlantic Niño (Niña) to a delay and prolongation of a Indian Ocean basin-wide cooling (warming) accompanying a Pacific La Niña (El Niño). From the composites an asymmetric SST response may be assumed. An Indian Ocean basin-wide cooling appears mainly in central and western parts of the ocean whereas warming affects the entire basin. However, this observation is more likely due to an asymmetric response of the Indian Ocean basin-wide mode to ENSO and may not be an asymmetric signal propagated from the Atlantic Ocean.

7.3.4 Teleconnections to the Indian Ocean Dipole

This section focuses on the second mode of Indian Ocean SST variability, namely the Indian Ocean Dipole, and its potential link to the tropical southeast Atlantic Ocean. Similar to the previous section, co-variability of the two oceans is explored using partial correlation analysis to exclude the influence of the Pacific ENSO. However, unlike the previous section, this section discusses the results for the simultaneous summer and following autumn seasons, which correspond to the developing and peak seasons of a typical Indian Ocean Dipole event.

Figure 7.15 depicts results for the boreal summer (JJA) ATLN3 index correlated with the IOD index of the summer (JJA, lag +00) and autumn (SON, lag +03) seasons. Similar to Figure 7.11, the black vertical line indicates the season of the IOD index. The partial correlation coefficient is displayed as red curve. The corresponding bivariate correlation coefficient between the ATLN3 and IOD indices is displayed as green horizontal line. The Figure additionally depicts the bivariate results for the relation of the ATLN3 and IOD indices to the disturbing variable, i.e. the ATLN3 and Niño3 indices (blue curve) as well as IOD and Niño3 indices (orange curve). X-axis labels correspond to the central month of the 3-month season of the disturbing variable (Niño3 index).

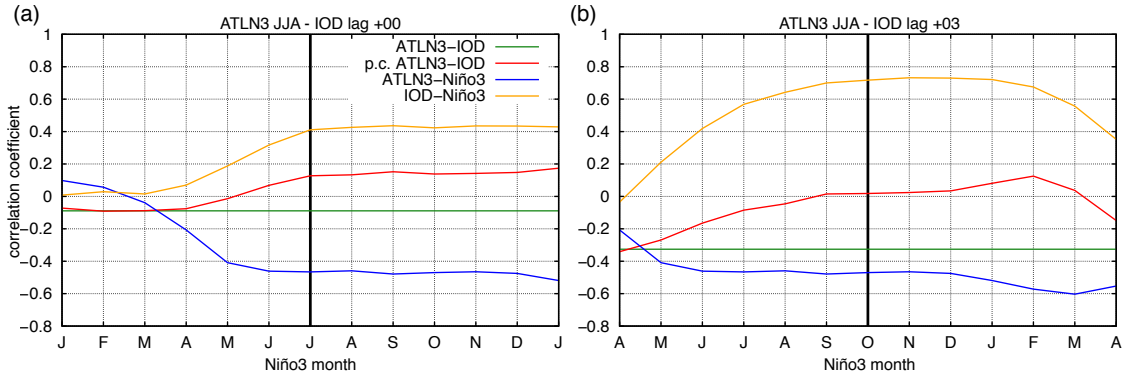

Figure 7.15: Partial correlations (red curve) between the boreal summer (JJA) ATLN3 and the IOD index for the (a) boreal summer (JJA, lag+00), (b) and following autumn (SON, lag +03), excluding the effect of the Niño3 index (disturbing variable). The black vertical line indicates the season of the TIO index. The single value of the corresponding bivariate correlation coefficient between the ATLN3 and IOD indices is displayed as green curve. The blue (orange) curve indicates the bivariate correlations between the ATLN3 (IOD) and the Niño3 index. X-axis labels indicate the central month of the 3-months season Niño3 index.

As shown in Figure 7.15 (a), both bivariate and partial correlation coefficients between the ATLN3 and IOD indices are close to zero, notwithstanding the time lag selected for the exclusion of the ENSO signal. That is, there is no simultaneous relationship between an Atlantic warm or cold event to a developing Indian Ocean Dipole event. Furthermore, Figure 7.15 (b) indicates an anticorrelation between the JJA ATLN3 index and the following autumn season (SON, lag +03). However, this correlation is weak and insignificant. With the effect of the Niño3 index removed, the partial correlation coefficient is close to zero. Thus, the weak bivariate anticorrelation is a result of the strong relationship between the Indian and Pacific Oceans and also reflects the anticorrelation of the Atlantic and Pacific Oceans. But there appears to be no link between southeast Atlantic SST variability and Indian Ocean Dipole variability.

In addition to the index correlation analyses, Figure 7.16 displays spatial patterns of bivariate and partial correlation coefficients between the ATLN3 index and the SSTs of the Atlantic-Indic domain. The patterns of bivariate correlations clearly explain the missing link between the ALTN3 and IOD indices: a typical dipole pattern is found in neither the boreal summer nor the autumn season. A large area in the central Indian Ocean is uncorrelated while only parts of the eastern and the far western basin are significantly correlated at the 95 % level. Most of these significant correlations disappear after the removal of the influence of the Niño3 index. For the boreal summer seasons, a small area of significant positive values remains in the eastern Indian Ocean. In the autumn pattern significant positive values extend from Madagascar to the center of the southern tropical Indian Ocean. However, large parts of the significant response in the bivariate results may be attributed to the influence of ENSO. In the partial correlation results, none of the two patterns corresponds to the response of the main modes of Indian Ocean SST variability, i.e. the basin-wide mode or the Indian Ocean mode. That means, the positive link to the Indian Ocean in boreal summer reported by Wang et al. (2009) is not confirmed by the

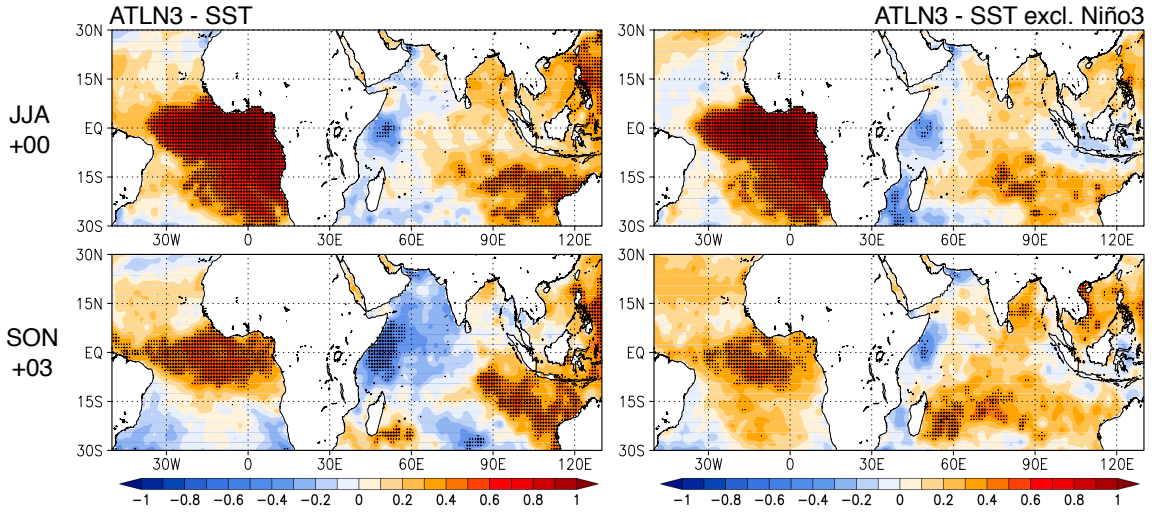

Figure 7.16: Spatial patterns of bivariate and partial correlation analysis between the boreal summer ATLN3 index and the summer and autumn SST fields of the Atlantic-Indic sector for the period 1981–2012. The ENSO signal is removed using the DJF Niño3 index as disturbing variable. Significant values (95 % level) are highlighted with dots.

results presented here. However, the study of the former authors uses a different time period (1950–1999) that includes both decades with and without significant correlations between the Atlantic and Pacific Oceans. This may explain the different results.

Although the correlation analyses discussed above have shown that there is no significant link between southeast Atlantic SST variability and the Indian Ocean dipole, additional composites are computed to investigate a potential asymmetric response. For that, the case study carried out for the TIO index as well as the boreal summer SST and atmospheric patterns in the previous section is now applied to the IOD index and to patterns of the IOD peak season boreal autumn. Composite time series for the ATLN3 and IOD indices are displayed in Figure 7.17. Boreal autumn SST, SLP and 200 hPa velocity potential (CHI) and stream function (PSI) composites are shown in Figure 7.18. The four cases of a Pacific La Niña (1) with and (2) without preceding summer peak Atlantic Niño as well as a Pacific El Niño (3) with and (4) without preceding summer peak Atlantic Niña correspond to the four cases introduced in Section 7.2.2.

As can be seen from the Niño3 index composite time series in Figure 7.17 (a), a pronounced dipole appears in neither the case of a Pacific La Niña with nor without a preceding Atlantic Niño. Only weak negative anomalies are observed in the autumn season. This explains why both the bivariate and the partial correlation coefficients for the ATLN3 and IOD indices are insignificant or even close to zero (Figure 7.15). Figure 7.18 confirms these results as the corresponding SST patterns for Case 1 and 2 do not depict a typical IOD pattern. Furthermore, in the associated atmospheric patterns, an anomalous downward branch (indicated by anomalous upper-level convergence) of the Indian Walker cell over the eastern Indian Ocean off the African continent corresponding to an IOD cold event is missing. Thus, none of the typical characteristics corresponding to an Indian Ocean Dipole event (as described by e.g. Saji and Yamagata 2003a) is found in the

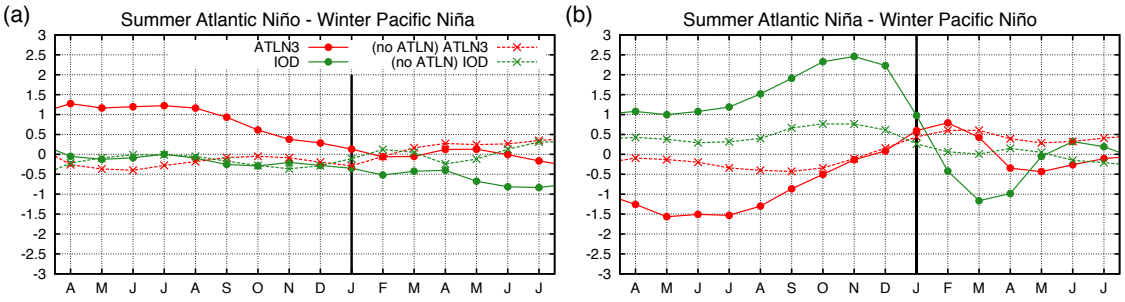

Figure 7.17: Composite time series of seasonal mean ATLN3 and IOD SST for ENSO events selected according to the following cases: (a) Pacific Niñas (1) with and (2) without preceding summer peak Atlantic Niño (ATLN) as well as (b) Pacific Niños (3) with and (4) without preceding summer peak Atlantic Niña. X-axis labels indicate the center month of each 3-month seasonal mean, i.e. DJF is plotted at central month J. Time lag 0 (black vertical line) corresponds to the ENSO mature season boreal winter (DJF). Negative (positive) lags of the lagging (leading) indices are plotted to the left (right) of the line.

composites. Therefore, in the selected study period 1981–2012, a developing Pacific La Niña does not appear to be accompanied by a pronounced IOD cold event.

By contrast, the Niño3 index composite time series in 7.17 (b) and the corresponding SST pattern in Figure 7.18 (Case 3) show a strong typical dipole response of the Indian Ocean to a Pacific El Niño with a preceding Atlantic Niño and a weaker response without a preceding Atlantic Niño (Figure 7.18, Case 4). The corresponding atmospheric patterns show the picture of an altered Indian Walker cell with anomalous upper-level convergence (divergence) and thus downward (upward) motion over the Indonesian Archipelago (off the African continent), inducing low-level equatorial easterly wind anomalies. Thus, the typical atmospheric patterns associated with an IOD warm event are found in the composites. Consistent with a weaker dipole pattern, the corresponding Walker cell anomaly is less well developed in the case of a Pacific El Niño without preceding Atlantic Niño. Therefore, results of the present case study suggest the enhancement of an IOD warm event accompanying a developing Pacific El Niño in boreal autumn. However, as already noted earlier, the sample of Case 3 only contains two events and may contain two particularly strong events. The magnitude of the difference between Case 3 and 4 can therefore not be evaluated. That means, it is likely that the enhancement of the IOD warm events is a coincidental result. Furthermore, the difference in the response to an Atlantic warm and cold event may rather reflect an asymmetric response of IOD variability to Pacific SST variability. Therefore, from the results presented in this section, it is assumed that no link between an Atlantic Niña and an Indian Ocean Dipole event exists, as was already suggested by the correlation analyses.

7.4 Summary

This chapter has discussed the teleconnections of the tropical Atlantic Ocean to the tropical Pacific and Indian Oceans. Co-variability of these oceans has been assessed by means of bivariate correlation analyses. Additional partial correlation analyses have been carried

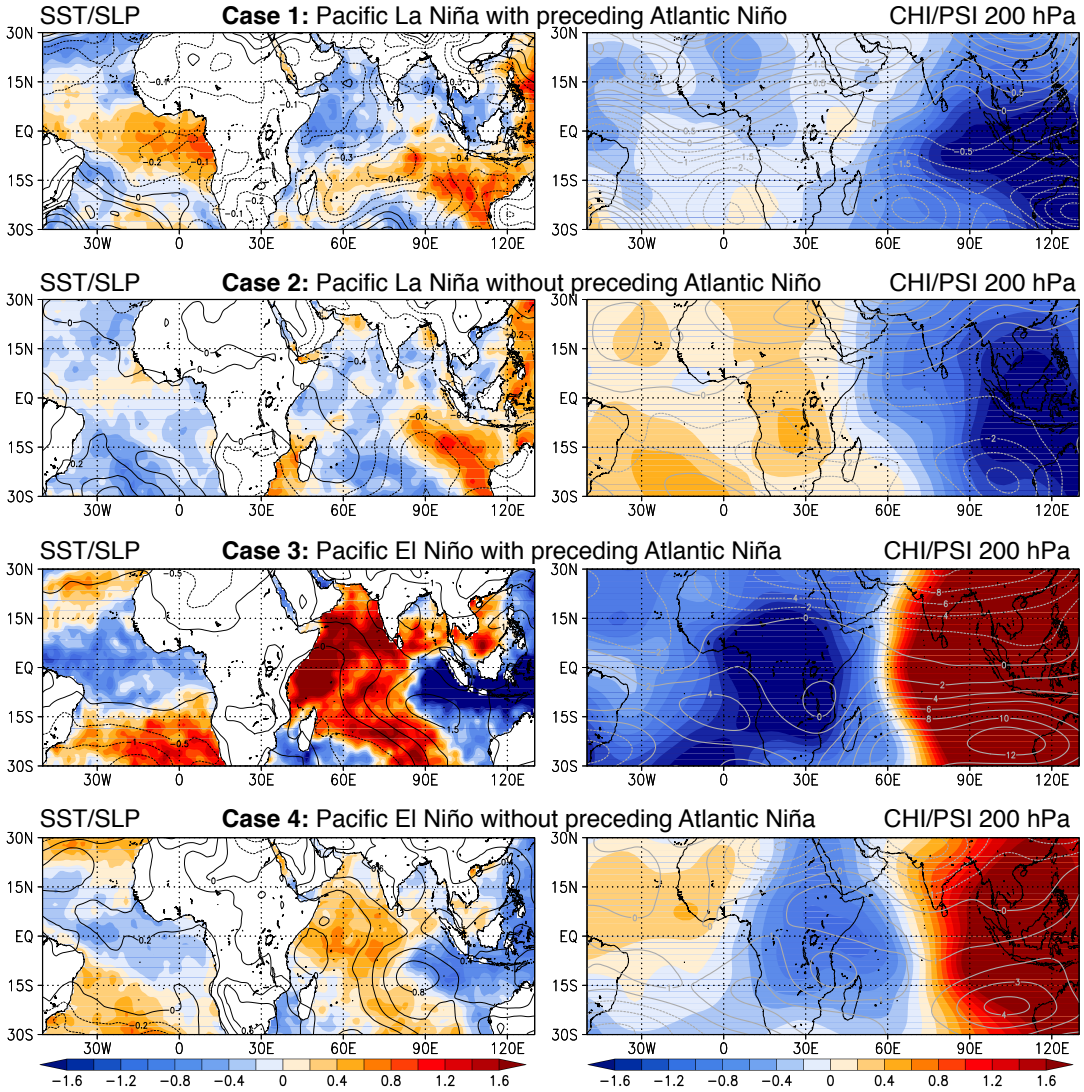

Figure 7.18: Composites of boreal autumn (SON) mean standardized high-pass filtered SST (shaded) and high-pass filtered SLP (hPa, contours), 200 hPa velocity potential (CHI, $10^6 m^2 s^{-2}$, shaded) and stream function (PSI, $10^6 m^2 s^{-2}$, contours) for ENSO events selected during 1981–2012 according to the following four cases from top to bottom: Pacific La Niña with (**Case 1**) and without (**Case 2**) preceding summer Atlantic Niño as well as Pacific El Niño with (**Case 3**) and without (**Case 4**) preceding summer Atlantic Niña. The selected SON season corresponds to the autumn season three months after the Atlantic event and 3 months before the corresponding ENSO event.

out for the analyses of the teleconnections between the Atlantic and Indian Oceans that are independent of ENSO. Furthermore, a case study of selected ENSO events with and without preceding Atlantic summer events in the period 1981–2012 has been performed in order to investigate whether an Atlantic influence on the Pacific and Indian Oceans applies to both the Niño and the Niña case.

For the tropical Atlantic and Pacific Oceans, results reveal a non-stationary linear relationship between the two ocean basins. No significant link is found for the earlier sub-period 1951–1980. By contrast, in the recent sub-period 1981–2012 boreal summer Atlantic SSTs are significantly anticorrelated with late boreal winter Pacific SSTs, i.e. when

the Atlantic leads the Pacific by 8 months. Consistent with earlier work, analyses of both SST and atmospheric patterns suggest an enhancement of a Pacific La Niña (El Niño) by a preceding Atlantic Niño (Niña) via an altered Walker circulation. However, the present results indicate a strengthened peak delayed to boreal spring in contrast to the suggested enhanced boreal winter peak.

An additional case study for the period 1981–2012 investigating boreal winter Pacific La Niña (El Niño) events with preceding summer Atlantic Niño (Niña) events further confirms the hypothesized influence of the Atlantic on the Pacific Ocean. Despite the small sample size, results are consistent with those from correlation analysis. That is, the case study confirms a delayed and enhanced peak for ENSO events with preceding Atlantic events. Furthermore, results indicate that the observed delay and enhancement of the peak applies to both a Pacific La Niña and an El Niño in response to an inverse anomaly in the Atlantic Ocean, i.e. a warm and cold event, respectively.

For the tropical Atlantic and Indian Oceans, no significant links were found that are independent of ENSO. Boreal summer Atlantic SSTs and the Indian basin-wide mode are significantly correlated in bivariate analyses when the Atlantic leads the Indian Ocean by $9-10$ months. However, partial correlation results are insignificant, revealing that the basin-wide mode is mainly influenced by the Pacific ENSO. This ENSO-dependent link is further investigated in a case study comparing the cases of an Indian basin-wide response to a Pacific La Niña (El Niño) with and without preceding Atlantic Niño (Niña). Consistent with the bivariate correlation analyses, results from the case study indicate a potential delay and prolongation of the basin-wide cooling (warming) accompanying a Pacific La Niña (El Niño) when preceded by an Atlantic warm (cold) event.

Furthermore, a significant response of the Indian Ocean Dipole to southeast Atlantic SSTs was neither found in the results including nor in those excluding the influence of the ENSO signal. Altogether, the influence of the Atlantic Ocean on Indian Ocean SST variability appears to be inferior to that of the Pacific ENSO system.

8

Conclusions and Outlook

Conclusions

This thesis has investigated sea surface temperature variability in the tropical southeast Atlantic Ocean and presents detailed analyses of Atlantic warm and cold water events, their impact on African west coast precipitation as well as their global interactions with the tropical Pacific and Indian Oceans.

Several important conclusions can be drawn from the results presented in this work:

I) A thorough analysis of south Atlantic sea surface temperatures has shown that there exists one dominant and persistent mode of SST variability in the tropical southeast Atlantic Ocean. Its center of variation extends from the western equatorial Atlantic to the coast off Angola and Namibia, covering the entire Gulf of Guinea in between. This clearly indicates that both the equatorial Atlantic and the coastal waters off Angola share a great portion of interannual variability. From this observation it may further be assumed that there is at least a strong link between Atlantic and Benguela Niños if they are not even part of one phenomenon. Consequently, three new Atlantic Niño (ATLN) regions and corresponding indices are defined such that they cover both the equatorial and coastal region and the area in between. The strong correlation found amongst the indices further confirms the link between equatorial Atlantic and coastal SST variability. Thus, in this thesis, Atlantic and Benguela Niños, previously considered as separate phenomena, are now integrated into one single classification. Warm and cold events in the tropical southeast Atlantic are thereby classified into three sub-types of one comprehensive Atlantic Niño with regard to their different regional character. That is, one major contribution of this work is that it provides a unified classification that serves as a solid base for further research on Atlantic warm and cold events.

II) SST anomalies in the tropical southeast Atlantic are associated with profound large-scale changes in the overlaying atmosphere. During warm events, a southward displacement of an intensified ITCZ, a weakened South Atlantic Anticyclone as well as a southward shift of the mid-latitude westerlies can be observed, along with a weakening of the trade winds covering large parts of the south Atlantic. This altered circulation pattern strongly impacts rainfall distribution along the entire African west coast. Major changes include:

- Increased rainfall in Gabon in late boreal spring as well as an intensification of the summer monsoon over West African are observed due to the southward shift of the ITCZ.
- Boreal winter precipitation in Angola and northern Namibia is increased, which may be attributed to increased moisture flux from the Indian Ocean and weakened southeasterly flux away from the southeast Atlantic coast.
- Boreal autumn precipitation is reduced in South Africa due to a southward shift of the mid-latitude westerlies.

A similar but inverse response may be observed for Atlantic cold events although results indicate an asymmetry in season and magnitude in some of the regions. For instance, Atlantic Niña events appear to contribute to a stronger decrease in West African monsoon rainfall than the increase is for Atlantic Niño events.

Furthermore, in several regions non-stationarities are observed in the SST-rainfall relationship. Changes in the link may be partly attributed to the counteracting effects of Atlantic Niños and Pacific La Niñas, which co-occur in recent decades.

III) The aforementioned altered large-scale circulation not only affects the distribution of regional rainfall. An altered zonal circulation also contributes to changes in remote tropical regions:

- Results presented in this thesis indicate that boreal summer Atlantic Niños (Niñas) are associated with an altered Walker circulation and anomalous ascending (descending) motion in the equatorial Atlantic. These changes contribute to a strengthening (weakening) of the Pacific Walker cell and thus to an enhancement of a Pacific La Niña (El Niño) during the following boreal winter. Consistent with a significant anticorrelation when the Atlantic Ocean leads by 8 months, the peak of a Pacific La Niña appears to be enhanced and delayed by two months to boreal spring. From a composite case study carried out in this thesis, it may be further assumed that these changes apply to both the Atlantic warm and cold case in a similar but inverse way.
- No ENSO-independent links appear to exist between the Atlantic and Indian Ocean SST variability. ENSO is the dominant influence in the Indian Ocean sector. Yet, results indicate that the Atlantic signal enhancing ENSO events is also propagated to the Indian Ocean. Thus, an Atlantic Niño (Niña) contributes to a strengthening and prolongation of an Indian Ocean basin-wide cooling (warming).

- Both these links are non-stationary and were established after the climate shift in the late 1970s. Since then, Atlantic and Pacific events co-occur. That is, only in the recent three decades, boreal Atlantic Niños (Niñas) are followed by subsequent winter Pacific La Niñas (El Niños) and an associated Indian Ocean basin-wide cooling (warming) in the following spring.

From all analyses based on the three ATLN indices and the new Niño classification another important conclusion can be drawn: all three indices and all Niño event classes have been shown to be relevant on both regional and global scales. Yet, interesting differences have been observed, as one would already expect from their different geographical location. In the regional impact analyses, the strongest links between precipitation regions and SSTs are not limited to one specific ATLN index but differ amongst the precipitation regions. In the tropical teleconnection analyses, the strongest links are observed to the equatorial ATLN3 index although the remaining indices also reflect these connections at weaker but still significant magnitudes. It is further assumed that the ATLN1 and 2 regions are more relevant in teleconnections to the extratropics.

Comparing these observations to that of the Pacific Ocean, both similarities and differences are discovered. The Pacific Ocean similarly holds two phenomena associated with strong positive SST anomalies, namely the well-known and well-studied conventional El Niño and the only recently described El Niño Modoki. The conventional type is associated with anomalies in the eastern Pacific Ocean while the Modoki type is centered in the central Pacific Ocean. One may at first compare these two to the two types in the Atlantic Ocean, namely the Benguela Niño and the equatorial Atlantic Niño, previously regarded as separate phenomena. However, the conventional Pacific El Niño and El Niño Modoki clearly differ in their associated atmospheric patterns. In contrast, in the Atlantic Ocean the two Niño types are associated with fairly similar large-scale atmospheric patterns, in support of the hypothesis of one Niño phenomenon in the Atlantic Ocean.

Instead, the regional differences between individual Atlantic Niño events and their associated response can be compared to the differences between individual events of the conventional Pacific El Niño type. For both the Atlantic Niño and the conventional Pacific El Niño types, the regional character of warm and cold events varies from case to case, with differences in the magnitude of SST values off the adjacent continents and in the central part of the ocean basins. But despite varying magnitudes in the SST patterns, the general oceanic and atmospheric patterns remain the same.

To conclude, the generalized concept of one comprehensive Atlantic Niño presented in this thesis seems justified and useful for subsequent analyses. Yet, future studies should be carried out with respect to the different regional character of the events.

Outlook

Results presented in this thesis have clearly shown the importance and relevance of the Atlantic Niño on both regional and global scales. The present analyses provide an important contribution towards a better understanding of the still comparably little studied

phenomenon. Based on the new generalized concept of one comprehensive Atlantic Niño, several aspects may be worth exploring in future work and are sketched in the following.

- The extensive analysis performed to investigate the impact of tropical southeast Atlantic SSTs on the regional rainfall distribution of the adjacent continents had its main focus on the west coast of sub-Saharan Africa. This analysis should be extended to the east and southeast of Africa as well as the South American continent to achieve a deeper understanding of the impact of Atlantic warm and cold events with respect to their different regional character.

- Both regional and global analyses have indicated non-stationaries. Especially the co-occurrence of Atlantic and ENSO events since the climate shift appears to have profound effects on both scales. Thus, future work should further explore non-stationarities in the regional rainfall relationship as well as in tropical teleconnections with respect to decadal-scale variations in the influence of the ENSO system.

- Regarding teleconnection analyses, this thesis has focused on the connections between the tropical ocean basins. Future work should further explore extratropical teleconnections. The present analyses have provided valuable insights into the character of both Atlantic Niños and Niñas as well as associated changes in the large-scale circulation that may help to further investigate known and to discover yet unknown links to the extratropics.

Bibliography

Ångström, A. (1935). Teleconnections of the climatic changes in present time. *Geografiska Annaler* **17**: 242–258.

Alexander, M. A., Bladé, I., Newman, M., Lanzante, J. R. and Lau, N.-C. (2002). The Atmospheric Bridge: The Influence of ENSO Teleconnections on Air-Sea Interaction over the Global Oceans. *Journal of Climate* **15**: 2205–2231.

Allan, R. and Ansell, T. (2006). A New Globally Complete Monthly Historical Gridded Mean Sea Level Pressure Dataset (HadSLP2): 1850-2004. *Journal of Climate* **19**: 5816–5842.

Allan, R., Chambers, D., Drosdowsky, W., Latif, M., Nicholls, N., Smith, I., Stone, R. and Tourre, Y. (2001). Is there an Indian Ocean dipole, and is it independent of the El Niño-Southern Oscillation? *CLIVAR Exchanges* **6**: 18–22.

An, S.-I. and Jin, F.-F. (2004). Nonlinearity and Asymmetry of ENSO. *Journal of Climate* **17**: 2399–2412.

Annamalai, H., Liu, P. and Xie, S.-P. (2005a). Southwest Indian Ocean SST Variability: Its Local Effect and Remote Influence on Asian Monsoons. *Journal of Climate* **18**: 4150–4167.

Annamalai, H., Kida, S. and Hafner, J. (2010). Potential Impact of the Tropical Indian Ocean-Indonesian Seas on El Niño Characteristics. *Journal of Climate* **23**: 3933–3952.

Annamalai, H., Xie, S.-P. and McCreary, J. P. (2005b). Impact of Indian Ocean Sea Surface Temperature on Developing El Niño. *Journal of Climate* **18**: 302–319.

Ashok, K., Behera, S. K., Rao, S. A., Weng, H. and Yamagata, T. (2007). El Niño Modoki and its possible teleconnection. *Journal of Geophysical Research* **112**: C11007.

Ashok, K. and Yamagata, T. (2009). The El Niño with a difference. *Nature* **461**: 481–483.

Backhaus, K., Erichson, B., Plinke, W. and Weiber, R. (2011). *Multivariate Analysemethoden: Eine anwendungsorientierte Einführung*. Springer, Heidelberg.

Bahrenberg, G., Giese, E. and Nipper, J. (1990). *Statistische Methoden in der Geographie. Band 1 - Univariate und Bivariate Statistik*. Teubner, Stuttgart.

Bahrenberg, G., Giese, E. and Nipper, J. (1992). *Statistische Methoden in der Geographie. Band 2 - Multivariate Statistik*. Teubner, Stuttgart.

Balas, N., Nicholson, S. E. and Klotter, D. (2007). The relationship of rainfall variability in West Central Africa to sea-surface temperature fluctuations. *International Journal of Climatology* **27**: 1335–1349.

Baquero-Bernal, A., Latif, M. and Legutke, S. (2002). On Dipolelike Variability of Sea Surface Temperature in the Tropical Indian Ocean. *Journal of Climate* **15**: 1358–1368.

Barimalala, R., Bracco, A. and Kucharski, F. (2011). The representation of the South Tropical Atlantic teleconnection to the Indian Ocean in the AR4 coupled models. *Climate Dynamics* **38**: 1147–1166.

Barnett, T. P. and Preisendorfer, R. W. (1987). Origins and levels of monthly and seasonal forecast skill for United States surface air temperatures determined by canonical correlation analysis. *Monthly Weather Review* **115**: 1825–1850.

Beck, C. and Philipp, A. (2010). Evaluation and comparison of circulation type classifications for the European domain. *Physics and Chemistry of the Earth, Parts A/B/C* **35**: 374–387.

Behera, S. K. and Yamagata, T. (2003). Influence of the Indian Ocean Dipole on the Southern Oscillation. *Journal of the Meteorological Society of Japan* **81**: 169–177.

Bjerknes, J. (1969). Atmospheric teleconnections from the equatorial Pacific. *Monthly Weather Review* **97**: 163–172.

Boyd, A. J., Salat, J. and Masó, M. (1987). The seasonal intrusion of relatively saline water on the shelf off northern and central Namibia. *South African Journal of Marine Science* **5**: 107–120.

Bracco, A., Kucharski, F., Molteni, F., Hazeleger, W. and Severijns, C. (2005). Internal and forced modes of variability in the Indian Ocean. *Geophysical Research Letters* **32**: L12707.

Buckle, C. (1996). *Weather and climate in Africa*. Longman, Harlow, UK.

Camberlin, P., Janicot, S. and Poccard, I. (2001). Seasonality and atmospheric dynamics of the teleconnection between African rainfall and tropical sea-surface temperature: Atlantic vs. ENSO. *International Journal of Climatology* **21**: 973–1005.

Carton, J. A. and Huang, B. (1994). Warm Events in the Tropical Atlantic. *Journal of Physical Oceanography* **24**: 888–903.

Chang, P., Fang, Y., Saravanan, R., Ji, L. and Seidel, H. (2006a). The cause of the fragile relationship between the Pacific El Niño and the Atlantic Niño. *Nature* **443**: 324–328.

Chang, P., Ji, L. and Li, H. (1997). A decadal climate variation in the tropical Atlantic Ocean from thermodynamic air-sea interactions. *Nature* **385**: 516–518.

Chang, P., Yamagata, T., Schopf, P., Behera, S. K., Carton, J. A., Kessler, W. S., Meyers, G., QU, T., Schott, F., Shetye, S. and Xie, S.-P. (2006b). Climate Fluctuations of Tropical Coupled Systems-The Role of Ocean Dynamics. *Journal of Climate* **19**: 5122–5174.

Chiang, J. C. H. and Lintner, B. R. (2005). Mechanisms of Remote Tropical Surface Warming during El Niño. *Journal of Climate* **18**: 4130–4149.

Chiang, J. C. H. and Sobel, A. H. (2002). Tropical Tropospheric Temperature Variations Caused by ENSO and Their Influence on the Remote Tropical Climate. *Journal of Climate* **15**: 2616–2631.

Compo, G. P., Whitaker, J. S., Sardeshmukh, P. D., Matsui, N., Allan, R. J., Yin, X., Gleason, B. E., Vose, R. S., Rutledge, G., Bessemoulin, P., Brönnimann, S., Brunet, M., Crouthamel, R. I., Grant, A. N., Groisman, P. Y., Jones, P. D., Kruk, M. C., Kruger, A. C., Marshall, G. J., Maugeri, M., Mok, H. Y., Nordli, Ø., Ross, T. F., Trigo, R. M., Wang, X. L., Woodruff, S. D. and Worley, S. J. (2011). The Twentieth Century Reanalysis Project. *Quarterly Journal of the Royal Meteorological Society* **137**: 1–28.

Czaja, A., van der Vaart, P. and Marshall, J. (2002). A Diagnostic Study of the Role of Remote Forcing in Tropical Atlantic Variability. *Journal of Climate* **15**: 3280–3290.

Delecluse, P., Servain, J., Levy, C., Arpe, K. and Bengtsson, L. (1994). On the connection between the 1984 Atlantic warm event and the 1982-1983 ENSO. *Tellus A* **46**: 448–464.

Deser, C., Alexander, M. A., Xie, S.-P. and Phillips, A. S. (2010). Sea Surface Temperature Variability: Patterns and Mechanisms. *Annual Review of Marine Science* **2**: 115–143.

Dezfuli, A. K. and Nicholson, S. E. (2013). The Relationship of Rainfall Variability in Western Equatorial Africa to the Tropical Oceans and Atmospheric Circulation. Part II: The Boreal Autumn. *Journal of Climate* **26**: 66–84.

Ding, H., Keenlyside, N. S. and Latif, M. (2012). Impact of the Equatorial Atlantic on the El Niño Southern Oscillation. *Climate Dynamics* **38**: 1965–1972.

Doi, T., Behera, S. K. and Yamagata, T. (2013). Predictability of the Ningaloo Niño/Niña. *Scientific Reports* **3**.

Dommenget, D. and Latif, M. (2000). Interannual to Decadal Variability in the Tropical Atlantic. *Journal of Climate* **13**: 777–792.

Dommenget, D. and Latif, M. (2002). A Cautionary Note on the Interpretation of EOFs. *Journal of Climate* **15**: 216–225.

Dommenget, D., Semenov, V. and Latif, M. (2006). Impacts of the tropical Indian and Atlantic Oceans on ENSO. *Geophysical Research Letters* **33**: L11701.

Feng, M., McPhaden, M. J., Xie, S.-P. and Hafner, J. (2013). La Niña forces unprecedented Leeuwin Current warming in 2011. *Scientific Reports* **3**.

Florenchie, P., Lutjeharms, J. R. E., Reason, C. J. C., Masson, S. and Rouault, M. (2003). The source of Benguela Niños in the South Atlantic Ocean. *Geophysical Research Letters* **30**: 1505.

Florenchie, P., Reason, C. J. C., Lutjeharms, J. R. E., Rouault, M., Roy, C. and Masson, S. (2004). Evolution of Interannual Warm and Cold Events in the Southeast Atlantic Ocean. *Journal of Climate* **17**: 2318–2334.

Foltz, G. R. and McPhaden, M. J. (2010). Interaction between the Atlantic meridional and Niño modes. *Geophysical Research Letters* **37**: L18604.

Frauen, C. and Dommenget, D. (2012). Influences of the tropical Indian and Atlantic Oceans on the predictability of ENSO. *Geophysical Research Letters* **39**: L02706.

Gammelsrød, T., Bartholomae, C. H., Boyer, D. C., Filipe, V. L. L. and O'Toole, M. J. (1998). Intrusion of warm surface water along the Angolan-Namibian coast in February-March 1995: the 1995 Benguela Niño. *South African Journal of Marine Science* **19**: 41–56.

Ghil, M. (2002). Advanced spectral methods for climatic time series. *Reviews of Geophysics* **40**: 1–41.

Giannini, A., Saravanan, R. and Chang, P. (2003). Oceanic forcing of Sahel rainfall on interannual to interdecadal time scales. *Science* **302**: 1027–30.

Gimeno, L., Drumond, A., Nieto, R., Trigo, R. M. and Stohl, A. (2010). On the origin of continental precipitation. *Geophysical Research Letters* **37**.

Gimeno, L., Stohl, A., Trigo, R. M., Dominguez, F., Yoshimura, K., Yu, L., Drumond, A., Durán-Quesada, A. M. and Nieto, R. (2012). Oceanic and terrestrial sources of continental precipitation. *Reviews of Geophysics* **40**: RG4003.

Ham, Y.-G., Kug, J.-S. and Park, J.-Y. (2013a). Two distinct roles of Atlantic SSTs in ENSO variability: North Tropical Atlantic SST and Atlantic Niño. *Geophysical Research Letters* **40**: 4012–4017.

Ham, Y.-G., Kug, J.-S., Park, J.-Y. and Jin, F.-F. (2013b). Sea surface temperature in the north tropical Atlantic as a trigger for El Niño/Southern Oscillation events. *Nature Geoscience* **6**: 112–116.

Harris, I., Jones, P., Osborn, T. and Lister, D. (2013). Updated high-resolution grids of monthly climatic observations - the CRU TS3.10 Dataset. *International Journal of Climatology* **34**: 623-642.

Hastenrath, S. (1984). Interannual Variability and Annual Cycle: Mechanisms of Circulation and Climate in the Tropical Atlantic Sector. *Monthly Weather Review* **112**: 1097–1107.

Hermes, J. C. and Reason, C. J. C. (2009). Variability in sea-surface temperature and winds in the tropical south-east Atlantic Ocean and regional rainfall relationships. *International Journal of Climatology* **21**: 11–21.

Hertig, E. (2004). *Niederschlags- und Temperaturabschätzungen für den Mittelmeerraum unter anthropogen verstärktem Treibhauseffekt*. PhD thesis, University of Augsburg.

Hertig, E. and Jacobeit, J. (2010). Predictability of Mediterranean climate variables from oceanic variability. Part I: Sea surface temperature regimes. *Climate Dynamics* **36**: 811–823.

Heymans, J. J., Shannon, L. J. and Jarre, A. (2004). Changes in the northern Benguela ecosystem over three decades: 1970s, 1980s, and 1990s. *Ecological Modelling* **172**: 175–195.

Hirst, A. C. and Hastenrath, S. (1983). Atmosphere-Ocean Mechanisms of Climate Anomalies in the Angola-Tropical Atlantic Sector. *Journal of Climate* **13**: 1146–1157.

Hoerling, M. P., Kumar, A. and Zhong, M. (1997). El Niño, La Niña, and the Nonlinearity of Their Teleconnections. *Journal of Climate* **10**: 1769–1786.

Houghton, R. W. and Tourre, Y. M. (1992). Characteristics of Low-Frequency Sea Surface Temperature Fluctuations in the Tropical Atlantic. *Journal of Climate* **5**: 765–772.

Hu, Z.-Z., Kumar, A., Huang, B. and Zhu, J. (2013). Leading Modes of the Upper-Ocean Temperature Interannual Variability along the Equatorial Atlantic Ocean in NCEP GODAS. *Journal of Climate* **26**: 4649–4663.

Huang, B. (2002). The ENSO effect on the tropical Atlantic variability: A regionally coupled model study. *Geophysical Research Letters* **29**: 2039.

Huang, B. (2004). Remotely forced variability in the tropical Atlantic Ocean. *Climate Dynamics* **23**: 133–152.

Jacobeit, J. (1993). Regionale Unterschiede im atmosphärischen Zirkulationsgeschehen bei globalen Klimaveränderungen. *Die Erde* **124**: 63–77.

Janicot, S., Harzallah, A., Fontaine, B. and Moron, V. (1998). West African Monsoon Dynamics and Eastern Equatorial Atlantic and Pacific SST Anomalies (1970-88). *Journal of Climate* **11**: 1874–1882.

Jansen, M., Dommenget, D. and Keenlyside, N. S. (2009). Tropical Atmosphere-Ocean Interactions in a Conceptual Framework. *Journal of Climate* **22**: 550–567.

Jolliffe, I. T. (2002). *Principal Component Analysis*. Springer, New York.

Joly, M. and Voldoire, A. (2010). Role of the Gulf of Guinea in the inter-annual variability of the West African monsoon: what do we learn from CMIP3 coupled simulations? *International Journal of Climatology* **1856**: 1843–1855.

Kalnay, E., Kanamitsu, M., Kistler, R., Collins, W., Deaven, D., Gandin, L., Iredell, M., Saha, S., White, G., Woollen, J., Zhu, Y., Chelliah, M., Ebisuzaki, W., Higgins, W., Janowiak, J., Mo, K. C., Ropelewski, C., Wang, J., Leetmaa, A., Reynolds, R., Jenne, R. and Joseph, D. (1996). The NCAR/NCEP 40-year Reanalysis Project. *Bulletin of the American Meteorological Society* **77**: 437–470.

Kao, H.-Y. and Yu, J.-Y. (2009). Contrasting Eastern-Pacific and Central-Pacific Types of ENSO. *Journal of Climate* **22**: 615–632.

Kataoka, T., Tozuka, T., Behera, S. and Yamagata, T. (2013). On the Ningaloo Niño/Niña. *Climate Dynamics*.

Kayano, M. T., Andreoli, R. V. and Ferreira de Souza, R. A. (2011). Evolving anomalous SST patterns leading to ENSO extremes: relations between the tropical Pacific and Atlantic Oceans and the influence on the South American rainfall. *International Journal of Climatology* **31**: 1119–1134.

Keenlyside, N. S., Ding, H. and Latif, M. (2013). Potential of equatorial Atlantic variability to enhance El Niño prediction. *Geophysical Research Letters* **40**: 2278–2283.

Keenlyside, N. S. and Latif, M. (2007). Understanding Equatorial Atlantic Interannual Variability. *Journal of Climate* **20**: 131–142.

Kistler, R., Kalnay, E., Collins, W., Saha, S., White, G., Woollen, J., Chelliah, M., Ebisuzaki, W., Kanamitsu, M., Kousky, V., van den Dool, H., Jenne, R. and Fiorino, M. (2001). The NCEP/NCAR 50-Year Reanalysis: Monthly Means CD-ROM and Documentation. *Bulletin of the American Meteorological Society* **82**: 247–268.

Klein, S., Soden, B. J. and Lau, N.-C. (1999). Remote Sea Surface Temperature Variations during ENSO: Evidence for a Tropical Atmospheric Bridge. *Journal of Climate* **12**: 917–932.

Kouadio, Y. K. (2003). Tropical Atlantic and rainfall variability in Côte d'Ivoire *Geophysical Research Letters* **30**: 8005.

Krishna Kumar, K., Rajagopalan, B. and Cane, M. A. (1999). On the weakening relationship between the indian monsoon and ENSO. *Science* **284**: 2156–2159.

Krishnamurthy, V. and Kirtman, B. P. (2003). Variability of the Indian Ocean: Relation to monsoon and ENSO. *Quarterly Journal of the Royal Meteorological Society* **129**: 1623–1646.

Kucharski, F., Bracco, A., Yoo, J. H. and Molteni, F. (2007). Low-Frequency Variability of the Indian Monsoon-ENSO Relationship and the Tropical Atlantic: The "Weakening" of the 1980s and 1990s. *Journal of Climate* **20**: 4255–4266.

Kucharski, F., Bracco, A., Yoo, J. H. and Molteni, F. (2008). Atlantic forced component of the Indian monsoon interannual variability. *Geophysical Research Letters* **35**: L04706.

Kucharski, F., Bracco, A., Yoo, J. H., Tompkins, A. M., Feudale, L., Ruti, P. and Dell'Aquila, A. (2009). A Gill-Matsuno-type mechanism explains the tropical Atlantic influence on African and Indian monsoon rainfall. *Quarterly Journal of the Royal Meteorological Society* **579**: 569–579.

Kucharski, F., Kang, I.-S., Farneti, R. and Feudale, L. (2011). Tropical Pacific response to 20th century Atlantic warming. *Geophysical Research Letters* **38**: L03702.

Kucharski, F., Syed, F. S., Burhan, A., Farah, I. and Gohar, A. (2014). Tropical Atlantic influence on Pacific variability and mean state in the twentieth century in observations and CMIP5. *Climate Dynamics*. DOI: 10.1007/s00382-014-2228-z

Kug, J.-S., Jin, F.-F. and An, S.-I. (2009). Two Types of El Niño Events: Cold Tongue El Niño and Warm Pool El Niño. *Journal of Climate* **22**: 1499–1515.

Kug, J.-S. and Kang, I.-S. (2006). Interactive Feedback between ENSO and the Indian Ocean. *Journal of Climate* **19**: 1784–1801.

Larkin, N. K. and Harrison, D. E. (2005). On the definition of El Niño and associated seasonal average U.S. weather anomalies. *Geophysical Research Letters* **32**: L13705.

Latif, M. and Grötzner, A. (2000). The equatorial Atlantic oscillation and its response to ENSO. *Climate Dynamics* **16**: 213–218.

Lau, K.-M. and Weng, H. (1995). Climate signal detection using wavelet transform: How to make a time series sing. *Bulletin of the American Meteorological Society* **76**: 2391–2402.

Liu, Z. and Alexander, M. (2007). Atmospheric bridge, oceanic tunnel, and climatic teleconnections. *Reviews of Geophysics* **45**: RG2005.

Lohmann, K. and Latif, M. (2007). Influence of El Niño on the Upper-Ocean Circulation in the Tropical Atlantic Ocean. *Journal of Climate* **20**: 5012–5018.

Losada, T., Rodríguez-Fonseca, B., Janicot, S., Gervois, S., Chauvin, F. and Ruti, P. (2010a). A multi-model approach to the Atlantic Equatorial mode: impact on the West African monsoon. *Climate Dynamics* **35**: 29–43.

Losada, T., Rodríguez-Fonseca, B., Mohino, E., Bader, J., Janicot, S. and Mechoso, C. R. (2012). Tropical SST and Sahel rainfall: A non-stationary relationship. *Geophysical Research Letters* **39**: L12705.

Losada, T., Rodríguez-Fonseca, B., Polo, I., Janicot, S., Gervois, S., Chauvin, F. and Ruti, P. (2010b). Tropical response to the Atlantic Equatorial mode: AGCM multimodel approach. *Climate Dynamics* **35**: 45–52.

Lübbecke, J. F. (2013). Climate science: Tropical Atlantic warm events. *Nature Geoscience* **6**: 22–23.

Lübbecke, J. F., Böning, C. W., Keenlyside, N. S. and Xie, S.-P. (2010). On the connection between Benguela and equatorial Atlantic Niños and the role of the South Atlantic Anticyclone. *Journal of Geophysical Research* **115**: C09015.

Lübbecke, J. F. and McPhaden, M. J. (2012). On the Inconsistent Relationship between Pacific and Atlantic Niños. *Journal of Climate* **25**: 4294–4303.

Lutz, K., Jacobeit, J. and Rathmann, J. (2014). Atlantic warm and cold water events and impact on African west coast precipitation. *Journal of International Climatology*. DOI: 10.1002/joc.3969.

Lutz, K., Rathmann, J. and Jacobeit, J. (2013). Classification of warm and cold water events in the eastern tropical Atlantic Ocean. *Atmospheric Science Letters* **14**: 102–106.

Matsuura, K. and Willmott, C. J. (2012). Terrestrial Precipitation: 1900-2010 Gridded Monthly Time Series (Version 3.02). Newark: Center for Climatic Research, Department of Geography, University of Delaware.

Meeuwis, J. M. and Lutjeharms, J. R. E. (1990). Surface thermal characteristics of the Angola-Benguela front. *South African Journal of Marine Science* **9**: 261–279.

Mélice, J.-L. and Servain, J. (2003). The tropical Atlantic meridional SST gradient index and its relationships with the SOI, NAO and Southern Ocean. *Climate Dynamics* **20**: 447–464.

Merle, J. (1980). Variabilité thermique annuelle et interannuelle de l'océan Atlantique équatorial Est. L'hypothèse d'un "El Niño" Atlantique. *Oceanologica Acta* **3**: 209–220.

Miller, A. J., Cayan, D. R., Barnett, T. P., Graham, N. E. and Oberhuber, J. M. (1994). The 1976-77 Climate Shift of the Pacific Ocean. *Oceanography* **7**: 21–26.

Mitchell, T. D. and Jones, P. D. (2005). An improved method of constructing a database of monthly climate observations and associated high-resolution grids. *International Journal of Climatology* **25**: 693–712.

Mohino, E., Rodríguez-Fonseca, B., Losada, T., Gervois, S., Janicot, S., Bader, J., Ruti, P. and Chauvin, F. (2011a). Changes in the interannual SST-forced signals on West African rainfall. AGCM intercomparison. *Climate Dynamics* **37**: 1707–1725.

Mohino, E., Rodríguez-Fonseca, B., Mechoso, C. R., Gervois, S., Ruti, P. and Chauvin, F. (2011b). Impacts of the Tropical Pacific/Indian Oceans on the Seasonal Cycle of the West African Monsoon. *Journal of Climate* **24**: 3878–3891.

Muller, A., Reason, C. J. C. and Fauchereau, N. (2008). Extreme rainfall in the Namib Desert during late summer 2006 and influences of regional ocean variability. *International Journal of Climatology* **28**: 1061–1070.

National Center of Atmospheric Research Climate Prediction Center (NCAR) (2014). Southern Oscillation Index (SOI).
URL: *http://www.cgd.ucar.edu/cas/catalog/climind/soi.html* (visited on 28/07/2014)

Nicholson, S. E. (2001). A semi-quantitative, regional precipitation data set for studying African climates of the nineteenth century, part I. Overview of the data set. *Climatic Change* **50**: 317–353.

Nicholson, S. E. (2013). The West African Sahel: A Review of Recent Studies on the Rainfall Regime and Its Interannual Variability. *ISRN Meteorology* **2013**: 1–32.

Nicholson, S. E. and Entekhabi, D. (1987). Rainfall variability in Equatorial and Southern Africa: Relationship with sea surface temperatures along the Southwestern coast of Africa. *Journal of Climate and Applied Meteorology* **26**: 561–578.

Nnamchi, H. C., Li, J. and Anyadike, R. N. C. (2011). Does a dipole mode really exist in the South Atlantic Ocean? *Journal of Geophysical Research* **116**: D15104.

National Oceanic and Atmospheric Administration Climate Prediction Center (NOAA CPC) (2014). Historical El Niño/ La Niña episodes (1950-present).
URL: *http://www.cpc.ncep.noaa.gov/products/analysis_monitoring/ensostuff/ensoyears.shtml* (visited on 28/07/2014)

Nobre, P. and Shukla, J. (1996). Variations of Sea Surface Temperature, Wind Stress, and Rainfall over the Tropical Atlantic and South America. *Journal of Climate* **9**: 2464–2479.

Okumura, Y. M. and Deser, C. (2010). Asymmetry in the Duration of El Niño and La Niña. *Journal of Climate* **23**: 5826–5843.

Okumura, Y. and Xie, S.-P. (2006). Some Overlooked Features of Tropical Atlantic Climate Leading to a New Niño-Like Phenomenon. *Journal of Climate* **19**: 5859–5874.

Ott, I., Romberg, K. and Jacobeit, J. (2014). Climate Dynamics Teleconnections of the tropical Atlantic and Pacific Oceans in a CMIP5 model ensemble. *Climate Dynamics*, *under review*.

Palmén, E. and Holopainen, E. O. (1962). Divergence, Vertical Velocity and Conversion between Potential and Kinetic Energy in an Extratropical Disturbance. *Geophysica* **8**: 89–113.

Parker, D., Good, E. and Chadwick, R. (2011). Reviews of Observational Data Available over Africa for Monitoring, Attribution and Forecast Evaluation. *Hadley Centre Technical Note* **86**: 1–63.

Philander, S. G. H. (1986). Unusual conditions in the tropical Atlantic Ocean in 1984. *Nature* **322**: 236–238.

Philipp, A. (2003). *Zirkulationsdynamische Telekonnektivität des Sommerniederschlags im südhemisphärischen Afrika*. PhD thesis, University of Würzburg.

Philipp, A., Della-Marta, P. M., Jacobeit, J., Fereday, D. R., Jones, P. D., Moberg, A. and Wanner, H. (2007). Long-Term Variability of Daily North Atlantic-European Pressure Patterns since 1850 Classified by Simulated Annealing Clustering. *Journal of Climate* **20**: 4065–4095.

Polo, I., Rodríguez-Fonseca, B., Losada, T. and García-Serrano, J. (2008). Tropical Atlantic Variability Modes (1979-2002). Part I: Time-Evolving SST Modes Related to West African Rainfall. *Journal of Climate* **21**: 6457–6475.

Preisendorfer, R. W. (1988). *Principle Component analysis in meteorology and oceanography*. Elsevier, Amsterdam.

Preston-Whyte, R. A. and Tyson, P. D. (1989). *The atmosphere and Weather of Southern Africa*. Oxford University Press, Cape Town, South Africa.

Rajeevan, M. and Sridhar, L. (2008). Inter-annual relationship between Atlantic sea surface temperature anomalies and Indian summer monsoon. *Geophysical Research Letters* **35**: L21704.

Rasmusson, E. M. and Carpenter, T. H. (1982). Variations in tropical sea surface temperature and surface sind fields associated with the Souther Oscillation/El Niño. *Monthly Weather Review* **110**: 354–384.

Rasmusson, E. M. and Carpenter, T. H. (1983). The Relationship Between Eastern Equatorial Pacific Sea Surface Temperatures and Rainfall over India and Sri Lanka. *Monthly Weather Review* **111**: 517–258.

Rathmann, J. (2009). *Klima- und Zirkulationsvariabilität im südhemisphärischen Afrika seit Beginn des 20. Jahrhunderts*. Geographica Augustana 6, Augsburg.

Rayner, N. A., Parker, D. E., Horton, E. B., Folland, C. K., Alexander, L. V., Rowell, D. P., Kent, E. C. and Kaplan, A. (2003). Global analyses of sea surface temperature, sea ice, and night marine air temperature since the late nineteenth century. *Journal of Geophysical Research* **108**.

Reason, C. J. C., Florenchie, P., Rouault, M. and Veitch, J. (2006). Influences of Large Scale Climate Modes and Agulhas System Variability on the BCLME Region. *In:* V. Shannon, G. Hempel, C. Malanotte-Rizzoli, C. Moloney and J. Woods (eds), *Large Marine Ecosystems 14*, Vol. 14, Elsevier, pp. 225–241.

Reason, C. J. C. and Rouault, M. (2006). Sea surface temperature variability in the tropical southeast Atlantic Ocean and West African rainfall. *Geophysical Research Letters* **33**: L21705.

Reynolds, R. W., Rayner, N. A., Smith, T. M., Stokes, D. C. and Wang, W. (2002). An Improved In Situ and Satellite SST Analysis for Climate. *Journal of Climate* **15**: 1609–1625.

Richter, I., Behera, S. K., Masumoto, Y., Taguchi, B., Komori, N. and Yamagata, T. (2010). On the triggering of Benguela Niños: Remote equatorial versus local influences. *Geophysical Research Letters* **37**: L20604.

Richter, I., Behera, S. K., Masumoto, Y., Taguchi, B. and Sasaki, H. (2013). Multiple causes of interannual sea surface temperature variability in the equatorial Atlantic Ocean. *Nature Geoscience* **6**: 43–47.

Richter, I., Xie, S.-P., Behera, S. K., Doi, T., and Masumoto, Y. (2014). Equatorial Atlantic variability and its relation to mean state biases in CMIP5. *Climate Dynamics* **42**: 171-188.

Robertson, A. W., Farrara, J. D. and Mechoso, C. R. (2003). Simulations of the Atmospheric Response to South Atlantic Sea Surface Temperature Anomalies. *Journal of Climate* **16**: 2540–2551.

Rodríguez-Fonseca, B., Janicot, S., Mohino, E., Losada, T., Bader, J., Caminade, C., Chauvin, F., Fontaine, B., García-Serrano, J., Gervois, S., Joly, M., Polo, I., Ruti, P., Roucou, P. and Voldoire, A. (2011). Interannual and decadal SST-forced responses of the West African monsoon. *Atmospheric Science Letters* **12**: 67–74.

Rodríguez-Fonseca, B., Polo, I., García-Serrano, J., Losada, T., Mohino, E., Mechoso, C. R. and Kucharski, F. (2009). Are Atlantic Niños enhancing Pacific ENSO events in recent decades? *Geophysical Research Letters* **36**: L20705.

Rouault, M. (2012). Bi-annual intrusion of tropical water in the Northern Benguela Upwelling. *Geophysical Research Letters* **39**: L12606.

Rouault, M., Florenchie, P., Fauchereau, N. and Reason, C. J. C. (2003). South East tropical Atlantic warm events and southern African rainfall. *Geophysical Research Letters* **20**: 8009.

Rouault, M., Illig, S., Reason, C. J. C. and Bentamy, A. (2007). Propagation and origin of warm anomalies in the Angola Benguela upwelling system in 2001. *Journal of Marine Research* **68**: 473–488.

Roxy, M., Gualdi, S., Drbohlav, H.-K. L. and Navarra, A. (2011). Seasonality in the relationship between El Nino and Indian Ocean dipole. *Climate Dynamics* **37**: 221–236.

Rudolf, B. and Schneider, U. (2005). Calculation of Gridded Precipitation Data for the Global Land-Surface using in-situ Gauge Observations. *2nd Workshop of the International Precipitation Working Group, Monterey October 2004*, pp. 231–247.

Ruiz-Barradas, A., Carton, J. A. and Nigam, S. (2000). Structure of Interannual-to-Decadal Climate Variability in the Tropical Atlantic Sector. *Journal of Climate* **13**: 3285–3297.

Sachs, L. and Hedderich, J. (2009). *Angewandte Statistik: Methodensammlung mit R*. Heidelberg, Springer.

Saji, N. H., Goswami, B. N., Vinayachandran, P. N. and Yamagata, T. (1999). A dipole mode in the tropical Indian Ocean. *Nature* **401**: 360–363.

Saji, N. H. and Yamagata, T. (2003a). Possible impacts of Indian Ocean Dipole mode events on global climate. *Climate Research* **25**: 151–169.

Saji, N. H. and Yamagata, T. (2003b). Structure of SST and Surface Wind Variability during Indian Ocean Dipole Mode Events: COADS Observations. *Journal of Climate* **16**: 2735–2751.

Saravanan, R. and Chang, P. (2000). Interaction between Tropical Atlantic Variability and El Niño-Southern Oscillation. *Journal of Climate* **13**: 2177–2194.

Schönwiese, C. (2013). *Praktische Statistik für Meteorologen und Geowissenschaftler*. 5 edn, Borntraeger, Berlin, Stuttgart.

Schott, F. A., Xie, S.-P. and McCreary, J. P. (2009). Indian Ocean circulation and climate variability. *Reviews of Geophysics* **47**.

Servain, J., Picaut, J. and Merle, J. (1982). Evidence of Remote Forcing in the Equatorial Atlantic Ocean. *Journal of Physical Oceanography* **12**: 457–463.

Servain, J., Wainer, I., McCreary, J. P. and Dessier, A. (1999). Relationship between the equatorial and meridional modes of climatic variability in the tropical Atlantic. *Geophysical Research Letters* **26**: 485–488.

Seubert, S. (2010). *Telekonnektionen des Niederschlags im Mittelmeerraum zur Zirkulation in den Tropen*. PhD thesis, University of Augsburg.

Shannon, L. V., Boyd, A. J., Brundrit, G. B. and Taunton-Clark, J. (1986). On the existence of an El Niño-type phenomenon in the Benguela System. *Journal of Marine Research* **44**: 495–520.

Shannon, L. V. and Nelson, G. (1996). The Benguela: Large Scale Features and Processes and System Variability. *In:* G. Wefer, W. Berger, G. Siedler and D. Webb (eds), *The South Atlantic: Present and Past Circulation*. Springer, Berlin, Heidelberg, pp. 163–210.

Shinoda, T., Hendon, H. H. and Alexander, M. A. (2004). Surface and subsurface dipole variability in the Indian Ocean and its relation with ENSO. *Deep Sea Research Part I: Oceanographic Research Papers* **51**: 619–635.

Slutz, R. J., Lubker, S. J., Hiscox, J. D., Woodruff, S. D., Jenne, R. L., Joseph, D. H., Steurer, P. M. and Elms, J. D. (1985). Comprehensive Ocean-Atmosphere Data Set: Release 1. *I: Climate Research Program, ERL/NOAA, Boulder, CO*.

Smith, T. M. and Reynolds, R. W. (2003). Extended Reconstruction of Global Sea Surface Temperatures Based on COADS Data (1854-1997). *Journal of Climate* **16**: 1495–1510.

Smith, T. M., Reynolds, R. W., Peterson, T. C. and Lawrimore, J. (2008). Improvements to NOAA's Historical Merged Land-Ocean Surface Temperature Analysis (1880-2006). *Journal of Climate* **21**: 2283–2296.

Torrence, C. and Compo, G. P. (1998). A Practical Guide to Wavelet Analysis. *Bulletin of the American Meteorological Society* **79**: 61–78.

Tozuka, T., Kataoka, T. and Yamagata, T. (2014). Locally and remotely forced atmospheric circulation anomalies of Ningaloo Niño/Niña. *Climate Dynamics*.

Trenberth, K. E. (1984). Signal versus Noise in the Southern Oscillation. *Monthly Weather Review* **112**: 326–332.

Trenberth, K. E. (1997). The Definition of El Niño. *Bulletin of the American Meteorological Society* **78**: 2771–2777.

Trenberth, K. E., Caron, J. M., Stepaniak, D. P. and Worley, S. (2002). Evolution of El Niño-Southern Oscillation and global atmospheric surface temperatures. *Journal of Geophysical Research* **107**.

Trenberth, K. E. and Stepaniak, D. P. (2001). Indices of El Niño Evolution. *Journal of Climate* **14**: 1697–1701.

Vigaud, N., Richard, Y., Rouault, M. and Fauchereau, N. (2009). Moisture transport between the South Atlantic Ocean and southern Africa: relationships with summer rainfall and associated dynamics. *Climate Dynamics* **32**: 113–123.

von Storch, H. and Zwiers, W. (1999). *Statistical Analysis in Climate Research*. Cambridge University Press, Cambridge.

Walker, N. D. (1987). Interannual sea surface temperature variability and associated atmospheric forcing within the Benguela system. *South African Journal of Marine Science* **5**: 121–132.

Wang, C. (2001). A Unified Oscillator Model for the El Niño-Southern Oscillation. *Journal of Climate* **14**: 98–115.

Wang, C. (2002). Atlantic Climate Variability and Its Associated Atmospheric Circulation Cells. *Journal of Climate* **15**: 1516–1536.

Wang, C. (2006). An overlooked feature of tropical climate: Inter-Pacific-Atlantic variability. *Geophysical Research Letters* **33**: L12702.

Wang, C., Deser, C., Yu, J.-Y., DiNezio, P. and Clement, A. (2013). El Niño and Southern Oscillation (ENSO): A Review. *Coral Reefs of the Eastern Pacific*. Springer, Miami, in press.

Wang, C., Kucharski, F., Barimalala, R. and Bracco, A. (2009). Teleconnections of the tropical Atlantic to the tropical Indian and Pacific Oceans: A review of recent findings. *Meteorologische Zeitschrift* **18**: 445–454.

Wang, C. and Picaut, J. (2004). Understanding ENSO Physics-A Review. *Geophysical Monograph Series* **147**: 21–48.

Wang, C. and Wang, X. (2013). Classifying El Niño Modoki I and II by Different Impacts on Rainfall in Southern China and Typhoon Tracks. *Journal of Climate* **26**: 1322–1338.

Webster, P. J., Moore, A. M., Loschnigg, J. P. and Leben, R. R. (1999). Coupled ocean-atmosphere dynamics in the Indian Ocean during 1997-98. *Nature* **401**: 356–60.

Wilks, D. (2005). *Statistical Methods in the Atmospheric Sciences*. Academic Press Inc., U.S.

Willmott, C. J. and Robeson, S. M. (1995). Climatologically Aided Interpolation (CAI) of terrestrial air temperature. *International Journal of Climatology* **15**: 221–229.

Willmott, C. J., Rowe, C. M. and Philpot, W. D. (1985). Small-scale climate maps: A sensitivity analysis of some common assumptions associated with grid-point interpolation and contouring. *The American Cartographer* **12**: 5–16.

Woodruff, S. D., Worley, S. J., Lubker, S. J., Ji, Z., Freeman, E. J., Berry, D. I., Brohan, P., Kent, E. C., Reynolds, R. W., Smith, S. R. and Wilkinson, C. (2011). ICOADS Release 2.5: extensions and enhancements to the surface marine meteorological archive. *International Journal of Climatology* **31**: 951–967.

Wu, R. and Kirtman, B. P. (2004). Understanding the Impacts of the Indian Ocean on ENSO Variability in a Coupled GCM. *Journal of Climate* **17**: 4019–4031.

Wu, R., Kirtman, B. P. and Krishnamurthy, V. (2008). An asymmetric mode of tropical Indian Ocean rainfall variability in boreal spring. *Journal of Geophysical Research* **113**: D05104.

Xie, S.-P., Annamalai, H., Schott, F. A. and McCreary, J. P. (2002). Structure and Mechanisms of South Indian Ocean Climate Variability. *Journal of Climate* **15**: 864–878.

Xie, S.-P. and Carton, J. A. (2004). Tropical Atlantic Variability: Patterns, Mechanisms, and Impacts. *Geophysical Monograph* **147**: 121–142.

Xie, S.-P. and Philander, S. G. H. (1994). A coupled ocean-atmosphere model of relevance to the ITCZ in the eastern Pacific. *Tellus A* **46**: 340–350.

Yadav, R. K. (2008). Role of equatorial central Pacific and northwest of North Atlantic 2-metre surface temperatures in modulating Indian summer monsoon variability. *Climate Dynamics* **32**: 549–563.

Yeh, S.-W., Kirtman, B. P., Kug, J.-S., Park, W. and Latif, M. (2011). Natural variability of the central Pacific El Niño event on multi-centennial timescales. *Geophysical Research Letters* **38**: L02704.

Yeh, S.-W., Kug, J.-S., Dewitte, B., Kwon, M.-H., Kirtman, B. P. and Jin, F.-F. (2009). El Niño in a changing climate. *Nature* **461**: 511–515.

Yu, J.-Y., Mechoso, C. R., Mcwilliams, J. C. and Arakawa, A. (2002). Impacts of the Indian Ocean on the ENSO cycle. *Geophysical Research Letters* **29**: 46–1–3.

Zebiak, S. E. (1993). Air-Sea Interaction in the Equatorial Atlantic Region. *Journal of Climate* **6**: 1567–1586.

A

Publications

Publications in peer-reviewed Journals

Parts of the work presented in this thesis have been published in the following papers:

1. Lutz, K., Rathmann, J. and Jacobeit, J. (2013). Classification of warm and cold water events in the tropical southeast Atlantic. *Atmospheric Science Letters* **14**: 102–106.
2. Lutz, K., Jacobeit, J. and Rathmann, J. (2014). Atlantic warm and cold water events and impact on African west coast precipitation. *Journal of International Climatology*. DOI: 10.1002/joc.3969.